AD-A094 433   WOODS HOLE OCEANOGRAPHIC INSTITUTION MASS   F/G 8/3
               1980 SUMMER STUDY PROGRAM IN GEOPHYSICAL FLUID DYNAMICS - COHER--ETC(U)
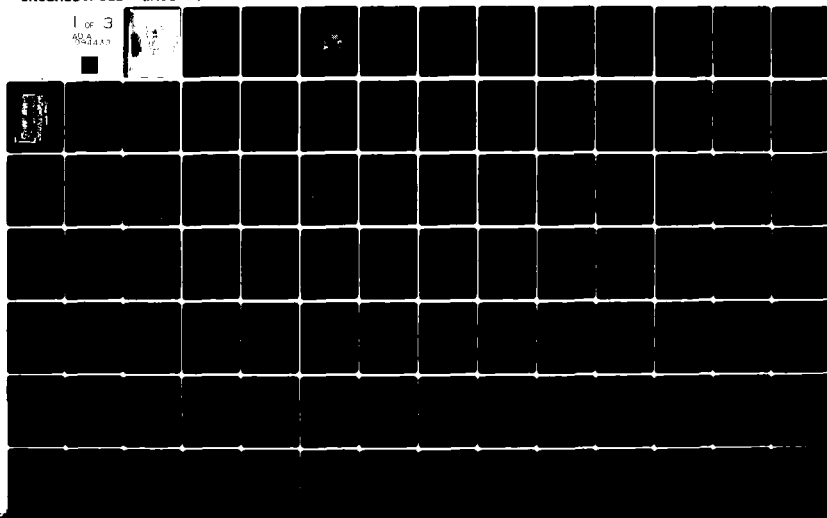   NOV 80   G VERONIS, F K MELLOR   N00014-79-C-0671
UNCLASSIFIED   WHOI-80-53   NL

| | OF | 3 |

SECURITY CLASSIFICATION OF THIS PAGE (When Data Entered)

REPORT DOCUMENTATION PAGE		READ INSTRUCTIONS BEFORE COMPLETING FORM
1. REPORT NUMBER WHOI-80-53	2. GOVT ACCESSION NO. AD-A094433	3. RECIPIENT'S CATALOG NUMBER
4. TITLE (and Subtitle) 1980 SUMMER STUDY PROGRAM IN GEOPHYSICAL FLUID DYNAMICS - COHERENT FEATURES IN GEOPHYSICAL FLOWS.		5. TYPE OF REPORT & PERIOD COVERED Technical rept.
		6. PERFORMING ORG. REPORT NUMBER
7. AUTHOR(s) George Veronis, Director Florence K. Mellor, Editor		8. CONTRACT OR GRANT NUMBER(s) N00014-79-C-0671
9. PERFORMING ORGANIZATION NAME AND ADDRESS Woods Hole Oceanographic Institution Woods Hole, Massachusetts 02543		10. PROGRAM ELEMENT, PROJECT, TASK AREA & WORK UNIT NUMBERS
11. CONTROLLING OFFICE NAME AND ADDRESS NORDA National Space Technology Laboratory Bay St. Louis, MS 39529		12. REPORT DATE November 1980
		13. NUMBER OF PAGES 249
14. MONITORING AGENCY NAME & ADDRESS(If different from Controlling Office)		15. SECURITY CLASS. (of this report) Unclassified
		15a. DECLASSIFICATION/DOWNGRADING SCHEDULE

16. DISTRIBUTION STATEMENT (of this Report)

Approved for public release; distribution unlimited.

17. DISTRIBUTION STATEMENT (of the abstract entered in Block 20, if different from Report)

18. SUPPLEMENTARY NOTES

19. KEY WORDS (Continue on reverse side if necessary and identify by block number)

1. Geophysical fluid dymanics
2. Coherent features
3. Geophysical flows

Accession For

NTIS CRA&I	☑
DTIC TAB	☐
Unannounced	☐
Justification	

By_____
Distribution/
Availability Codes

Dist	Avail and/or Special
A	

20. ABSTRACT (Continue on reverse side if necessary and identify by block number)

See reverse side.

DD FORM 1473 EDITION OF 1 NOV 65 IS OBSOLETE
S/N 0102-014-6601

Four principal lecturers shared the task of presenting the subject "Coherent Features in Geophysical Flows" to the participants of the twenty-second geophysical fluid dynamics summer program. Glenn Flierl introduced the topic and the Kortweg-de Vries equation via a model of finite amplitude motions on the beta plane. He extended the analysis to more complex flows in the ocean and the atmosphere and in the process treated motions of very large amplitude. Larry Rdekopp's three lectures summarized an extensive body of the mathematical literature on coherent features. Andrew Ingersoll focussed on the many facinating features in Jupiter's atmosphere. Joseph Keller supplemented an interesting summary of laboratory observations with suggestive models for treating the flows.

The seminars by participants and invited speakers, abstracts of which are included, cover a broad range of topics in geophysical fluid dynamics. Among the abstracts are the seminars presented by McWilliams, Flierl, Redekopp, Rizzoli, Pierrehumbert and Hendershott during the one-week workshop on coherent features.
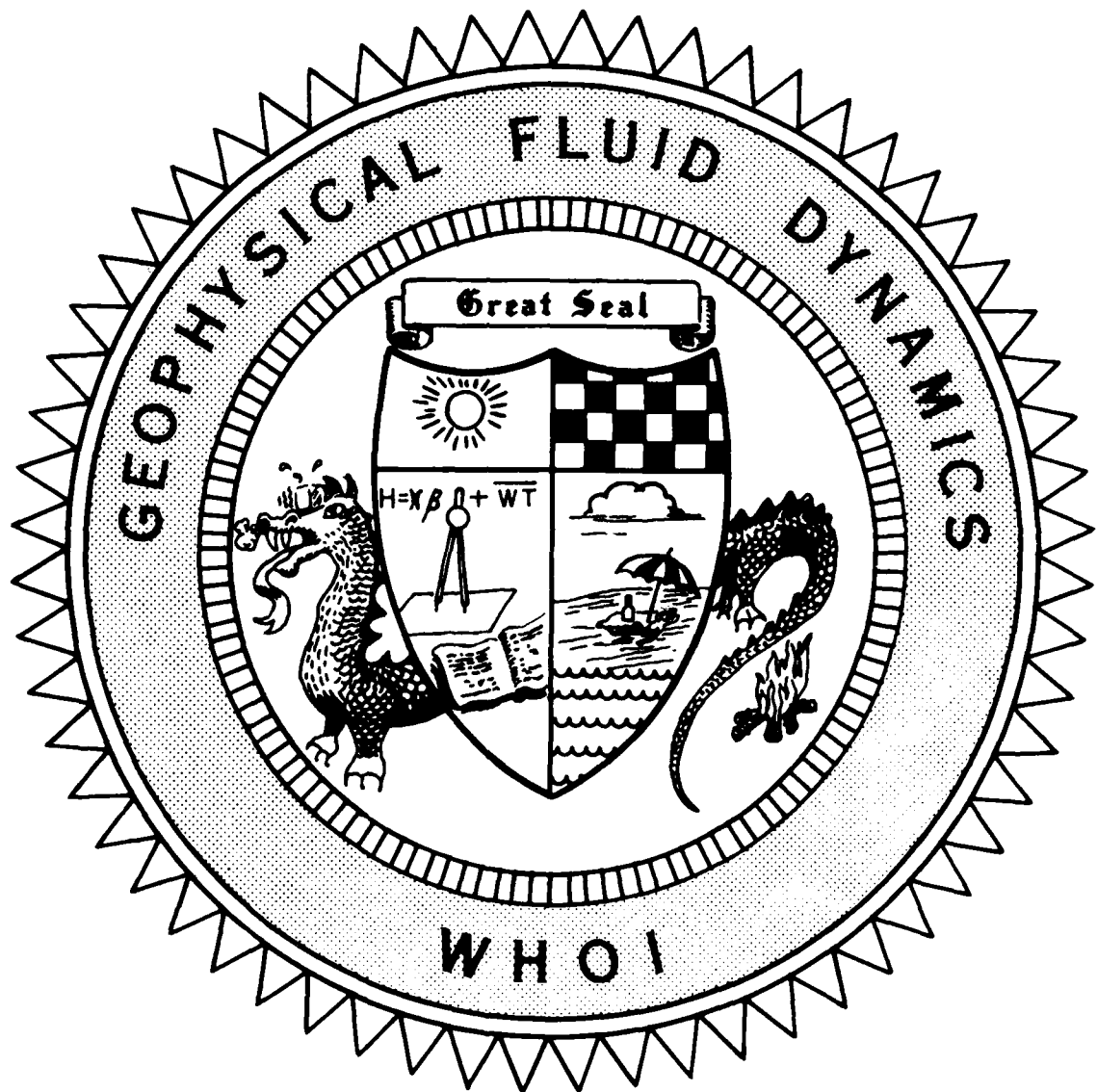
The nine student lectures summarize the most creative product of the summer program. This year was most unusual in that most of the students worked on some aspect of the central theme. Some of these projects will be reworked and extended for publication.

WHOI-80-53

1980

GEOPHYSICAL FLUID DYNAMICS

Great Seal

$H = X \beta \Omega + \overline{WT}$

WHOI

COURSE LECTURES

SEMINARS

ABSTRACTS OF SEMINARS

LECTURES OF THE FELLOWS

WHOI-80-53

1980 SUMMER STUDY PROGRAM
IN
GEOPHYSICAL FLUID DYNAMICS
THE WOODS HOLE OCEANOGRAPHIC INSTITUTION

COHERENT FEATURES IN GEOPHYSICAL FLOWS

By

George Veronis, Director
and
Florence K. Mellor, Editor

WOODS HOLE OCEANOGRAPHIC INSTITUTION
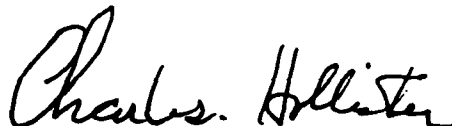Woods Hole, Massachusetts 02543

November 1980

TECHNICAL REPORT

Approved for Distribution

Charles D. Hollister
Charles D. Hollister
Dean of Graduate Studies

1980 SUMMER STUDY PROGRAM

in

GEOPHYSICAL FLUID DYNAMICS

at

THE WOODS HOLE OCEANOGRAPHIC INSTITUTION

COHERENT FEATURES IN GEOPHYSICAL FLOWS

STAFF MEMBERS AND PARTICIPANTS

Blumen, William	University of Colorado
Boyd, John	Harvard University
Chu, B. T.	Yale University
Flierl, Glenn	Massachusetts Institute of Technology
Gans, Roger	University of Rochester
Grimshaw, Roger	University of Melbourne
Hendershott, Myrl	Scripps Institution of Oceanography
Hide, Raymond	Geophysical Fluid Dynamics Laboratory, Berkshire
Hohenberg, Martin	Bell Laboratories, Murray Hill
Howard, Louis	Massachusetts Institute of Technology
Hunkins, Kenneth	Lamont-Doherty Geological Observatory
Pierrehumbert, Raymond	Massachusetts Institute of Technology
Ingersoll, Andrew	California Institute of Technology
Keller, Joseph	Stanford University
Lesser, Martin	University of Rochester
Malkus, Willem	Massachusetts Institute of Technology
Maxworthy, Anthony	University of Southern California
McWilliams, James	National Center for Atmospheric Reserch
Nelkin, Mark	Cornell University
Redekopp, Larry	University of Southern California
Rhines, Peter	Woods Hole Oceanographic Institution
Rizzoli, Paola	Laboratorio Dinamica Grandi Masse-Venice
Salusti, Ettore	Instituto di Fisico Universita Rome
Smith, Ron	Yale University
Spence, Thomas	Texas A & M University
Spiegel, Edward	Columbia University
Stern, Melvin	University of Rhode Island
Veronis, George	Yale University
Whitehead, John	Woods Hole Oceanographic Institution

FELLOWS

Aref, Hassan	Cornell University
Deininger, Richard	Massachusetts Institute of Technology
Depassier, M. Cristina	Columbia University
Gregory-Allen, Richard	Massachusetts Institute of Technology
Griffiths, Ross	D.A.M.T.P., Cambridge, England
Meiss, James	University of California
Webb, Spahr	Scripps Institution of Oceanography
Young, William	WHOI/MIT

EDITOR'S PREFACE

Four principal lecturers shored the task of presenting the subject "Coherent Features in Geophysical Flows" to the participants of the twenty-second geophysical fluid dynamics summer program. Glenn Flierl introduced the topic and the Kortweg-de Vries equation via a model of finite amplitude motions on the beta plane. He extended the analysis to more complex flows in the ocean and the atmosphere and in the process treated motions of very large amplitude. Larry Redekopp's three lectures summarized an extensive body of the mathematical literature on coherent features. Andrew Ingersoll focussed on the many fascinating features in Jupiter's atmosphere. Joseph Keller supplemented an interesting summary of laboratory observations with suggestive models for treating the flows.

The seminars by participants and invited speakers, abstracts of which are printed in the following pages, cover a broad range of topics in geophysical fluid dynamics. Included among the abstracts are the seminars presented by McWilliams, Flierl, Redekopp, Rizzoli, Pierrehumbert and Hendershott during the one-week workshop on coherent features.

The nine student lectures summarize the most creative product of the summer program. This year was most unusual in that most of the students worked on some aspect of the central theme. Some of these projects will be reworked and extended for publication.

We are deeply indebted to Ralph Cooper of the Office of Naval Research for arranging the funding from several government agencies. We are also grateful to Florence Mellor and Maryanne Macaluso, who assembled the reports and handled the practical functioning of the program and to A. L. Peirson who helped in the administration of the program.

George Veronis

iii

TABLE OF CONTENTS

COHERENT FEATURES IN GEOPHYSICAL FLOWS

SEMINARS and ABSTRACTS OF SEMINARS

LECTURES OF FELLOWS

Top Row: Rhines, Hendershott, Pierrehumbert, Spiegel, Redekopp, Meiss,
           Flierl, Griffiths, Deinenger, Webb, Veronis, Depassier.
Front Row: Whitehead, McWilliams, Spence, Howard, Gregory-Allen, Rizzoli,
           Aref, Stern, Mellor, Salusti, Young, Charney, Malkus.

INTRODUCTION TO COHERENT FEATURES

Glenn R. Flierl

LECTURE #1.

1. INTRODUCTION

In this lecture we shall quickly derive several nonlinear equations governing the propagation of Rossby waves in a homogeneous β-plane ocean. Some of these equations, such as the Korteweg-de Vries equation, are familiar from surface wave theory; others such as the modon solutions were first derived in the context of β-plane dynamics. All these equations, however, describe the evolution of features with finite total energy which retain their identity for long periods of time, i.e., coherent features. Nonlinearity is an essential part of their dynamics since it combats the linear wave dispersion and holds the features together.

Because an infinite plane Rossby wave is an exact nonlinear solution on a uniform depth β - plane, additional mechanisms are needed to induce non-trivial nonlinearity. The mechanisms discussed in this lecture are nonuniform depth, gradual modulation of a wave train and shear in a mean zonal current.

Finally, we distinguish between solitary waves and solitons. Solitons are solitary waves which survive collisions with other solitary waves.

2. *NONUNIFORM DEPTH*

In this section we show that the KdV equation governs the propagation of Rossby waves in a zonal channel of uneven depth. The symbols associated with the geometry of the channel are defined in Figure 1.
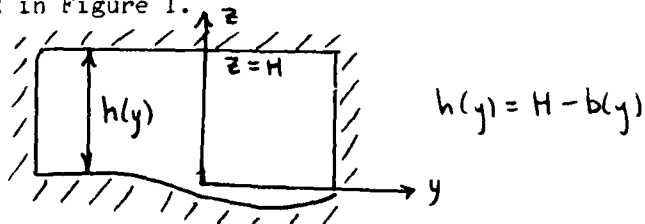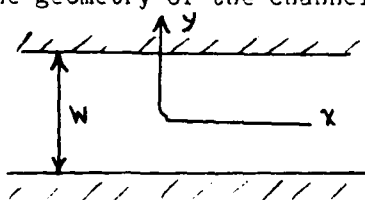
The shallow water equations:

$$\frac{Du}{Dt} - fv = -p_x \tag{1a}$$

$$\frac{Dv}{Dt} + fu = -p_y \tag{1b}$$

$$(uh)_x + (vh)_y = 0 \tag{1c}$$

imply potential vorticity conservation :

$$\frac{D}{Dt}\left(\frac{\zeta+f}{h}\right) = 0 \tag{2a}$$

$$f = f_0 + \beta y \tag{2b}$$

$$\zeta = v_x - u_y \tag{2c}$$

The mass conservation Eqn. (2c) allows the introduction of a mass streamfunction:

$$hu = -\psi_y \tag{3a}$$

$$hv = \psi_x \tag{3b}$$

so that (2a) is an equation in one unknown, ψ . This equation is simplified using the following approximations:

1) The channel is rapidly rotating, i.e.

$$\frac{\zeta}{f} \sim \frac{u}{f_0 L} = R_0 \ll 1$$

2) The depth variation is slight, i.e.

$$\frac{b}{H} \lesssim O(R_0)$$

3) The channel is narrow, i.e.

$$W \ll \beta^{-1} f_0 \sim \text{Radius of Earth}$$

Using the above (2a) becomes

$$\left(\partial_t + \varphi_x \partial_y - \varphi_y \partial_x\right)\left(\nabla^2\varphi + \beta y + \frac{f_0}{H} b\right) = O\left(R_0, \frac{W\beta}{f_0}\right) \tag{4}$$

where $\varphi = H^{-1}\psi$. Equation (4) is the quasigeostrophic potential vorticity equation.

Equation (4) is now nondimensionalized using $\varphi \sim UW$, $y \sim W$, $x \sim L$ $t \sim (L/\beta W^2)$; the x and y scales are different. The subsequent perturbation analysis uses the nondimensional numbers

$$\varepsilon = \frac{\text{particle speed}}{\text{wave speed}} = \frac{u}{\beta W^2}$$

$$\varsigma = \frac{\text{y scale}}{\text{x scale}} = \frac{W}{L}$$

$$s = \frac{\text{vortex stretching}}{\text{planetary vorticity variations}} = \frac{f_0\,(\text{slope})}{\beta H}$$

We will analyze the simplest case $\varepsilon \sim \delta \sim s \ll 1$. Because $\delta \ll 1$, the perturbation solutions cannot be applied strictly to synoptic weather systems or mesoscale ocean eddies which have comparable EW and NS length scales.

The scale separation, however, allows the y dependence to be removed and produces an x-t problem which ultimately reduces to the KdV equation.

The nondimensional form of (4) is

$$\left[\partial_t + \varepsilon \left(\varphi_x \partial_y - \varphi_y \partial_x \right) \right] \left[\varepsilon \varphi_{yy} + \varepsilon \delta^2 \varphi_{xx} + y + sb \right] = 0 \quad (5)$$

Now, it is easily seen that a naive expansion of φ in powers of ε must fail; simply consider the dispersion relation calculated using linear theory; when b = 0:

$$\omega = - \frac{k}{k^2 \delta^2 + \ell^2} \simeq - \frac{k}{\ell^2} + \frac{\delta^2 k^3}{\ell^4} - \cdots \quad (6)$$

Because ℓ is constant all the dispersive effects, which must balance nonlinear steepening, are in the term $\delta^2 k^3/\ell^4$. This term can only be important on time scales of order δ^{-2}. Thus a successful perturbation expansion must contain the time scale $T = \delta^2 t$ explicitly. This motivates the multiple time scale expansion

$$\varphi = \varphi^{(0)}(x,y,t,T) + \varepsilon \varphi^{(1)}(x,y,t,T) + \varepsilon^2 \varphi^{(2)}(x,y,t,T) \quad (7a)$$
$$+ \cdots$$

and in (5)

$$\frac{\partial}{\partial t} \rightarrow \frac{\partial}{\partial t} + \delta^2 \frac{\partial}{\partial T} \quad (7b)$$

The ε expansion of Eqn. (7a) is motivated by $\varepsilon \sim \delta$

Equations (7a and b) are now substituted into Eqn. (4) and like powers of ε collected to produce a hierarchy of problems the first of which is:

$$O(\varepsilon): \qquad \partial_t \varphi^{(0)}_{yy} + \varphi^{(0)}_x = 0 \quad (8)$$

The solution of Eqn. (8) which satisfies the boundary condition:

$$\varphi = 0 \qquad at \qquad y = 0 \text{ and } 1$$

is

$$\varphi^{(0)} = F\left(x + (m\pi)^{-2} t, T \right) \sin m\pi y \quad (9)$$

F is unknown at the moment; it is determined by requiring that the subsequent problems in the hierarchy be free of resonant forcing so that all the $\varphi(n)$ are bounded as $t \rightarrow \infty$. For simplicity make the nonessential simplification m = 1 in (9).

The next problem in the hierarchy is then

$$O(\varepsilon^2): \qquad \partial_t \varphi^{(1)}_{yy} + \varphi^{(1)}_x = - \frac{s}{\varepsilon} b_y \varphi^{(0)}_x \quad (10)$$

Note how the expected nonlinear term $\dfrac{\partial(\varphi^{(0)}, \nabla^2 \varphi^{(0)})}{\partial(x,y)}$ vanishes identically. The nonlinear Jacobians appear at the next order and so the nonlinear terms are important on times of $O(\varepsilon^{-2})$. Since the dispersive effects are important on times of order S^{-2} the scaling $\varepsilon \sim S$ is necessary for a balance. With stronger topography ($S \sim 1$) the y structure of the lowest order solution would be more complicated and $\dfrac{\partial(\varphi^{(0)}, \nabla^2\varphi^{(0)})}{\partial(x,y)}$ would not be zero. Then we would choose $\varepsilon \sim S^2$ to bring dispersion and nonlinearity in together. The weak topography shows explicitly the necessity of curvature in b(y) steepening.

To solve Eqn. (10) it is necessary to specify a particular topography; for illustrative purposes $b = \sin(\pi y)$ is simple. The solution of Eqn. (10) in this case is

$$\varphi^{(0)} = \frac{\pi}{6}\frac{S}{\varepsilon}\, \sin 2\pi y \; F(x + \pi^{-2}t, T) \tag{11}$$

The next problem in the hierarchy is

$$O(\varepsilon^3): \quad \frac{S^2}{\varepsilon^2}\left[\varphi^{(0)}_{yyT} + \varphi^{(0)}_{xxt}\right] + \frac{S}{\varepsilon} b_y \varphi^{(1)}_x + \frac{\partial(\varphi^{(0)}, \varphi^{(1)}_{yy})}{\partial(x,y)}$$
$$+ \frac{\partial(\varphi^{(1)}, \varphi^{(0)}_{yy})}{\partial(x,y)} + \varphi^{(2)}_{yyt} + \varphi^{(2)}_x = 0 \tag{12}$$

Substituting Eqn. (9) and Eqn. (10) into Eqn. (12) one obtains

$$\left(\frac{S}{\varepsilon}\right)^2 \left[-\pi^2 F_T + \pi^{-2} F_{xxx}\right]\sin \pi y + \left(\frac{S}{\varepsilon}\right)^2 \frac{\pi^2}{6} F_x \cos \pi y \, \sin 2\pi y$$
$$+ \left(\frac{S}{\varepsilon}\right) \frac{\pi^4}{2} F F_x \left[\sin 2\pi y \, \cos \pi y - 2\sin \pi y \, \cos 2\pi y\right] + \varphi^{(2)}_{yyt} + \varphi^{(2)}_x = 0 \tag{13}$$

From the structure of the inhomogeneous terms it is clear that $\varphi^{(2)}_t = \pi^{-2}\varphi^{(2)}_x$. If $\varphi^{(2)}_x$ is to remain bounded the forcing terms in (13) must be orthogonal to the adjoint solution of $(\pi^{-2}\frac{\partial^2}{\partial y^2}+1)\chi = 0$; thus if (13) is multiplied by $\sin(\pi y)$ and integrated across the channel the inhomogeneous term must vanish. This condition is the desired evolution equation for F

$$F_T - \frac{1}{12}\left(\frac{S}{\delta}\right)^2 F_x - \pi^{-4} F_{xxx} - \frac{3\pi^2}{4}\left(\frac{\varepsilon S}{\delta^2}\right) F F_x = 0 \tag{14}$$

Apart from the constant coefficients Eqn. (14) is the standard form of the Korteweg-de Vries equation. If s = 0, corresponding to a flat bottom, the nonlinear term in Eqn. (14) is removed. Without it the straightforward linear solution is, in fact, an exact nonlinear solution and the above perturbation theory merely generates successive terms in the Taylor series expansion of the dispersion relation as in Eqn. (6).

3. PROPERTIES OF THE KORTEWEG-DE VRIES EQUATION

The transformation

$$F = \frac{8\delta^2}{\varepsilon S \pi^4}\, q\left(x + \frac{1}{12}\left(\frac{S}{\delta}\right)^2 T, \; -\pi^{-4}T\right)$$

puts Eqn. (14) into the more elegant form

$$q_\tau + q q_\zeta + 6 q_{\zeta\zeta\zeta} = 0 \qquad (15)$$

with

$$\zeta = x + \frac{1}{12}\left(\frac{5}{8}\right)^2 T \quad \text{and} \quad \tau = -\pi^{-4} T$$

One can write (formally) an exact solution to Eqn. (15)

In order to gain some simple intuition about Eqn. (14), however, let us consider two special cases:

1) The linear cases $F_T - \frac{1}{12}\left(\frac{5}{8}\right)^2 F_x - \pi^{-4} F_{xxx} = 0$. The initial tendency of a symmetric hump to steepen at the rear is sketched in Figure (2a). This rear steepening occurs because long waves travel faster (c total for a wave with wavenumber k is given by $-(m\pi)^{-2} - \frac{1}{12}s^2 + \pi^{-4} k^2 \delta^2$).

2) The strongly nonlinear case $F_T - \frac{3\pi^2}{4}\left(\xi^5/\delta^2\right) F F_x$. The initial tendency of a positive symmetric hump to steepen at the front is sketched in Figure (2b). Negative humps steepen at the rear.

(a)   (b)
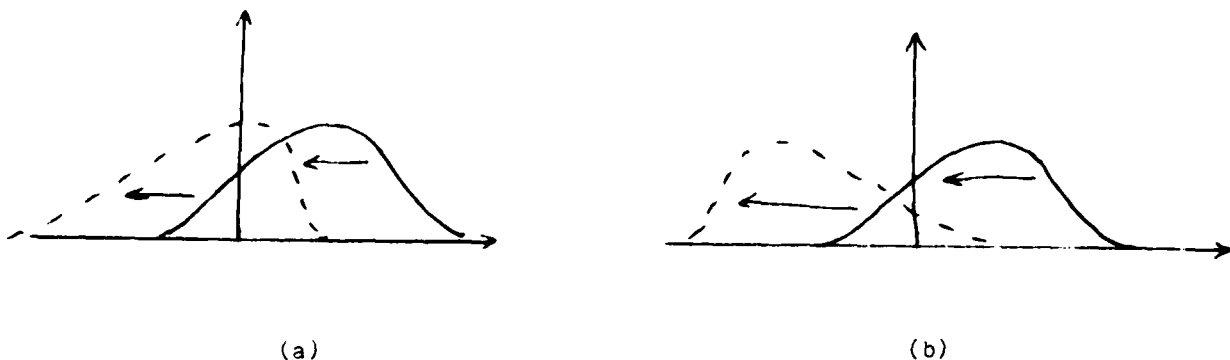
Figure 2

These special cases suggest that for positive humps it may be possible to strike a balance between forward and rear steepening to produce a hump which travels without distortion. To prove conclusively that this balance can be achieved, construct a solitary wave solution of Eqn. (15); it is found that

$$q = q_0 \operatorname{sech}^2\left[\frac{1}{2}\sqrt{c}\,(x - ct)\right] \qquad (16)$$

where the amplitude and the speed are related by

$$q_0 = \tfrac{1}{2} c$$

or in terms of our original variables

$$F = \frac{16 \, s^2 \, k^2}{\pi^6 \, \varepsilon \, s} \, sech^2 \left[k \, (x - ct) \right]$$

$$c = - \pi^{-2} - \tfrac{1}{12} s^2 - \tfrac{4}{\pi^4} k^2 s^2$$

One might expect that the soliary wave solution Eqn. (16) is a delicate structure which would arise from a limited class of initial conditions. However, one of the major successes of the inverse scattering method was to prove that all reasonable initial conditions eventually break up into a finite number of solitary waves plus a weakly nonlinear wave train. Moreover, the solitary solutions of the KdV equation can collide and pass unchanged through other solitary waves. Thus since the larger waves move faster the eventual behaviour as $t \to \infty$ consists of a finite number of solitary waves lined up with size and velocity increasing to the front. In the following lectures we will reserve the term _soliton_ for robust solitary waves such as these which survive interactions.

4. MODULATED ROSSBY WAVES

In this section we will investigate the nonlinear evolution of a slowly modulated Rossby wave group (Yamagata, 1979)

$$\varphi = A(X, T) \, e^{i(kx - \varpi t)} \, \sin \pi y \qquad \text{+ complex conjugate} \quad (17)$$

Our goal is to determine the evolution of the envelope A on the slow space and time scales X and T.

The nondimensionalized equation is

$$\left[\partial_t + \varepsilon (\varphi_x \, \partial_y - \varphi_y \, \partial_x) \right] \left[\varepsilon \, \varphi_{yy} + \varepsilon \, \varphi_{xx} + y \right] \qquad (18)$$

Note the following differences between Eqn. (18) and Eqn. (5):

1) There is no topographic term in Eqn. (18); nonlinear effects are provided
   by the slow modulation of the plane wave.

2) The x and y scales are the same in Eqn. (18), this is because the zonal wavelength of the carrier may be comparable to the width of the channel.

Equation (18) is solved using a multiple scale perturbation expansion

$$\varphi = \varphi^{(o)}(x, y, t; X, T) + \varepsilon \, \varphi^{(1)}(x, y, t, X, T) \qquad (19)$$

$$X = \varepsilon (x - v_g t)$$

$$T = \varepsilon^2 t$$

where V_g is the X-component of group velocity. We will see below that the well known result $v_g = \frac{\partial \varpi}{\partial k}$ will be recovered at second order in the perturbation expansion.

The first problem in the hierarchy is

$$O(\varepsilon^1): \qquad (\partial_t \nabla^2 + \partial_x) \, \varphi^{(0)} = 0 \tag{20}$$

the solution of which is

$$\varphi^{(0)} = A(X,T) \, e^{i(kx - \varpi t)} \sin \pi y \tag{21}$$

$$\varpi = - k / (k^2 + \pi^2)$$

The next problem is

$$O(\varepsilon^2): \qquad (\partial_t \nabla^2 + \partial_x) \, \varphi^{(1)} + (1 - v_g \nabla^2 + 2 \partial_t \partial_x) \, \varphi^{(0)}_X \tag{22}$$
$$= - \frac{\partial(\varphi^{(0)}, \nabla^2 \varphi^{(0)})}{\partial(x,y)}$$

The term proportional to $\varphi^{(0)}_X$ in Eqn. (22) is resonant, to eliminate it take

$$v_g = - \frac{1 + 2 \varpi k}{k^2 + \pi^2} = \frac{\partial \varpi}{\partial k} \tag{23}$$

The general solution of Eqn. (22) is then an infinite sum of plane waves, the only one of which produces resonant terms at next order is the quasi-zonal flow:

$$\varphi^{(1)} = B(X,T) \, \theta(y) \tag{24}$$

The next order is

$$O(\varepsilon^3): \quad (\partial_t \nabla^2 + \partial_x) \, \varphi^{(2)} + (1 - v_g \partial_j^2) \, \varphi^{(1)}_X + (\nabla^2 \varphi^{(0)}_T + \varphi^{(0)}_{XXt} - 2 v_g \varphi^{(0)}_{XXX}) \tag{25}$$
$$= - \frac{\partial(\varphi^{(0)}, \nabla^2 \varphi^{(0)})}{\partial(X,y)} - 2 \frac{\partial(\varphi^{(0)}, \varphi^{(0)}_{XX})}{\partial(x,y)} - \frac{\partial(\varphi^{(1)}, \nabla^2 \varphi^{(0)})}{\partial(x,y)} - \frac{\partial(\varphi^{(0)}, \nabla^2 \varphi^{(1)})}{\partial(x,y)}$$

When Eqn. (21) and Eqn. (24) are substituted into Eqn. (25) there are two types of resonant forcing terms which must be eliminated.

1) Terms independent of the fast time and length scales such as $(1 - v_g \partial_j^2) \varphi^{(1)}_X$. Elimination of these terms implies

$$\varphi^{(1)} = - 2 k^2 \pi (1 + 4\pi^2 v_g)^{-1} |A|^2 \sin 2\pi y \tag{26}$$

Since we shall choose $1 + 4\pi^2 v_g \neq 0$, there will be no second harmonic resonance.

2) Terms dependent on $kx - \varpi t$. Elimination of these terms implies

$$i A_T + \left[\frac{k(3\pi^2 - k^2)}{(k^2 + \pi^2)^2} \right] A_{XX} = \left[\frac{2 k^3 \pi^2 (3\pi^2 - k^2)(k^2 + \pi^2)}{k^4 + 5\pi^2 k^2 - 5\pi^4} \right] A |A|^2 \tag{27}$$

Equation (27) is the cubic Schroedinger equation. Time can be rescaled to put it in the form

$$i \hat{A}_\tau + \hat{A}_{xx} = \nu \hat{A} |\hat{A}|^2$$

$$\nu = \frac{2 k^2 \pi^2 (k^2 + \pi^2)^4}{k^4 + 6\pi^2 k^2 - 3\pi^4} \tag{28}$$

Eq. (28) has soliton solutions:

$$\hat{A} = \sqrt{\frac{-2s^2}{\nu}} \operatorname{sech} s x \, e^{is^2 T}$$

This is a solution of Eqn. (28) only when $\nu < 0$ or equivalently $k < \pi \sqrt{2\sqrt{3} - 3}$.

This is the wave number range in which our infinite train of waves is modulationally unstable (Plumb, 1977).

5. ROSSBY WAVES IN SHEAR FLOWS AND NONQUASIGEOSTROPHIC EFFECTS

In this section we will use a model equation which is not strictly derivable from the equations of motion but which crudely represents some of the nonlinearities associated with nonquasigeostrophic effects. The model equation is

$$\left[\partial_t + \bar{u} \partial_x + \psi_x \partial_y - \psi_y \partial_x \right] \left[\frac{\nabla^2 \psi + f - \bar{u}_y}{1 - \frac{b}{H} + \psi/fR^2} \right] = 0 \tag{29}$$

The nonquasigeostrophic term is the ψ/fR^2 in the denominator of the potential vorticity. The closest physical analog is a two layer system with an upper layer which is passive because it is much thicker than the lower layer. The nonquasigeostrophic term represents the perturbation of the density structure (i.e., the interface displacement) associated with the disturbance.

Now look for steadily moving solutions to Eqn. (29) so that $\partial_t = -c\,\partial_x$ and a first integral is then

$$\nabla^2 \psi + f - \bar{u}_y = \left(1 - \frac{b}{H} + \frac{\psi}{fR^2}\right) P\left(\psi + cy - \int^y \bar{u}\right) \tag{30}$$

where P is an, as yet, arbitrary function.

For streamlines which extend to $\pm\infty$, P can be evaluated by requiring that the eddy be isolated ($\psi \to 0$ as $x \to \pm\infty$) so that:

$$\frac{f - \bar{u}_y}{1 - b/H} = P\left(cy - \int^y \bar{u}\right) \tag{31}$$

We can use Eqn. (31) to rewrite Eqn. (30) in the form

$$\nabla^2 \psi - \frac{(1 - \bar{u}_y/f)}{(1 - b/H)} \frac{\psi}{R^2} = \left(1 - \frac{b}{H} + \frac{\psi}{fR^2}\right)\left[P\left(\psi + cy - \int^y \bar{u}\right) - P\left(cy - \int^y \bar{u}\right)\right] \tag{32}$$

which is a type of nonlinear oscillator equation. In the quasigeostrophic approximation, the lefthand side of Eqn. (31) becomes $f_o + \beta y + \frac{f_o b}{H} - \bar{u}_y$ while (32) is partially linearized to

$$\nabla^2 \psi - \frac{\psi}{R^2} = P\left(\psi + cy - \int^y \bar{u}\right) - P\left(cy - \int^y \bar{u}\right)$$

In principle Eqn. (31) can be solved to find P as a function of its argument and Eqn.(32) can then be solved for the wave shape ψ and speed c . In practice, to make analytic progress it is necessary to use approximations. The first is the __weak wave approximation__ which simplifies the righthand side of Eqn. (32) by expanding the square bracket in a Taylor series in ψ so that finally

$$\nabla^2 \psi = A(y,c)\,\psi + B(y,c)\,\psi^2 \qquad\qquad \text{+ (higher order terms)} \qquad (33)$$

A and B in Eqn. (33) contain derivatives of P evaluated at $cy - \int^y \bar{u}$. For example, the linear coefficient is

$$A(y,c) = \frac{1 - \bar{u}_y/f}{1 - b/H}\,1/R^2 + (1 - b/H)\,P'(cy - \int^y \bar{u})$$

$$= \frac{1 - \bar{u}_y/f}{1 - b/H}\,1/R^2 + (1 - b/H)\left(\frac{1}{c - \bar{u}}\right)\frac{\partial}{\partial y}\left(\frac{f - \bar{u}_y}{1 - b/H}\right)$$

These derivatives can be written in terms of known functions such as u and b using Eqn. (31). In general A in Eqn. (33) depends on y and the linear term is much greater than the ψ^2 term. In this case we get a balance by forcing the waves to be elongated in the x-direction, $\partial_y^2 \gg \partial_x^2$, so that at lowest order

$$\frac{\partial^2 \psi^{(0)}}{\partial y^2} = A(y, c^{(0)})\,\psi^{(0)} \qquad\qquad (34)$$

The solution of Eqn. (34) is

$$\psi^{(0)} = F(x)\,H(y) \qquad \text{and } c = c^{(0)} \quad \text{+ higher order terms where } c(0)$$

is an eigenvalue determined by the y boundary conditions. F(x) is determined at the next order where dispersion and nonlinearity enter. The equation for $\psi^{(1)}$ is an inhomogeneous boundary value problem, and the solvability condition is an equation for F:

$$\left[\int H^2 dy\right] F'' = \left[\int \frac{\partial A}{\partial c^{(0)}}(y, c^{(0)}) H^2 dy\right](c - c^{(0)})F + \int H^3 B(y, c^{(0)})\,dy\,\frac{F^2}{(35)}$$

This equation determines the structure of F and the correction to $c^{(0)}$. As in section 1, F has a sech^2 shape and the correction to $c^{(0)}$ is positive so that the nonlinear wave moves faster than the fastest linear wave.

There is an exceptional class of solutions to Eqn. (33) which are worth noting. When $\frac{\partial A}{\partial y} = 0$, as happens when u = b = 0, then it is possible to find radially symmetric solutions in which nonquasigeostrophic effects provide the nonlinear steepening. In this case, the potential vorticity functional is just

$$P(z) = f_0 + \frac{\beta}{c}\,z$$

so that

$$\nabla^2 \psi = \left(\frac{1}{R^2} + \frac{\beta}{c}\right)\psi + \frac{\beta}{cfR^2}\,\psi^2$$

The lowest order balance for scales large compared to R is just

$$A(c^{(0)}) = 0$$

or $c^{(0)} = -\beta R^2$. At first order

$$\nabla^2 \psi = -\frac{\beta}{c^{(0)2}}(c - c^{(0)})\psi - \frac{1}{fR^4}\psi^2$$

which has both sech^2 and radially symmetric solutions if the scale is small enough so that f can be replaced by f_o.

The other assumption which simplifies the general form Eqn. (32) is the strong eddy approximation. Assume that both mean flow and topography are weak; P in Eqn. (31) is approximately linear since

$$cy - \int^y \bar{u} = z \qquad \text{implies} \qquad y \simeq c^{-1} z + c^{-1} \int^{c^{-1} z} \bar{u}$$

and so
$$P(z) = \frac{f - \bar{u}_y}{1 - b/H} \simeq (f_0 + c^{-1}\beta z)(1 + b/H) + c^{-1}\beta \int^{c^{-1}z} \bar{u} - \bar{u}_y(c^{-1}\beta z)$$

With simple choices of topography and shear Eqn. (33) is recovered and the subsequent analysis is applicable.

Both the weak wave approximation and the strong eddy approximation are based on (31) and so apply only to streamlines which extend to ∞ , i.e., open streamlines. It is possible to construct solutions having closed streamlines and in this case it is necessary to specify P in the region where the streamlines close. There are two different approaches:

1) Assume P is an analytic function and continue to use Eqn. (31) to define P.

2) Let P be a multivalued function and use different branches in the open and closed regions.

The simplest solution with closed streamlines is the quasigeostrophic modon with u = b = 0. In the exterior region the equation is linear and

$$\psi = - \frac{ca \; K_1 \left[r \sqrt{\beta c^{-1} + R^{-2}} \right]}{K_1 \left[a \sqrt{\beta c^{-1} + R^{-2}} \right]} \sin \theta$$

is one convenient solution. This solution has a closed streamline at r = a and within this circle P need not satisfy Eqn. (31). Instead take

$$P(z) = - \left(\frac{k^2}{a^2} + R^{-2} \right) z$$

where k is an arbitrary constant and then the corresponding interior solution which is continuous at r = a is

$$\psi = \left\{ \beta a^3 \left(1 + \frac{c}{\beta R^2} \right) \frac{J_1(k \frac{r}{a})}{k^2 J_1(k)} - \frac{r}{k^2} \left(\beta a^2 + c \left[k^2 + \frac{a^2}{R^2} \right] \right) \right\} \sin \theta$$

Continuity of ψ_r at r = a implies the dispersion relation:

$$\frac{K_2(a \sqrt{\beta c^{-1} + R^{-2}})}{a \sqrt{\beta c^{-1} + R^{-2}} \; K_1(a \sqrt{\beta c^{-1} + R^{-2}})} = - \frac{J_2(k)}{k J_1(k)}$$

Equation (36) connects the speed, amplitude and size of the nonlinear modons; the dispersion curves are sketched in Lecture 2.

The following table shows how various published Rossby solitary wave solutions fit within the classifications discussed above.

TABLE 1

Effects Included

	Topographic	Mean Flow	Nonquasigeostrophic	Multi-valued P
Weak	Rizzoli (1978)	Maxworthy & Redekopp Redekopp (1976) Redekopp (1976)	Clarke (1971) Charney & Flierl (1980)* Boyd (1978)	
Strong	Rizzoli (1980) Henrotay (1980)*	Flierl (1979)* Long (1964) Larsen (1965) Benney (1966)	Flierl (1977)* or Charney & Flierl (1980)*	

Modon		Ingersoll (1973)		Stern (1975)
				Larichev & Reznik (1976)
				Flierl, Larichev,
				  McWilliams & Reznik
				  (1980)

*Indicates radially symmetric cases.

REFERENCES

Benney, D. J., 1966. J. Math. & Phys., 45, 52.

Boyd, J. P., 1978. Review Papers of Equat. Oc. FINE Workshop Proceedings.

Charney, J. and G. Flierl, 1980. Oceanic analogues of large-scale atmospheric motion (Preprint).

Clarke, R. A., 1971. G. F. D., 2, 343-354.

Flierl, G., 1977. Warm Core Rings Workshop notes.

Flierl, G., 1977. D. A. O., 3, 15-38.

Flierl, G., V. Larichev, J. McWilliams and G. Reznik, 1980. D. A. O. (current or next issue.

Ingersoll, A., 1973. Science, 182, 1346-1348.

Larsen, L. H., 1965. Jour. Acoust. Soc., 22, 222-224.

Long, R. R., 1964. Jour. Acoust. Soc., 21, 197-200.

Maxworthy, A. and L. Redekopp, 1976. Icarus, 29, 261-271.

Plumb, R. A., 1977. Jour. Fluid Mech., 80, 705.

Redekopp, L., 1977. Jour. Fluid Mech., 82, 725-745.

Rizzoli, P. M., 1978. Solitary Rossby waves over variable relief and
     their stability properties. PhD. Thesis, SIO.

Stern, M., 1975. Jour. Mar. Res., 33, 1-13.

Yamagata. T., 1979. Submitted to J. Met. Soc., Japan.

NOTES SUBMITTED BY
WILLIAM YOUNG

MODONS AND ATMOSPHERIC BLOCKING

Glenn Flierl

LECTURE #2

Isolated features with long lifetimes are associated with atmospheric
blocking. The 700 mb surface from June 1963 illustrates this phenomena. A
paired high and low were observed over the North Atlantic. The high lay north
of the low and both features were nearly stationary.

A possible model for these features is a "Modon" solitary Rossby wave.
The modon solutions are exact solutions of the quasigeostrophic equation and
exhibit strong nonlinearity and strong dispersion which still cancel each
other. These solutions are isolated in both the north-south (y) and east-west
(x) directions.

The single layer quasigeostrophic equation in nondimensional form is

$$\partial_t (\nabla^2 - 1) \psi + \psi_x + J(\psi, \nabla^2 \psi) = 0 \tag{1}$$

Here x is nondimensionalized by the radius of deformation $R_d = \sqrt{gH}/f_0$,
time by $(\beta R_d)^{-1}$ and velocity by βR_d^2. If the solutions are steadily
moving the time derivative ∂_t may be replaced by $-c \partial_x$ where c is
the velocity of propagation in the east-west direction. [Conservation of
vorticity prohibits steady motion with a component in the north-south directio
for any wave which carries fluid with it. Particles in these trapped regions
(closed streamlines in the moving reference frame) would after one period have
moved north or south without a corresponding change in relative vorticity.]
Equation 1 becomes:

$$J(\psi + cy, \nabla^2 \psi - \psi + y) = 0 \tag{2}$$

and therefore

$$\nabla^2 \psi - \psi + y = P(\psi + cy) \tag{3}$$

where $P(Z)$ is any function of Z. Far from an isolated feature $\psi \to 0$,

$$P(Z) = \frac{1}{c} Z \tag{4}$$

In any region with streamlines which extend to infinity:

$$\nabla^2 \psi - \psi = \frac{1}{c} \psi \tag{5}$$

The linear form of this equation is a consequence of dynamics, not just an ad-
hoc choice. Vertical shear and stratification does not change the linearity
of the exterior equation although topography and horizontal shear will.

The solution to this equation is:

$$\psi = \sum_{n=1}^{\infty} D_n K_n\left(\sqrt{\tfrac{1}{c}+1}\; r\right) \sin n\theta + \sum_{n=0}^{\infty} E_n K_n\left(\sqrt{\tfrac{1}{c}+1}\; r\right) \cos n\theta \qquad (6)$$

$$r = \sqrt{(x-ct)^2 + y^2} \qquad \theta = \tan^{-1}\frac{y}{x-ct}$$

The requirement that the eddy be isolated and energy and enstrophy be finite restricts the propagation velocity c to c $\gtrless$ 0 or c < -1. Linear waves are possible only in the complement of this domain, $-1 \leqslant c < 0$. Initially, we shall consider only a single term of this solution. The stream function written in a coordinate frame moving with the wave is

$$\chi = \psi + cy = D K_1\left(\sqrt{\tfrac{1}{c}+1}\; r\right) \sin\theta + cr\sin\theta \qquad (7)$$

If Dc > 0, this solution will be singular with all streamlines closing at this singularity at the origin (see sketch). When Dc < 0, however, there is a streamline $\psi + cy = 0$ at position $r = a$, where a is related to D and c by

$$D K_1\left(a\sqrt{\tfrac{1}{c}+1}\right) + ca = 0$$

CONTOURS
OF χ
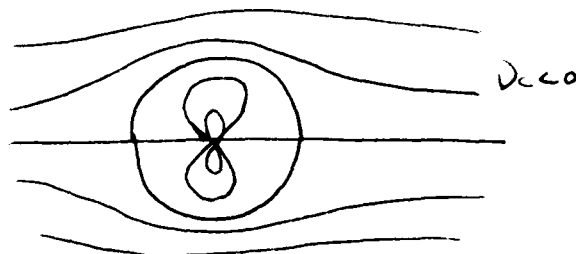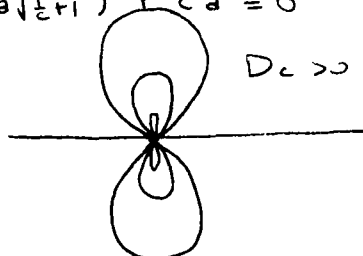
Since equation 4 applies only to regions with streamlines extending to infinity, a different choice of P(Z) can be made inside any closed streamline. P(Z) can be chosen which allows solutions which are nonsingular, have finite energy and enstrophy, and match to the exterior solutions.

The matching conditions are continuity of ψ and $\frac{\partial \psi}{\partial n}$ where n is normal to the boundary closed streamline. Higher order derivatives may also be made continuous, but some discontinuous derivatives are necessary.

The continuity of the first derivative is a consequence of this Bernouilli equation

$$\frac{D}{Dt}\left[\frac{(u-c)^2 + v^2}{2} + p + c\int^y f(y')dy'\right] = 0 \qquad (8)$$

which can be obtained from the equations of motion:

$$\frac{D}{Dt}(u-c) - fv = -\left(p + c\int^y f\right)_x , \quad \frac{D}{Dt}v + f(u-c) = -\left(p + c\int^y f\right)_y \quad (9)$$

The last two terms in Eqn. (8) are continuous across a boundary; therefore, the change in the square of this tangential velocity with tangential distance must be the same on either side of the dividing streamline. The simpliest condition which accomplishes this and simultaneously avoids potentially unstable shear layers is to require that the tangential velocity be continuous.

An auxilliary constraint on the modon solutions is evident from the x-moment of the quaisgeostrophic Eqn. (1). The constraint can be relaxed if there is a mean shear, stratification or topography. If this equation times x is integrated over all x and y, all terms except the β effect (ψ_x) give no contribution. The result is

$$\iint \psi \, dx\,dy = 0 \tag{10}$$

or no mean surface displacement. This is equivalent to no net coriolis force on the modon.

The idea of matching one solution within a closed streamline to an exterior solution can be carried to three dimensional solutions. A volume will be found within closed streamlines and an exterior solution matched onto the solution within the volume.

For the one term exterior solution (Eqn. 7) there is a circular closed streamline at radius a if a = -DK$_1$(q)/c (q = $a\sqrt{\frac{1}{c}+1}$). This choice of closed streamline (required by keeping only the simple term) will lead to only a few of a large class of solutions. P(Z) can be made a linear function of Z within the circle:

$$P(Z) = Q - S \cdot Z \tag{11}$$

Unlike the exterior regions, the linearity in the interior is a completely ad hoc assumption made to lead to soluable equations. However, this linearization does not lead to vanishing of the advection terms in Eqn. (1); this solution is not linear.

Let $S = 1 + k^2/a^2$ then Eq. (3) becomes

$$\nabla^2 \psi + \frac{k^2}{a^2} \psi = Q - \left(1 + \frac{k^2}{d^2}\right) y \tag{12}$$

This equation has the solution:

$$\psi = \frac{Qd}{k^2} - \left[1 + c\left(1 + \frac{k^2}{d^2}\right)\right] \cos\vartheta + \sum_{n=1}^{\infty} B_n J_n\left(\frac{kr}{d}\right)\sin n\vartheta + \sum_{n=0}^{\infty} C_n J_n\left(\frac{kr}{d}\right)\cos n\vartheta \tag{13}$$

Let Q = 0. The matching conditions allow only B$_1$ to be nonzero and require:

$$\frac{J_2(k)}{k J_1(k)} = -\frac{K_2(q)}{q K_1(q)} \tag{14}$$

These solutions are antisymmetric about an east-west axis. A high lies south of a low for eastward moving waves and north of the low for westward moving waves.
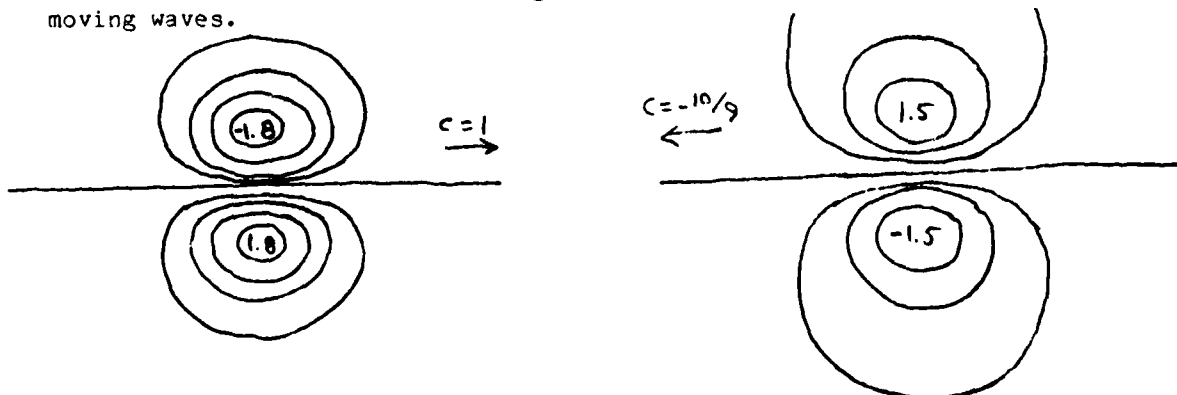
These solutions may be better understood by first examining the vortex pair solutions of Batchelor (1967). A southern high drives a northern low to the east and the low pushes the high also to the east. If the right amount of this eastward tendency is added to the westward β tendency, Stern's (1975) modon solution is recovered. Increasing the strength of the vortex pair leads to eastward motion as in Larichev and Reznick (1976) and where the pair is very strong Batchelor's solution is again the correct description.

The wave speed is a function of the size and amplitude. Small scale (short distance between vortex centers) and large amplitude waves travel faster.

ψ at NORTHERN CENTER
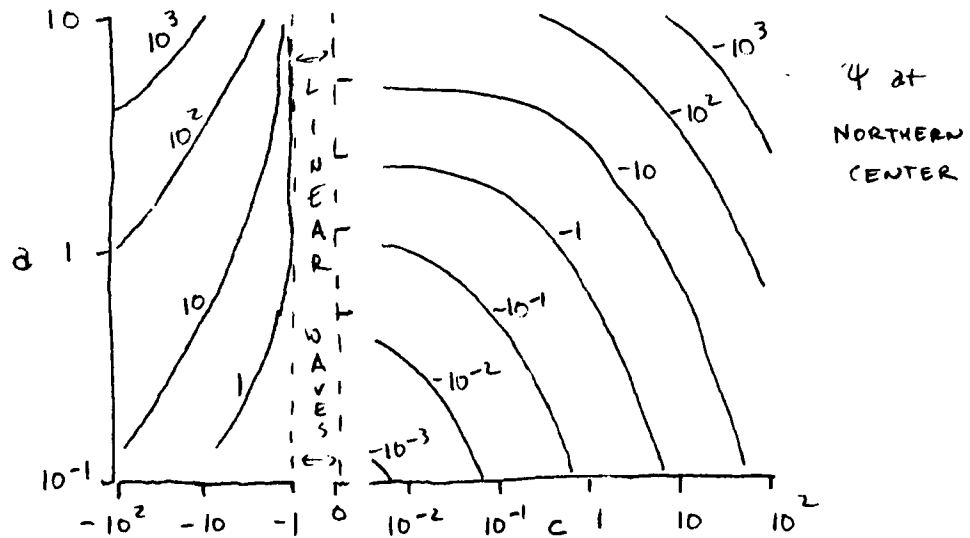
Riders

Additional solutions can be found by adding an arbitrary constant (E_0) times the K_0 Bessel function to the exterior solution. The solution in the interior now requires a Jo term. The new matching conditions are:

$$E_0 \, K_0\left(\sqrt{\tfrac{1}{c}+1}\; a\right) = \frac{Q a^2}{k^2} + C_0 \, J_0(k)$$

$$E_0 \, {}^{q}/_{a} \, K_0'\left(\sqrt{\tfrac{1}{c}+1}\; a\right) = C_0 \, {}^{k}/_{a} \, J_0'(k) \tag{15}$$
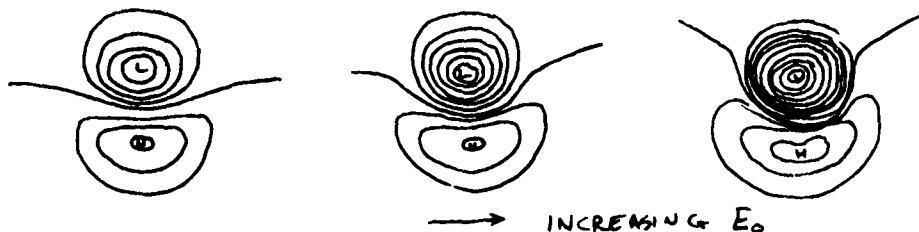
$\longrightarrow$ INCREASING E_0

These solutions become more symmetric (more like a single vortex) as E_o is increased. The name "riders" has been given to these solutions because the radially symmetric fields have no influence upon the shape, strength or speed of the $\sin\theta$ solutions. The riders move with the original solution.

Numerical Studies

A number of experiments have indicated that solutions evolve only slowly. Numerical studies by McWilliams et al. (1980) suggest the solutions without riders are stable. This study also illustrated the necessity of fine resolution (15 or more grid points per diameter) to obtain the correct wave speed for these nonlinear features. Poorly resolved features moved as little as half as fast as the actual wave speed.

The stability of the solutions without riders to finite perturbations was also examined. The stability depends both on the scale and amplitude of the perturbations. Large amplitude, small scale perturbations allowed the two vortex centers to drift apart until they were independent features. The larger scale perturbations did not need to be as strong to destroy the modons, and destroyed the modons by shearing out the features. The modons appear stable to perturbations with an r.m.s. stream function amplitude less than 10-20% of the modon amplitude.

A last set of numerical experiments included parameterized friction in the equations. The amplitude of a modon solution was found to decay slowly. The velocity of the wave decreased, following the dispersion curve until the amplitude was too small for the wave to be sufficiently nonlinear to avoid dispersion (essentially when c decreases to 0 for eastward moving eddies). The wave then dispersed.

This model will not allow stationary features in an eastward mean flow. The single layer quasigeostrophic Eqn. (1) is not Galilean invariant. Requiring a wave speed c = 0 in a mean flow at U leads to this equation:

$$J(-Uy + \psi, \nabla^2 \psi - y) = 0 \tag{16}$$

There are only solutions with flow from the east. This is contrary to atmospheric observations of the blocking phenomena.

Vertical Shear and Stratification

In order to apply this model, we need to construct a one mode description of motions in an atmosphere with vertical stratification and shear. The equations for a stratified atmosphere are:

$$\frac{Du}{Dt} - fv = -\Phi_x \qquad \frac{Dv}{Dt} + fu = -\Phi_y \qquad \frac{\partial \Phi}{\partial p} = -\alpha \tag{17}$$

$$\nabla \cdot \underset{\sim}{u} = 0 \qquad \frac{D}{Dt} \ln \alpha + \frac{\omega}{\gamma p} = 0$$

(p coordinates)

The vertical velocity in pressure coordinates is ω and α is the specific volume. ϕ is the geopotential gz. The boundary condition is $\frac{D}{Dt}\phi = 0$ at a pressure p_o such that $\phi(x, y, p_o, t) = 0$. A quasigeostrophic stream function can be defined

$$\psi = \phi / f_o \tag{18}$$

The boundary condition linearized in accordance with the quasigeostrophic approximation is

$$\frac{D}{Dt}\psi = \omega\,\frac{\bar{\alpha}(p_o)}{f_o} \tag{19}$$

with $\bar{\alpha}(p)$ a mean specific volume profile.

The equations in (17) can be approximated by a pair of coupled equations

$$\frac{D}{Dt}(\nabla^2\psi + \beta y) = f_o\frac{\partial\omega}{\partial p} \tag{20}$$

$$\frac{D}{Dt}\left(\frac{\partial\psi}{\partial p}\right) + \frac{\sigma\omega}{f_o} = 0 \qquad \sigma = \frac{\bar{\alpha}^2 N^2}{g^2} \tag{21}$$

For solutions which are stationary in a mean flow, these equations become:

$$U\partial_x\nabla^2\psi + (\beta - U_{yy})\psi_x + J(\psi, \nabla^2\psi) = f_o\frac{\partial\omega}{\partial p} \tag{22}$$

$$U\partial_x\frac{\partial\psi}{\partial p} - U_p\psi_x + J\left(\psi, \frac{\partial\psi}{\partial p}\right) + \frac{\omega\sigma}{f_o} = 0 \tag{23}$$

The boundary condition is reduced to $\omega = 0$ at $p = p_o$. The stream function may be written as a modal expansion.

$$\psi = \sum_i \alpha_i(x, y)\,F_i(p) \tag{24}$$

$$\frac{1}{p_o}\int_0^{p_o} F_i\,F_j\,dp = \delta_{ij} \tag{25}$$

The mean velocity is assumed to have only p dependence (vertical shear).

$$U = U_o\,G(p) \tag{26}$$

An equation describing a one mode approximation for standing motions in the atmosphere can be obtained by first plugging their expressions into Eqns. (22) and (23). Eqn. (22) is then multiplied by F_j, and Eqn. (23) by $\frac{1}{\sigma}\partial_p F_j$; both equations are integrated in p from 0 to p. Eliminating the terms in ω between the equations and truncating to one term gives this result:

$$\hat{U}\partial_x\nabla^2\hat{\alpha} - \frac{\hat{U}}{R^2}\partial_x\hat{\alpha} + \beta\partial_x\hat{\alpha} + J(\hat{\alpha}, \nabla^2\hat{\alpha}) = 0 \tag{27}$$

$$\hat{U} = \langle F^2 U\rangle \qquad \frac{\hat{U}}{R^2} = \left\langle \frac{f_o^2}{\sigma}\left(\frac{\partial F}{\partial p}\right)^2 U - \frac{f_o^2}{\sigma}\frac{\partial F}{\partial p}F\frac{\partial U}{\partial p}\right\rangle \qquad \hat{\alpha} = \alpha\langle 1 \rangle$$

The brackets are used to signify integration in p from 0 to p_0. An appropriate choice for F (the first term in the expansion) is the first empirical orthogonal function as determined from observations. The values of R, and $\hat{U}$ are not very precise, but R is close to the internal radius of deformation.

Equation (27) may be put in the same form as Eqn. (2) by nondimensionalizing. Thus the one vertical mode model will have the same modon solutions as the single layer quasigeostrophic equation. However, it is necessary that the vertical structure of the mean flow be different from the vertical structure of the waves. Otherwise there are no stationary solutions in an eastward mean flow.

Two Layer Models

Flierl, et al. (1980) describe modon solutions for a two layer model. Solutions are possible with closed streamlines in either layer or in both layers. The exterior solution (defined in the same way as for a single layer model) can have both barotropic and baroclinic parts, but if there is a barotropic part the motion must be eastward.

$$\psi = b_T K_1 \left(\sqrt{\tfrac{1}{c}} \, r \right) \sin \theta + b_c K_1 \left(\sqrt{\tfrac{1}{c}+1} \, r \right) \sin \theta + \dots \tag{28}$$

The solutions are sums of modes with the mode number k, the k_{th} zero of the Bessel function. Which modes are possible in each layer depends principally on the ratio of layer depths $\delta = H_1/H_2$, but also on the scale of the features (a).

For the typical ocean model $\delta = .2$. A possible solution with four centers is sketched.
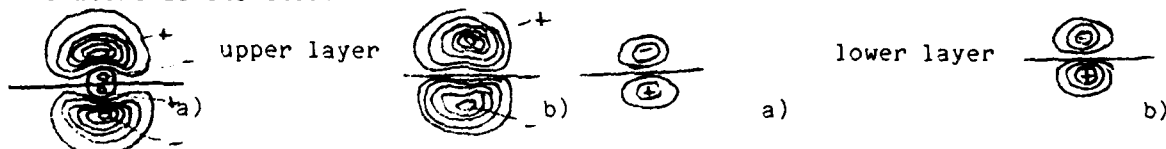
The solution is antisymmetric and propagates westward at C = 1.1. There is very little motion in the lower layer.

In the atmosphere $\delta \sim 1$ which changes the solutions considerably because we must use the first and third roots of (14) rather than the first and second.
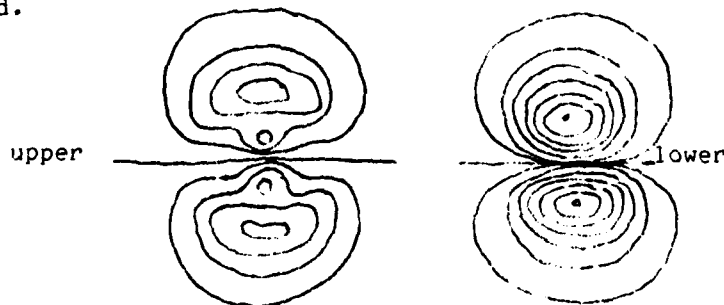
In both cases the solutions exist only for a limited range of wave velocity and scale. Riders can be added to these solutions also.

Vertical structure seems to be important. These solutions have similar patterns to observations, but lack close dynamical similarity. In all solutions vortex pairing is apparent. The vortices advect each other in such a way as to stay together and move with constant velocity.

This theory also suggests moving features should exist that have not been observed. Perhaps they have not been recognized in the data or else forcing and dissipation are important.

Forcing and Dissipation

An example of the effect of forcing and dissipation can be examined with the model equation.

$$J(\psi - \bar{u}y, \nabla^2 \psi + \beta y + b_0(y) + b_1(x,y)) = -\sigma \nabla^2 \psi \qquad (29)$$

The last term represents dissipation. The local topography and forcing is modeled by $b_1(x,y)$. Some terms arising from the mean shear have been modeled as topography $b_0(y)$ to make the problem more tractable.
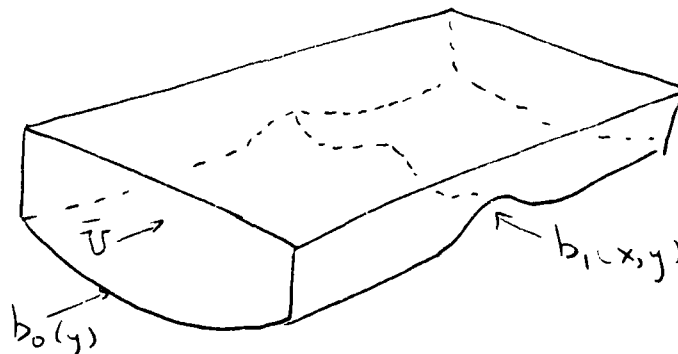
The length scale is assumed to be much longer than the width. Then the first order terms (e.g., Lecture 1) from the Eqn. (29) are

$$\mu^{(1)} F_x - D F_{xxx} + N F F_x = f'(x) - \nu F \qquad (30)$$

Here F(x) is the amplitude of the stream function as a function of the east-west direction. The x-variable topography leads to f(x) which is proportional to an integral of some function of y times b_1; D, N, ν are the coefficients of the dispersive, nonlinear and dissipative terms. The first order correction to the wave velocity is $\mu^{(1)}$. This equation with no forcing (f'(x) = 0) or dissipation ($\nu = 0$) has solitary wave solutions.

$$F = -\frac{3\mu^{(1)}}{N} \operatorname{sech}^2\left(\sqrt{\frac{\mu^{(1)}}{4D}}\, x\right) \qquad (31)$$

Periodic forcing by topography, but with no nonlinear term (N = 0) exhibits resonances:

$$f(x) = e^{ikx} \qquad F(x) = \frac{-1}{(\mu^{(1)}+k^2 D) + \frac{\nu}{ik}} e^{ikx} \qquad (32)$$

The nonlinear term (N = 0) adds the possibility of multiple states in a periodic system.

$$F(x) \cong A e^{ikx} + c.c. \qquad |A|^2 = \frac{-1}{\left(\mu^{(1)}+k^2 D - \frac{|A|^2}{N^{2/3}} \frac{1}{6k^2 D}\right)^2 + \frac{\nu^2}{k^2}}$$
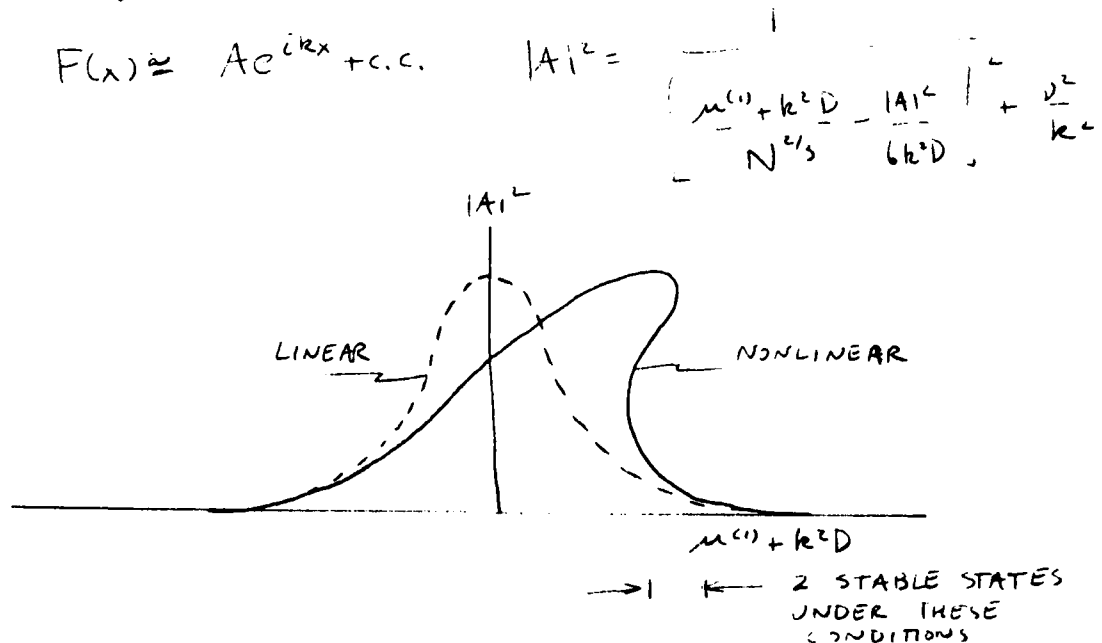
A stationary solution exists for tanh(x) topography. In this solution friction balances topography and nonlinearity balances dispersion:

$$F(x) = \frac{1}{\nu} \operatorname{sech}^2 x \;, \quad \mu^{(1)} = 4D \;, \quad f(x) = \tanh x \;, \quad \nu = -\frac{N}{12D} \qquad (33)$$

This special solution indicates that forced and dissipative systems can have solitary wave responses given the proper relationship between the topographic scale, amplitude and mean flow speed.

REFERENCES

Batchelor, G. K., 1967. An Introduction to Fluid Dynamics, Cambridge Univ. Press, London, 615 p.

Flierl, G. R., V. D. Larichev, S. C. McWilliams, and G. M. Reznik, 1980. The dynamics of baroclinic and barotropic solitary eddies. Dyn. Atmos. and Oceans, 4, in press.

Larichev, V. and G. Reznik, 1976a. Two dimensional Rossby soliton, an exact solution. Reports U.S.S.R. Acad. of Sci. 231(5). Also Polymode News, 19.

Larichev,V. and G. Reznik, 1976b. Strongly nonlinear two-dimensional isolated
    Rossby waves. Oceanologia, 16, 547-550.

McWilliams, J. C., G. R. Flierl, V. D. Larichev, and G. M. Reznik, 1980.
    Numerical studies of barotropic modons. Dyn. of Atmos. and Oceans.

Stern, M. E., 1975. Minimal properties of planetary eddies. Jour. Mar. Res.,
    33, 1-13.

NOTES SUBMITTED BY
SPAHR WEBB

GULF STREAM RING DYNAMICS

Glenn Flierl

LECTURE #3.

1. SOME OBSERVATIONS OF RINGS

Gulf Stream rings are formed when a meander of the stream pinches off into a ring.

A cold core ring "Bob" was formed in February-March 1979 and disappeared in November of the same year. It was observed to interact with the stream in April and May, spinning up and entraining cold water. Such interactions appear to be very common. After detaching again, it moved steadily southwest at about 5 1/2 cm/s from June through August. In September, it coalesced with the Stream through a process very much the reverse of its formation. The ring formed onto the Gulf Stream, opened up, and left the center of the ring again on the northside of the Stream.

Other rings have apparently been destroyed by mixing into the Stream after being sheared out in the Stream. Every r ng that has been observed has eventually reattached to the Gulf Stream, but some have had lifetimes as long as two years.

Warm rings break off to the north of the Stream and travel southwest, trapped between the Stream and the topography of the shelf. Cold rings form south of the Stream. They also travel roughly southwest but are not constrained by a coast as the warm rings are and can be found thousands of kilometers from the Stream.

The isotherms in a ring are displaced $\sim$ 300-400 meters from their depths in the surrounding environment. The maximum azimuthal velocities occur at radius 60-90 km from the center. The velocity profile is not well known, but velocities are largest above the thermocline reaching 150 cm/sec at the surface. It is not clear whether the velocity reverses with the depth. In a newly formed ring the isotherms all the way to the bottom show displacement. The velocity field is strong enough to transport material at least above the thermocline. The rings have anomalous T-S, $T-O_2$ and biological characteristics which can persist for well over a year. There is some indication of a jump in potential vorticity from outside the ring into the edge of the ring; i.e., potential vorticity is not a function of density alone.

The rings decay slowly. The isotherms fall (for a cold ring) about .8 m/day. Likely decay processes include friction, radiation due to dispersion; instabilities and meridional circulation probably caused by surface processes.

Gulf Stream rings are common. Nine or ten cold rings, three warm rings and one ring being formed were observed from March to July 1975 in a twenty-five by twenty degree area near the Gulf Stream. The rings covered 10-20% of the total area. Five cold rings and five warm rings may be formed each year.

Two rings may coalesce. Rings Al and Bob collided during which a single feature with two centers was observed. Later it split apart. At times, azimuthal waves can be seen and occasionally rings appear to split in two.

2. MODELING WITH SOLITARY WAVES

The Gulf Stream rings have been modeled as radially symmetric baroclinic solitary waves by Flierl (1979). The quasigeostrophic; β plane equations in continuously stratified fluid are the basis for these solutions. A mean horizontal shear flow or topography is necessary for the solutions to exist.

The stream function is governed by the conservation of quasigeostrophic potential vorticity

$$\partial_t P + J(\psi, P) = 0 \qquad P = \left(\nabla^2 + \frac{\partial}{\partial z}\frac{f_o^2}{N^2}\frac{\partial}{\partial z}\right)\psi + \beta y \tag{1}$$

The stream function is written as the sum of a part due to the mean velocity and a traveling wave

$$\psi = \Psi(y, z) + \varphi(x - ct, y, z) \tag{2}$$

The time derivative is replaced by $-c\frac{\partial}{\partial x}$ where c is the velocity of propagation.

$$J(\Psi + cy, P) = 0 \tag{3}$$

Therefore

$$\left(\nabla^2 + \frac{\partial}{\partial z}\frac{f_o^2}{N^2}\frac{\partial}{\partial z}\right)(\Psi + \varphi) + \beta y = Q(\Psi + \varphi + cy, z) \tag{4}$$

where $Q(\xi, z)$ is any function of ξ.

Far from an isolated solitary wave $\varphi \to 0$ and $Q(\xi, z)$ may be determined from the mean flow. Then:

$$\left(\nabla^2 + \frac{\partial}{\partial z}\frac{f_o^2}{N^2}\frac{\partial}{\partial z}\right)\varphi = Q(\Psi + \varphi + cy, z) - Q(\Psi + cy, z) \tag{5}$$

If the external shear flow $\bar{u}(y, z) = \alpha y$ then

$$Q(-\frac{\alpha}{2}y^2 + cy, z) = \beta y - \alpha \tag{6}$$

and therefore

$$Q(\xi, z) = -\alpha + \frac{\beta c}{\alpha}\left[1 - \sqrt{1 - \frac{2\alpha}{c}\xi}\right] \tag{7}$$

Plugging into Eqn. (5):

$$\left(\nabla^2 + \frac{\partial}{\partial t}\frac{f_0^2}{N^2}\frac{\partial}{\partial t}\right)\varphi = \frac{\beta c}{\alpha}\left\{\left(1-\frac{\alpha y}{c}\right) - \sqrt{\left(1-\frac{\alpha y}{c}\right)^2 - \frac{2\alpha\varphi}{c^2}}\right\} \tag{8}$$

The argument of the square root must be positive. This is assured by making the mean shear small enough and the possibility of a critical layer is excluded.

Under certain assumptions the right side of Eqn. (8) can be made nearly linear. Let ΔU be the change in the mean flow over the scale of an eddy, ℓ , U be the particle speed in the eddy and R the radius of deformation.

Require:

$$\frac{\Delta u}{c} \ll \frac{\Delta u}{c}\frac{u}{c} \sim \frac{R^2}{\ell^2} \ll 1 \tag{9}$$

then the righthand side can be Taylor expanded

$$\left(\nabla^2 + \frac{\partial}{\partial t}\frac{f_0^2}{N^2}\frac{\partial}{\partial t}\right)\varphi \simeq \frac{\beta\varphi}{c} + \frac{\beta\alpha}{2c^3}\varphi^2 \tag{10}$$

The scale is chosen so that $|\nabla^2\varphi| \ll \left|\frac{\partial}{\partial t}\frac{f_0^2}{N^2}\frac{\partial\varphi}{\partial t}\right|$. Then the lowest order balance is:

$$\frac{\partial}{\partial t}\frac{f_0^2}{N^2}\frac{\partial}{\partial t}\varphi^{(0)} = \frac{\beta}{c^{(0)}}\varphi^{(0)} \tag{11}$$

The stream function is approximated by

$$\varphi = \psi(x,y)\, F(t) + \varphi^{(1)} \quad ; \quad c^{(0)} = -\beta R^2$$

At next order, the governing equation for G is derived as a solvability condition:

$$\nabla^2 x + \frac{c + \beta R^2}{\beta R^4} \cdots + \frac{\alpha^2}{2\beta^2 R^3}\cdots^2 = 0 \quad ; \quad \varepsilon = \cdots \tag{12}$$

If G is only a function of x, a "ridge wave" soliton is a solution

$$\cdots = \cdots \tag{13}$$

This propagates at a velocity $c = -\beta R^2 (1 + 4\frac{R^2}{\ell^2})$ A second solution can be found which is radially symmetric. The solution is parabolic in the interior and decays as $e^{-r}/\sqrt{r}$ in the exterior (outside the closed streamlines).

Figure 2

This solution is intrinsically baroclinic and lies embedded in a barotropic mean flow. In these solutions dispersion is balanced by the steepening effects of the interaction with the mean shear.

Anticyclonic rings are observed only north of the Gulf Stream and cyclonic to the south. This model of the rings would require recirculating regions on either side of the Gulf Stream if the mean shear is to be the right sign to support the rings.

anticyclonic eddies

Gulf Stream

~ 1000 km

cyclonic eddies
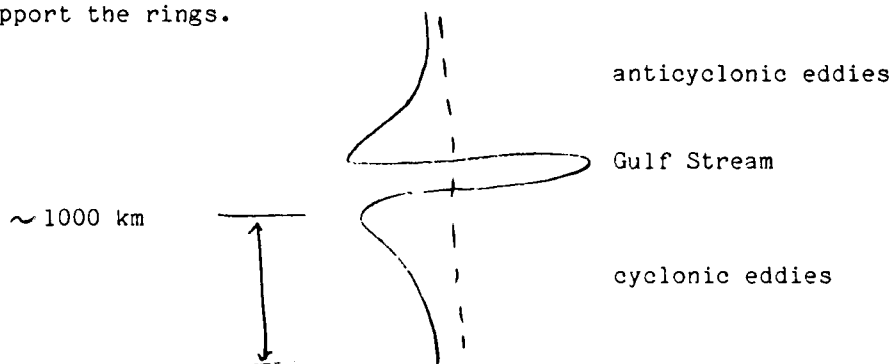
Figure 3

Circulation models suggest some regions of recirculations may exist. As an eddy moves the mean shear it experiences will change. The eddy therefore may always be adjusting towards a new equilibrium.

In the absence of shear these solutions do not exist. Other possible models for the rings were discussed in the preceding lecture. The "modon" solutions do not require a mean shear flow. The solutions with riders can be single centered in the baroclinic field and look like rings, but propagate eastward. These have developed in numerical initial value problems, but appear to be unstable.

3. DYNAMICS OF THE INTERMEDIATE SCALE

The quasigeostrophic equations have been applied to mesoscale motions in the ocean for many years. These equations can be derived for small Rossby number and a horizontal scale on the order of the deformation radius (50 km for the ocean). Charney and Flierl (1980) have recently shown that other terms begin to enter at larger scales (200 km) such that the dynamics permit solitary waves. In these waves, linear dispersion can be balanced by a non quasigeostrophic effect, vertical density advection. The scales at which this may occur can be found from the vorticity, (vertical component) and buoyancy equations

$$\zeta_t + \underline{v}\cdot\nabla\zeta + \beta\underline{v} - f_0\omega_z = -(\omega_x v_z - \omega_y u_z) + (\beta y + \zeta)\omega_z$$

$$b_t + \underline{v}\cdot\nabla b + \omega N^2 = -\omega b_z$$

where ∇ is the horizontal gradient, ζ the vorticity and b the buoyancy. The terms on the righthand sides are not included in quasigeostrophic

dynamics. For larger scale waves, the underlined terms are comparable, (non-dispersive long wave dynamics) leading to the following estimates for time and vertical velocity scales

$$t \sim L/\beta R^2 \qquad \text{and} \qquad w \sim \beta H V/f_0$$

where L is the horizontal scale, $R = NH/f_0$ the deformation radius scale and V the horizontal velocity scale. Thermal wind has been used. The vertical density advection will be comparable in effect to vorticity changes if

$$w b_z / w N^2 \sim \zeta_t / \beta v$$

implying $V/f_0 L \sim R^4/\ell^4$. For a given V, the vertical density advection becomes important for some scale larger than the deformation radius. Horizontal advection of vorticity enters at the same order as these terms if $\underline{v} \cdot \nabla \zeta \sim \zeta_t$, implying $V \sim \beta R^2$ which leads to

$$\ell \sim (f_0 R^2/\beta)^{1/3}$$

a scale of 200 km for the ocean. At this "intermediate" scale, the $\beta y \, w_t$ term is also comparable to $\zeta_t + v \cdot \nabla \zeta$.

We can demonstrate the existence of solitary wave solutions near the intermediate scale by describing the linear and nonlinear free oscillations of a single-layer, homogeneous, incompressible fluid with a free surface on the β-plane. The analog to vertical density advection is the $\eta(u_x + v_y)$ term in Eqn. (14c) below. In dimensional form, the shallow water equations are

$$\frac{Du}{Dt} - (f_0 + \beta y) v = -g \eta_x \tag{14a}$$

$$\frac{Dv}{Dt} + (f_0 + \beta y) u = -g \eta_y \tag{14b}$$

$$\frac{D\eta}{Dt} + (H + \eta)(u_x + v_y) = 0 \tag{14c}$$

$$\frac{D}{Dt} = \frac{\partial}{\partial t} + u \frac{\partial}{\partial x} + v \frac{\partial}{\partial y} \tag{14d}$$

where η is the surface displacement, H the mean depth and g the reduced gravity.

With the geostrophic scalings

$$u, v \sim u \qquad x, y \sim L \qquad \text{and} \qquad \eta \sim f_0 u L/g \quad t \sim L/\beta R^2$$

Eqn. (14a) and Eqn. (14d) become

$$\hat{\beta} \, \frac{Du}{Dt} - (1 + \hat{\beta} y) v = -\eta_x \tag{15a}$$

$$\hat{\beta} \, \frac{Dv}{Dt} + (1 + \hat{\beta} y) u = -\eta_y \tag{15b}$$

$$\hat{\beta} \frac{D\eta}{Dt} + \left(1 + \frac{\varepsilon}{\hat{s}} \eta\right)(u_x + v_y) = 0 \tag{15c}$$

$$\frac{D}{Dt} = \frac{\partial}{\partial t} + \frac{\varepsilon}{\hat{\beta}\hat{s}} \left(u \frac{\partial}{\partial x} + v \frac{\partial}{\partial y}\right) \tag{15d}$$

The three nondimensional numbers in Eqn. (15) are

$$\varepsilon = U/f_0 L \qquad , \qquad \hat{\beta} = \beta L/f_0 \qquad , \qquad \hat{s} = R^2/L^2 \tag{16}$$

It is useful to think of these parameters as the ratio of L to various natural length scales: the radius of an inertial circle U/f_0, the distane to the equator in the tangent plane approximation $L_\beta = f_0/\beta$ and the deformation radius $R = \sqrt{gH}/f_0$.

In Figure 4 the dependence of these three nondimensional numbers on L and U is shown.
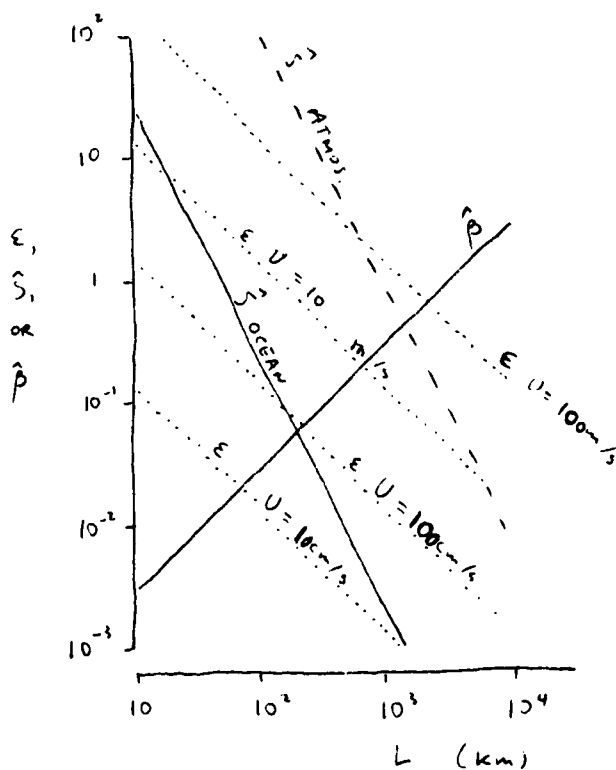
Figure 4:

The quasigeostrophic approximation is valid when $\hat{S} \sim 1$ and $\hat{\beta} \sim \epsilon \ll 1$. As L increases one moves into a parameter range where $\hat{\beta} \sim 1$ and $\hat{S}, \epsilon \ll 1$. In this range the term $\epsilon/\hat{S} \, \eta$ in Eqn. (15c) is not negligible and consequently the quasigeostrophic approximation is invalid. For the ocean this transition to nonquasigeostrophic dynamics occurs when $\hat{\beta} \sim \hat{S} \sim (\epsilon/\hat{S})$ which is at a relatively small scale (~ 200 km) because the deformation radius is so small compared to L_β.

To completely characterize the wavelike solutions admitted by Eqn. (15a-d) and further elucidate the role of the different nonlinearities, look for motions translating steadily with a speed c. In this case, there are two conserved quantities

1) The Bernoulli function:

$$\frac{1}{2}(u-c)^2 + \frac{1}{2} v^2 + g(H+\eta) + c\left(f_0 y + \frac{1}{2}\beta y^2\right)$$

2) The Potential vorticity

$$\left(v_x - u_y + f_0 + \beta y\right) / (H+\eta)$$

Since the mass conservation equation becomes

$$\left[(u-c)(H+\eta)\right]_{,x} + \left[v(H+\eta)\right]_{,y} = 0$$

it is possible to introduce a streamfunction

$$(u-c)(H+\eta) = -\frac{\partial \psi}{\partial y} = -\frac{\partial}{\partial y}(\psi + cH_y) \tag{17a}$$

$$v(H+\eta) = \frac{\partial \psi}{\partial x} = \frac{\partial}{\partial x}(\psi + cH_y) \tag{17b}$$

and write our conservation statements in the form

$$\frac{1}{2}\left[v^2(f+c\psi)\right]^2 + g(H+\eta)^3 + c(H+\eta)^2\left(f_0 y + \frac{1}{2}\beta y^2\right) \tag{18a}$$
$$= (H+\eta)^2 B(f+c\psi)$$

$$v \cdot (H+\eta)^{-1} v(f+c\psi) + f_0 + \beta y = (H+\eta) B'(f+c\psi) \tag{18b}$$

If the streamlines extend to ∞, B can be evaluated in the familiar fashion by requiring that the eddy be isolated. In this case,

$$B(\psi) = \frac{1}{2} c^2 + gH + \frac{f_0}{H} \psi + \frac{\beta}{H^2} \psi^2 \tag{19}$$

and Eqns. (18a, b) are the two equations for the two unknowns f and η. We shall assume Eqn. (19) is valid throughout the fluid even within closed streamlines. In nondimensional form these equations are

$$\tfrac{1}{2}\epsilon|\nabla\varphi|^2 + \hat\beta\hat s = f_y + \eta\left(1+\tfrac{\epsilon}{s}\varphi\right)^2 - \hat\beta^2\hat s\epsilon^2\left[1+\tfrac{\epsilon}{2s}\eta\right] + f\left(1+\hat\beta\right)y\left(1+\tfrac{\epsilon}{s}\eta\right)^2 \quad (20a)$$

$$+ \tfrac{\epsilon}{s}\,f_{ss}\left(1+\tfrac{\epsilon}{s}\eta\right)^2$$

$$\hat s\nabla^2 f\left(1+\tfrac{\epsilon}{s}\right) - \epsilon\nabla f\cdot\nabla_j - \hat\beta\hat s\epsilon\eta_j = \eta_j(1+\hat\beta)y\left(1+\tfrac{\epsilon}{s}\eta\right)^2 + \tfrac{\epsilon}{\epsilon}\left(1+\tfrac{\epsilon}{s}\eta\right)^3 \quad (20b)$$

Before discussing the nonlinear terms in Eqn. (20a,b) it is essential to determine the various linear balances. The linear case is recovered by setting $\epsilon = 0$ in Eqn. (20a,b). Then Eqn. (20a) can be solved for η in terms of φ; this relation is substituted into Eqn. (20b) to yield

$$\hat s\nabla^2 f - \tfrac{1}{\epsilon}f - (1+\hat\beta)y^2 f = \hat\beta^2\hat s^2\epsilon^{-1}f_{xx} \quad (21)$$

The righthand side of Eqn. (21) corresponds to gravity wave terms and is negligible on th scales we're considering. With this term absent there are four different types of behaviour:

1) Midlatitude Rossby Waves, $\hat\beta \ll 1$ $\hat s \sim 1$

$$\varphi = e^{ix}\cos y \qquad c = -(1+\epsilon\hat s)^{-1}$$

2) Intermediate Scale Waves, $\hat\beta \sim \hat s \ll 1$. The above dispersion relation is invalid, instead $c = -1+\hat s c^{(1)}$ where $c^{(1)}$ is the eigenvalue of

$$\nabla^2 f + c^{(1)}f - 2\hat\beta/\hat s\, y f = 0$$

3) The Sverdrup-Burger limit $\hat\beta \sim 1$ $\hat s \ll 1$. In this limit all the terms on the lefthand side of Eqn. (21) are equally important.

4) The equatorial limit $\hat\beta \gg 1, \hat s \ll 1$. In this limit $f = \hat\beta y$ and the NS structure functions are parabolic cylinder functions. These eigenfunctions confine the motion about the equator with a meridional scale of $\hat\beta^{-1/4}\hat s^{1/4}$ (corresponding to a dimensional scale $(L_\beta R)^{1/2}$).

As the amplitude of the motion increases (or equivalently ϵ increases) nonlinearity modifies the linear solutions described above. On the mid-latitude synoptic scale, $\hat s \sim 1$, the nonlinearity modifies the phase speed and shape but does not produce solitons. As the scale increases the dispersive effects become weaker until they can be balanced by nonlinearity to produce solitons. The structure of the isolated disturbances is the same as the sech[2] solutions of the KdV equation. The relationship of these solutions to the KdV equation will be clarified in the next section when we derive an equation governing the time evolution of arbitrary initial disturbances. For the moment return to Eqns. (20a,b) and observe that for nonlinearity to be important one of the ϵ terms must be balanced by a linear

term. For the oceanic intermediate scale this implies the scaling

$$\hat{\beta} = B\,\hat{S} \qquad \text{and} \qquad \varepsilon = E\,\hat{S}^2$$

where E and B are order unity. Then from Eqn. (20a)

$$\eta = \varphi + B\,\hat{S}\, _y\varphi + E\,\hat{S}\left(\frac{\varphi^2}{2c}\right) + O(\hat{S}^2)$$

so that Eqn. (20b) becomes

$$\hat{S}\,\nabla^2\varphi = \varphi\left(1+\frac{1}{c}\right) + 2B\,\hat{S}\,_y\varphi + 3\tfrac{1}{2}\,E\,\hat{S}\,\frac{\varphi^2}{c} + 2E\,\hat{S}\,\varphi^2$$

The order one terms in the above imply

$$c = -1 + \hat{S}\,c^{(1)}$$

and so

$$\nabla^2\varphi^{(0)} + c^{(1)}\varphi^{(0)} - 2B_y\,\varphi^{(0)} + \tfrac{3}{2}E\,\varphi^{(0)^2} = 0 \qquad (22)$$

Equation (22) can be simplified in two limits

1) $B \ll 1$, $E \sim 1$. In this case the coefficients of Eqn. (22) are independent of position coordinates and there is x-y symmetry. Various solutions such as cnoidal and solitary waves can be found. Perhaps the most interesting is the radially symmetric solitary wave found by Flierl:

φ = G (k $(x^2 + y^2)^{1/2}$)

c = -1 - S k^2

E = 1.59 k^2

The shape + dispersion relation are sketched in Figure 5.
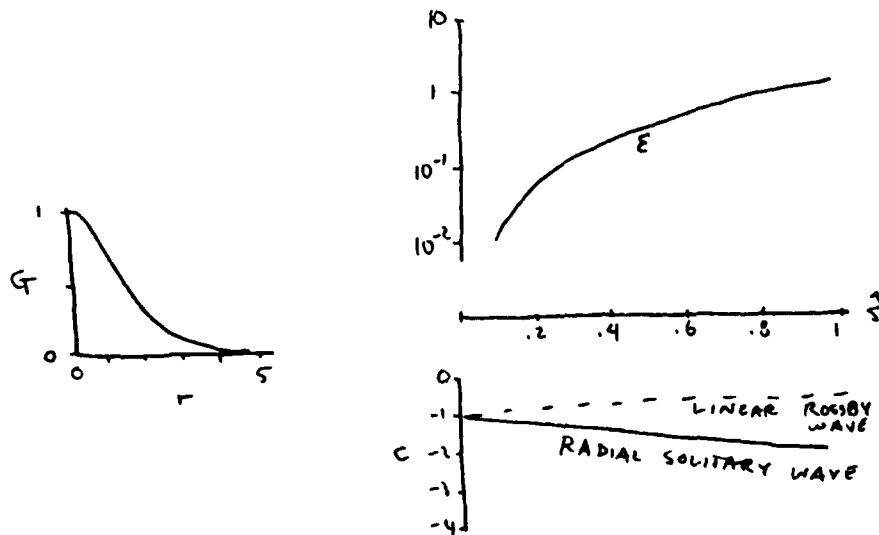
Figure 5

2) $\underline{B \gg 1 \quad E \sim 1}$. In this case y can be rescaled by $B^{-1/3}$ and the equation solved by expanding in powers of $B^{-2/3}$. At first order there is a linear equation for the y-structure. At next order x dispersion and nonlinear steepening balance and the x-structure has a sech^2 form.

When the fluid is continuously stratified, similar results can be obtained in density coordinates except that the quadratic factor in Eqn. (22) is multiplied by $\mathbf{\mathcal{E}}$.

4. INTERMEDIATE SCALES - KORTEWEG DE VRIES DYNAMICS

In the previous section, it was shown that the steadily translating, intermediate scale solutions have a sech^2 shape when $B \ll 1$ and $E \sim 1$. This is suggestive of Korteweg - de Vries dynamics. However, we must still determine the form of the time evolution equation for intermediate scale motions; for this, we return to the governing Eqns. (15a-d) and derive the time evolution equation in the limit $\mathbf{\mathcal{E}} = ES^2, \hat{\beta} = BS$ by expanding in powers of S. For the ocean, this parameter range corresponds to $(U,L) = (5 \text{ cm S}^{-1}, 200 \text{ km})$ and for the atmosphere $(U,L) = (20 \text{ ms}^{-1}, 1500 \text{ km})$.

The zero order equations

$$u^{(o)} = -\eta^{(o)}_y \tag{23a}$$

$$v^{(o)} = \eta^{(o)}_x \tag{23b}$$

$$u^{(o)}_x + v^{(o)}_y = 0 \tag{23c}$$

tell us the flow is geostrophic. At first order in S we have:

$$u^{(1)} + By\, u^{(o)} = -\eta^{(1)}_y \tag{24a}$$

$$v^{(1)} + By\, v^{(o)} = \eta^{(1)}_x \tag{24b}$$

$$B\eta^{(o)}_t + E\, \underline{v}^{(o)} \cdot \nabla \eta^{(o)} + E\eta^{(o)} \nabla \cdot \underline{v}^{(o)} + \nabla \cdot \underline{v}^{(1)} = 0 \tag{24c}$$

The above imply

$$\eta^{(o)}_t - \eta^{(o)}_x = 0$$
$$\eta^{(o)} = \eta(x+t, y, T) \tag{25}$$

T in Eqn. (25) is a slow time, $T = St$, which is required to remove secular effects at 0 $(\hat{S}^2)$. At second order in $\hat{S}$ the vorticity and density equations are

$$B \frac{D^{(o)}}{Dt} \zeta^{(o)} + \nabla \cdot \underline{v}^{(2)} + By\, \nabla \cdot v^{(1)} + B\, v^{(1)} = 0$$

and

$$B \frac{D^{(o)}}{Dt} \eta^{(1)} + B \frac{D^{(1)}}{Dt} \eta^{(o)} + \nabla \cdot \underline{v}^{(2)} + E\eta^{(o)} \nabla \cdot \underline{v}^{(1)} + E\eta^{(1)} \nabla \cdot \underline{v}^{(o)} = 0$$

Elimination of $\nabla \cdot \underline{\iota}^{(2)}$ between these equations leads to an evolution equation for $\eta^{(0)}$.

$$E \eta_T^{(0)} = E B \cdot \eta^{(0)} \eta_x^{(0)} + B \langle \nabla^2 \eta^{(0)} \rangle_x - 2 B^2 y \eta_x^{(0)} + E J \langle \eta^{(0)}, \nabla^2 \eta^{(0)} \rangle$$

When $B \ll 1$ and $E \sim 1$, and $\eta^{(0)} = \eta^{(0)}(x,T)$, surface height is indeed governed by the KdV equation. For B large and $E \sim 1$, the solution takes a model form in y with the x-structure governed by the KdV equation. However, for two dimensional disturbances, we must include vorticity advection as well as quadratic nonlinearity and the evolution may be much more complicated.

NOTES SUBMITTED BY
SPAHR WEBB AND WILLIAM YOUNG

MEAN FLOWS, EDDIES, AND LONG-LIVED VORTICES

Andrew Ingersoll

Lecture #1

A. Jupiter

i) Is a fluid planet composed mainly of Hydrogen and Helium (solar composition atmosphere), i.e.

H_2	0.886
He	0.112
H_2O	1.5×10^{-3}
CH_4	6.3×10^{-4}
NH_3	1.52×10^{-4}
H_2S	2.9×10^{-5}

ii) Has a radius ten times bigger than the earth's

iii) Bulk density 1.3 g/cm^3

iv) Period of rotation $9^h 55^m 29.7^s$ - measured by the rotation of the magnetic dipole (tilted 10°)

v) Interior adiabatic (or nearly so) due to the presence of convection (and internal cooling)

vi) Internal heat flux ~ 6 Wm^{-2}
Sun's input ~ 8 Wm^{-2}
Total output ~ 14 Wm^{-2} which is relatively uniform across latitude circles.

vii) How much latent heat? If all three gases condense
(H_2O, NH_3 and NH_4 SH of fractional abundance 10^{-3})
$\Delta T \approx 2^o$K, a significant amount

viii) Colors come from the compounds S_n, P_m, $C_k H_l$. In a hydrogen atmosphere, these elements tend to be present as (H_2S, PH_3, CH_4). Thus chemical equilibrium must be destroyed. This can occur by the presence of

a) lightning
b) charged particles
c) solar ultraviolet

Pictures of the dark side show the presence of (a) and the possibility of (b).

ix) Interior structure
There is a gradual transition from gas to liquid (at .97R) and a phase transition from molecular to metallic at r = 0.75R.

B. Heat Balance and Thermal Inputs

An observational fact which has to be explained is that there are no appreciable meridional currents on the surface of the planet. This should not be the case if we just take into account the solar heating which is much stronger on the equator than on the poles. There is no difference in temperature between the equator and the poles so there must be a distribution of internal heat which compensates for the sunlight.
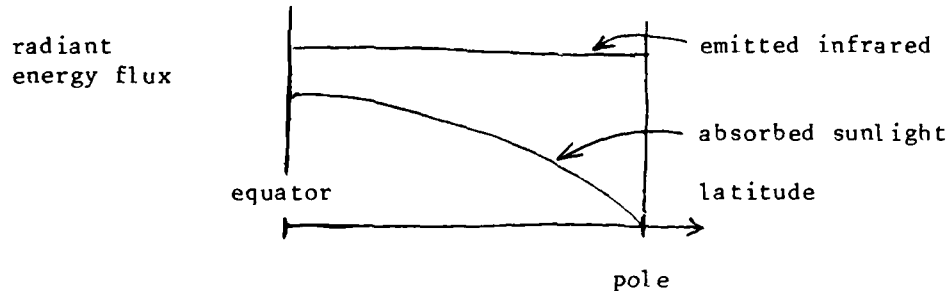
The model proposed to explain this is that the interior is a better heat conductor than the atmosphere so that the temperature is adjusted in the interior. The mechanism of heat transfer will be by convection. There can be poleward heat transfer in the interior so that the surface will be essentially isothermal.

A simple example of this effect is the following: consider a sphere of any good conductor rotating fast and the sunlight incident perpendicular to the axis of rotation
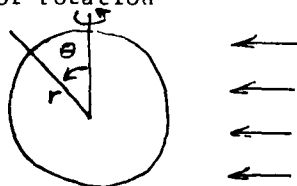
the equation for the interior is

$$\rho c \frac{\partial T}{\partial t} = k \nabla^2 T \qquad (1)$$

At the surface, the normal heat flux must be continuous

$$-k \frac{\partial T}{\partial r} = \sigma T^4 - \text{solar flux} \qquad (2)$$

The solar flux can be averaged over longitude if the sphere is rotating fast, in which case it is $(1-A) \frac{S}{\pi} \sin\theta$ S = solar constant
                                                        A = albedo

There are two time scales which characterize the problem: the internal time τ_i which is the time it takes to reach an internal equilibrium configuration and an external time τ_e which is the time it takes to reach equilibrium with the ambient medium.

From (1) $\tau_i = \frac{\rho c r^2}{k}$

$$\int (1) \, dVol = \frac{\rho c T r^3}{\tau_e} = r^2 \sigma T^4 \; ; \; \tau_e = \frac{\rho c r}{\sigma T^3}$$

The ratio of these two times $\epsilon = \tau_i / \tau_e$ is small for high conductivities. We want to consider what happens for times t, $\tau_i \ll t \ll \tau_e$. First for all, from the boundary condition we see that the ratio of temperature differences to mean temperature is also small $\Delta T/T = 1 \sigma T^3/k \approx \epsilon$. To order ϵ, the problem can be solved and the equilibrium isothermal pattern in the sphere is found to depend on the parameter

$$E = \left(\frac{\text{total emitted heat}}{\text{absorbed sunlight}} \right)$$

There are three different patterns of isotherms depending on the value of E:

a) For $E < 4/\pi = 1.27$ the heat flow at the surface is inwards which is contradictory with the assumption that there will be convection.
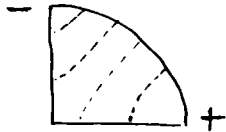
b) For $\frac{4}{\pi} < E < 1.3125$ the heat flow at the surface is outward near the surface but inside a ring of radius R it is directed inwards. Taking the radial variations of density into account raises the upper limit from 1.3125 to $\gtrsim 2.0$.
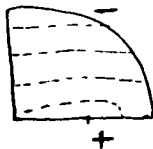
c) For $E > 1.3125$ heat is conducted outwards at all latitudes

It turns out that the behavior of the isotherm pattern with E in this example is very similar to the isotherm pattern found when considering a convecting interior for Jupiter. The radial and horizontal heat fluxes are computed using mixing length theory. Since the value of E for Jupiter probably falls in category (b), the horizontal heat transfer must be considered also in stably stratified regions where it will be possible due to baroclinic instabilities. The external equilibrium time τ_e can be estimated to be longer than the age of the solar system and the internal readjustment time τ_i is short compared to it. The model is consistent with 4.5×10^9 yrs for the age of Jupiter. The results of the calculation show the same qualitative behavior as that of the example. For small values of E the tendency of the sun to heat the equator is the dominant factor. As E is increased the isotherm pattern becomes spherically symmetric with heat flow always directed outwards. The estimated value of E for Jupiter gives a configuration in which there is a central stably stratified region where the vertical heat transfer will depend on the existence of horizontal gradients. The outer part of the planet will have a spherically symmetric (to order ϵ) pattern which would account for the temperature differences between the pole and the equator being unobservable.

RECENT NUMERICAL EXPERIMENTS ON LONG-LIVED VORTICES

Andrew Ingersoll

LECTURE #2
Jovian Spots

There are some qualitative features of the main coherent features observed which may be synthesized as follows:

i) the most coherent, compact and time independent features tend to be anticyclonic (for example red spot, white ovals)

ii) cyclonic "wakes" exist to the west of the spots. Here the flow varies rapidly. The typical form of the flow (in the southern hemisphere) is

SP = stagnation points
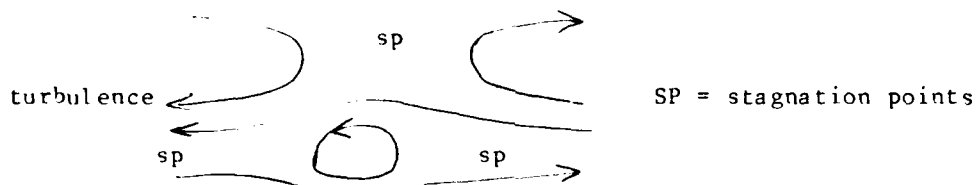
Size of the red spot is 10,000 x 25,000 km (NS diameter x EW diameter).

iii) ratio of relative vorticity is ζspot/ ζ shear $\approx$ 4, i.e., the spot is a large amplitude disturbance.

iv) large scale eddies do not occur on the equator. The most prominent are in mid latitudes (for example red spot is at 22°S, a white oval at 30°S), smaller scale features occur near the poles, having a more granular like appearance.

v) the structure of the flow near the stagnation points is not constant in time, for example it was seen to change from a $\quad$ to a $\quad$

vi) there is an exception to this pattern: a brown cyclonic spot in the northern hemisphere (which is a hole in the clouds). It has very large eccentricity. It oscillates in length and width roughly conserving area with a period of about 15 days.

vii) there is a region at 35°N where there are small spots which rotate very fast, sometimes colliding and merging, emitting a stream of fluid.

Some quantitative observations:

i) The spots have approximately elliptic form. The velocity of the flow tangent to the ellipses has no angular dependence. For the red spot

$\dot{\nu}'_{Tan}$

ellipse
2.2/1

$d(\text{semi-major axis})$

for a white oval

ellipse
1.6/1
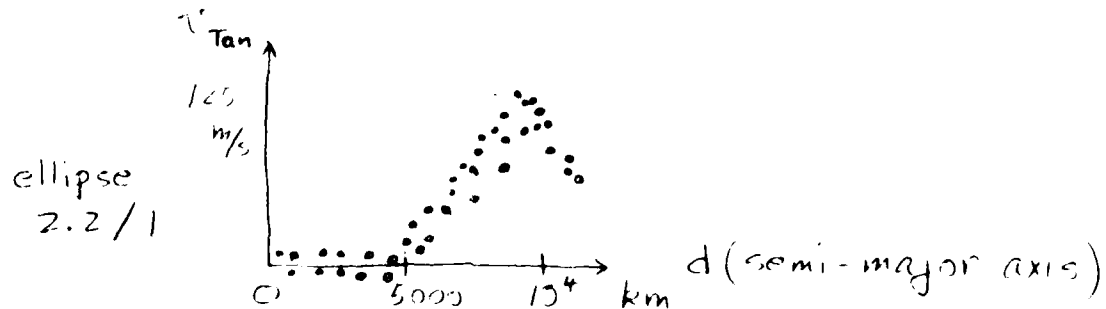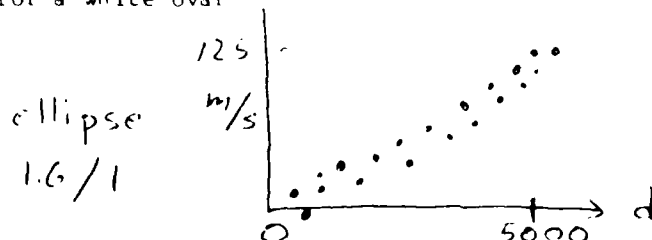
The contribution of these larger features to the correlation $\overline{u'v'}$ is too small to be resolved. The net tilt is at most 5, which would correspond to $(\overline{u'v'})^{1/2} \approx 5$ m/sec. Since $v_{tang} \approx 100$ m/sec it is beyond the resolution possible.

ii)

	latitude	Red Spot 22°S	White Oval 30°S
units $(10^{-5} s^{-1})$ {	ζ_{max}	6	6
	f	13	19
	$\beta y = \Delta f$ (NS diam)	6	2.6

ζ shear outside spots $1.5 \times 10^{-5} s^{-1}$

Red spot has a longitude oscillation of about $2°$.

Models for Steady Isolated Features

Three models are considered:

1) A two-dimensional quasigeostrophic, barotropic single layer of fluid.

2) A two-layer model. The lighter upper layer is the one of interest. Below there is a very deep layer with no mean flow. The mean flow $\bar{u}(y)$ of the upper layer is given.

3) Same as (2) but the lower layer has mean horizontal flow $\bar{u}(y)$, which is assumed to be a given function independent of time and of the motion of the upper layer. The upper and lower layer have the same mean flow $\bar{u}(y)$.

In these two last models the motion of the interface is negligible for the lower layer. When applying a two fluid model to Jupiter the upper layer can be taken to be about the depth of the clouds, the deep bottom layer would correspond to the adiabatic zone below the clouds.

First consider the field far away in a moving reference frame.

Model I: The equation for this model is $\dfrac{d}{dt}\left(\nabla^2 \psi + f\right) = 0$, $f = f_0 + \beta y$

The stream function $\psi = -\displaystyle\int \bar{u}\,dy + \phi(x - ct, y)$ and the linear equation for the field far away is

$$\nabla^2 \phi_x + \left(\frac{\beta - \bar{u}_{yy}}{\bar{u} - c}\right)\phi_x = 0$$

For a regular (non-singular) solution ϕ, the speed c is determined requiring that $\lambda^2 = (\beta - \bar{u}_{yy})/(\bar{u} - c)$ be an analytic function. It is measured that $\beta - \bar{u}_{yy} = 0$ at some latitudes. The value of $\bar{u}$ where this occurs is c. For $U = \cos y/L$, we get $\lambda^2 = 1/L^2 > 0$. $(\nabla^2 + \lambda^2)\phi_x = 0$ does not have exponentially decaying solutions in the plane. It is possible to get decay in one direction by confining in one direction. Let $\phi \sim e^{ik_y y}$, then

$$\frac{d^2\phi_x}{dx^2} + \left(\lambda^2 - k_y^2\right)\phi_x = 0$$

For k_y^2 large enough (in a narrow channel), there is exponential decay in x, and isolated, closed-streamline features can exist.

Two Layer Models

The usual two layer model equation can be written in the form

$$\left(\frac{\partial}{\partial t} + \frac{\partial \psi_n}{\partial x}\frac{\partial}{\partial y} - \frac{\partial \psi_n}{\partial y}\frac{\partial}{\partial x}\right)\left[\nabla^2 \psi_n \pm F_n(\psi_2 - \psi_1) + \beta y\right] = 0$$

for n = 1, 2, the upper and lower layers respectively. The (+) sign applies for n = 1, and the (-) sign for n = 2. The F_n are

$$F_n = f_0^2 L^2 \Big/ \left(g \frac{\Delta \rho}{\rho} H_n\right)$$

If the lower layer is much deeper than the upper layer, $F_2 \ll F_1$, so the vortex stretching in the lower layer is negligible compared to that of the upper layer. For this case the two layer equations become

$$\left(\frac{\partial}{\partial t} + \frac{\partial \psi_1}{\partial x}\frac{\partial}{\partial y} - \frac{\partial \psi_1}{\partial y}\frac{\partial}{\partial x}\right)\left[\nabla^2 \psi_1 + k_0^2(\psi_2 - \psi_1) + \beta y\right] = 0$$

where $k_0^2 = F_1$

$$\left(\frac{\partial}{\partial t} + \frac{\partial \psi_2}{\partial x}\frac{\partial}{\partial y} - \frac{\partial \psi_2}{\partial y}\frac{\partial}{\partial x}\right)\left[\nabla^2 \psi_2 + \beta y\right] = 0$$

<u>Model II</u>: $\Psi_2 = 0.$ The equation for the far field in a moving frame is

$$\nabla^2 \phi_x + \left(\frac{\beta - \bar{u}_{yy} + k_o^2 \bar{u}}{\bar{u} - c} \right) \phi_x - k_o^2 \phi_x = 0$$

Here too, C is determined requiring that $\lambda^2 = (\beta - \bar{u}_{yy} + k_o^2 \bar{u})/(\bar{u} - c)$ be analytic. For example, for $\bar{u} = \cos y/L$ we find $c = -\beta/(k_o^2 + L^{-2})$ and the equation for ϕ is

$$\nabla^2 \phi_x + \frac{1}{L^2} \phi_x = 0$$

which is the same as obtained in Model I and again there is no exponential decay in the plane. Isolated structures cannot exist except in a channel.

<u>Model III</u> $\quad \dfrac{d}{dt} \left(\nabla^2 \Psi_1 + f - k_o^2 \Psi_1 + k_o^2 \Psi_2 \right) = 0 \qquad\qquad (1)$

where $\Psi_2 = -\int \bar{u} dy$ is given.

Introducing $\Psi_1 = -\int \bar{u} dy + \phi$ (x-ct, y) the linear equation for ϕ is

$$\nabla^2 \phi_x - k_o^2 \phi_x + \left(\frac{\beta - \bar{u}_{yy}}{\bar{u} - c} \right) \phi_x = 0$$

Choosing for ex. $\bar{u} = \cos y/L$ we get

$$\nabla^2 \phi_x + \left(L^{-2} - k_o^2 \right) \phi_x = 0 \qquad$$ which has decaying solution in the

plane for $k_o^2 > L^{-2}$. In this case it is possible to obtain an isolated vortex.

The time dependent equation (1) was integrated then numerically. For the reference frame moving with speed C it is found that a stable isolated vortex is formed at latitudes in which $\beta - \bar{u}_{yy}$ is zero.
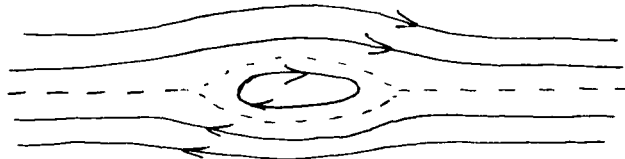
$$\bar{u}^* = \bar{u} - c$$

The structure is unstable if perturbed by a finite displacement in latitude. A tilt develops giving rise to a $\overline{u'v'}$ which destroys the eddy. The structure is stable to infinitesimal perturbations. This solution is not analytic, i.e., there is a discontinuity in the derivative of potential vorticity across the critical streamline.

INTERACTION BETWEEN LARGE-SCALE EDDIES AND MEAN FLOW

Andrew Ingersoll

LECTURE #3.

Interaction of Eddies and Zonal Flow

Eddies form perhaps by convection and are then ripped apart by shear. The zonal currents have been determined to be permanent features, only the clouds changing patterns. The currents also show north-south symmetry up to about 45° in latitudes. From maps of velocity vectors it is found that the correlation $\overline{u'v'}$ of deviations of zonal and meridional winds from their longitudinal mean is positively correlated with the meridional gradient $d\bar{u}/dy$ in such a manner that it implies a large rate of conversion from eddy kinetic energy to zonal mean kinetic energy.
$\{K'\bar{K}\} = \overline{u'v'}\,d\bar{u}/dy \cdot M$, the rate of conversion, is calculated to be 3 $W\,m^{-2}$, M the mass per unit area equivalent to a layer 2.5 bar thick. This is a large rate of energy transfer which is comparable to the total IR emission (14 $W m^{-2}$).

Conversion of eddy kinetic energy to mean kinetic energy divided by the total infrared radiation emitted by Jupiter is $3/14$ while the same ratio on earth is about $0.3/300$. A rough time scale is $\bar{K}$ over $\{K'K\}$ which is 50 earth days. Here we are taking $\bar{K} \approx \frac{1}{2}(50\ ms^{-1})^2$. If $\{K'K\}$ were the only term acting the mean kinetic energy and $\{K'K\}$ would have to oscillate with a period ≤ 50 days. Such oscillatory behavior is predicted in Williams' model (1979). The longitudinal gradient of vorticity, $\beta - \bar{u}_{yy}$ is negative at westward jets and positive at eastward jets, the observed limits are $-3\beta \leq \bar{u}_{yy} \leq 2\beta$. There have been different numerical experiments to see whether it is possible to obtain flows with such an extreme behavior for $\bar{u}_{yy}$.

For example, in two dimensional turbulence, given initially a state with an energy spectrum $\mathcal{E}(k)$, so that the total kinetic energy $= \int_0^\infty \mathcal{E}(k)dk$, the deviation σ_k from the average wave number $\langle k \rangle = \int k\mathcal{E}(k)dk / \int \mathcal{E}(k)dk$ is

$$\sigma_k^2 = \frac{\int (k - \langle k \rangle)^2 \mathcal{E}(k)dk}{\int \mathcal{E}(k)dk} = \langle k^2 \rangle - \langle k \rangle^2 = \frac{\int k^2 \mathcal{E}(k)dk}{\int \mathcal{E}(k)dk} - \langle k \rangle^2$$

If both energy $\int \mathcal{E}(k)dk$ and mean square vorticity $\int k^2 \mathcal{E}(k)dk$ are constant,

then $\qquad \frac{\partial}{\partial t}\sigma_k^2 > 0 \qquad$ implies $\qquad \frac{\partial}{\partial t}\langle k \rangle^2 < 0$.

This means that the energy is transferred to smaller values of k so the large sizes eddies end up carrying away most of the energy.

Now, if the β effect is included not only this phenomenon occurs but, due to the possibility of Rossby waves, the eddies may drift apart before interacting so the cascade of energy to low wave numbers stops in the horizontal direction. This leads to the formation of zonal flows. For wave numbers $k \leq k_\beta = (\beta/2u)^{1/2}$ this is a significant effect. The numerical results indicate that for such flows $-\beta \leq \bar{u}_{yy} \leq \beta$ which is not in very good agreement with the Jupiter observations.

The β plane models correspond to thin spherical shells. If we suppose that the currents may be circulating deep within the planet. A more appropriate model to consider is a rotating sphere of density ρ .
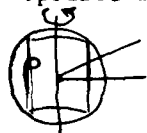
The linear equation for inertial oscillations is

$$\frac{\partial^2}{\partial t^2}\nabla^2 P + 4\Omega^2 \frac{\partial^2 P}{\partial z^2} = 0$$

, where P = pressure, the boundary condition being no normal velocity at the surface. If the modes considered correspond to oscillations of thin cylinders then the variation in Z is slow and we can approximate

$$P(r, \theta, Z) = P_1(r, \theta)Q(r,Z)$$

with Q a slowly varying function of Z and r.

$$\left| \frac{1}{P_1}\frac{\partial^2 P_1}{\partial r^2} \right| , \left| \frac{1}{P_1}\frac{1}{r^2}\frac{\partial^2 P_1}{\partial \theta^2} \right| \gg \frac{1}{r^2} \approx \left| \frac{1}{Q}\frac{\partial^2 Q}{\partial z^2} \right|$$

The result of the problem is that the surface flow is mainly horizontal and the speed is strongly dependent on latitude. The "effective β " is larger than β. Distance from the origin gives phase speed in units of βk^{-2}.

Rossby waves (spherical shell)
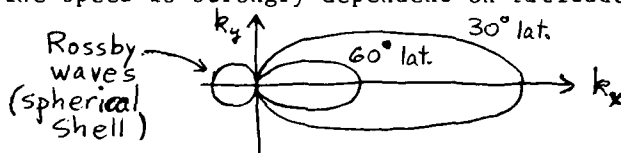
This can be compared with a Rossby wave which for the same value of Ω gives smaller speed and the flow in opposite direction independent of latitude.

For spherical shells we do not get $\bar{u}_{yy}$ large enough. In the sphere configuration, however, at some latitudes $\bar{u}_{yy}$ is as large as 3β . Of course the result is not correct at all latitudes. This indicates that it may be possible in some geometries to obtain values of $\bar{u}_{yy}$ more consistent with the observations.

REFERENCE

Williams, G. P., 1979. J. Atmospheric Sci., 36, 932.

LONG INTERNAL WAVES: GENERAL THEORY AND THE EFFECT OF DENSITY STRUCTURE AND VELOCITY SHEAR

L. G. Redekopp

LECTURE #1

1. INTRODUCTION

The theoretical development for the propagation of long, finite-amplitude internal waves can be clarified and motivated by considering the simple model of interfacial gravity waves in a stably stratified two-layer system. For this model the linear dispersion relation is given by
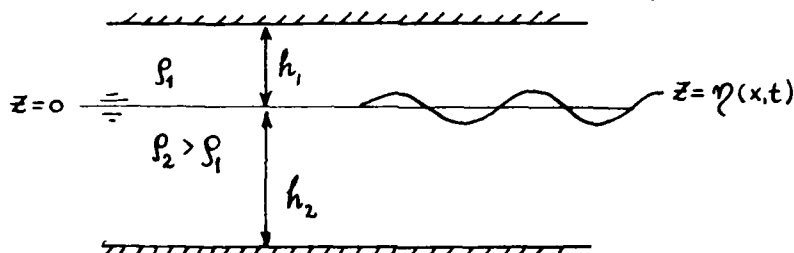
$$\omega^2 = \frac{g(\rho_2 - \rho_1) T_1 T_2}{\rho_2 T_1 + \rho_1 T_2} \quad, \quad T_i = \tanh(k h_i), \tag{1.1}$$

where (ω, k) are the frequency and wave number of an infinitesimal, sinusoidal disturbance of the interface. There are several long-wave limits for this system which imply different space/time scalings relevant to the weakly nonlinear theory.

(i) <u>The shallow-water limit</u>. In this case we consider the limit of long-wave ($k \rightarrow 0$) disturbances holding the wave guide length scale h = h_1 + h_2 fixed

$$\lim_{\substack{k \to 0 \\ h_1, h_2 \text{ fixed}}} \omega^2 = c_0^2 k^2 - 2 c_0 \gamma k^4 + \cdots , \tag{1.2}$$

$$c_0^2 = \frac{g(\rho_2 - \rho_1) h_1 h_2}{\rho_2 h_1 + \rho_1 h_2} \quad , \quad \gamma = \frac{1}{6} c_0 h_1 h_2 \frac{\rho_1 h_1 + \rho_2 h_2}{\rho_1 h_2 + \rho_2 h_1} \quad .$$

Then, considering only waves propagating in one direction (to the right, say) and truncating the expansion after the first dispersive term, we obtain

$$(\omega - c_0 k) = - \gamma k^3 . \tag{1.3}$$

This relation defines a unique scaling relationship between the slow space and time scales in a frame moving with the nondispersive motion

$$\xi = \mu (x - c_0 t) \quad , \quad \tau = \mu^3 t \quad , \quad \mu \ll 1 . \tag{1.4}$$

μ is the long-wave parameter measuring the ratio of the wave-guide scale to the wave length.

(ii) <u>The deep-water limit</u>. In this case we take the sequence of limits where first the depth of one of the layers (h_2, say) is allowed to increase indefinitely and then we take the long-wave limit ($k \to 0$) holding h_1 fixed.

$$\lim_{\substack{k \to 0 \\ h_1 \text{ fixed}}} \left\{ \lim_{\substack{h_2 \to \infty \\ k_1 h_1 \text{ fixed}}} \omega^2 \right\} = c_o^2 k^2 - 2\beta c_o k^3 \, \text{sgn} \, k + \cdots \tag{1.5}$$

$$c_o^2 = \frac{\rho_2 - \rho_1}{\rho_1} g h_1 \, , \qquad \beta = \frac{1}{2} \frac{\rho_2}{\rho_1} c_o h_1 \, .$$

The truncated dispersion relation for waves propagating in one direction is

$$\omega - c_o k = -\beta k |k| . \tag{1.6}$$

The space/time scaling for this limit has

$$\xi = \mu (x - c_o t) , \qquad \tau = \mu^2 t . \tag{1.7}$$

(iii) <u>The intermediate limit</u>. An intermediate case exists where the lower depth is much larger than the upper depth ($h_2 \gg h_1$), but not infinite (i.e., $kh_1 \ll 1$, $kh_2 = 0(1)$). The truncated dispersion relation for this case is

$$\omega - c_o k = -\frac{1}{2} \frac{\rho_2}{\rho_1} c_o h_1 k^2 \left[\coth (kh_2) - \frac{1}{kh_2} \right] . \tag{1.8}$$

Each of the limiting dispersion laws quoted here implies the existence of a linear evolution equation for the field variables like $\eta(x,t)$. The equation corresponding to an arbitrary dispersion relation $\omega(k) = kc(k)$ is given by (Whitham, 1974)

$$\eta_t + \int_{-\infty}^{\infty} K(x-z) \eta_z (z,t) \, dz = 0 , \tag{1.9}$$

where the kernal is the inverse Fourier transform of $c(k)$,

$$K(x) = \frac{1}{2\pi} \int_{-\infty}^{\infty} c(k) e^{ikx} dk . \tag{1.10}$$

For the respective cases we have the following equations:

(i) Shallow-water limit:

$$c = c_o - \gamma k^2 ,$$

$$K(x) = c_o \delta(x) + \gamma \delta''(x) , \tag{1.11}$$

$$\eta_t + c_o \eta_x + \gamma \eta_{xxx} = 0 .$$

(ii) Deep-water limit:

$$c = c_o - \beta |k| , \tag{1.12}$$

$$K(x) = c_o \delta(x) - \frac{\beta}{2\pi} \int_{-\infty}^{\infty} |k| e^{ikx} dk ,$$

$$\eta_t + c_o \eta_x - \beta \frac{\partial^2}{\partial x^2} H(\eta) = 0 ,$$

where $\mathcal{H}(\eta)$ denotes the Hilbert transform

$$\mathcal{H}(\eta) \equiv \frac{1}{\pi} \int_{-\infty}^{\infty} \frac{\eta(\bar{z},t)\, d\bar{z}}{x - \bar{z}} .$$

(iii) Intermediate limit:

$$C = C_0 - \frac{C_0}{2} \frac{\rho_2}{\rho_1} k h_1 \left[\coth(k h_2) - \frac{1}{k h_2} \right]$$

$$K(x) = C_0 \delta(x) - \frac{C_0}{4} \frac{\rho_2 h_1}{\rho_1 h_2} \frac{\partial}{\partial x} \left[\coth\left(\frac{\pi x}{2 h_2}\right) - \mathrm{sgn}\, x \right] . \tag{1.13}$$

Evaluating the first nonlinear correcton to these equations for long waves we obtain

$$\eta_t + C_0 \eta_x + \alpha \eta \eta_x + \int_{-\infty}^{\infty} \left[K(x-\bar{z}) - C_0 \delta(x-\bar{z}) \right] \eta_{\bar{z}}(\bar{z},t)\, d\bar{z} = 0. \tag{1.14}$$

This generalized KdV equation incorporates the leading effects of nonlinearity and dispersion on the evolution of long waves, where the adjective "long" has been made precise by the different limits applied to the linear dispersion relation (1.1). For the present model, the coefficient α is

$$\alpha = \frac{3}{2} \frac{C_0}{h_1 h_2} \frac{\rho_2 h_1^2 - \rho_1 h_2^2}{\rho_2 h_1 + \rho_1 h_2} , \tag{1.15}$$

and does not require a separate evaluation for the deep-water limit. Its form for the deep-water case is obtained from the above expression by allowing h_2 to be large compared to h_1; namely

$$\lim_{h_2 \to \infty} \alpha = - \frac{3}{2} \frac{C_0}{h_1} . \tag{1.16}$$

In some cases (e.g., when $\rho_1 h_2^2 \cong \rho_2 h_1^2$) $\alpha = 0$ and it is necessary to go to higher order in order to discuss the combined effects of nonlinearity and dispersion on the long-wave evolution. However, restricting the discussion to those situations with quadratic nonlinearity and defining the amplitude parameter $\epsilon = a/h$, where a is the wave amplitude, the space/time scales for which the nonlinear and dispersive effects balance are:

(i) shallow-water theory:

$$\xi = \epsilon^{1/2}(x - C_0 t) , \quad \tau = \epsilon^{3/2} t . \tag{1.17}$$

(ii) deep-water theory:

$$\xi = \epsilon (x - C_0 t) , \quad \tau = \epsilon^2 t . \tag{1.18}$$

This preliminary discussion is presented to demonstrate the role of the linear dispersion relation in selecting the appropriate space/time scales for the weakly nonlinear theory. The usefulness of this general approach will be emphasized again in Lecture #3.

2. THE EFFECT OF AMBIENT DENSITY STRUCTURE ON LONG WAVES IN A THERMOCLINIC WAVE GUIDE: DEEP WATER THEORY

Consider the 2-D equations of motion for a continuously stratified fluid

$$\nabla \cdot \vec{u} = 0,$$
$$\rho \frac{D\vec{u}}{Dt} = -\nabla p - \rho g \, \hat{e}_z,$$
$$\frac{D\rho}{Dt} = 0. \tag{2.1}$$

The total density ρ is represented as a background stable stratification plus a perturbation

$$\rho = \rho_s(z) + \tilde{\rho}(x,z,t). \tag{2.2}$$

We define a perturbation buoyancy σ and the Brunt-Väisälä frequency by

$$\sigma = \frac{g\tilde{\rho}}{\rho_s}, \qquad N^2 = -\frac{g}{\rho_s}\frac{d\rho_s}{dz}. \tag{2.3}$$

Let N_0 denote the maximum value of $N(z)$ and introduce the following scales to make the problem dimensionless.

Scale

x,z	with h
t	with N_0^{-1}
$\bar{u}$	with $N_0 h$
σ	with $N_0^2 h$
N(z)	with N_0

Introduce a streamfunction defined by

$$u = \psi_z, \qquad w = -\psi_x. \tag{2.5}$$

For convenience we invoke the Boussinesq approximation in which terms of order σ/g and ρ_s'/ρ_s are neglected. The governing equations in dimensionless form are then

$$\nabla^2 \psi_t + J(\nabla^2\psi, \psi) = \sigma_x,$$
$$\sigma_t + J(\sigma, \psi) + N^2(z)\,\psi_x = 0 \tag{2.6}$$

where $J(a,b)$ is the Jacobian operator.

The analysis which follows will address the specific thermocline model shown here.
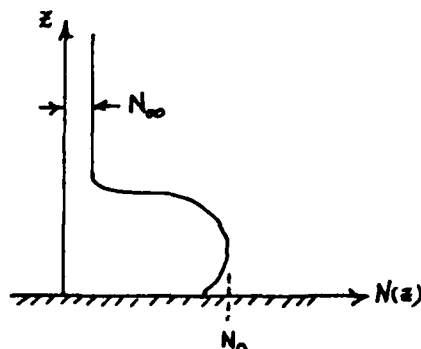
Later we will quote results when velocity shear is included and when the lower boundary is removed. The space/time scales for this "deep-water" case are those given in (1.18). Then the equations are

$$\left\{ \epsilon \partial_\tau - c_o \partial_\xi + (\psi_z \partial_\xi - \psi_\xi \partial_z) \right\} (\partial_{zz}^2 + \epsilon^2 \partial_{\xi\xi}^2) \psi = \sigma_\xi' ,$$

$$(2.7)$$

$$\left\{ \epsilon \partial_\tau - c_o \partial_\xi + (\psi_z \partial_\xi - \psi_\xi \partial_z) \right\} \sigma + N^2 \psi_\xi = 0,$$

and we seek solutions by the perturbation expansions

$$\psi(\xi, z, \tau) = \epsilon \psi^{(1)} + \epsilon^2 \psi^{(2)} + \cdots ,$$

$$\sigma(\xi, z, \tau) = \epsilon \sigma^{(1)} + \epsilon^2 \sigma^{(2)} + \cdots .$$

$$(2.8)$$

The leading order equations are

$$- c_o \psi_{\xi zz}^{(1)} = \sigma_\xi^{(1)} ,$$

$$- c_o \sigma_\xi^{(1)} + N^2 \psi_\xi^{(1)} = 0 ,$$

$$(2.9)$$

which can be combined to give

$$\frac{\partial}{\partial \xi} \left(\frac{\partial^2}{\partial z^2} + \frac{N^2}{c_o^2} \right) \psi^{(1)} = 0 .$$

$$(2.10)$$

Looking for a separable solution

$$\psi^{(1)} = A(\xi, \tau) \, \phi(z) ,$$

$$\sigma^{(1)} = A \frac{N^2}{c_o} \phi ,$$

$$(2.11)1$$

yields the problem

$$\phi'' + \frac{N^2}{c_o^2} \phi = 0 , \qquad \phi(o) = 0, \quad \phi(\infty) \to 0 .$$

$$(2.12)$$

When $N_\infty = O(1)$, long waves cannot be confined to the thermocline with vertical scale h and it is meaningless to talk about "long waves". When $N_\infty < O(\epsilon)$, the solution as $z \to \infty$ is $\phi \to \phi_\infty + \phi_\infty' z$ and we cannot satisfy the condition that the velocity perturbation decays as $z \to \infty$. The resolution of this difficulty requires an inner-outer matching since, in the deep fluid $O(z) \gg h$, h is no longer the vertical scale for the motion. Instead, the deep fluid is forced by the thermocline heaving which has the wavelength scale h/ϵ. We will account for this explicitly by defining the outer variables

$$\zeta = \epsilon z ,$$

$$\psi_{outer} = \tilde{\psi}(\xi, \zeta, \tau) ,$$

$$(2.13)$$

$$\sigma_{outer} = \tilde{\sigma}(\xi, \zeta, \tau) .$$

Before discussing the outer flow, however, we continue the inner problem to second order and get

$$\frac{\partial}{\partial \xi}\left(\frac{\partial^2}{\partial z^2} + \frac{N^2}{C_o^2}\right)\psi^{(2)} = -2\,\frac{N^2\phi}{C_o^3}\,A_\tau + ?\,\frac{(N^2)'\phi^2}{C_o^3}\,A\,A_\xi\;.$$

(2.14)

Multiplying by ϕ and integrating yields

$$\frac{\partial}{\partial \xi}\left(\phi\,\psi_z^{(2)} - \phi'\psi^{(2)}\right)\Big|_{z\to\infty} = -A_\tau\,\frac{2}{C_o^3}\int_0^\infty N^2\phi^2\,dz - A\,A_\xi\,\frac{2}{C_o^3}\int_0^\infty (N^2)'\phi^3\,dz,$$

(2.15)

after using the boundary conditions $\phi(0) = \psi_\xi^{(2)} = 0.$ The evaluation of the lefthand side can be made only after the outer flow solution has been obtained and the matching accomplished.

Introducing the outer flow variables (2.13) into the governing equations (2.6) yields

$$\left[\epsilon\partial_\tau - C_o\partial_\xi + \epsilon\,(\tilde\psi_\zeta\partial_\xi - \tilde\psi_\xi\partial_\zeta)\right]\tilde\nabla^2\tilde\psi = \frac{\tilde\sigma_\xi}{\epsilon^2}\;,$$

$$\left[\epsilon\partial_\tau - C_o\partial_\xi + \epsilon\,(\tilde\psi_\zeta\partial_\xi - \tilde\psi_\xi\partial_\zeta)\right]\tilde\sigma + N_\infty^2\,\tilde\psi_\xi = 0,$$

(2.16)

$$\tilde\nabla^2 \equiv \partial_{\xi\xi}^2 + \partial_{\zeta\zeta}^2\;.$$

Notice that the Laplacian ($\tilde\nabla^2\tilde\psi$) now appears in the vorticity equation so that decaying solutions are possible. The outer flow scaling requires $\tilde\psi = 0(\epsilon)$ to match the vertical velocity forced by thermocline motion. Then, we must require $\tilde\sigma \le O(\epsilon^2\tilde\psi)$ to avoid the result $\tilde\sigma_\xi = \tilde\psi_\xi = 0$ which implies either that the flow is blocked or that the scaling is wrong and the wave disperses throughout the entire fluid column. This forces a restriction on the magnitude of N_∞ $\left[N_\infty^2 \le O(\epsilon^2)\right]$ in order for long waves to remain ducted along the thermocline. In dimensional form, this ducting condition is

$$\frac{N_\infty}{N_o} \lesssim O\left(\frac{a}{h}\right).$$

(2.17)

Ducting of a linear wave with wave number k requires that $\omega(k) > N_\infty$ so that the motion is evanescent in the outer region. However, this is clearly impossible for $N_\infty \ne 0$ because $\omega \to o$ as $k \to 0$. Ducting of long-wave modes is possible with $N_\infty \ne 0$ only on a nonlinear basis whereby the linear frequency correction is sufficiently large to give $\omega > N_\infty$.
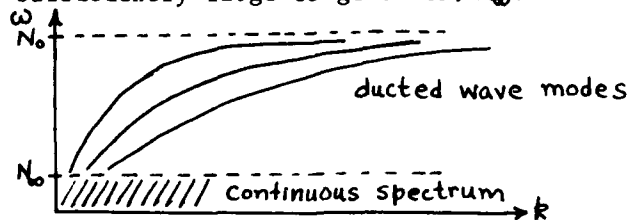
Assuming that $N_\infty = \epsilon\Omega$, $\Omega = 0(1)$, the outer flow expansion has the form

$$\tilde\psi(\xi,\zeta,\tau) = \epsilon\,\tilde\psi^{(1)} + \epsilon^2\,\tilde\psi^{(2)} + \cdots,$$

$$\tilde\sigma(\xi,\zeta,\tau) = \epsilon^3\,\tilde\sigma^{(1)} + \epsilon^4\,\tilde\sigma^{(2)} + \cdots.$$

(2.18)

The leading order equations valid in the outer region are

$$-C_0 \widetilde{\nabla}^2 \widetilde{\psi}^{(1)}_\xi = \widetilde{\sigma}^{(1)}_\xi ,$$

$$-C_0 \widetilde{\sigma}^{(1)}_\xi + \Omega^2 \widetilde{\psi}^{(1)}_\xi = 0,$$

(2.19)

which can be combined to give

$$\frac{\partial}{\partial \xi} \left[\widetilde{\nabla}^2 + \frac{\Omega^2}{C_0^2} \right] \widetilde{\psi}^{(1)} = 0$$

or, after one integration,

$$\widetilde{\nabla}^2 \widetilde{\psi}^{(1)} + \alpha^2 \widetilde{\psi}^{(1)} = 0 , \qquad \alpha^2 = \frac{\Omega^2}{C_0^2} .$$

(2.20)

If the stratification in the outer region is weaker, the outer flow is potential and one recovers the situation analyzed independently by Benjamin (1967) and Davis and Acrivos (1967). The boundary conditions for (2.20) are

(i) $\quad \widetilde{\psi}^{(1)}(\zeta \to 0) = a(\xi, \tau)$

(ii) the radiation condition as $\xi^2 + \zeta^2 \to \infty$

The relation of $a(\xi, \tau)$ to the wave amplitude $A(\xi, \tau)$ will be found by matching. The problem defined by (2.20) is analogous to the classical lee-wave problem except that here the shape of the "mountain" is unknown and time-dependent.

The solution of (2.20) is readily obtained by Fourier transforms:

$$\widehat{\psi}^{(1)}(k, \zeta, \tau) = \int_{-\infty}^{\infty} \widetilde{\psi}^{(1)} e^{-ik\xi} d\xi,$$

$$\frac{d^2 \widehat{\psi}^{(1)}}{d\zeta^2} + (\alpha^2 - k^2) \widehat{\psi}^{(1)} = 0,$$

(2.21)

$$\widehat{\psi}^{(1)}(\zeta \to 0) = \widehat{a}(k, \tau) = \int_{-\infty}^{\infty} a(\xi, \tau) e^{-ik\xi} d\xi.$$

The solution satisfying the radiation condition is

$$\widehat{\psi}^{(1)}(k, \zeta, \tau) = \begin{cases} \widehat{a}(k, \tau) e^{-\zeta\sqrt{k^2 - \alpha^2}} , & |k| > \alpha \\[2mm] \widehat{a}(k, \tau) e^{-i\zeta\sqrt{\alpha^2 - k^2}} , & 0 < k < \alpha \\[2mm] \widehat{a}(k, \tau) e^{i\zeta\sqrt{\alpha^2 - k^2}} , & -\alpha < k < 0 . \end{cases}$$

(2.22)

The choice of branch for $|k| < \alpha$ can be understood by recalling the propagation of linear internal waves in an environment with N = const. (i.e., $\omega = N \cos\Theta$ where Θ is the angle the wave vector makes with

respect to the horizontal).
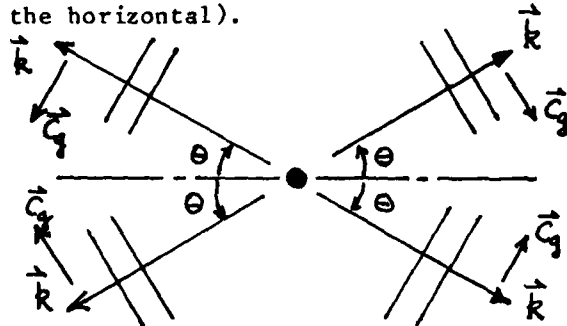
In the present situation, if we consider the ducted wave mode travelling to the right with speed c (or, in a frame stationary with respect to the wave, a mean flow with speed c from the right), we must choose that branch circled in the diagram above and having phase fronts with a positive slope. The phase for

Energy
Flux vector
relative to stationary "mountain"
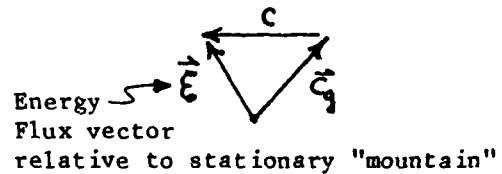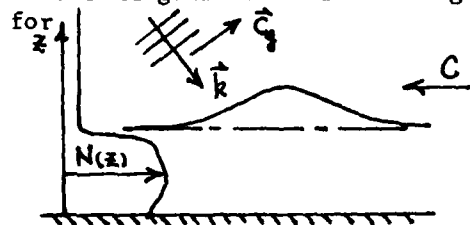
in the solution (2.22) is

$$\tilde{\Theta} = k\xi \pm \zeta \sqrt{\alpha^2 k^2},$$
(2.23)

and we have chosen that branch to which the lines of constant phase have a positive slope

$$\frac{d\zeta}{d\xi}\Bigg|_{\tilde{\Theta}=const.} = -\frac{\partial\tilde{\Theta}/\partial\xi}{\partial\tilde{\Theta}/\partial\zeta} = -\frac{k}{\left(\pm\sqrt{\alpha^2 k^2}\right)} > 0,$$
(2.24)

Hence, we must choose the ($\mp$) sign in (2.23) when $k \gtrless 0$.

In order to carry out the matching with the inner solution we need the behavior of $\tilde{\psi}^{(1)}$ as $\zeta \to 0$. This is obtained by expanding (2.22) for small ζ and taking the inverse transform:

$$\lim_{\zeta\to 0} \tilde{\psi}^{(1)} = \int_{-\infty}^{\infty} a(\xi',\tau)\, d\xi' \left\{ \delta(\xi-\xi') - \frac{\zeta}{\pi}\left[\int_{\alpha}^{\infty}\sqrt{k^2-\alpha^2}\, \cos k(\xi-\xi')dk \right.\right.$$

$$\left.\left. - \int_{0}^{\alpha}\sqrt{\alpha^2-k^2}\, \sin k(\xi-\xi')dk\right] - \frac{\zeta^2}{2}\left[\delta''(\xi-\xi') + \alpha^2\delta(\xi-\xi')\right] + O(\zeta^3) \right\}.$$
(2.25)

We make the approximation, purely for analytical convenience,

$$\int_{\alpha}^{\infty}\sqrt{k^2-\alpha^2}\, \cos k(\xi-\xi')dk \cong \int_{0}^{\infty} k\cos k(\xi-\xi')dk,$$
(2.26)

which is only valid as $\alpha \to 0$. What is really involved in this approximation is neglecting the effect of the ambient environment (N_∞) on the first dispersive correction for the ducted wave modes. However, we do retain the radiation damping effect contained in the integral $[0, \alpha]$.

Then, we can write

$$\lim_{\zeta \to 0} \tilde{\psi}^{(1)} = a(\xi, \tau) - \zeta \, D(\xi, \tau) - \frac{\zeta^2}{2} \left(a_{\xi\xi} + \alpha^2 a \right) + O(\zeta^3), \qquad (2.27)$$

where

$$D(\xi, \tau) \equiv \frac{\partial}{\partial \xi} \mathcal{H}(a) - \frac{\alpha}{2} \int_{-\infty}^{\infty} a(\xi', \tau) \frac{H_1(\alpha |\xi - \xi'|)}{\xi - \xi'} \, d\xi',$$

and $\mathcal{H}(a)$ is the Hilbert transform and H_1 is the Struve function of order one. The leading order matching gives

$$\lim_{z \to \infty} \psi_{inner} = \epsilon \, A(\xi, \tau) \left\{ \phi_\infty + \phi_\infty' \, z \right\} + O(\epsilon^2),$$

$$\lim_{\zeta \to 0} \psi_{outer} = \epsilon \, a(\xi, \tau) - \epsilon^2 z \, D(\xi, \tau) + O(\epsilon^3), \qquad (2.28)$$

so that $\phi_\infty' = 0$, $\phi_\infty = 1$ and $a(\xi, \tau) = A(\xi, \tau)$. Matching the velocity gives

$$\lim_{z \to \infty} \frac{\partial \psi_{inner}}{\partial z} = \epsilon^2 \left. \frac{\partial \psi^{(2)}}{\partial z} \right|_{z \to \infty} + O(\epsilon^3), \qquad (2.29)$$

$$\lim_{\zeta \to 0} \frac{\partial \psi_{outer}}{\partial z} = -\epsilon^2 D(\xi, \tau) + O(\epsilon^3),$$

so that $\left. \frac{\partial \psi^{(2)}}{\partial z} \right|_{z \to \infty} = -D(\xi, \tau)$. With these results the lefthand side of (2.15) is known yielding the evolution equation for the ducted long-wave modes

$$A_\tau + \gamma A A_\xi - \beta \frac{\partial^2}{\partial \xi^2} \mathcal{H}(A) = -\beta \int_{-\infty}^{\infty} A(\xi', \tau) \, d\xi' \left[\frac{1}{\pi} \int_0^\alpha k \sqrt{\alpha^2 - k^2} \, \cos k(\xi - \xi') \, dk \right]$$

where

$$\gamma = - \frac{\int_0^\infty (N^2)' \phi^3 \, dz}{\int_0^\infty N^2 \phi^2 \, dz} \quad , \qquad \beta = \frac{1}{\int_0^\infty N^2 \phi^2 \, dz} \quad . \qquad (2.30)$$

At this point we will just note that, if there were another region of deep fluid below the thermoclinic wave guide, an additional dispersive and damping term would appear in the evolution equation characterizing the effect of the additional ambient region on the confined wave modes.

Considering a wave packet solution, (2.30) has the following properties.

(i) $$\frac{\partial}{\partial \tau} \int_{-\infty}^{\infty} A(\xi, \tau) \, d\xi \equiv \frac{\partial}{\partial \tau} \langle A \rangle = 0. \qquad (2.31)$$

This implies a relation between the amplitude and length of the packet as the wave "volume" is conserved (essentially a conservation of mass).

(ii)
$$\frac{\partial}{\partial \tau} \langle A^2 \rangle = - \frac{\beta}{\pi} \int_0^\alpha k\sqrt{\alpha^2 - k^2} \; |F(k,\tau)|^2 dk ,$$
(2.32)

where
$$F(k,\tau) = \int_{-\infty}^\infty A(\xi,\tau) \, e^{-ik\xi} d\xi .$$

This relation gives the energy decay of the wave packet via excitation and radiation of internal waves in the deep fluid surrounding the thermocline wave guide.

The same results are obtained for a periodic wave train solution if we integrate over a wave length instead of the unbounded domain.

At this point we return to the proto-type model discussed at the beginning of the lecture (except we now allow the lower layer to be weakly stratified) and seek an estimate for the lifetime of a coherent long-wave structure propagating along the density interface. In dimensional form, equation (2.30) is
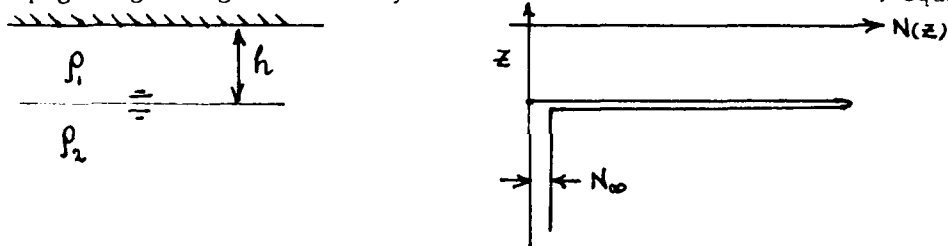
$$\eta_t + c_0 \eta_x - \frac{3}{2} \frac{c_0}{h} \eta \eta_x - \frac{1}{2} \frac{\rho_2}{\rho_1} c_0 h \frac{\partial^2}{\partial x^2} \mathcal{H}(\eta) = -\frac{1}{2} \frac{\rho_2}{\rho_1} c_0 h \int_{-\infty}^\infty \eta(x',t) dx' \left[\frac{1}{\pi} \int_0^\alpha k\sqrt{\alpha^2 - k^2} \cos k(x-x') dk \right]$$
(2.33)

$$c_0^2 = \frac{\rho_2 - \rho_1}{\rho_1} gh , \qquad \alpha = \frac{N_\infty}{c_0}$$

We assume that the term on the right is small and that the long-wave structure is a solitary wave solution of the equation with the LHS = 0

$$\eta(x,t) = - \frac{a_0 \lambda^2}{(x-ct)^2 + \lambda^2} , \qquad a_0 \lambda = \frac{4}{3} \frac{\rho_2}{\rho_1} h^2 , \qquad \frac{c - c_0}{c_0} = \frac{3}{8} \frac{a_0}{h} .$$
(2.34)

The integral relations (Eqn. 2.31, 2.32) give

$$\langle \eta \rangle = \pi a_0 \lambda = \text{constant} ,$$
(2.35)

$$\langle \eta^2 \rangle = \frac{\pi a_0}{2} (a_0 \lambda) ,$$

$$F(k,\tau) = \pi a_0 \lambda \, e^{-\lambda |k|} .$$

We assume that the solitary wave structure is maintained even when the damping term on the right is included, but that the solitary wave parameters are slowly varying in time ($a_o = a_o(t)$, $\lambda = \lambda(t)$). In this adiabatic approximation the decay is given by

$$\frac{da_o}{dt} = 2 c_o h \,(a_o \lambda)\, \alpha^3 \, I(p),$$

$$I(p) = \frac{d}{dp} \int_0^1 \sqrt{1-t^2}\; e^{-pt}\, dt\,, \qquad p = 2\alpha\lambda. \tag{2.36}$$

Two limiting cases can be identified

(i) For $p \to 0$ (steep wave), $\quad I(p) = -\frac{1}{3} - \frac{\pi}{16}\, p\, + O(p^2).$
In this case the decay is linear in time.

(ii) For $p \to \infty$ (shallow wave), $I(p) \sim -\frac{1}{p^2}$ and the decay varies inversely with time. There is a threshold amplitude below which the wave can no longer remain ducted, but disperses throughout the deep fluid.
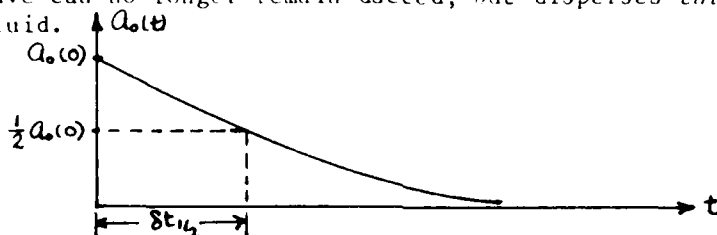
Defining a "half-life" as indicated in the sketch and using $\delta x_{1/2} = c_o\, \delta t_{1/2}$, one obtains

$$\frac{\delta x_{1/2}}{\lambda(0)} = \frac{3}{4}\, \frac{c_o/h}{N_\infty} \left[\frac{h/\lambda(0)}{N_\infty h/c_o} \right]^2. \tag{2.37}$$

The quantity in square brackets must be $\gtrsim 0(1)$ for ducting and the other factor ($\frac{c_o/h}{N_\infty}$) is essentially (N_0/N_∞). Hence, unless $N_\infty \ll N_0$, the wave will decay after propagating several initial wave lengths. This is probably why long-wave packets of internal waves are not observed in the deep ocean with nearly the frequency with which they are observed on the continental shelf.

The adiabatic theory presented here has been tested by numerical solution of Eqn. (2.30) for solitary wave initial conditions (Pereira and Redekopp, 1980). The adiabatic approximation slightly overestimates the decay, but gives a quantitatively useful result. The important point to make, however, is that we have here an example of a coherent structure which radiates and that the life-time of the structure depends crucially on its "radiation efficiency".

3. THE EFFECT OF VELOCITY SHEAR

A similar analysis can be carried out when velocity shear is included (Maslowe and Redekopp, 1980). Our purpose here is to provide an analytical example of the existence of solitary eddies in a shear flow which are

describable in terms of a nonlinear evolution equation which implies that these eddies exhibit special interaction properties. The discussion here will also set the stage for our next lecture.

Suppose we write the total streamfunction and perturbation buoyancy as

$$\Psi = \int_{z_c}^{z} U(z')dz' + \in A(\xi,\tau)\,\phi(z) + \epsilon^2 \psi^{(2)} + \cdots , \tag{3.1}$$

$$\sigma = - \in A \frac{\phi}{U-c_o} + \epsilon^2 \sigma^{(2)} + \cdots ,$$

and substitute into Eqn. (2.6). Then, for Couette flow with constant Brunt-Väisälä frequency, the linear eigenvalue
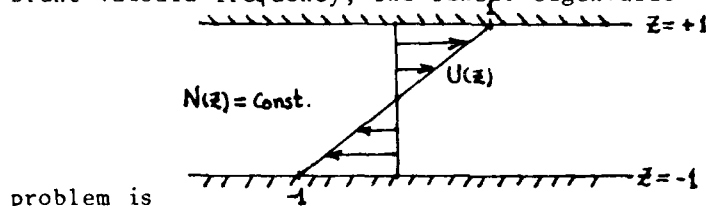
problem is

$$\phi'' + \frac{J}{(z-z_c)^2}\,\phi = 0 , \qquad \phi(\pm 1) = 0 , \tag{3.2}$$

$$J = \left[\frac{N(z)}{U'(z)}\right]^2 = \text{constant}$$

We consider only the case where the Richardson number $J > \frac{1}{4}$ so the flow is stable on a linear basis. The eigenvalue problem then has the solution

$$\phi = |z - z_c|^{1/2} \cos\left(\mu \ln|z-z_c| - \Delta\right), \tag{3.3}$$

$$\mu = \sqrt{J - \tfrac{1}{4}} ,$$

where z_c is the eigenvalue (the phase speed measured relative to the linear velocity profile with unit slope). There are two classes of solutions.

(i) Internal wave modes $|z_c| > 1$,

$$z_c = \pm \coth\left(\frac{n\pi}{2\mu}\right) , \qquad n = 1, 2, \ldots ; \tag{3.4}$$

(ii) Singular neutral modes $|z_c| < 1$

$$z_c = \pm \tanh\left(\frac{n\pi}{2\mu}\right) , \qquad n = 0, 1, 2, \ldots . \tag{3.5}$$

Miles proved that there were <u>no</u> singular neutral modes for $J > \frac{1}{4}$ based on a <u>viscous</u> critical layer theory. Here, we have implicitly invoked the result of <u>nonlinear</u> critical layer theory by which we make the interpretation that the quantity $(Z - Z_c)^{1/2 \pm i\mu}$ becomes simply $|Z - Z_c|^{1/2 \pm i\mu}$ when $Z < Z_c$. In the next lecture, we will give a detailed description of nonlinear critical layer theory in the context of Rossby waves in a shear flow.

We conclude our discussion by noting that, after adopting the KdV (shallow-water) scaling and computing the $\psi^{(2)}$, $\sigma^{(2)}$ terms in (3.1), one

obtains the KdV equation

$$A_t + \gamma A A_\xi + \beta A_{\xi\xi\xi} = 0 \qquad (3.6)$$

for either of the modes (3.4) or (3.5). For the singular neutral modes we have

$$\beta = -\frac{2 z_c (1 - z_c^2)}{4J + 3},$$

$$\gamma = \frac{\mu}{J+2} \frac{(1 - z_c)^{3/2} - (-1)^n (1 + z_c)^{3/2}}{(1 - z_c^2)^{1/2}}. \qquad (3.7)$$

These modes will always have closed streamline regions whose shape can be determined by a detailed analysis of the critical layer region.

REFERENCES

Benjamin, T. B., 1967. Internal waves of permanent form in fluids of great depth. J. Fluid Mech., 29, 559-592.

Davis, R. E. and A. Acrivos, 1967. Solitary internal waves in deep water. J. Fluid Mech., 29, 593-607.

Pereira, N. R. and L. G. Redekopp, 1980. Radiation damping of long, finite amplitude internal waves. Phys. of Fluids (to appear, vol. 23, Nov. 1980).

Maslowe, S. A. and L. G. Redekopp, 1980. Long nonlinear waves in stratified shear flows. J. Fluid Mech. 101, 321-348.

Whitham, G. B., 1974. Linear and nonlinear waves. John Wiley & Sons, Inc., N. Y., p. 368.

Notes Submitted by
Richard Gregory-Allen

SOLITARY ROSSBY WAVES WITH CRITICAL LAYERS

L. G. Redekopp

LECTURE #2

1. INTRODUCTION

We consider in this lecture a zonal shear flow $U(y)$ which goes to constant values U_{min} and U_{max} as $y \to -\infty$ and $y \to +\infty$ respectively, and we study the question: Can a solitary wave evolve and exist with a propagation velocity c between U_{min} and U_{max}? There will then be a critical value of y for which $U(y) = c$. This level $y = y_c$ and a band in y around it, the so-called critical layer, will be seen to deserve special attention.

Let the total streamfunction Ψ in a frame moving with speed c be

$$\Psi = \int_{y_c}^{y} dy' \left(U(y') - c \right) + \epsilon \psi \tag{1.1}$$

where ψ is a perturbation. If we furthermore adopt the KdV type scaling from Lecture #1:

$$x \to \epsilon^{1/2} x \, , \qquad t \to \epsilon^{3/2} t, \tag{1.2}$$

the model equation for ψ that we consider becomes

$$\left\{ \epsilon \partial_t + (U-c)\partial_x + \epsilon(\psi_y \partial_x - \psi_x \partial_y) \right\} \left[\partial_{yy}^2 - k^2 + \epsilon \partial_{xx}^2 \right] \psi$$
$$+ (\beta - U'') \psi_x = \frac{\nu}{\epsilon^{1/2}} \psi_{yyyy} . \tag{1.3}$$

In Sec. 2 we consider perturbation expansions for ψ in the region away from the critical layer and derive the matching problem that the critical layer gives rise to. In Sec. 3 we consider the critical layer region and solve the matching problem. In Sec. 4 the time evolution of the vorticity in the critical layer is discussed.

2. THE OUTER REGION

We first look at the region away from the critical layer and consider a straightforward expansion of the perturbation stream function in powers of ϵ

$$\psi = \psi^{(1)} + \epsilon \psi^{(2)} + \cdots . \tag{2.1}$$

Since the perturbation, $\epsilon \psi$, is itself $O(\epsilon)$ the first term has superscript (1). We substitute Eqn. (2.1) into Eqn. (1.3) and collect terms $O(\epsilon^0)$. Since we are assuming that we are away from the critical layer, $|U-c| \gg \epsilon$, we can divide through by U-c to obtain an equation

$$\mathcal{L} \psi^{(1)} = 0, \tag{2.2}$$

where $\mathcal{L}$ is the linear operator

$$\mathcal{L} \equiv \frac{\partial}{\partial x} \left(\frac{\partial^2}{\partial y^2} - k^2 + B(y) \right), \tag{2.3}$$

with

$$B(y) \equiv \frac{\beta - U''}{U - c} . \tag{2.4}$$

We look for separable solutions to this equation

$$\psi^{(1)} = A(x,t) \, \phi(y), \tag{2.5}$$

where ϕ then must satisfy the eigenvalue problem

$$\phi'' - k^2 \phi + B \phi = 0 \tag{2.6}$$

with bounday conditions

$$\phi(y_s) = \phi(y_n) = 0 \tag{2.7}$$

at stations far below and far above the critical layer, $y_s \ll y_c \ll y_n$.
We note that for Eqn. (2.6) one can identify at least three possibilities:

(i) $U(y) \neq c$ for all y, i.e., there is no critical layer at all, $B(y)$ is regular and the equation for ϕ has no singularities. This case leads to what we shall call propagating neutral modes (PNM), Rossby waves modified by the shear.

(ii) $U(y_c) = c$ but $\beta - U''(y_c)$ vanishes. In this case $B(y)$ can have a series expansion about y_c
$B(y) = B_c + B_c (y-y_c) + \dots$
Then ϕ will also be regular
$\phi(y) = \phi_c + \phi'_c (y-y_c) + \dots$
and the solutions will be called regular neutral modes (RNM).

We shall consistently use the notation $U(y_c) = U_c$, $U'(y_c) = U'_c$, $U''(y_c) = U''_c$, etc.

Finally we have

(iii) $U(y_c) = c$ but $B(y) = \dfrac{B_{-1}}{y-y_c} + B_0 + B_1 (y-y_c) + \dots$
is singular at the critical layer. From Eqn. (2.4)
$B_{-1} = (\beta - U''_c)/U'_c$
$B_0 = -(2U'_c U'''_c + (\beta - U''_c)U''_c)/2(U'_c)^2$
and so on.

According to the theory of Eqn. (2.6) there will be two linearly independent solutions $\phi_a(y)$ and $\phi_b(y)$. These will be given by Frobenius series. The regular solution is

$$\phi_a(y) = \sum_{n=0}^{\infty} a_n (y-y_c)^n \tag{2.8a}$$

and the singular solution is

$$\phi_b(y) = \sum_{n=0}^{\infty} b_n (y-y_c)^n + b_{00} \phi_a(y) \ln|y-y_c| . \tag{2.8b}$$

The coefficients a_0, a_1,...b_0, b_1... and b_{00} are determined by substitution of (2.8) into (2.6) using the expansion given for $B(y)$. By straightforward calculation we find

$$B_{-1} a_0 = 0, \tag{2.9a}$$

$$2a_2 - k^2 a_0 + a_1 B_{-1} + a_0 B_0 = 0 , \tag{2.9b}$$

$$6a_3 - k^2 a_1 + a_2 B_{-1} + a_1 B_0 + a_0 B_1 = 0, \tag{2.9c}$$

and so on. Hence $a_0 = 0$, we fix $a_1 = 1$ and then

$$a_2 = -\tfrac{1}{2} B_{-1} = -\frac{\beta - U''_c}{2U'_c} , \tag{2.10a}$$

$$a_3 = \frac{1}{6}\left(k^2 - B_0 + \frac{1}{2}B_{-1}^2\right) = \frac{k^2}{6} + \frac{U_c''}{6U_c'} + \frac{\beta(\beta - U_c'')}{12(U_c')^2} ,$$

(2.10b)

and so on. Similarly we find

$$b_{\infty} a_1 + B_{-1} b_0 = 0 ,$$

(2.11a)

$$2b_2 + 3b_{\infty} a_2 - k^2 b_0 + B_{-1} b_1 + B_0 b_0 = 0 .$$

(2.11b)

We normalize ϕ_b by demanding that $b_0 = 1$ and we fix $b_1 = 0$ to assure that no multiple of ϕ_a is added to the regular part of ϕ_b. We then obtain

$$b_{\infty} = -B_{-1} = 2a_2 = -\frac{\beta - U_c''}{U_c'} ,$$

(2.12a)

$$b_2 = \frac{1}{2}\left(k^2 - B_0 - 6a_2^2\right) = \frac{k^2}{2} + \frac{U_c'''}{2U_c'} + \frac{(\beta - U_c'')(4U_c'' - 3\beta)}{4(U_c')^2} .$$

(2.12b)

For this case we can only assume the ansatz (2.5) to be valid for $y > y_c$ and we must have a similar outer solution for $y < y_c$. We write these

$$\psi_+^{(1)} = A(x,t)\left\{ \alpha_+ \phi_a(y) + \phi_b(y) \right\} , \qquad y > y_c ,$$

$$\psi_-^{(1)} = D(x,t)\left\{ \alpha_- \phi_a(y) + \phi_b(y) \right\} , \qquad y > y_c .$$

(2.13)

The problem posed is solved by examination of the critical layer region to determine a matching between A, D, α_+ and α_-.

Before considering this matching problem, let us go back to Eqn. (1.3) and extract the $0(\epsilon)$ terms.

We get

$$(U-c)\mathcal{L}\psi^{(2)} = -\frac{\partial}{\partial t}\left(\frac{\partial^2}{\partial y^2} - k^2\right)\psi^{(1)} - (U-c)\frac{\partial^3 \psi^{(1)}}{\partial x^3} - \left(\psi_y^{(1)}\partial_x - \psi_x^{(1)}\partial_y\right)\left(\frac{\partial^2}{\partial y^2} - k^2\right)\psi^{(1)} .$$

(2.14)

Using Eqn. (2.6) in the form

$$\left(\frac{\partial^2}{\partial y^2} - k^2\right)\psi^{(1)} = -B\psi^{(1)} ,$$

(2.15)

we get

$$\mathcal{L}\psi^{(2)} = \frac{B}{U-c}\frac{\partial \psi^{(1)}}{\partial t} - \frac{\partial^3 \psi^{(1)}}{\partial x^3} - \frac{B'}{U-c}\psi^{(1)}\psi_x^{(1)}$$

(2.16)

$$= \frac{B\phi}{U-c}\frac{\partial A}{\partial t} - \phi\frac{\partial^3 A}{\partial x^3} - \frac{B'\phi^2}{U-c}A\frac{\partial A}{\partial x} .$$

Note that the first and third terms here are singular even for RNM (they are strongly singular for SNM). To derive an equation of motion for A we want to consider

$$\int dy \, \phi \mathcal{L} \psi^{(2)}.$$

For both RNM and SNM we exclude from the integral an interval of size δ (to be determined) about y_c. For SNM we furthermore must change A to D for $y < y_c$. Now for any limits a, b

$$\int_a^b dy \, \phi \frac{\partial^2 \psi^{(2)}}{\partial y^2} = \left[\phi \frac{\partial \psi^{(2)}}{\partial y} - \psi^{(2)} \phi' \right]_a^b + \int_a^b dy \, \psi^{(2)} \phi''; \tag{2.17}$$

hence,

$$\int_a^b dy \, \phi \mathcal{L} \psi^{(2)} = \frac{\partial}{\partial x} \left\{ \left[\phi \frac{\partial \psi^{(2)}}{\partial y} - \psi^{(2)} \phi' \right]_a^b + \int_a^b dy \, \psi^{(2)} \left(\phi'' - k^2 \phi + B\phi \right) \right\}, \tag{2.18}$$

where the second integrand vanishes identically by Eqn. (2.6). Using this relation with $b = y_n$, $a = y_c + \delta$ and then with $b = y_c - \delta$, $a = y_s$ and finally adding the second result to the first we get

$$\fint_{y_s}^{y_n} dy \, \phi \mathcal{L} \psi^{(2)} = \frac{\partial}{\partial x} \left[\phi' \psi^{(2)} - \phi \frac{\partial \psi^{(2)}}{\partial y} \right]_{y_c - \delta}^{y_c + \delta} = \frac{\partial A}{\partial t} \fint_{y_s}^{y_n} \frac{B \phi^2 dy}{U - c} - A \frac{\partial A}{\partial x} \fint_{y_s}^{y_n} \frac{B' \phi^3 dy}{U - c} - \frac{\partial^3 A}{\partial x^3} \fint_{y_s}^{y_n} \phi^2 dy, \tag{2.19a}$$

where

$$\fint_{y_s}^{y_n} = \int_{y_s}^{y_c - \delta} + \int_{y_c + \delta}^{y_n}, \tag{2.19b}$$

and we have used the boundary conditions (Eqn. 2.7) and

$$\psi_x^{(2)}(y_s) = \psi_x^{(2)}(y_n) = 0. \tag{2.20}$$

For PNM the jump is zero and to this order in ϵ we obtain the KdV equation for A. For RNM ϕ is continuous and $\psi^{(2)}$ is continuous and the unknown jump term in Eqn. (2.19a) is

$$-\phi_c \frac{\partial}{\partial x} \left[\!\!\left[\frac{\partial \psi^{(2)}}{\partial y} \right]\!\!\right].$$

For this case, and for SNM where the corresponding term is

$$\frac{\partial}{\partial x} \left[\!\!\left[\phi' \psi^{(2)} - \phi \frac{\partial \psi^{(2)}}{\partial y} \right]\!\!\right],$$

an examination of the critical layer equation is necessary before the evolution equation for A can be determined.

Let us write $\psi^{(2)}$ as

$$\psi^{(2)} = \tfrac{1}{2} A^2 \phi_{nl}^{(2)} + A_{xx} \phi_{disp}^{(2)} + \left(\int_0^x dx' \cdot \frac{\partial A}{\partial t} \right) \phi_0^{(2)} \tag{2.21}$$

where $\phi_{nl}^{(2)}$, $\phi_{disp}^{(2)}$ and $\phi_0^{(2)}$, depend only on y. Then

$$\mathcal{L} \psi^{(2)} = A A_x \left(\frac{d^2}{dy^2} - k^2 + B \right) \phi_{nl}^{(2)} + A_{xxx} \left(\frac{d^2}{dy^2} - k^2 + B \right) \phi_{disp}^{(2)}$$
$$+ A_t \left(\frac{d^2}{dy^2} - k^2 + B \right) \phi_0^{(2)}, \tag{2.22}$$

and, from Eqn. (2.16), the most singular part is $\phi_{nl}^{(2)}$. We write a Frobenius expansion for $\phi_{nl}^{(2)}$:

$$\phi_{nl}^{(2)} = \frac{r_{-1}}{y - y_c} + \sum_{n=0}^{\infty} r_n (y - y_c)^n + \ln|y - y_c| \sum_{n=0}^{\infty} q_n (y - y_c)^n$$
$$+ \ln^2|y - y_c| \sum_{n=0}^{\infty} p_n (y - y_c)^n. \tag{2.23}$$

Then from

$$\left(\frac{d^2}{dy^2} - k^2 + B \right) \phi_{nl}^{(2)} = - \frac{B'}{U - c} \left(\alpha \tfrac{b}{a} + \phi_b \right)^2 \tag{2.24}$$

we can obtain all the coefficients r_n, q_n, p_n in terms of a_n, b_n and α ($= \alpha_\pm$ according as $y \gtrless y_c$). We shall not write out all the necessary equations but only extract r_{-1}. On the lefthand side of Eqn. (2.24) the only term to vary as $(y - y_c)^{-3}$ is $2 r_{-1} (y - y_c)^{-3}$. On the right the only such term is $(B_{-1}/ U_c)(y - y_c)^{-3}$.

Hence

$$r_{-1} = \frac{B_{-1}}{2 U_c'} = - \frac{b_{00}}{2 U_c'} . \tag{2.25}$$

Now we go to the critical layer region.

3. CRITICAL LAYER EQUATION

We write the total streamfunction in the critical layer as

$$\psi = \int_{y_c}^{y} dy' \left(U(y) - c \right) + \epsilon \phi(x, Y, t, T) \tag{3.1}$$

where:

(i) $Y = (y-y_c)/\delta$ we want $Y = O(1)$ in the critical layer region and so δ is a gauge function to be determined

(ii) $T = t/\mu$ (with μ so far undetermined) is a second time scale. We shall find that the critical layer is quasisteady on time scale t. To follow the time evolution of the vorticity in the critical layer we must go back and introduce T with the appropriate choice for μ.

The coefficient of Φ is ϵ in order to match to the dominant term outer flow as $y \rightarrow y_c$. Putting Ψ, Eqn. (3.1), into the basic Eqn. (1.3) we obtain the expansion

$$\left\{ \frac{\epsilon}{\mu\delta}\frac{\partial}{\partial T} + \frac{\epsilon}{\delta}\frac{\partial}{\partial t} + U_c'Y\left(1 + \frac{U_c''}{2U_c'}\delta Y + \ldots\right)\frac{\partial}{\partial x} + \frac{\epsilon}{\delta^2}\left(\Phi_Y\partial_x - \Phi_x\partial_Y\right)\right\} \cdot$$

$$\left[\frac{\partial^2}{\partial Y^2} - \delta^2 k^2 + \epsilon\delta^2\frac{\partial^2}{\partial x^2}\right]\Phi + \delta\left[\beta - U_c'' - U_c'''\delta Y - \ldots\right]\Phi_x = \frac{\nu}{\epsilon^{1/2}\delta^3}\frac{\partial^4\Phi}{\partial Y^4} . \tag{3.2}$$

The equation is written with the term $U_c'Y$ being $O(1)$ since it is the basic term giving rise to the singular behavior in the outer expansion. We now consider possible balances in Eqn. (3.2).

(i) Viscous balance: In this case $\dfrac{\nu}{\epsilon^{1/2}\delta^3} = O(1)$, $\delta = \left(\nu/\epsilon^{1/2}\right)^{1/3}$ and $\epsilon/\delta^2 \ll 1$. The $\epsilon^{1/2}$ term appears in the expression for δ because the wave number is $O(\epsilon^{1/2})$ for the long-wave motion considered here. This limit and those that follow are best characterized by the parameter λ (sometimes referred to as the Benney-Haberman parameter)

$$\lambda = \left[\frac{\left(\nu/\epsilon^{1/2}\right)^{1/3}}{\epsilon^{1/2}}\right]^3 .$$

The viscous balance occurs for $\lambda \gg 1$.

(ii) Nonlinear balance: In this case $\epsilon/\delta^2 = O(1)$ or $\delta = \epsilon^{1/2}$. Also we require $\lambda \ll 1$ so that the viscous terms are weak.

(iii) Hybrid case: A third possibility is $\lambda = O(1)$ so that both nonlinearity and viscosity are important to leading order in the critical layer.

We shall focus exclusively on case (ii) in this lecture. For earlier work dealing with this limit of the critical layer theory the reader should consult Benney and Bergeron (1969) and Haberman (1972).

Consider for SNM the outer solution (Sec. 2) ψ_+ as $y \to y_c^+$. From Eqn. (2.13) and Eqn. (2.23) the leading terms are

$$\psi_+ = A \left\{ 1 + \frac{b_{oo} Y}{2} \epsilon^{1/2} \ln \epsilon + \epsilon^{1/2} \left[\alpha_+ Y + b_{oo} Y \ln |Y| + \frac{r_1 A}{2Y} \right] + \cdots \right\} \tag{3.3}$$

To match this we consider an inner expansion of ϕ of the form

$$\phi = \phi^{(o)} + \epsilon^{1/2} \ln \epsilon \, \phi_1^{(1/2)} + \epsilon^{1/2} \phi^{(1/2)} + \cdots \ . \tag{3.4}$$

Substituting this into Eqn. (3.2) with the assumed scaling, viz.

$$\left\{ \frac{\epsilon^{1/2}}{\mu} \frac{\partial}{\partial T} + \epsilon^{1/2} \frac{\partial}{\partial t} + U_c' Y \left[1 + \frac{U_c''}{2U_c'} \epsilon^{1/2} Y + \cdots \right] \frac{\partial}{\partial x} + (\phi_Y \partial_x - \phi_x \partial_Y) \right\} \cdot \tag{3.5}$$

$$\left[\frac{\partial^2}{\partial Y^2} - \epsilon \zeta^2 + \epsilon^2 \frac{\partial^2}{\partial x^2} \right] \phi + \epsilon^{1/2} \left[\beta - U_c'' - U_c''' \epsilon^{1/2} Y - \cdots \right] \phi_x = \lambda \, \phi_{YYYY} \ ,$$

where $\lambda = \nu / \epsilon^{1/2} \delta^3 = \nu / \epsilon^2 \ll 1$, we get

$$O(\epsilon^o): \quad \mathcal{L}_c \frac{\partial^2 \phi^{(o)}}{\partial Y^2} \equiv \left\{ U_c' Y \frac{\partial}{\partial x} + \phi_Y^{(o)} \frac{\partial}{\partial x} - \phi_x^{(o)} \frac{\partial}{\partial Y} \right\} \frac{\partial^2 \phi^{(o)}}{\partial Y^2} = 0 .$$

A solution that matches uniformly is $\phi^{(o)} = A(x,t)$. Similarly, matching as $Y \to -\infty$ we obtain $\phi^{(o)} = D$ (see Eqn. (2.13)). Thus we have $A = D$ in Eqn. (2.13).

$$O(\epsilon^{1/2} \ln \epsilon): \quad \mathcal{L}_c \frac{\partial^2 \phi_1^{(1/2)}}{\partial Y^2} = 0 \text{ whence } \quad \phi_1^{(1/2)} = \frac{b_{oo}}{2} A Y \text{ matches identically!}$$

$$O(\epsilon^{1/2}): \quad \mathcal{L}_c \frac{\partial^2 \phi^{(1/2)}}{\partial Y^2} + \frac{\partial^3 \phi^{(o)}}{\partial t \partial Y^2} + (\beta - U_c'') \phi_x^{(o)}$$

$$+ \left[\frac{1}{2} U_c'' Y^2 \frac{\partial}{\partial x} + (\phi_Y^{(1/2)} \partial_x - \phi_x^{(1/2)} \partial_Y) \right] \frac{\partial^2 \phi^{(o)}}{\partial Y^2} = 0 .$$

The second and fourth terms vanish identically leaving

$$\left\{ U_c' Y \frac{\partial}{\partial x} - A_x \frac{\partial}{\partial Y} \right\} \frac{\partial^2 \phi^{(1/2)}}{\partial Y^2} + (\beta - U_c'') A_x = 0 . \tag{3.6}$$

To discuss this equation consider the transformation to new independent variables

$$S = \frac{1}{2} U_c' Y^2 + A , \tag{3.7}$$

$$X = x .$$

Since

$$U_c' Y \frac{\partial}{\partial x} - A_x \frac{\partial}{\partial Y} = U_c' Y \frac{\partial}{\partial X} + U_c' Y A_x \frac{\partial}{\partial S} - U_c' Y A_x \frac{\partial}{\partial S} ,$$

Eqn. (3.6) becomes simply

$$\frac{\partial \zeta}{\partial X} = - \frac{\beta - U_c''}{U_c' Y} A_X = \frac{b_\infty}{Y} A_X ,$$

where $\zeta = \Phi_{YY}^{(1/2)}$ gives the leading order perturbation vorticity. Before integrating this equation let us interpret the transformation Eqn. (3.7).

The total streamfunction in the critical layer region is (see Eqn. 3.1

$$\Psi = \int_{y_c}^{y} dy \left(U(y) - c \right) + \epsilon \Phi .$$

Expand $U(y)$ as

$$U(y) = U_c + U_c' (y - y_c) + \cdots ,$$

and integrate term by term to obtain

$$\Psi = \epsilon \tfrac{1}{2} U_c' Y^2 + \tfrac{1}{6} \epsilon^{3/2} U_c'' Y^3 + \cdots + \epsilon \left(\Phi^{(0)} + \epsilon^{1/2} \ln \epsilon \, \Phi_1^{(1/2)} + \cdots \right)$$

$$= \epsilon S + O(\epsilon^{3/2} \ln \epsilon) + O(\epsilon^{3/2}) + \cdots .$$

Thus S is simply the leading order part of the total streamfunction in the critical layer.

Now consider the streamline pattern, i.e., the level curves of $S(x, Y$ $= \tfrac{1}{2} U_c' Y^2 + A$. Since A is assumed to go to zero as $|x| \to \infty$, $S(x,Y)$ has least one stationary point given by $Y = 0$, $A_x = 0^*$). To determine its ty consider the matrix

$$\begin{pmatrix} \dfrac{\partial^2 S}{\partial x^2} & \dfrac{\partial^2 S}{\partial x \partial Y} \\[2mm] \dfrac{\partial^2 S}{\partial x \partial Y} & \dfrac{\partial^2 S}{\partial Y^2} \end{pmatrix} = \begin{pmatrix} A_{xx} & 0 \\[2mm] 0 & U_c' \end{pmatrix} .$$

Thus, if $U_c' > 0$, we have two possible cases:
  (a) For $A_{xx} < 0$, A has a maximum and the stationary point is a saddle
      point. In this case $A > 0$.

  (b) For $A_{xx} > 0$, A has a minimum and the stationary point is a maximu
      In this case $A < 0$.

Streamlines corresponding to the two cases are sketched in Figs. 1a a
1b. It is clear that as $X \to \pm \infty$ the streamlines have asymptotes
parallel to the X-axis.

---

*We assume that these equations have just one solution which we place at
origin of coordinates without loss of generality.
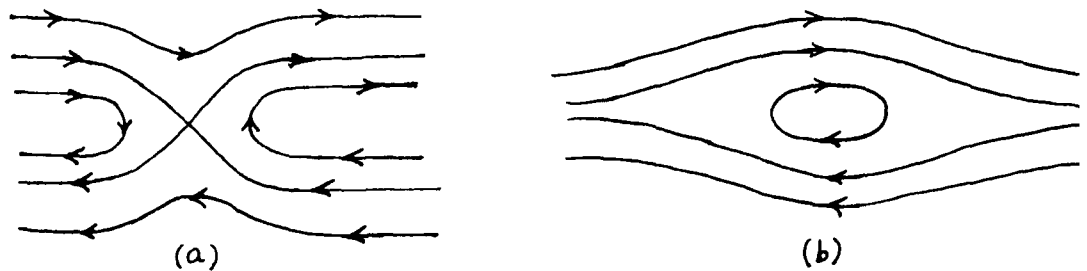
Fig. 1 Streamline patterns for solitary waves in a critical layer:
(a) $A > 0$, (b) $A < 0$.

(The case $U_c' < 0$ is analogous except that pattern (a) occurs for $A < 0$ ɛ
pattern (b) for $A > 0$). In both patterns there is a dividing streamline
separating those streamlines that run continuously from $-\infty$ to $+\infty$ (in
from those that do not. In case (a) this dividing streamline clearly ha:
A_{max}, the maximum value of A; in case (b) $S = 0$ on the dsl. In either cɛ
denoting the value of S on the dsl by S_c, the equation for the dsl becom∈

$$Y_{ds\ell} = \pm \left[\frac{2}{U_c'} \left(S_c - A(x,t) \right) \right]^{1/2}.$$

Outside the dividing streamline it is straightforward to integrate Ec
(3.8). Substituting, from (3.7),

$$Y = \text{sgn } Y \left(\frac{2}{U_c'} (S-A) \right)^{1/2}$$

we get

$$\frac{\partial \zeta}{\partial X} = b_\infty \, \text{sgn} Y \frac{A_X}{\sqrt{\frac{2}{U_c'} (S-A)}}$$

which is easily integrated to give

$$\zeta = b_\infty \sqrt{2 U_c'} \, \text{sgn} Y \left\{ \sqrt{S} - \sqrt{S-A} \right\}$$

using the boundary condition that $\zeta \to 0$ and $A \to 0$ as $|X| \to \infty$. In ter

$$\zeta = b_\infty \sqrt{2 U_c'} \, \text{sgn} Y \left\{ \sqrt{\tfrac{1}{2} U_c' Y^2 + A} - \sqrt{\tfrac{1}{2} U_c' Y^2} \right\}.$$

Hence for $|Y| \to \infty$,

$$\epsilon^{1/2} \zeta = \epsilon^{1/2} \left[b_\infty \frac{A}{Y} - \frac{b_\infty}{2 U_c'} \frac{A^2}{Y^3} + \cdots \right].$$

From Eqn. (3.3) this has to match with

$$\frac{\partial^2 \psi_+}{\partial Y^2} = \epsilon^{1/2} \left[b_\infty \frac{A}{Y} + r_1 \frac{A^2}{Y^3} + \cdots \right]$$

But this matching is valid uniformly according to Eqn. (2.25) (and the A = D derived previously.)

To determine the matching of the coefficients $\alpha_\pm$ we integrate Eq once to obtain

$$\frac{\partial \Phi^{(1/2)}}{\partial Y} = \int^Y d Y' \zeta(Y') + m(X,t)$$

$$- \frac{1}{2} b_\infty U_c' \left\{ |Y| \sqrt{Y^2 + \frac{2A}{U_c'}} + \frac{2A}{U_c'} \ln \left(|Y| + \sqrt{Y^2 + \frac{2A}{U_c'}} \right) - Y^2 \right\} + m$$

When we consider this expression for $|Y| \to \infty$ we get a term independen

$$\frac{\partial \Phi^{(1/2)}}{\partial Y} = \frac{1}{2} b_\infty U_c' \left\{ \frac{A}{U_c'} \ln(4e) + \frac{2A}{U_c'} \ln|Y| + \frac{A^2}{2(U_c')^3 Y^2} + \cdots \right\} + m$$

and, when this is compared with the first Y-derivative of ψ_+ in Eqn. (the main conclusion is that

$$\alpha_+ = \alpha_- .$$

Together with A = D (already derived twice) this completes the solution matching problem posed after Eqn. (2.13). Stated differently, the matc has shown that the leading order outer solution for ψ is the same on sides of the critical layer. It is also clear from the discussion in § that A evolves according to KdV.

We still need to obtain a solution valid inside the dsl. To do th rewrite Eqn. (3.6) as

$$\left(S_Y \frac{\partial}{\partial X} - S_X \frac{\partial}{\partial Y} \right) \Gamma = 0 ,$$

where

$$\Gamma = \frac{\partial^2 \Phi^{(1/2)}}{\partial Y^2} - (\beta - U_c'') Y .$$

The general solution is $\Gamma = F(S)$. (In our previous analysis of Eqn. via Eqn. (3.14), we found $\zeta = \Gamma + (\beta - U_c'') Y = \pm b_\infty \sqrt{2 U_c' S} + (\beta - U$

which is consistent with this type of general solution). To determ
form of F(S) inside the dsl we must consider the two basic streamli
patterns, (a) and (b) (cf. Fig. 1) separately.

For case (a) where all the streamlines extend to infinity we ha
Eqn. (3.7) that

$$0 = \Gamma' + (\beta - U_c'') \, sgn \, Y \, \sqrt{\frac{2}{U_c'} S}$$

as $X \to \pm \infty$ since both ζ and A vanish asymptotically. Thus Γ
discontinuous across the Y-axis:

$$\Gamma = F(S) = b_\infty \sqrt{2U_c'} \; sgn \, Y \; \sqrt{S}$$

the discontinuous jump being $[\![\Gamma]\!] = 2 \, b_\infty \sqrt{2U_c' A}$.

It is stated without proof that this can be avoided by allowin
appropriate distortion of the mean flow. It is clear from the disc
Eqn. (3.23) matches with Eqn. (3.15) on the dsl.

For case (b) the presence of closed streamlines suggests that w
F(S) by requiring that the steady solution being found is consisten
equations of motion in the limit of vanishing viscosity. For $\nu \neq 0$
(3.21a) becomes

$$\left(S_Y \frac{\partial}{\partial X} - S_X \frac{\partial}{\partial Y} \right) \Gamma = \lambda \, \Gamma_{YY} \; .$$

We seek Γ as a regular perturbation solution of this equation:

$$\Gamma = F(S) + \lambda \, \Gamma^{(1)} + \cdots \; ,$$

whence

$$\left(S_Y \partial_X - S_X \partial_Y \right) \Gamma^{(1)} = \frac{\partial^2 F}{\partial Y^2} \; .$$

This equation may be rewritten as

$$\nabla \cdot \vec{Q}$$

where the two-dimensional vector

$$\vec{Q} = \left(S_Y \Gamma^{(1)}, \; -S_X \Gamma^{(1)} - \frac{\partial F}{\partial Y} \right)$$

By the divergence theorem, we see that the integral of $\vec{Q} \cdot \hat{n}$ aroun
curve $\mathcal{C}$, where $\hat{n}$ is the normal to $\mathcal{C}$, is zero. We choose

a closed streamline so that

$$\hat{n} = \frac{(S_X, S_Y)}{\sqrt{S_X^2 + S_Y^2}} \ .$$

Then

$$\vec{Q} \cdot \hat{n} = - \frac{S_Y \frac{\partial F}{\partial Y}}{\sqrt{S_X^2 + S_Y^2}} = - F'(S) \frac{S_Y^2}{\sqrt{S_X^2 + S_Y^2}} \ .$$

Hence, in the contour integral, $\oint_C \vec{Q} \cdot \hat{n} \, d\ell$, the position depender the integrand is positive definite and the integral itself vanishe: follows that F'(S) = 0 or F(S) = const. This result is generally as the "Prandtl-Batchelor" theorem. The value of the constant is d matching on the dividing streamline. Since $S_c = 0$ for case (b) (so discussion just before Eqn. (3.13)) it follows that

$$\zeta \Big|_{ds\ell} = \Gamma_{ds\ell} + (\beta - U_c'')Y_{ds\ell} = b_\infty \sqrt{2U_c'} \ \text{sgn}\, Y \ \sqrt{S_c} + (\beta - U_c'') $$

or $\quad \Gamma_{ds\ell} = F(S_c) = 0$ and so the solution is simply

$$\zeta = (\beta - U_c'')Y$$

Notice that if we applied the result of this analysis to case (a) would give $F = b_{oo}\sqrt{2U_c'} \ \text{sgn}\, Y \ \sqrt{A_{max}}$ which is not a const Furthermore, Eqn. (3.26) would not match on the dsl and would not $x \longrightarrow \pm\infty$.

There is, of course, no paradox since in case (a) the streamlines closed and the Prandtl-Batchelor theorem need not apply.

Finally, we make some general comments about the effects of vi general, if one considers the eigenvalue problem (2.6) one has to solutions on the two sides of the critical layer of the form

$$\phi_\pm = a_\pm \phi_a(y) + b_\pm \phi_b(y)$$

It may be shown that for the steady problem considered here the ma the form of the following jump conditions on the coefficients a±,

$$[\![\, b \,]\!] \equiv b_+ - b_- = 0,$$

$$[\![\, a_+ \,]\!] \equiv a_+ - a_- = i \, \frac{\beta - U_c''}{|U_c'|} \, b \, \Theta(\lambda),$$

where b is the common value of b+ and b-. The quantity $\Theta(\lambda)$ pl

of a phase jump in the term $\ln(y-y_c)$. When Eqn. (3.27b) hol
interpret $\ln (y-y_c)$ as $\ln |y-y_c| + i \Theta(\lambda)$ sign U_c' for $y <$
argument, λ, of $\Theta(\lambda)$ is defined as

$$\lambda = \left[\frac{\left(\mathcal{V}/\epsilon''_2\right)^{4/3}}{\epsilon''_2} \right]^3 = \frac{\nu}{\epsilon^2} ,$$

and measures the relative importance of the viscous and nonl
both are important. The nonlinear analysis presented above v
yielded $\Theta \to 0$. The other limit $\lambda \to \infty$ (the viscous crit
known to give $\Theta \to -\pi$. In between these two limits the re:
varies as shown in Fig. 2.
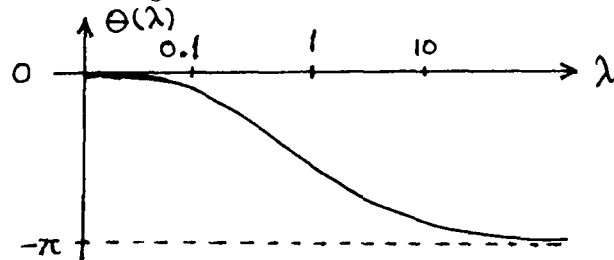
Fig. 2. Variation of phase jump $\Theta(\lambda$

In the general case the Reynolds stress averaged over on
the motion along the critical layer has a jump discontinuity

$$[\![\tau]\!] = 2 \frac{k (\phi - U_c'')}{|U_c'|} b \Theta$$

where k is the wave number.

4. TIME EVOLUTION OF VORTICITY IN THE CRITICAL LAYER

In this section we want to consider briefly the consequei
time dependence to the equation for ζ, (Eqn. 3.6). To in
derivative into (Eqn. 3.6) we must select the scaling $\mu =$
thus becomes a *fast* time scale compared to t. Introducing s

$$(X', Y') = U_c' (X, Y), \qquad T' = U_c' T, \qquad A' = U_c' A$$

we obtain

$$\frac{\partial \zeta}{\partial T} + Y \frac{\partial \zeta}{\partial X} - A_X \frac{\partial \zeta}{\partial Y} = b_\infty A_X ,$$

where the primes have been dropped for convenience. Let A b
solitary wave solution:

$$A = 12 \frac{s}{r} \operatorname{sech}^2(X-4st)$$

which solves the KdV equation

$$A_t + \mathbf{r}\, AA_x + sA_{xxx} = 0$$

We have

$$A_x = A_o \mathrm{sech}^2\theta \tanh\theta$$

where

$$A_o = -24\frac{s}{r}\ , \quad \theta \equiv X - 4st \approx X - 4s\epsilon^{1/2}T.$$

This expression for A_x is to be substituted into (4.1) and the eq
solved with $\zeta = 0$ at $T = 0$.

Particular solution of Eqn. (4.1) is

$$\zeta = -b_{oo}Y\ ,$$

and, since the equation is linear, all that remains is to find th
solution of the homogeneous equation

$$\frac{\partial\zeta}{\partial T} + Y\frac{\partial\zeta}{\partial X} - A_o\,\mathrm{sech}^2 X\,\tanh X\,\frac{\partial\zeta}{\partial Y} = 0$$

Note that $\mathrm{sech}^2 X$, $\tanh X$ appear here since by Eqn. (4.5) $\theta \sim X =$

We can again adopt the streamline coordinates (Eqn. 3.7) viz.

$$S = \tfrac{1}{2}Y^2 + A$$

to obtain

$$\frac{\partial\zeta}{\partial T} + Y\frac{\partial\zeta}{\partial X} = 0$$

We now seek a new variable p such that

$$\frac{dX}{dp} = Y = \sqrt{2(S-A)}$$

or (assuming $A_o/2S > 0$)

$$p = \int\frac{dX}{\sqrt{2\left(S + \tfrac{1}{2}A_o\,\mathrm{sech}^2 X\right)}} = \frac{1}{2\sqrt{S}}\,\sinh^{-1}\left\{\frac{\sinh X}{\sqrt{1 + \frac{A_o}{2S}}}\right\}$$

Then (Eqn. 4.9) becomes

$$\frac{\partial\zeta}{\partial T} + \frac{\partial\zeta}{\partial p} = 0\ ,$$

so that

$$\zeta = \zeta(p - T)$$

is the general solution sought. The full solution is

$$\zeta = -b_\infty Y + \zeta(p-T) \tag{4.14}$$

where the choice of the second term is determined by the initial condition $\zeta = 0$ at $T = 0$:

$$\zeta(p) = b_\infty Y. \tag{4.15}$$

Hence, all that remains is to express Y in terms of p. We have

$$Y^2 = 2(S-A) = 2\left(S + S\sinh^2 X + \tfrac{1}{2}A_0\right)\Big/\left(1+\sinh^2 X\right), \tag{4.16}$$

and from (Eqn. 4.11)

$$\sinh^2 X = \left(1 + \frac{A_0}{2S}\right)\sinh^2\left(p\sqrt{2S}\right). \tag{4.17}$$

Thus

$$Y^2 = \frac{2\left(S+\tfrac{1}{2}A_0\right)\cosh^2\left(p\sqrt{2S}\right)}{\cosh^2\left(p\sqrt{2S}\right) + \frac{A_0}{2S}\sinh^2\left(p\sqrt{2S}\right)} . \tag{4.18}$$

Finally then

$$\zeta = -b_\infty\left\{ Y - \sqrt{2S}\ \frac{\sqrt{1+\frac{A_0}{2S}}\ \cosh\left((p-T)\sqrt{2S}\right)}{\left[\cosh^2\left((p-T)\sqrt{2pS}\right) + \frac{A_0}{2S}\sinh^2\left((p-T)\sqrt{2S}\right)\right]^{1/2}} \right\}. \tag{4.19}$$

Equations   (4.8) and Eqn. (4.11) give the variable transformations to X, Y and T. We have assumed $Y > 0$ throughout but for $Y < 0$ we simply change T to $-T$ and change the sign of the second term.

As $T \to \infty$ we (formally) get from Eqn. (4.19) that

$$\zeta \cong -b_\infty\left(Y - \sqrt{2S}\right) \tag{4.20}$$

which is precisely Eqn. (3.15). (Recall that we are using units such that $U_c' = 1$).

If we look inside the recirculating region we have $S < 0$ for $A_0 > 0$ (since the dsl has $S = 0$). Then Eqn. (4.11) becomes

$$p = \frac{1}{\sqrt{2|S|}}\ \sin^{-1}\left\{\frac{\sinh X}{\sqrt{\frac{A_0}{2|S|} - 1}}\right\} \tag{4.21}$$

and the solution corresponding to Eqn. (4.19) becomes

$$\zeta = -b_\infty \,\text{sgn}\,Y \left\{ |Y| - \frac{\sqrt{A_0 - 2|S|}\; \cos\left(\sqrt{2|S|}\,(p - \text{sgn}\,Y\,T)\right)}{\left[\cos^2\left(\sqrt{2|S|}\,(p - \text{sgn}\,Y\,T)\right) + \frac{A_0}{2|S|}\,\sin^2\left(\sqrt{2|S|}\,(p - \text{sgn}\,Y\,T)\right)\right]^{1/2}} \right\} \quad (4.22)$$

This result has the unfortunate feature that it continues to oscillate as $T \longrightarrow +\infty$. However, we conjecture that the addition of a weak viscosity ($\lambda \ll 1$ as opposed to $\lambda = 0$) will effectively damp this oscillation and yield a constant vorticity in the closed streamline region consistent with the Prandtl-Batchelor criterion.

The theory presented in this lecture is the basis for the hypothesis that some of the large eddy structures in the Jovian atmosphere (e.g., the Great Red Spot) are solitary Rossby Waves (cf., Maxworthy and Redekopp, 1976, 1980).

REFERENCES

Benney, D. and R. F. Bergeron, 1969. A new class of nonlinear waves in parallel flows. Stud. Appl. Math, 48, 181-204.

Haberman, R., 1972. Critical layers in parallel flows. Stud. Appl. Math., 51, 139-161.

Maxworthy, T. and L. G. Redekopp, 1976. A solitary wave theory of the Great Read Spot and other observed features in the Jovian Atmosphere. Icarus, 29, 261-271 and A note on a possible fluid dynamical interpretation of some reported features in the Jovian atmosphere. Science, in press.

Notes Submitted by
Hassan Aref

HIGHER DIMENSIONAL SYSTEMS

L. G. Redekopp

LECTURE #3., Part I: The 2-D KdV Equation

The form of the 2-D KdV equation can be obtained quite simply through the long wave (shallow-water) limit of the dispersion relation for interfacial gravity waves (see Lecture 1, Eqn. 1.2).

$$\omega^2 = C_o^2 k^2 - 2 C_o \gamma k^4 + \cdots . \tag{1.1}$$

We want to bring the leading effects of transverse (y, say) variations into the usual KdV balance. Hence, we write $k^2 = k_x^2 + k_y^2$ and consider $k_y^2 \ll k_x^2 \ll h^{-2}$, where h is the wave guide scale. We obtain from Eqn. (1.1) the relation

$$\omega = C_o \sqrt{k_x^2 + k_y^2} \left\{ 1 - \frac{2\gamma}{C_o}(k_x^2 + k_y^2) + \cdots \right\}^{1/2}$$

$$= C_o k_x + \frac{C_o}{2}\frac{k_y^2}{k_x} - \gamma k_x^3 + O\left(\frac{k_y^4}{k_x^3}, k_x^5, k_y^2\right). \tag{1.2}$$

Truncating the expansion after the first longitudinal and transverse dispersive terms yields

$$k_x(\omega - C_o k_x) = \frac{C_o}{2} k_y^2 - \gamma k_x^4 , \tag{1.3}$$

with the corresponding linear evolution equation

$$\left(u_t + C_o u_x + \gamma u_{xxx} \right)_x + \frac{C_o}{2} u_{yy} = 0 \tag{1.4}$$

Transverse variations are coupled with longitudinal dispersion if $|k_y| = O(k_x^2)$. This dispersion law implies the space/time scalings.

$$\xi = \mu(x - C_o t), \qquad \tau = \mu^3 t , \qquad \eta = \mu^2 y . \tag{1.5}$$

If the first nonlinear term has the same quadratic form as in the 1-D KdV equation, we obtain the nonlinear equation
(with

$$\left\{ u_\tau^{(1)} + \alpha u^{(1)} u_\xi^{(1)} + \gamma u_{\xi\xi\xi}^{(1)} \right\}_\xi + \frac{C_o}{2} u_{\eta\eta}^{(1)} = 0 . \tag{1.6}$$

This equation was first obtained by Kadomstrev and Petviashvili (1970) to study the stability of the KdV solitary wave to transverse disturbances. It is found that the solitary wave is stable (unstable) if $\gamma > 0$ ($\gamma < 0$). The situation with $\gamma \gtrless 0$ corresponds to the long-wave phase speed c_o being a local maximum/minimum. We will focus on the stable case only in this lecture. However, it is worth pointing out that we had $\gamma < 0$ for the singular neutral mode case for internal waves (see Lecture #1, Eqn. 2.7). Also, Ablowitz and

Satsuma (1973) have shown that two-dimensional lump solitons exist for this equation with $\gamma < 0$.

For convenience we will write Eqn. (1.6) in the scaled form

$$\left(u_t + \frac{3}{2} u u_x + \frac{1}{4} u_{xxx} \right)_x + \frac{3}{4} u_{yy} = 0 , \tag{1.7}$$

and also restrict our discussion to the soliton solutions of this equation.*

Zakharov and Shabat (1974) have presented a linear (inverse) method for solving the equation. The essence of this method is as follows:

Step 1. Find solutions to the pair of linear equations involving the auxiliary independent variable r:

$$Q_t + Q_{xxx} + Q_{rrr} = 0,$$

$$Q_y + Q_{xx} - Q_{rr} = 0. \tag{1.8}$$

Note the relation of the first equation to the linear, 1-D KdV equation and that, when $\partial/\partial y = 0$, $Q = Q(x + r, t)$ which is the form arising in the inverse scattering transform for the 1-D KdV equation.

Step 2. Knowing Q, find $\tilde{K}$ (x,r; y,t) from the linear integral equation (Gelfand-Levitan eqn.)

$$\tilde{K}(x,r) + Q(x,r) + \int_x^\infty \tilde{K}(x,s) Q(s,r) ds = 0. \tag{1.9}$$

We have suppressed the y and t dependence which enters only parametrically.

Step 3. Obtain the solution u(x,y,t) from

$$u = 2 \frac{\partial}{\partial x} \tilde{K}(x,x; y,t). \tag{1.10}$$

This solution procedure is quite remarkable. Nevertheless, it suffers from the lack of any direct connection with the initial data. The direct scattering problem and the time evolution of the scattering data are not prescribed.

As an illustration of the solution method, we construct the single soliton solution. Suppose we look for separable solutions of the Q-equations having the form

$$Q = Q_0 \exp\left\{ -\ell x - nr - (\ell^2 - n^2)y + (\ell^3 + n^3)t \right\}. \tag{1.11}$$

The Gelfand-Levitan equation is also separable with the solution

$$\tilde{K}(x,r; y,t) = \tilde{k}(x; y,t) e^{-nr}; \quad Q(x,r; y,t) = q(y,t) e^{-\ell x - nr};$$

$$\tilde{k} + q e^{-\ell x} + q \tilde{k} \int_x^\infty e^{-(\ell+n)s} ds = 0 ; \quad \tilde{K} = -\frac{q e^{-\ell x - nr}}{1 + \frac{q}{\ell+n} e^{-(\ell+n)x}} . \tag{1.12}$$

---

*Interesting dispersive solutions of Eqn. (1.7) exist as well and are discussed by Redekopp (1980).

Hence, the solution for u is obtained

$$u(x,y,t) = 2 \frac{\partial}{\partial x} \tilde{K}(x,x;y,t) = \frac{1}{2}(l+n) \operatorname{sech}^2 \frac{\Theta}{2} \;,$$

$$\Theta = (l+n)(x-x_0) + (l^2-n^2)y - (l^3+n^3)t \;, \tag{1.13}$$

$$x_0 = \frac{1}{l+n} \ln\left(\frac{Q_0}{l+n}\right).$$

This is a plane solitary wave propagating oblique to the x-direction. In fact, it is useful to define the soliton wave vector $\vec{K} = (K, M)$ and write the phase as

$$\Theta = \vec{K}\cdot\vec{X} - \Omega t \;, \qquad \vec{X} = (x,y) \;,$$

$$K = l+n \;, \quad M = l^2-n^2 \;, \quad \Omega = l^3+n^3 = \frac{1}{4}\left(K^3 + 3\frac{M^2}{K}\right) \;, \tag{1.14}$$

$$l = \frac{1}{2}\left(K + \frac{M}{K}\right) \;, \qquad n = \frac{1}{2}\left(K - \frac{M}{K}\right).$$

One should note the close relation to the dispersion relation of the linear equation

$$u \sim \exp\{i(kx + my - \omega t)\} \;,$$

$$\omega = -\frac{1}{4}\left(k^3 - 3\frac{m^2}{k}\right). \tag{1.15}$$

Also, if $l = n$ so that $\vec{K} = (2l, 0)$, we recover the solitary wave solution of the KdV equation

$$u = l \operatorname{sech}^2\{l(x-x_0 - l^2 t)\}. \tag{1.16}$$

Interesting results are obtained when we seek to construct multi-soliton solutions. We then write

$$Q = \sum_j q_j(y,t)\, e^{-l_j x - n_j r} \;, \tag{1.17}$$

$$\tilde{K} = \sum_j \tilde{k}_j(x,y,t)\, e^{-n_j r}.$$

The integral term in the Gelfand-Levitan equation will have the form

$$\int_x^\infty \tilde{K}(x,s)\, Q(s,r)\, ds = \sum_j \sum_i q_j \tilde{k}_i\, e^{-n_j r} \int_x^\infty e^{-(l_j+n_i)s}\, ds. \tag{1.18}$$

This integral is singular and the solution method fails when

$$l_j + n_i = 0 \;, \qquad i \neq j. \tag{1.19}$$

The case $j = i$ is never singular because the solitary wave vanishes identically (Eqn. 1.13). To understand what this singular condition corresponds to, we construct the function

$$F(\vec{K}_1, \vec{K}_2) = \Omega(\vec{K}_1) + \Omega(\vec{K}_2) - \Omega(\vec{K}_1 + \vec{K}_2) \tag{1.20}$$

$$= -3 \frac{K_1 K_2}{K_1 + K_2}\, (l_1 + n_2)(l_2 + n_1).$$

The singular condition corresponds to a satisfaction of the triad resonance condition for soliton dispersion relation. In this case there is a strong resonance and a third soliton is created (corresponding to the third member of the triad) yielding the configuration
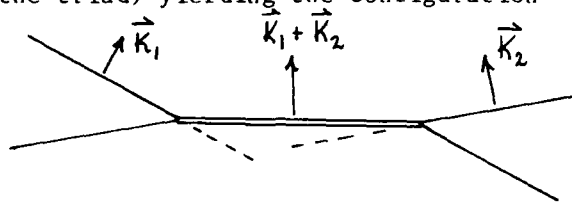
Further discussion on aspects of the interaction is provided in the following references.

REFERENCES

Maxworthy, T, 1980. On the formation of nonlinear internal waves from the gravitational collapse of mixed regions in two and three dimensions. J. Fluid Mech., 96, 47.

Melville, W. K., 1980. On the Mach reflexion of a solitary wave. J. Fluid Mech., 98. 285.

Newell, A. C., 1978. In Nonlinear Evolution Equations Solvable by the Spectral Transform. Edited by F. Calogero, p. 158, Pitman, London.

Newell, A. C. and L. G. Redekopp, 1977. Breakdown of Zakharov-Shabat theory and soliton creation. Phys. Rev. Lett., 38, 377.

Miles, J. W., 1979. Obliquely interacting solitary waves. J. Fluid Mech., 79, 157-170 and Resonantly interacting solitary waves. J. Fluid Mech., 79, 171-179.

Ze, F., N. Hershkowitz and K. E. Lonngren, 1980. Oblique collision of ion-acoustic solitons. Phys. Fluids, 23, 1155.

PERTINENT REFERENCES

Alblowitz, M. J. and J. Satsuma, 1978. Solitons and rational solutions of nonlinear evolution equations. J. Math. Phys., 19, 2180.

Kadomtsev, B. B. and V. I. Petviashvili, 1970. On the stability of solitary waves in weakly dispersive media. Soviet Physics DOKL., 15, 539.

Redekopp, L. G., 1980. Similarity solutions of some two-space-dimensional nonlinear wave evolution equations. Stud. Appl. Math. In press.

Zakharov, V. E. and A. B. Shabat, 1974. A scheme for integrating the nonlinear equations of mathematical physics by the method of the inverse scattering problem. Func. Anal. Appl. 8, 226.
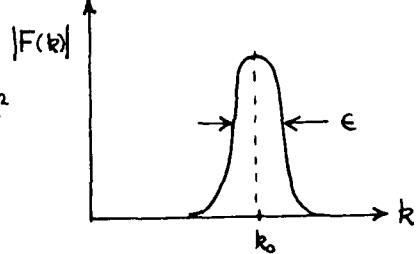
LECTURE #3, PART II. LONG-WAVE/SHORT-WAVE RESONANT INTERACTION

In our previous discussion we considered some examples of coherent structures described in terms of a single, weakly nonlinear wave mode. We will now present results for a particular multi-modal interaction which also admits coherent behavior with some interesting properties. First, however, w make some preliminary remarks concerning the <u>linear</u> evolution of a narrow-ban wave packet and also its <u>nonlinear</u> evolution which is described by the (cubic nonlinear Schrödinger (NLS) equation.

A linear wave packet in a dispersive media with linear dispersion relation $\omega(k)$ is given in terms of the Fourier integral

$$\phi = \frac{1}{2\pi}\int_{-\infty}^{\infty} F(k)\, e^{i(kx-\omega t)}\, dk, \qquad \omega = \omega(k), \tag{2.1}$$

where $F(k)$ is the transform of the initial packet. We suppose $F(k)$ has central wave number k_0, spectral width ϵ and, purely for analytical convenience, that its shape is Gaussian

$$\phi(x,0) = e^{i k_0 x}\, e^{-\left(\frac{\epsilon x}{2}\right)^2}$$

$$F(k) = \int_{-\infty}^{\infty} \phi(x,0)\, e^{-ikx} dx = \frac{2\sqrt{\pi}}{\epsilon}\, e^{-\left(\frac{k-k_0}{\epsilon}\right)^2} \tag{2.2}$$

If the spectral bandwidth is narrow ($\epsilon \ll 1$), the dispersion relation is well approximated by several terms in its Taylor series expansion about k_0

$$\omega(k) \cong \omega_0 + c_g (k-k_0) + \frac{\omega_0''}{2} (k-k_0)^2. \tag{2.3}$$

When $\omega(k)$ and $F(k)$ have these simple forms, the Fourier integral for $\phi(x,t)$ can be integrated directly and yields

$$\phi(x,t) = e^{i(k_0 x - \omega_0 t)}\, \frac{e^{-\frac{1}{2} \tan^{-1}(\omega_0'' \epsilon t^2/2)}}{\left[1 + \left(\frac{\omega_0'' \epsilon t^2}{2}\right)^2\right]^{1/4}}\, \exp\left\{-\frac{\epsilon^2 (x-c_g t)^2}{4\left(1 + i\frac{\omega_0''}{2}\epsilon^2 t\right)}\right\}$$

$$\equiv e^{i(k_0 x - \omega_0 t)}\, \Phi(\xi,\tau). \tag{2.4}$$

This defines the appropriate space and time scales which are relevant to the weakly nonlinear evolution of a wave packet

$$\xi = \epsilon (x - c_g t), \qquad \tau = \epsilon^2 t \tag{2.5}$$

In terms of these variables the envelope function Φ defined in Eqn. (2.4 satisfies the linear Schrödinger equation

$$i\, \frac{\partial \Phi}{\partial \tau} + \frac{\omega_0''}{2}\, \frac{\partial^2 \Phi}{\partial \xi^2} = 0. \tag{2.6}$$

In fact, the envelope function $\tilde{\phi}$ satisfies the equation defined in Eqn. (2.6) for arbitrary $F(k)$ whenever the dispersion relation has the form Eqn. (2.3). However, the approximate form of the dispersion relation is valid onl if the bandwidth is narrow $(\epsilon \ll 1)$ and then there exists a clear separatio in scales between the rapid phase $(k_0 x - \omega_0 t)$ and the envelope variation $\tilde{\phi}(\xi, \tau)$.

Considering the extension of Eqn. (2.6) to include the first nonlinear correction, a balance between the (self) nonlinearity and dispersion is achieved if we identify ϵ with the nondimensional wave amplitude ak (i.e., the maximum wave slope). One then finds that the envelope function obeys the NLS equation (written in dimensionless form)

$$i A_\tau + \lambda A_{\xi\xi} = \nu |A|^2 A. \qquad (2.7$$

Several remarks regarding this equation are in order.

(i) The NLS equation is implicity applicable only to the evolution of a narrow bandwidth wave packet or wave train in the weakly nonlinear regime. How narrow the spectral width must be for the equation to provide a good description of the motion in any physical situation i not so easy to define.

(ii) The coefficient ν of the nonlinear term has the general form

$$\nu \sim \frac{1}{D(2\omega, 2k)\,(C_g(k) - C(o))} \qquad (2.8$$

where $D(\omega, k) = 0$ is the linear dispersion relation, $c(k)$ is the phase speed and $c_g(k)$ is the group velocity. This coefficient is singular when either of two resonance conditions are satisfied:

a) Harmonic resonance, $D(2\omega, 2k) = 0$

b) Long-wave/short-wave resonance, $c(o) = c_g(k)$.

In either case, the single mode theory leading to the NLS equation is invalid and a multi-mode interaction occurs on a faster time scale. The following discussion will focus exclusively in the long-wave/short-wave resonant interaction.

The theoretical development leading to the coupled pair of equations describing the resonant interaction of a long and short wave can be briefly outlined as follows. The expansion of the dependent variable ψ (the streamfunction, say) is written in the form (assuming that the waves are loca in x and modal in z)

$$\psi(x,z,t) = \epsilon\left\{ S(\xi,\tau) e^{i(kx-\omega t)} + c.c. \right\} \phi(z) + \epsilon^{4/3} L(\xi,\tau)\tilde{\phi}(z) + \cdots, \qquad (2.9$$

where the slow space/time scales (ξ, τ) are defined by

$$\xi = \epsilon^{2/3}(x - c_g t), \qquad \tau = \epsilon^{4/3} t. \qquad (2.1$$

Note that ϵ is the nondimensional amplitude (e.g., the slope ak) o short wave. Hence, the long-wave amplitude is asymptotically smaller tha short-wave, but much larger than the streaming motion associated with the short wave (i.e., $\epsilon^2 |S|^2$). The time scale is much faster than that associated with single-mode modulation (cf. Eqn. (2.5) where $\tau = \epsilon^2 t$). Proceeding to higher order in the expansion (Eqn. (2.9)) we obtain the amplitude equations

$$i\, S_\tau + \frac{\omega_o''}{2} S_{\xi\xi} - \nu_1 SL = \epsilon^{2/3}\left\{\alpha_1 |S|^2 S + \alpha_2 S L_\xi + \alpha_3 S_\xi L + \frac{i\omega_o'''}{6} S_{\xi\xi\xi}\right\}$$
$$+ \alpha(\epsilon^{4/3}),$$

$$L_\tau + \frac{C(o) - C_g(k)}{\epsilon^{2/3} C_g(k)} L_\xi - \nu_2 (|S|^2)_\xi = \epsilon^{2/3}\left\{\beta_1 L L_\xi + \beta_2 L_{\xi\xi\xi} + \beta_3 (|S|^2)_{\xi\xi}\right.$$
$$\left. + \beta_4 |S|^2 L\right\} + O(\epsilon^{4/3}).$$

We have included the higher order terms on the righthand-side to exhibit relation of these equations to their respective single mode form: namely NLS equation and the KdV equation. It is clear from the second term in E (2.11b) that the bandwidth of the resonance is $O(\epsilon^{2/3})$. Detailed derivations of these equations are given by Djordjevic and Redekopp (1977 Grimshaw (1977).

In the remaining discussion we consider the leading order equations f on-resonance conditions. Furthermore, we choose to normalize the equatio such that we obtain

$$i\, S_\tau + S_{\xi\xi} = SL,$$
$$L_\tau = -2 (|S|^2)_\xi .$$

Based on the coupled set of equations, we note the following properties:

(i) The long wave is unstable (even if L (ξ , t = 0)=0) to modulati the short wave.

(ii) The equations permit a uniform amplitude, periodic wave train so

$$S = S_o\, e^{-i L_o \tau},$$
$$L = L_o ,$$

where S_o and L_o are constants. The short wave has a frequency correction proportional to the long wave amplitude. This solution, however, is unst to small modulational perturbations.

$$S = S_o\, e^{-i L_o \tau}\left\{ 1 + s_+\, e^{i(K\xi - \Omega\tau)} + s_-\, e^{-i(K\xi - \Omega^*\tau)}\right\},$$
$$L = L_o\left\{ 1 + \ell\, e^{i(K\xi - \Omega\tau)} + \ell^*\, e^{-i(K\xi - \Omega^*\tau)}\right\}.$$

Linearizing the equations for $\left| s_{\pm} \right|$, $\left| 1 \right| \ll 1$, we obtain the eiger relation

$$\Omega^3 - K^4 \Omega + 4 K^3 = 0$$

The perturbation is unstable (complex eigenvalues) for

$$0 < K < 2^{1/3} 3^{1/2} = 2.182\cdots$$

The maximum instability occurs for K = 1.51 with the growth rate Im Ω Numerical simulations of the equations confirm the instability and show the
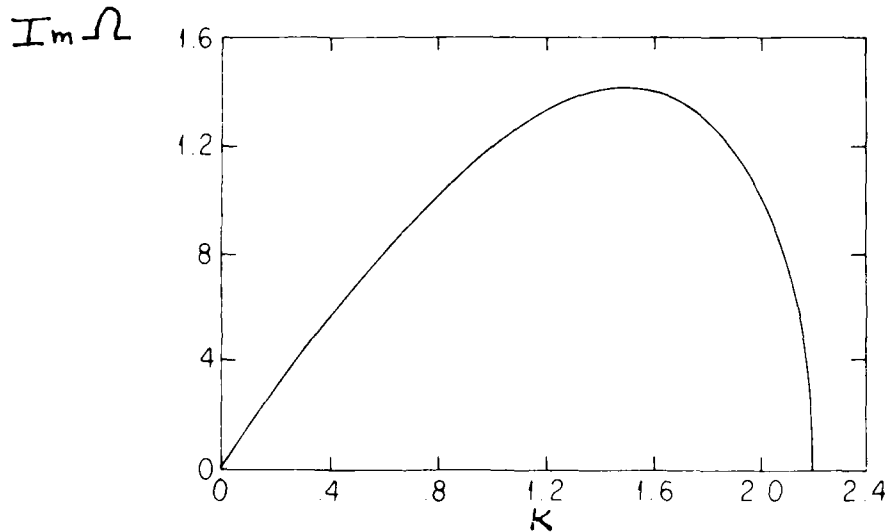
long-time character of the instability is one in which the energy of th shortwave is transferred reversibly to side-hands of the short wave as to the long wave and back again with periodic recurrence. Other aspec the long-time behavior of this interaction together with some experimer results on the initial instability and the resonance bandwidth are dis(by Koop and Redekopp (1980).
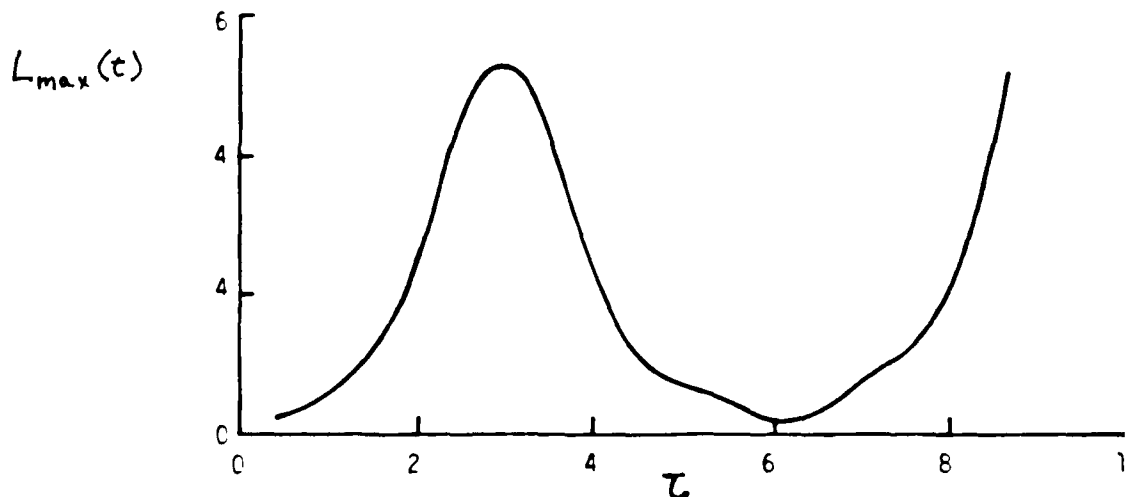
(iii) Envelope pulse soliton solutions exist also. The single s‹
wave form is

$$S = K(-c)^{1/2} e^{i\left[\frac{c}{2}(x-\frac{c}{2}t)\right]} \operatorname{sech}[K(x-ct)]$$

$$L = -2K^2 \operatorname{sech}^2[K(x-ct)]$$

Note that the wave travels to the left (c < 0); that is, its speed i‹
necessarily less than the carrier wave group velocity. Also, the wa›
K and the speed c are independent so that breather (or, bound state)
exist for which two (or more) solitons with different wave numbers c‹
the same velocity. Such solutions are localized in space, but are t‹
dependent.
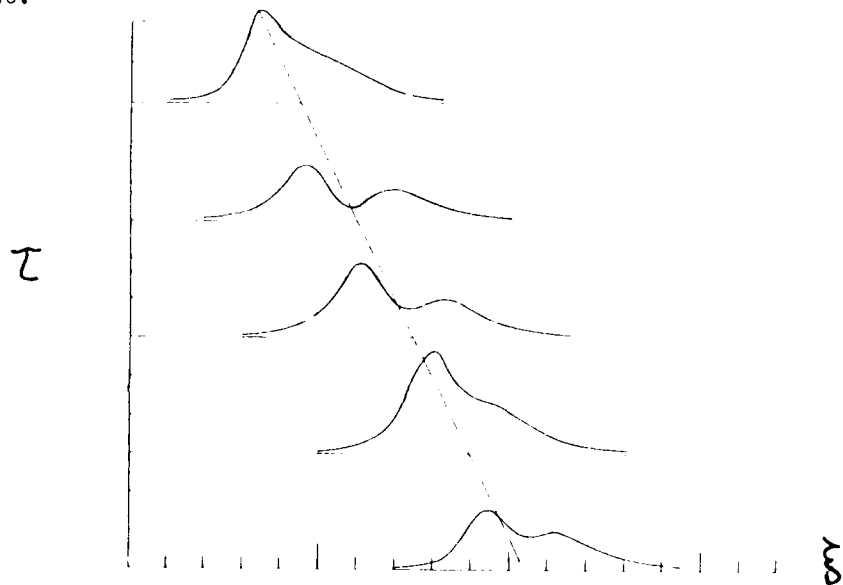
The long and short scale motions propagate together in a coherent
time-dependent manner. This example is presented to emphasize that c
features can be unsteady and exhibit motion on several length scales.
solitary wave solutions and others are described in Ma and Redekopp (

REFERENCES

Djordjevic, V. D. and L. G. Redekopp, 1977. On two-dimensional packe
capillary-gravity waves. ' J. Fluid Mech., 79, 703-714.

Grimshaw, R.H.J., 1977. The modulation of an internal gravity wave ⌐
resonance with the mean motion. Stud. Appl. Math., 56, 241.

Koop, C. G. and L. G. Redekopp, 1980. The interaction of long and sʰ
internal gravity waves: theory and experiment. Submitted to J.
Mech.

Ma, Y. C. and L. G. Redekopp, 1979. Some solutions pertaining to the
resonant interaction of long and short waves. Phys. Fluids, 22,

MIXING LAYERS AND SPATIAL STABILITY

Joseph B. Keller

LECTURE #1.

Introduction

It is well known that the interface between two fluid strear when the streams are moving parallel to the interface w velocities. This is called Helmholtz instability because Helmh it theoretically in 1863. We shall present his analysis later.

A typical wind tunnel or water tunnel demonstration of this sketched in Fig. 1. Fluids of densities ρ_1 and ρ_2 , with ve and U_2 , are separated by a flat plate[1] which ends in the passing the end of this plate, the streams produce an interface w with increasing amplitude. Ultimately, the streams mix together zone called a "mixing layer". The width $\delta(x)$ of the mixing lay to increase linearly with distance x from the end of the plate. the width is given by (Brown and Roskho, 1974)

$$\delta(x) \simeq 0.38 \frac{|U_1 - U_2|}{U_1 + U_2} x .$$
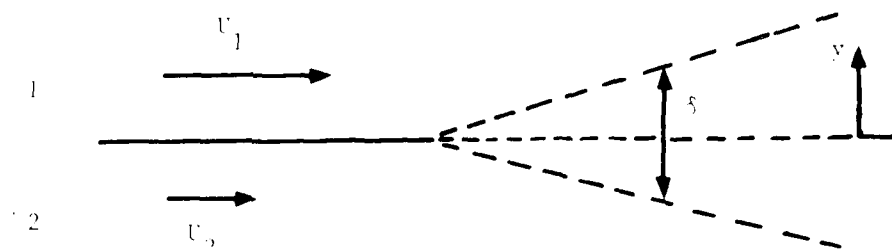
FIGURE 1.

Dimensional Analysis

The observed linear growth of $\delta(x)$ can be deduced t inviscid fluids as follows. For such fluids, the only quantit $\delta(x)$ can depend are ρ_1, ρ_2, U_1, U_2 and x:

$$\delta(x) = F(\rho_1, \rho_2, U_1, U_2, x) \ .$$

Dimensional analysis requires that the dimensionless ratio function of dimensionless quantities, so

$$\delta(x) = x f(\rho_1/\rho_2, U_1/U_2) \ .$$

Thus, the mixing layer thickness increases linearly with x.

Velocity Profile

To describe the mean horizontal velocity in the mixing la the averaged equation for the x-component of momentum of a fluid:

$$\bar{u}_t + \overline{u}\overline{u}_x + \overline{v}\overline{u}_y + \overline{w}\overline{u}_z = -\rho^{-1}\bar{p}_x + \tau_x \ .$$

Here u, v, w are the velocity components, p is the press density, $\bar{f}$ denotes the average of f, and $\rho\tau = \overline{(u - \bar{u})^2}$ is of the Reynolds stress. In the mixing layer we assume that $\bar{u}_t$ $\bar{u}_z = 0$ while $\overline{v}\overline{u}_y$ and $\rho^{-1}\bar{p}_x$ are small compared to terms. Then Eqn. (4) becomes

$$\overline{u}\overline{u}_x = \tau_x \ .$$

We now assume that τ_x can be written in terms of $\bar{u}(x,y)$ i $\tau_x = \nu_e \bar{u}_{yy}$ where ν_e is an eddy viscosity coeff: dimensions of ν_e are time/(length)^2, and ν_e should vanish w Therefore, we choose ν_e to be

$$\nu_e = c^2(\Delta U)^2 x/U \ .$$

Here $\Delta U = |U_1 - U_2|$, $U = |U_1 + U_2|/2$ and c is a dimensionless Eqn. (5) becomes

$$\overline{u}\overline{u}_x = c^2(\Delta U)^2 x \bar{u}_{yy}/U \ .$$

We expect Eqn. (7) to hold in the region $x > 0$, and the app conditions are

$$\bar{u}(0,y) = U_1 \ , \qquad y > 0 \ ,$$

$$= U_2 \ , \qquad y < 0 \ .$$

It is convenient to replace x in Eqn. (7) by the new vari

$$T = c^2 \left(\frac{\Delta U}{U}\right)^2 x^2 \qquad . \text{ Then } \bar{u}(T,y) \text{ satisfies the equation}$$

$$2\bar{u}\bar{u}_T/U = \bar{u}_{yy} \quad .$$

The nonlinear parabolic Eqn. (9) and the boundary conditi
invariant in form under the transformation $y = Ly'$, T
choice of L. Therefore the solution also must be inva
transformation. Consequently, the solution must be a funct
variable $z = y/T^{1/2}$, which is itself invariant. Therefore, w
$\bar{u}(T,y) = w(z)$ and then Eqns. (8) and (9) become

$$-zww'/U = w'' \quad ,$$

$$w(\infty) = U_1 \quad , \qquad w(-\infty) = U_2 \quad .$$

The two-point boundary value problem Eqns. (10) and (11) fo
of $w(z)$ can be solved numerically. However, many features o
be found by introducing into Eqn. (10) the simplification w/l
(10) becomes, upon division by w',

$$\frac{w''}{w'} = -z \quad .$$

Integration yields $\log w' = -z^2/2 + \log B$ where B is an int
Solving for w', integrating again, and using the boundary co
leads to the solution

$$\bar{u}(x,y) = w(z) = U_2 + (U_1 - U_2) \int_{-\infty}^{yU/c\Delta Ux} e^{-s^2/2} ds \Big/ \int_{-\infty}^{\infty} e^{-s^2/2}$$

This solution indicates how u varies across the mixing la
layer width increases linearly with x.

From Eqn. (13) we can find the layer width. We may
difference in y values between the places where $u(x,y) - U_2/$
takes on two particular values, say .25 and .75. The result
form Eqn. (1) with the numerical factor dependent upon the val

Recent Observations

More recent observations of mixing layers have reveale
patterns within the turbulent zone (Brown and Roshko, 1974; W
1974; Roshko, 1976; Dimotakis, 1980; Browand and Troutt, 1980
vortex-like structures form and "roll up" the interface bet
shown in Figure 2.
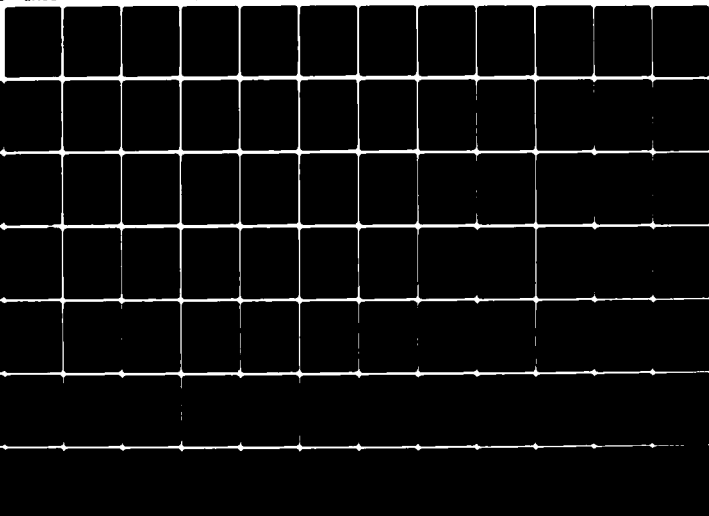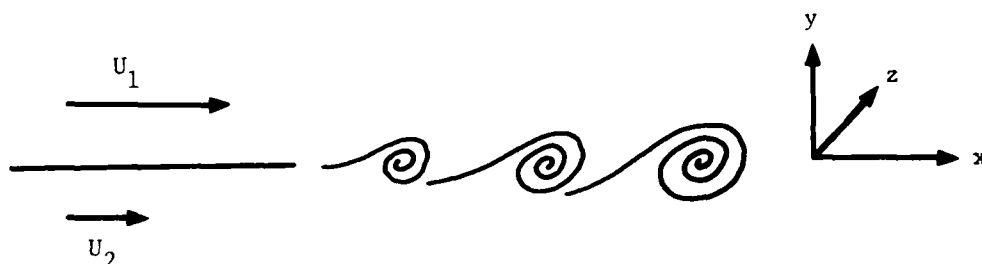
Figure 2

These structures extend very far in the cross-stream (z) direction. However, the motions appear to be de-correlated over very large distances in this direction because the structures have a small tilt (Browand and Troutt, 1980). Pairing of vortices is also observed, and the pairing or coalescence of two vortices occurs repeatedly as the structures move downstream. The overall growth of the mixing layer appears to be due primarily to the vortex pairing process, rather than to the growth of individual vortices.

When two vortices coalesce they produce a single vortex whose dimensions are roughly double the dimensions (in x and y) of the initial structures. A linear growth of the mixed layer results.

Temporal or Helmholtz Instability of an Interface

We shall now determine when an interface is unstable, and also examine the initial stages of its unstable evolution, following the procedure of Helmholtz (See Lamb, 1916). Thus, we consider the two dimensional irrotational motion of a fluid with density ρ_1 and velocity potential Φ_1 in the region $y > \eta(x,t)$, and of a fluid with density ρ_2 and velocity potential Φ_2 in $y < \eta(x,t)$. Both Φ_1 and Φ_2 are harmonic functions, and in terms of them the pressure P is given by the Bernoulli equation. At the interface the pressure must be continuous and the normal component of the fluid on each side must equal the normal velocity of the interface. Far from the interface $y = \eta(x,t)$, the velocity must tend to ($U_1,0$) above the interface and to (U_2 , 0) below it.

We write ϕ_j in the form

$$\Phi_j = U_j x + \phi_j(x,y,t) - \frac{1}{2}(U_j)^2 t , \qquad j = 1,2 . \qquad (14)$$

Here ϕ_j is the perturbation potential which is also harmonic. When $\phi_j = 0$ and $\eta = 0$ the flows are uniform, the interface is flat and the three boundary conditions are satisfied on it. When the ϕ_j and η are small, we linearize the boundary conditions around the uniform state. Then we seek a solution of the form

$$\phi_j = C_j e^{i(\sigma t - kx) - k|y|} ,$$

$$\eta = A e^{i(\sigma t - kx)} , \qquad Re(k) > 0 . \qquad (15)$$

Here σ and k are respectively the frequency and wave number of the perturbation while C_1, C_2 and A are constants. These constants are related by three homogeneous linear algebraic equations obtained by substituting Eqn. (15) into the three linearized boundary conditions.

In order that these equations have a non-trivial solution, the determinant of the coefficient matrix must vanish. This yields the dispersion equation

$$\rho_1[(\sigma - U_1 k)^2 + gk] = \rho_2[-(\sigma - U_2 k)^2 + gk] \ . \tag{16}$$

Here g is the acceleration of gravity, which points along the negative y-axis. When $g = 0$ and $U_1 = U_2$, Eqn. (16) yields the Rayleigh-Taylor instability which occurs when a heavy fluid is accelerated toward a lighter fluid. We shall consider only the case $g = 0$.

Upon setting $g = 0$ in Eqn. (16) and solving for σ we obtain the two solutions

$$\sigma_{\pm}(k) = \left[\frac{\rho_1 U_1 + \rho_2 U_2}{\rho_1 + \rho_2} \pm i \frac{(\rho_1 \rho_2)^{1/2}|U_1 - U_2|}{\rho_1 + \rho_2}\right] k \ . \tag{17}$$

The solution $\sigma_-(k)$ has a negative imaginary part so the corresponding perturbation (15) grows exponentially in time. For $\rho_1 = \rho_2$ we have from Eqns. (15) and (17),

$$\eta(x,t) = e^{ik(Ut-x)-\Delta Ukt/2} \ . \tag{18}$$

Thus the flat interface $\eta = 0$ is temporally unstable. Initial perturbations of any wave number $k > 0$ can grow, and the growth rate is proportional to k. There is no finite wave number of maximum growth rate.

When $U_1 = U_2$ then σ_+ and σ_- are real and equal, and the two solutions given by Eqn. (15) are identical and not growing. However, then there is another solution with the time factor $te^{i\sigma t}$. It can be obtained by differentiating Eqn. (15) with respect to U_1 with R fixed, and then setting $U_1 = U_2$. In this case an initial perturbation can grow linearly in time.

Spatial Instability

In the mixing layer problem the interface perturbation grows with x but not with t. Such growth is usually called spatial instability, although in plasma physics it is called drift instability. To analyze spatial stability we must consider σ to be real and solve the dispersion Eqn. (16) for $k(\sigma)$. Next, we must see if there are solutions for which Im $k(\sigma)$ is positive. If so, the corresponding solutions will grow exponentially with increasing x but just oscillate with increasing t. Then, if there are disturbances of the upstream flow which can excite these growing modes, the interface is spatially unstable.

The two solutions of Eqn. (16) for $k(\sigma)$ with $g = 0$ are

$$k_{\pm}(\sigma) = \frac{\rho_1 U_1 + \rho_2 U_2 \pm i(\rho_1 \rho_2)^{1/2}|U_1 - U_2|}{\rho_1 U_1^2 + \rho_2 U_2^2} \sigma . \tag{19}$$

The solution $k_+(\sigma)$ has a positive imaginary part so the corresponding disturbance (Eqn. 15) grows exponentially with increasing x. The growth rate is Im $k_+(\sigma)$.

It is of interest to compare the spatial growth rate Im $k_+(\sigma)$ given by Eqn. (19) with an approximate value. It is that given by the usual method of converting the temporal growth rate to a spatial growth rate. The conversion is performed by writing $t = x/c$ and $k = \sigma/c$, in the growth exponent $-\text{Im }\sigma_-(k)t$, where c is the phase velocity of the disturbance. This yields the new growth exponent $-c^{-1}\text{Im }\sigma_-(c^{-1}\sigma)x$, so the approximate spatial growth rate is $-c^{-1}\text{Im }\sigma_-(c^{-1}\sigma)$. From this result and Eqn. (17) we get

$$\text{Im }k_+(\sigma) \approx \frac{(\rho_1 \rho_2)^{1/2}|U_1 - U_2|}{(\rho_1 U_1 + \rho_2 U_2)^2} (\rho_1 + \rho_2)\sigma . \tag{20}$$

Comparison of Eqn. (20) with Eqn. (19) shows that the approximation (Eqn. 20) is good when $|\text{Im }\sigma_-| \ll |\text{Re }\sigma_-|$.

When $U_1 = U_2$ the two solutions k_+ and k_- become real and equal. Then there is another solution, in addition to (15), in which e^{-ikx} is replaced by xe^{-ikx}. This solution grows linearly in x. It can be found by differentiating Eqn. (15) with respect to U, with σ held fixed, and then setting $U_1 = U_2$.

The spatial growth rate increases linearly with σ, as we see from Eqn. (19). However, in a real mixing layer, the disturbance has a rather definite frequency. That frequency is presumably the frequency of maximum spatial growth rate of waves in the viscous boundary layer and shear layer near the edge of the plate. We shall not consider it further because it has not been determined theoretically.

Are Unstable Modes Excited?

We have seen that there are spatially unstable modes associated with an interface. We must now consider whether these modes are actually produced or excited by any perturbation. The example of potential flow in a semi-infinite pipe extending from $x = 0$ to $x = \infty$ with cross section D will be examined to illustrate this point.

Let $\phi(x,y,z)$ be the potential function for the perturbed velocity field and let $U(y,z)$ be the prescribed perturbation of the x-component of velocity at the pipe entrance $x = 0$. Then ϕ satisfies the equations

$$\Delta\phi = 0 , \quad x > 0 , \qquad (y,z) \text{ in } D , \tag{21}$$

$$\partial_n \phi = 0 \qquad \text{on boundary} \qquad (22)$$

$$\phi_x(0,y,z) = U(y,z) . \qquad (23)$$

To solve this problem we seek normal modes of the form

$$\phi_j = e^{\pm \lambda_j x} \psi_j(y,z) . \qquad (24)$$

Then Eqns. (21) and (22) become

$$(\partial_y^2 + \partial_z^2)\psi_j + \lambda_j^2 \psi_j = 0 \text{ in } D , \qquad (25)$$

$$\partial_n \psi_j = 0 \quad \text{on boundary of } D . \qquad (26)$$

For each positive eigenvalue λ_j^2, $j = 1,2,\ldots$, we obtain the two solutions (24). For $\lambda_j^2 = 0$ we find instead the solutions $\phi = $ constant and $\phi = x$. Thus, there is one growing mode and one decaying mode for each positive eigenvalue. For $\lambda_j = 0$ both modes yield constant velocities, so they do not grow.

It appears likely that the flow is unstable because there exists growing modes, in fact infinitely many of them. However, there is a solution satisfying the boundary condition (Eqn. 23) at the pipe entrance, which does not involve any of the growing modes no matter what the perturbation $U(y,z)$ is. This solution is

$$\phi(x,y,z) = \phi_0 + U_0 x - \sum_{j=1}^{\infty} \frac{U_j}{\lambda_j} \psi_j(y,z)e^{-\lambda_j x} . \qquad (27)$$

Here ϕ_0 is an arbitrary constant and U_j is defined by the quotient of inner products

$$U_j = (U,\psi_j)/(\psi_j,\psi_j) . \qquad (28)$$

Thus, despite the existence of the growing modes, they are not excited in this problem.

Modes of the Interface Behind a Plate

Let us now consider the spatial stability of the flow with an interface behind a semi-infinite flat plate. This problem differs from that considered above because of the presence of the plate, so that the interface is also semi-infinite. This problem was solved by John Neu (1980, unpublished) and we shall now outline his results. The flow configuration is shown in Figure 3.

We seek solutions of the linearized problem of the form

$$\Phi_1 - U_1 x = \phi_1(x,y)e^{i\sigma t} , \qquad (29)$$

$$\Phi_2 - U_2 x = \phi_2(x,y)e^{i\sigma t} ,$$

$$N(x,t) = \eta(x)e^{i\sigma t} .$$
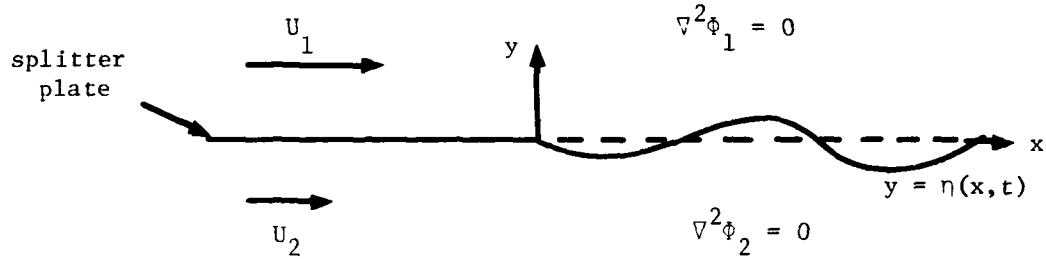
Figure 3

In order to simplify the resulting boundary value problem, we introduce the new variables u and v by the conformal transformation

$$x = u^2 - v^2 , \qquad y = 2uv .$$ (30)

We then find that the solution for $\eta(x)$ satisfying $\eta(0) = 0$ is a multiple of

$$\eta(x) = \int_C \sin kx^{1/2} [e^{i\Omega k^2/4} - e^{i\Omega*k^2/4}] dk .$$ (31)

In Eqn. (31), $\Omega = \sigma^{-1}[U + i\Delta U]$ and the contour C_1 goes from the origin to infinity in the k-plane with $1/2 \arg \Omega < \arg k < \frac{\pi}{2} - \frac{1}{2} \arg \Omega$. The asymptotic form of Eqn. (31) for x large is, with A a certain constant,

$$\eta(x) \sim A \exp\left[\frac{\sigma\Delta U}{U^2 + (\Delta U)^2} x - i \frac{\sigma U}{U^2 + (\Delta U)^2} x\right] .$$ (32)

This is a spatially growing mode of the form we obtained before for the infinitely extended interface. In the special case when $\Delta U = 0$, we find instead that for large x, with B another constant,

$$\eta(x) \sim Bxe^{i\sigma x/U} .$$ (33)

Again, this is the linear growth we found before for the unbounded interface. Thus both for $\Delta U \neq 0$ and for $\Delta U = 0$, the interface behind a flat plate has spatially growing modes.

Vortices and the Roll-up of Interfaces

In order to construct a model of the roll-up observed in mixing layers, Jimenez (1980) considered the influence of a single point vortex placed at the initial fluid interface. The vortex models the vorticity that is present in

the real shear flow. Each point on the interface will move along a streamline with velocity

$$\frac{dz}{dt} = \frac{i\Gamma(t)}{2\pi z} \,,$$

where $\Gamma(t)$ is the circulation in the vortex that is placed at $z = 0$. To model the shear due to a velocity difference ΔU between the fluids, we require $\Gamma(t) = 2\eta\Delta U$, where $2\eta(t)$ is the initial length of that part of the interface which is rolled up at time t. The interface position $x(\eta,t)$ of the point initially at $z = \eta$ is found to be

$$z(t) = \eta \, \exp\left[i \int_0^t \Gamma(t)dt/2\pi\eta^2\right] \,.$$

To find $\eta(t)$ we set $\arg z(\eta,t) = -\frac{\pi}{2} = -\int_0^t \Gamma(t)dt/2\pi\eta^2$. This yields

$$\eta = \frac{\Delta}{\pi^2}t\,. \qquad \text{Then} \quad \Gamma(t) = \frac{2(\Delta U)^2}{\pi^2}t\,.$$

Thus points on the interface move along circular streamlines and those closest to the point vortex move with greatest angular velocity. The interface becomes "rolled up" to form a spiral structure reminiscent of those observed in mixing layers.
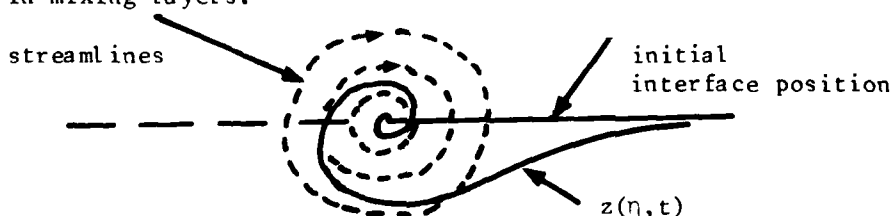
The cross-stream width (2η) of the region occupied by the rolled-up interface also increases linearly with time. Thus, an analogy between these spiral structures produced by a point vortex and those observed in mixing layers would predict that the overall growth of the mixing layer thickness is

$$\frac{\delta}{x} \sim \frac{2\eta}{\frac{1}{2}(U_1 + U_2)t} = \frac{4}{\pi^2} \cdot \frac{\Delta U}{U_1 + U_2} \,.$$

This growth is simply due to growth of individual vortex structures. The coefficient (0.4) is very close to that observed in experiments. However, it is also necessary to consider the interactions of vortex structures with each other.

Jimenez (1980) has also studied the flow induced by placing a row of equally spaced point vortices along a straight line (to be identified with the interface in the mixing layer problem). A velocity difference between fluids is simulated by requiring the strength of each vortex to be $\kappa = \lambda\Delta U$, where λ is the distance between adjacent vortices. The vortices are fixed in space and moving with the mean flow velocity $1/2 \, (U_1 + U_2)$. Summing the logarithmic potentials of the infinite line of vortices gives the complex streamfunction

$$w(z) = \phi + i\psi = \frac{i\kappa}{2\pi} \log \sin(\frac{\pi z}{\lambda}) \,.$$

The complex velocity of any point on the interface is then

$$\frac{dw}{dz} = u - iv = - \frac{i\kappa}{2\lambda} \cot\left(\frac{\pi z}{\lambda}\right) ,$$

so that the position of any point on the interface can be found by solving the equation

$$\frac{dz(t)}{dt} = - \frac{i\kappa}{2\lambda} \cot\left(\frac{\pi z}{\lambda}\right) .$$

The solution shows that the streamlines take the shape of the broken lines in the sketch, and the interface "rolls-up" about the closest vortex. The resulting
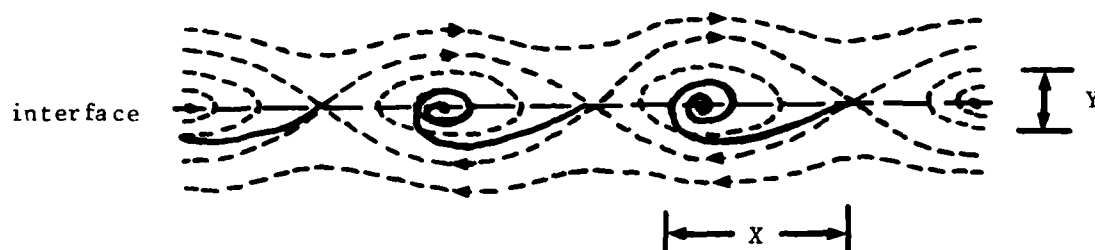
structure has an aspect ratio X:Y that varies in time. Because both scales X and Y increase toward upper limits (determined by the vortex spacing), the area occupied by the spiral structure, $\sigma \sim XY$, also tends toward a well-defined upper limit.

However, there is no reason why the point vortices should be fixed relative to each other. Suppose a small perturbation is imposed on their initial positions so that the vortices lie at the points

$$x_m (t = 0) = m \lambda + \beta \lambda , \quad m \text{ odd}$$

$$= m \lambda \quad , \quad m \text{ even}$$

$$y_m (t = 0) = 0,$$

where $\beta \ll \lambda$. Then relative motion of the vortices ensues.
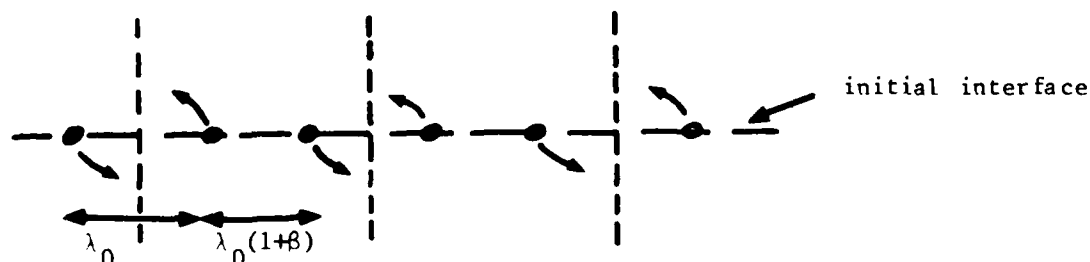
Each vortex moves on an elliptic path, and so each pair must reach a "point of closest approach" when odd and even numbered vortices lie on a vertical line. This occurs at a time θ_o , where

$$\theta_o = \frac{4\lambda K}{\pi \Delta U} , \qquad K \approx -\log 2\beta .$$

Pairing, or coalescence, of vortices is assumed to occur at this time. The distance between the new, larger vortices will be 2λ , and the whole pairing process is free to recur. If the initial vortices were the zeroth generation, then the nth generation vortices will be at a distance $2^n\lambda$ apart and will pair at a time $\theta_n = (1 + 2 + 2^n + \ldots + 2^{n-1})\theta_o$. From this, the lifetime of an individual vortex structure in the nth generation can be shown to approach the value

$$\frac{\text{lifetime of vortex}}{\text{birthtime of vortex}} \quad \to \quad 1 \qquad \text{as} \quad n \to \infty .$$

Some observations of mixing layers by Roshko (1976) and Hernon (   ) have given the values 0.43 and 0.89, respectively, for this ratio of time scales.

The area occupied by the "rolled-up" structure at the beginning of the $(n + 1)^{st}$ generation of vortices will be given by

$$\sigma_{n+1} = 2(1 + \alpha)\sigma_n ,$$

where σ_n is the area covered at the beginning of the nth generation. The factor α^n includes the influence of the growth of the nth generation structures during their lifetime, as well as any deviation from a simple area doubling when two equal sized vortices coalesce. A normalized area may be defined as

$$S_{n+1} = \frac{\sigma_{n+1}}{(2^{n+1})^2} ,$$

so that

$$S_{n+1} = \frac{1}{2}(1 + \alpha)S_n .$$

By making a suitable renormalization of the area (multiplying by $2/1+\alpha$) after each pairing, Jimenez (1980) obtained a limit cycle for the sequence of successive areas.

An analogy can now be drawn between the observed pairing of vortex-like structures in mixing layers and the pairing of point vortices. This suggests that the mixing layer thickness should increase with distance from the splitter plate according to

$$\frac{\delta}{x} = \frac{Y_L \Delta U}{k(U_1 + U_2)} ,$$

where the distance is again given by $x = 1/2 \, (U_1 + U_2)t$ and Y_L is a constant. This predicts the observed linear growth and dependence upon ΔU.

REFERENCES

Browand, F. K. and T. R. Troutt, 1980. A note on spanwise structure in the two dimensional mixing layer. J. Fluid Mech., 97, 771-782.

Brown, G. and A. Roshko, 1974. On density effects and large structure in turbulent mixing layer. J. Fluid Mech., 64, 775-816.

Dimotakis, P., 1980. Preprint.

Helmholtz, H. von, 1868. Ueber discontinuirliche Flussigkeitsbewegungen. Phil. Mag.

Lamb, H., 1916. Hydrodynamics. Cambridge Univ. Press.

Roshko, A., 1976. Structure of turbulent shear flows. AIAA Jour., 14, 1349-1357.

Notes Submitted by
J. Meiss

BOUNDARY LAYERS AND TURBULENT SPOTS

Joseph B. Keller

LECTURE #2.

Turbulent spots in boundary layers are the analogs of the vortex structures observed in mixing layers. The net effect of observations of these "coherent features" has been to reintroduce fluid dynamics into the theory of turbulence. Theorists must now develop dynamical models of these flows which are, in some sense, embedded in turbulence.

We begin by recalling some properties of boundary layers. For the Eulerian fluid equations

$$\underset{\sim}{u}_t + (\underset{\sim}{u} \cdot \nabla)\underset{\sim}{u} = -\nabla p \, , \tag{1a}$$

$$\nabla \cdot \underset{\sim}{u} = 0 \tag{1b}$$

governing fluid flow in some region D, the appropriate boundary conditions are that the fluid velocities normal to the boundary vanish

$$\underset{\sim}{u} \cdot n = 0 \text{ on } \partial D \, . \tag{2}$$

The Navier-Stokes (N-S) equations - when the viscous term, $\nu\Delta\underset{\sim}{u}$, is added to the righthand side of (1a) - are a higher order system and the boundary condition (2) must be supplemented by the requirement that the tangential velocities also vanish

$$\underset{\sim}{u}\cdot\hat{t} = 0 \text{ on } \partial D \ . \tag{3}$$

The limit of vanishing viscosity is therefore a singular limit for the N-S equations, and it is not obvious how to treat the tangential boundary condition in this case. If this condition were applied to the Euler equations there would, in general, be no solution.

In 1903 Prandtl investigated this problem and thus began the theory of singular perturbations. He postulated that in the limit $\nu \rightarrow 0$ the solution to the N-S equations approaches the Eulerian one everywhere except within a vanishingly small layer near the boundaries. To analyze this boundary layer, where viscosity dominates, he introduced a simplified set of equations assuming that the boundary layer is so thin that longitudinal derivatives are small compared to transverse derivatives. In 1907 Blasius found a similarity solution to these equations for uniform flow along a flat plate, reducing the problem to a single nonlinear ordinary differential equation. This equation must be solved with boundary conditions both at the surface and far from the surface, where the Eulerian solution is valid. Without a computer the solution of the Blasius equation is difficult; however, it is interesting to note that in 1941 Weyl developed an iterative technique for this purpose. The Blasius solution is the standard laminar boundary layer when the external stream velocity is uniform. A slightly more general case, when the external velocity varies as a power of downstream distance, was studied by Falkner and Skan (1930).

In the 1920's Heisenberg studied the stability of the Blasius boundary layer. Tollmien and Schlichting concluded this work in 1935. They assumed a perturbation to the boundary layer solution of the form

$$\phi(y)e^{i(kx-\omega t)} \ , \tag{4}$$

where x is the longitudinal and y is the normal coordinate. For certain wave numbers and a range of Reynolds number, they showed that there is temporal instability. (Here is another problem where it would be more appropriate to study spatial instability). If the perturbation varies in the transverse (z) direction then, as Squires has shown, instability sets in at a higher Reynolds number than before. Therefore, a study of two dimensional perturbations is sufficient to find the onset of instability. In the 1940's Schubauer and Skramstad demonstrated the existence of the Tollmien-Schlichting waves. In their experiments a vibrator was inserted into the boundary layer with the appropriate real frequency to excite the instability. (Note again, that it is spatial instability that is being observed.) These experiments led to the supposition that these waves are involved in the transition to a turbulent boundary layer. Turbulence may occur when the waves reach sufficient amplitude to "break". Measurements of the wave amplitudes show that typically growth occurs by a factor of e^9 to e^{11} before the boundary layer becomes turbulent.

In 1951 Emmons discovered that just before the transition point, localized spots of turbulence could be observed. These spots probaly play a role in the breakdown of the laminar flow. Emmons' student Mitchner (1954) examined these further and Schubauer and Klebanoff also reported observations in 1955. Observations of the flow by Elder in 1960 showed that if a thin layer of dye was placed along the plate, then some of it would become entrained by the spots. The impact of these experiments was small until the 1964-67 observations by Kline and Reynolds. They claimed to observe these same spots in the turbulent boundary layer itself.

Since this time there have been many quantitative measurements due to the development of laser-Doppler velocity measuring techniques. The 1976 measurements of Wygnanski revealed the 3-D structure of these spots and in 1978 Cantwell, Coles and Dimotakis examined the flow in the symmetry plane of the spot. All of these observations were done with artifically generated spots in a laminar boundary layer.

The experimental apparatus was a water tunnel with uniform flow in the x-direction. A laminar boundary layer is formed on a plate inserted in the flow. Spots are generated by perturbing the flow with a pulse of water from a nozzle near the head of the plate. The spots grew linearly in size with distance downstream after an initial region of more rapid growth. Linear growth continued over a large distance until (presumably) viscous effects become important and the growth rate declined (see Fig. 1).
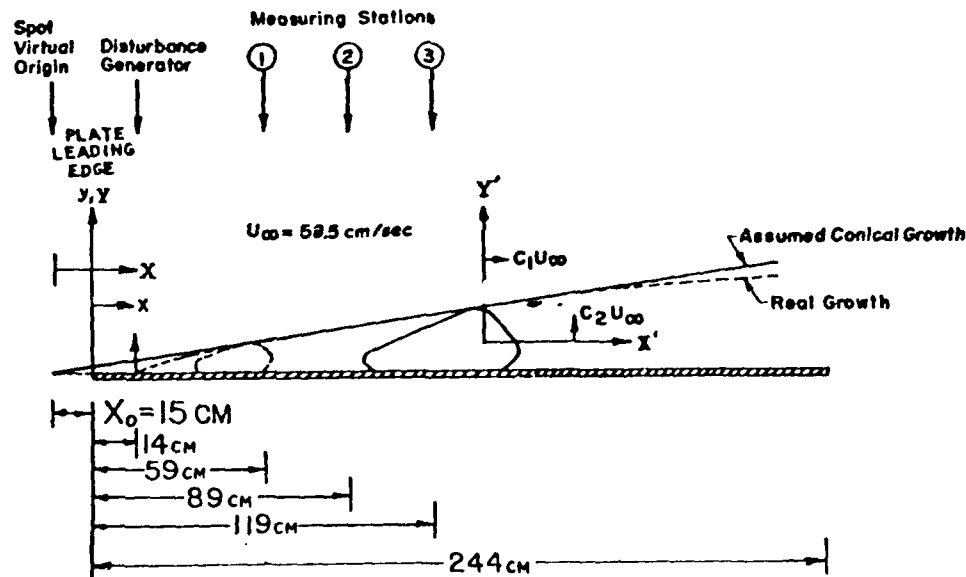
Fig. 1. Sketch of Cantwell, Coles, and Dimotakis (1978) Experiment.

The plan view of the spots show that they develop a characteristic arrowhead shape. In the photograph, dye that was placed in a thin layer next to the plate was swept into, and entrained by, the spot leaving a clear region behind.

In the Cantwell, Coles and Dimotakis experiment a laser was positioned at three positions along the plate ($x = 19$, 59 and 119 cm) pointing in the z direction and focussed on the symmetry plane of the spot. Measurements of the streamwise velocity as a function of y showed that near the plate the spot enhanced the unperturbed velocity while far from the plate the velocities were reduced. This suggests a vortical nature for the flow in the spots.

While the velocity profile for an individual spot contains large wiggles, an average over an ensemble of spots produces a smooth velocity profile.

With these profiles it is possible to follow the evolution of features on the profile moving downstream. This analysis shows that the velocity scales as

$$v = f(x/t, y/t) ,\qquad(5)$$

with high accuracy.

Wyganski showed that in the symmetry plane of the spot $w_z = 0$, so the continuity equation becomes $u_x + v_y = 0$ in that plane. Therefore, a stream function, ψ , can be introduced in the x, y plane with $\psi_y = u$ and $\psi_x = -v$. The conical scaling of v given above implies that

$$\psi = tg(x/t, y/t) .\qquad(6)$$

This is a consistent form for solution to Euler's equations in 2-dimensions. The streamline patterns of the spot show closed streamlines, and an integration of the fluid particle trajectories shows that some particles are indeed entrained by the flow. The streamline patterns show that the center of the spot moves at .78 times the free stream velocity.

Wyganski's measurements show that there are stream-wise striations in the flow which may be Taylor-Gortler vortices. It appears that a good model for the spot is a horseshoe shaped vortex where the feet of the horseshoe are planted in the generation region. As the head of the horseshoe moves downstream the vortex lines are stretched.

There have not been many theoretical studies of turbulent spots. Theodorsen suggested long before these measurements that horseshoe vortices might play a role in turbulence, and as noted above this appears to be a reasonable model for the spots.

Most of the theoretical work has been linear analysis. In 1960 Kovaszny and Criminale considered a point disturbance to the laminar boundary layer. If a perturbation of the form

$$f(z)e^{i(\omega t - k_x x - k_y y)}\qquad(7)$$

is assumed then an ordinary differential equation for f (the Orr-Sommerfeld equation) can be obtained. A Fourier integral of these solutions can be used to describe the flow due to an initial point disturbance. This solution shows that a kidney shaped region develops downstream from this disturbance. This may be the initial stage of a turbulent spot.

Additional work along these lines was done by Gasster and Grant (1975). They treated both stable and unstable boundary layers.

The only nonlinear case so far treated was by Landahl (1979). He studied short linear waves growing on large waves and inducing an instability.

Extensive numerical computations have been done by Leonard (1978-80). He represented the inviscid flow by an array of vortex lines aligned in the z direction. A small localized wiggle was put on some of the lines and allowed to propagate. The equations of motion for a point x_i (ξ) on the ith vortex line at a distance ξ along the line are given by

$$\frac{\partial}{\partial t} x_i(\xi) = -\frac{\Gamma_i}{4\pi} \sum_j \Gamma_j \int d\xi' \frac{(x_i - x_j) \frac{\partial x_j}{\partial \xi'}}{[|x_i - x_j|^2 + \alpha(\sigma_i - \sigma_j)^2]^{3/2}} . \quad (8)$$

Here Γ_i is the strength of the vortex line and σ_j represents the radius of the core. The constant α is empirically adjusted to obtain the correct velocity for the known ring vortex solution. This constant is an ad hoc computational device to avoid singularities when two vortex lines are close together. Leonard has produced a movie of the evolution of this system showing the generation of a horseshoe shaped region which is suggestive of the experimental measurements.

Let us now suppose that a turbulent flow is composed of a collection of spots. *Consider, for example, the flow through a cylindrical pipe with axis in the z direction.* Assume that the fluid velocity and pressure can be written as a sum of contributions due to individual spots.

$$u = \sum_{i=1}^{N} u^i , \qquad P = \sum_{i=1}^{N} P^i , \quad (9)$$

where N represents the number of spots. Each spot is assumed to satisfy the N-S equations

$$u_t^i + (u \cdot \nabla) u^i = -\nabla p^i + \nu \Delta u^i , \quad (10)$$

$$\nabla \cdot u^i = 0 , \quad (11)$$

$$u^i = 0 \text{ on } \partial D . \quad (12)$$

Note, however, that the full fluid velocity is retained in the nonlinear term so that no approximation is made.

The velocity profile of each spot may have a rapidly varying or stochastic part as well as a mean component. Of course, we do not know the form of this profile although experimental measurements could be used. In any case, suppose that the functional form of the spot is universal

$$u^i = U(x-x^i, t-t^i, s) , \quad (13)$$

$$p^i = P(x-x^i, t-t^i, s) . \quad (14)$$

Here, $\underset{\sim}{U}$ and P are universal functions and (x^i, t^i) represent the position and time where the ith spot forms. We suppose that this formation takes place on the pipe boundary and therefore if the pipe is not circular, the functions $\underset{\sim}{U}$ and P will depend on the parameter s, which indicates the arc position of formation on the pipe boundary.

The idea is to attempt a self-consistent formulation where the equations for determination of U and u are intertwined. To this end, we define the mean fluid velocity by

$$\underset{\sim}{\bar{u}}(x,y) = \lim_{\substack{T\to\infty \\ L\to\infty}} \frac{1}{LT} \int_{-L/2}^{L/2} \int_{-T/2}^{T/2} u(x,y,z,t)dt\,dz , \tag{15}$$

where we average over downstream position as well as time. Now we substitute into Eqn. (15) the assumed form (9) and (13) for U, and introduce the spot number density: n(s) = number of spots per unit arc length per unit distance downstream per unit time. Then n(s)LT is the number per unit arc length in a section of pipe of length L during time T, and Eqn. (15) becomes

$$\underset{\sim}{\bar{u}}(x,y) = n(s) \int_{-\infty}^{\infty} \int_{-\infty}^{\infty} \underset{\sim}{U}(x-x_0(s),y-y_0(s),z,t,s)dt\,dz . \tag{16}$$

For a circular pipe, $\underset{\sim}{U}$ is independent of s. In this case we integrate the above equation over $s = ad\theta$ obtaining

$$\underset{\sim}{\bar{u}}(r) = na \int_{-\infty}^{\infty} \int_{-\infty}^{\infty} \int_{0}^{2\pi} U(r,\theta,z,t)d\theta,dt,dz . \tag{17}$$

Here $\underset{\sim}{U}(r,\theta,z,t)$ represents the velocity in a spot born at $r = a, \theta = z = t = 0$. Similarly the pressure gradient is given by

$$\bar{P}_z(r) = na \int_{-\infty}^{\infty} \int_{0}^{2\pi} [P(r,\theta,+\infty,t) - P(r,\theta,-\infty,t)]d\theta dt$$

$$= 2\pi na \int_{-\infty}^{\infty} [P(+\infty,t) - P(-\infty,t)]dt \tag{18}$$

where the righthand side contains the pressure drop along the pipe, which is independent of r and θ. Therefore, from (18) the local mean pressure gradient and the total pressure drop along the pipe due to one spot determine the number density of the spots.

If the number of spots is large (or infinite as it is in the infinite pipe) then it seems reasonable that the total fluid velocity could be approximated by the mean. Thus, the sum over a great number of spots acts as an averaging. In this case the N-S equation for a spot would become

$$\underset{\sim}{u}^i + (\underset{\sim}{\bar{u}}\cdot\nabla)\underset{\sim}{u}^i = -\nabla p^i + \nu\Delta\underset{\sim}{u}^i ,$$

which is an integro-differential equation for the universal function $\underset{\sim}{U}$. An improved theory could be obtained by replacing $\bar{u}$ by $\bar{\underset{\sim}{u}} + \underset{\sim}{u}^1$, retaining the velocity $\underset{\sim}{u}^1$ of the ith spot itself.

As a computation with this equation one could assume that $\bar{u}$ is given by the experimentally measured profile and that at $t = 0$ $u^1 = \overset{\sim}{} \delta^3 (x-x^i)$. In this case would the $\bar{u}$ obtained from computation of u^1 be approximately the same as the assumed ~profile? Perhaps an iterative ~technique could be developed.

This theory does not account for the triggering mchanism for the spots. The computations of Landahl show how new spots could be triggered by the flow field of other developed spots.

In view of its importance, we shall call a turbulent spot a turbulon - an acronym for The Universal Rapid Burst upon Laminar Outer Flow.

REFERENCES

Blasius, 1907. Grenzschichten in flussigkeiten mit kleiner reibung, Berlin.

Cantwell, B., D. Coles and P. Dimotakis, 1978. Structure and entrainment in the plane of symmetry of a turbulent spot. J. Fluid Mech., _87_, 641.

Criminale, W. O. and L. S. Kovasznay, 1962. The growth of localized disturbances in a laminar boundary layer. J. Fluid Mech., _14_, 59.

Elder, J. W., 1960. An experimental investigation of turbulent spots and breakdown to turbulence. J. Fluid Mech. _9_, 235.

Emmons, H. W., 1931. The laminar-turbulent transition in a boundary layer, Part 1. J. Aeron. Sci., _18_, 490.

Falkner, V. M. and S. W. Skan, 1930. Aero. Res. Coun. Rep. and Memo. No. 1314.

Gasster, M. and I. Grant, 1975. An experimental investigation of the formation and development of a wave packet in a laminar boundary layer. Proc. Roy. Soc. Lond. _A347_, 253.

Kline, S. J., W. C. Reynolds, F. A. Schraub and P. W. Runstadler, 1967. The structure of turbulent boundary layers. J. Fluid Mech., _30_, 741.

Landahl, M. T., 1975. Wave breakdown and turbulence. Siam J. Appl. Math., _28_, 735.

Leonard, A., 1980. Vortex simulation of three-dimensional, spotlike disturbances in a laminar boundary layer. In: Turbulent Shear Flows II, Bradbury (ed.) Springer-Verlag.

Leonard, A., 1980. Turbulent structures in wall-bounded shear flows observed via 3-dimensional numerical simulations. Preprint for turbulence conference, Madrid.

Mitchner, M., 1954. Progpagation of turbulence from an instantaneous point disturbance. J. Aeron. Sci. 21, 350.

Prandtl, L., 1904. Ueber Flussigkeitsbewegung bei sehr kleiner Reibung. 1904 Verh. d. III. Int. Math. - Kongress, Heidelberg.

Schubauer, G. B. and P. S. Klebanoff, 1955. Contributions on the mechanics of boundary-layer transition. NAC TN 3489.

Wyganski, I., M. Sokolov, D. Friedman, 1976. On the turbulent 'spot' in a boundary layer undergoing transition. J. Fluid Mech., 78, 785.

Notes Submitted by R. Griffiths

SOLITARY WAVES AND BIFURCATION THEORY

Joseph B. Keller

LECTURE #3

Shallow Water Theory and Solitary Waves Derived by the Scaling Method

The analysis of long waves in shallow water, such as the tides, is usually based upon certain simplified equations called the equations of shallow water theory. These equations are inadequate to describe solitary waves or cnoidal waves, however. Therefore, Boussinesq (1871) derived another set of simplified equations which were adequate to describe such waves. Lord Rayleigh also devised an equation to describe solitary waves, and later Korteweg and DeVries (1895) devised their well known equation which accounts for these waves and their interactions.

The derivations of all these equations were unsystematic. They involved the neglect of some terms and retention of others without a definite basis for estimating their relative sizes. Thus, it was not clear whether or not the derivations were consistent, nor how the equations could be improved upon if that were necessary.

K. O. Frederichs (1948) introduced a new method to derive the equations of the nonlinear shallow water theory in a systematic way. It involved the explicit scaling of horizontal and vertical distances and velocities with different scales. The ratio ε of the vertical scale length to the horizontal scale length was then defined and assumed to be a small parameter. Then all the unknown functions were written as power series in ε, substituted into the equations, and coefficients of each power of ε were equated. In this way, the nonlinear shallow water theory was obtained for the leading terms in the expansion.

When applied to steady progressing waves, the nonlinear shallow water theory yields only two types of solutions: uniform flows and bores. In order to obtain other steady progressing waves, Keller (1948) extended the expansion to higher order in ε, starting with the uniform flow. In that way he obtained the solitary wave as well as the nonlinear periodic waves which are called cnoidal waves. Since then the scaling method has been used to derive the Korteweg-DeVries equation and the equation for solitary internal waves. In fact, it has become a standard tool in fluid dynamics.

A particularly interesting development of this method was made by Shen and Keller (1973). They considered waves which did not have to be plane, in a stratified fluid which could vary in depth and in stratification in both horizontal directions. However, the horizontal variations had a length scale large compared to the length scale of the waves, and the length scale of the waves was large compared to the vertical length scale. From these assumptions, they found that the waves travelled along rays, as in geometrical optics. The wave amplitude satisfied an equation like the Korteweg-DeVries equation along these rays. Thus, the theory of these waves combines the essential feature of short waves, i.e., propagation along rays, with the finite amplitude effects usually associated with long waves.

Solitary Waves Derived via Bifurcation Theory

Keller's (1948) derivation of the solitary and cnoidal waves leads to an interpretation of these waves in terms of bifurcation theory. There is a family of solutions, the uniform flows, which exist for every flow speed. At the critical flow speed $(gH)^{1/2}$ another family of solutions branches off from this family. It is the family of cnoidal waves parameterized by a wavelength, an amplitude, and a phase. The infinite wavelength members of this family are the solitary waves.

There is also another way of viewing the occurrence of a solitary wave as a bifurcation phenomenon. It is based upon the fact that the solitary wave solution tends to a uniform flow at $x = -\infty$. Thus, by considering a steady flow as evolving in the direction of increasing x, we see that two different flows can evolve from a uniform flow at $x = -\infty$. One is the uniform flow itself, and the other is a solitary wave of arbitrary phase.

In order to make this description more explicit, let us consider the amplitude A(t) of any unstable motion of a dynamical system. Linear theory yields for the evolution of A, an equation of the form

$$A_t = \alpha A .$$

(1)

Because the growth rate α is positive, this equation predicts unbounded exponential growth. However, as Landau pointed out, nonlinear terms will ultimately become important enough to limit the growth of A. Therefore he proposed that Eqn. (1) should be replaced by

$$A_t = \alpha A - \beta A^3 .$$

(2)

The coefficients α and β can be obtained from the original problem governing the field of which A is the amplitude. For example, let us suppose that the field u(t,x) satisfies the equation

$$u_t = F(u) .$$

(3)

Let $\phi(x)$ be the most unstable mode of the equation linearized about the steady solution $u_o(x)$ for which $F(u_o) = 0$. Then we write

$$u(t,x) = u_0(x) + A(t)\phi(x) .$$

(4)

By substituting Eqn. (4) into Eqn. (3) and taking the inner product of the resulting equation with ϕ , we get

$$A_t = \frac{<\phi, F(u_0 + A\phi)>}{<\phi, \phi>} \tag{5}$$

Upon expanding the right side of Eqn. (5) in a Taylor series, and keeping terms up to order A^3 we get Eqn. (2), provided that the quadratic term vanishes. In this way, we find explicit expressions for α and β .

Each solution of the Landau equation grows from zero at $t = -\infty$ to $\pm (\alpha/\beta)^{1/2}$, except for the solution $A(t) \equiv 0$. Thus the solutions bifurcate from $A = 0$ at $t = -\infty$. If we interpret t as a space variable, the Eqn. (2) describes the spatial growth of a disturbance. By interpreting shock waves in this way, we have been able to analyze weak shocks governed by the Boltzmann equation as well as by the Navier-Stokes equations. The shock solutions bifurcate from a sonic flow at $x = -\infty$.

The preceding considerations, based upon the Landau equation (2), show why the profile shown in Figure 1 is of such common occurrence in nonconservative systems. We shall now examine the analogous equation for the amplitude of motion of a conservative system. Let us begin with the energy equation, which we assume to be of the form

$$A_t^2 + V(A) = E . \tag{6}$$

Here V is the potential energy and E is the total energy. We suppose that $A = 0$ is a state of rest so that $V(0) = E$ and $V_A(0) = 0$. Then we write

$$E - V(A) = \alpha^2 A^2 - \beta A^3 + \cdots . \tag{7}$$

Now omitting the higher order terms, we can rewrite Eqn. (6) in the form

$$A_t = [\alpha^2 A^2 - \beta A^3]^{1/2} . \tag{8}$$

This equation replaces the Landau equation for conservative systems.

Each solution of Eqn. (8) which starts at $A = 0$ when $t = -\infty$ increases until $A = \alpha^2/\beta$. (See Fig. 2.) Then if $A(t)$ has a continuous second derivative, the solution decreases to $A = 0$ at $t = +\infty$. When we interpret t as a space variable, these solutions are solitary waves. They differ from one another only by a phase shift. This analysis indicates why solitary waves are so prevalent. When $V(0) \neq E$, Eqn. (6) describes periodic waves, such as the cnoidal waves.

REFERENCES

Boussinesq, J., 1871. Theorie de L'intumescence liquide appelee onde solitaire ou de translation se propageant dans un canal rectangulaire. Comptes Rendus, 72, 755-759.

Frederichs, K. O., 1948. On the derivation of the shallow water theory. Appendix to J. J. Stoker, Breakers and Bores, Communications on Pure and Applied Mathematics, 1.

Keller, J. B., 1948. Solitary waves and periodic waves in shallow water. Communications on Pure and Applied Mathematics, 1.

Rayleigh, Lord, 1916. See H. Lamb, "Hydrodynamics", Cambridge Univ. Press.

Shen, M. C. and J. B. Keller, 197 .

Notes Submitted by
R. Griffiths and J. Meiss

NON-LINEAR EQUATORIAL WAVES

John P. Boyd

Using the method of multiple scales, I show that long, weakly nonlinear equatorial Rossby waves are governed by either the Korteweg-deVries (KdV) equation (symmetric modes of odd mode number n) or modified Korteweg-deVries (MKDV) equation. From the same localized initial conditions, the nonlinear and corresponding linearized waves evolve very differently. When nonlinear effects are neglected, the whole solution is an oscillatory wave-train which decays algebraically in time so that the symptotic solution as $t \to \infty$ is everywhere zero. The nonlinear solution consists of two parts: solitary waves plus an oscillatory tail. The solitary waves are horizontally localized disturbances in which nonlinearity and dispersion balance to create a wave of permanent form.

The solitary waves are important because (i) they have no linear counterpart and (ii) they are the sole asymptotic solution as $t \to \infty$. The oscillatory wave-train, which lags behind and is well-separated from the solitary waves for large time, dies out algebraically like its linear counterpart, but the leading edge decays faster rather than slower than the rest of the wave-train. Graphs of explicit case studies, chosen to model impulsively excited equatorial Rossby waves propagating along the thermocline in the Pacific, illustrate these large differences between the linearized and nonlinear waves. The case studies suggest that Rossby solitary waves should be clearly identifiable in observations of the western Pacific.

DYNAMICS AND STATISTICS OF POINT VORTICES

Hassan Aref

The motion of N point vortices in a plane was considered for $1 \leq N \leq O(10^4)$. The system is integrable for N = 1, 2, 3 (Novikov, 1975 and Aref, 1979). For NN = 4 stochasticity sets in (Novikov and Sedov, 1978, 1979 and Aref and Pomphrey, 1980). Numerical experiments revealing chaos were

described and the result was related to the question of predictability of two-dimensional fluid motions and to the ideas of KAM theory.

For $N \cong O(10)$ configurations of identical vortices in uniform rotation were sought. The classical results were reviewed and the recent numerical study by Campbell and Ziff (1979) mentioned. Results of some recent work in collaboration with F. Calogero was briefly touched upon.

For $N \gtrsim O(100)$ the detailed motion of every single point vortex is of little interest and the emphasis is on using the point vortices as a convenient discretization of the continuum equations (the two-dimensional Euler equation). The Brown and Roshko (1974) structure of the shear layer provided the motivation to do a large scale numerical study of this problem (Aref and Siggia, 1980a). In the simulation discussed 4096 point vortices were followed in time using the vortex-in-cell algorithm of Christansen (1973) with a 256x256 background grid. A lengthy exposition of the conclusions would be out of place here and the reader is referred to our paper.

More recently we have considered the evolution of two parallel rows of oppositely signed vortices (Aref and Siggia, 1980b). Depending on the symmetry of the initial perturbation the flow evolves either toward a two-dimensional wake or jet. From the large number of pictures shown we select Figure 1 which illustrates the pairing of vortex structures in a plane jet. Each dot corresponds to a point vortex; the bottom ones are all positive, the top ones all negative. The large, diffuse vortex blobs are our "coherent structures" and the pairing interaction is a basic mechanism in the evolution (Winant and Browand, 1974; Crow and Champagne, 1971).

REFERENCES

Aref, H.,, 1979. Phys. Fluids, 22, 393.

Aref, H. and N. Pomphrey, 1980. Integrable and chaotic motions of four vortices. Phys. Lett. A (to appear).

Aref, H. and E. D. Siggia, 1980a. Vortex dynamics of the two-dimensional turbulent shear layer. J. Fluid Mech. (to appear).

Aref, H. and E. D. Siggia, 1980b. Evolution and breakdown of a vortex street in two dimensions. Cornell preprint.

Brown, G. L. and A. Roshko, 1974. J. Fluid Mech., 64, 775.

Campbell, L. J. and R. M. Ziff, 1979. Phys. Rev., B20, 1886.

Christiansen, J. P., 1973. J. Comp. Phys., 13, 363.

Crow, S. C. and F. H. Champagne, 1971. J. Fluid Mech., 48, 547.

Novikov, E. A., 1975. Sov. Phys. - JETP, 41, 937.

Novikov, E. A. and Yu. B. Sedov, 1978. Sov. Phys. - JETP, 48, 440.
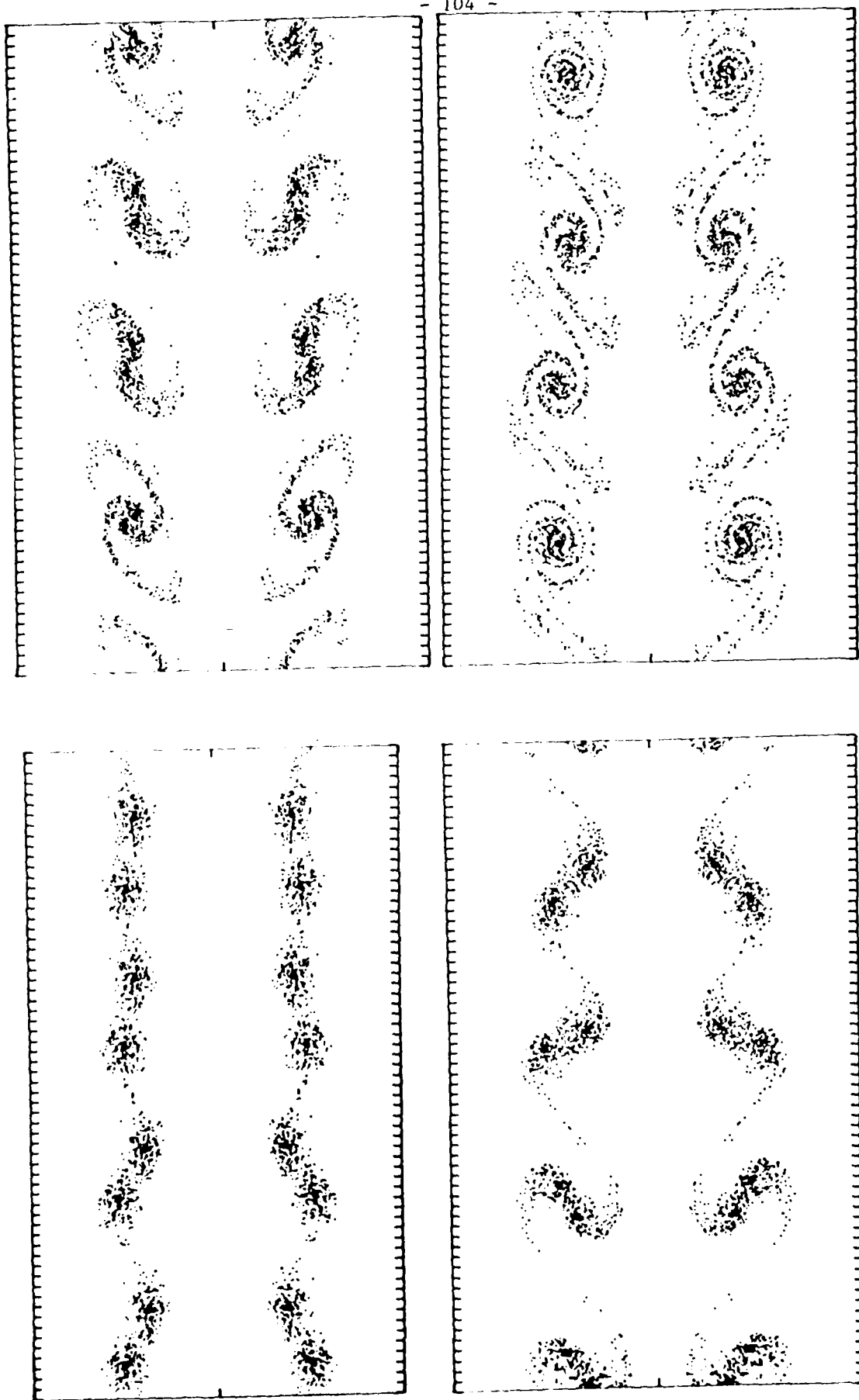
Fig. 1. Vortex pairing in a plane jet (from Aref and Siggia (1980b)).

Novikov, E. A. and Yu. B. Sedov, 1979. JETP Lett. 29, 677.

Winant, C. D. and F. K. Browand, 1974. J. Fluid Mech., 63, 237.

CANONICAL EQUATIONS FOR SLOWLY VARYING SOLITARY WAVES

Roger Grimshaw

A general theory is developed for the evolution of a dispersive and weakly nonlinear wave packet in an inhomogeneous medium. The wave packet propagates along rays determined by the linear dispersion relation, and the equation describing the evolution of the wave amplitude A along a ray is obtained. For unidirectional modulations the equation is the nonlinear Schrodenger equation

$$ i\, \frac{\partial A}{\partial s} + \sigma\, \frac{\partial^2 A}{\partial \xi^2} + \nu |A|^2 A = 0, $$

with appropriate generalization for multi-dimensional modulations. Here the coefficients σ , ν are functions of s alone, s is a time-like coordinate which varies along a ray, and ξ is a coordinate which is constant along a ray, but whose spatial projection defines the spatial direction of wave propagation. $|A^2|$ is the wave action flux along a ray if there is no dissipation in the system. The scaling required to produce this equation scales s with a^{-2}, ξ with a^{-1} and the inhomogeneous medium with a^{-2}, where a is a small parameter measuring amplitude.

Plane wave solutions of the nonlinear Schrodinger equation are unstable when $\sigma \nu$ 0, but it will be shown that for long waves σ and ν necessarily have opposite signs. For the case $\sigma \nu > 0$, and both constant, there is a solitary wave solution. The behavior of this solitary wave is described when σ and ν are not constant, but vary slowly with respect to the solitary wave. The principal result here is that the solitary wave deforms so that $A^2 \sigma \nu^{-1}$ remains constant. Also, for some special forms of σ, ν there exist transformations which convert the variable coefficient equation into a constant coefficient equation.

For long waves a related theory is developed to describe the evolution of a weakly nonlinear wave in an inhomogeneous medium. The wave propagates along rays determined by the linear long wave dispersion relation. The equation describing the evolution of the wave amplitude A along a ray is the Korteweg-de Vries equation

$$ \frac{\partial A}{\partial s} + \lambda \frac{\partial^3 A}{\partial \theta^3} + \mu A \frac{\partial A}{\partial \theta} + B = 0 $$

$$ \frac{\partial B}{\partial \theta} = \sigma \frac{\partial^2 A}{\partial \eta^2} $$

Here the coefficients λ , μ , and σ are functions of s alone, s is a time-like coordinate which varies along a ray, θ is a phase variable, and η is a coordinate transverse to a ray. A^2 is the wave action flux along a ray if there is no dissipation in the system. The scaling required to produce this equation scales s with a^{-3}, θ with a^{-1}, η with a^{-2}, the inhomogeneous medium with a^{-3}, where a is a small parameter measuring amplitude. The behavior of the solitary wave solution is described when λ and μ are not constant, but vary slowly with respect to the solitary wave.

The principal results here is that the solitary wave deforms so that
$A^{3/2}\lambda\mu^{-1}$ remains constant, with a shelf developing behind the wave.

UNSTABLE VORTICES IN A ROTATING, TWO-LAYER FLUID

R. W. Griffiths

There are a number of geophysically important situations in which surfaces
of constant density, under the influence of the Coriolis force due to the
Earth's rotation, intersect one horizontal boundary and in which the fluid
motion is not constrained by rigid vertical walls. Isolated eddies, con-
taining closed streamlines and with horizontal length scales of the order of
10^2 km, are found at the surface in many parts of the oceans. More
rectilinear frontal zones between air or water masses of unequal density,
intersecting the free surface of the ocean or the rigid bottom boundary of the
atmosphere, also exist far away from vertical boundaries.

In the laboratory, density fronts can be established in an axisymmetric
configuration. We released either a constant flux of fluid from a point
source or a constant volume of fluid into a rotating environment with a
different density. In the constant volume experiments, fresh water was placed
inside a bottomless cylinder which was surrounded by a homogeneous layer of
salt solution. After the system was brought to solid body rotation, the
cylinder was carefully removed. The buoyant fluid then collapsed and spread
radially until it reached a state in which the radial pressure gradient, due
to buoyancy forces, is balanced by the Coriolis and centrifugal forces. The
resultant anticyclonic vortex was always unstable to wave-like azimuthal
disturbances, and broke up into a well-defined number of smaller vortices. In
the point source experiments the source was placed at the free surface and the
resulting anticyclonic vortex grew continuously with time. It reached a
critical size at which the flow became non-axisymmetric.

The transition to non-axisymmetric flow can be described by two
parameters: θ, the square of the ratio of the internal Rossby radius of
deformation to the horizontal length scale of the flow, and δ , the fraction
of the total fluid depth occupied by the layer inside the front. For $\theta \ll 1$
and $\delta > 10^{-1}$ unstable disturbances obtain most of their energy from the
potential energy of the flow, whilst for $\delta < 10^{-1}$ extraction of kinetic
energy from the basic shear becomes the dominant driving mechanism. When δ
is not too small in the point source experiments, we observe an azimuthal
disturbance whose phase increases with depth, a characteristic feature of
baroclinically unstable waves. When the front intersects the free surface (as
opposed to the rigid bottom of the tank) n = 2 is the minimum azimuthal wave
number for an unstable disturbance.

At large amplitude of the growing waves, baroclinic and barotropic
processes combine to form n vortex dipole structures which entrain buoyant
fluid from the original vortex and propagate radially over the free surface.
The relative strengths of the paired cyclone and anticylone appear to depend
upon the ratio, δ , of layer depths. Also, the anticyclones are confined to
the upper layer, while the cyclones extend throughout the depth of the tank

(at least for δ not too small). The vortex pairs are long-lived features and eventually dissipate their energy due to friction.

REFERENCE

Griffiths, R. W. and P. F. Linden, 1980. The stability of vortices in a two-layer, rotating fluid. J. Fluid Mech. (to appear).

EVOLUTION OF LONG NONLINEAR WAVES IN STRATIFIED SHEAR FLOWS

Roger Grimshaw

There are now a number of reports of long nonlinear internal gravity waves occurring on the thermocline in inland lakes, fjords or coastal waters, or on the nocturnal inversion in the atmosphere. When these long waves can be identified as solitary waves, the appropriate equation to model their evolution in the first instance is either the Korteweg-de Vries (KdV) equation when the horizontal wave-guide has limited vertical extent, or the Benjamin-Davis-Ono (BDO) equation for a deep fluid. Here these equations are derived for the case when the waves are propagating on a basic stratified shear flow.

The basic state, as well as having the usual dependence on the vertical coordinate which defines the wave modal structure, is allowed a slow variation in the horizontal and temporal coordinates. The waves then propagate along rays defined by this basic state, and the evolution equations, either KdV or BDO, describe the evolution of the wave action flux as the wave propagates along the ray. For the KdV equation, if $\mathcal{E}^2$ is a small parameter measuring the amplitude of the vertical particle displacement, the phase of the waves varies on the scale $\mathcal{E}^{-1}$, while the evolution of the wave and the basic state vary on the scale $\mathcal{E}^{-3}$. For the BDO equation, $\mathcal{E}$ measures the amplitude of the vertical particle displacement, the phase varies on the scale $\mathcal{E}^{-1}$, and the evolution of the wave and the basic state vary on the scale $\mathcal{E}^{-2}$. To derive the equations, an operator formalism is developed to handle the analytical complexities, and this formalism may be readily applied to other complex wave systems.

A brief discussion is given of the solutions of each of these equations in three special cases. First, if the coefficients are constant, there is the solitary wave solution, the N-soliton solution and the inverse scattering formalism is available to solve certain initial value problems. Second, the asymptotic solution describing a slowly varying solitary wave is presented; this deforms so as to conserve its energy, and a shelf develops behind the wave so that overall the mass is conserved. Third, it is shown that a solitary wave incident on an abrupt change in the basic state will generally either fission into a number of solitons, or break up into a dispersive wave train.

Both the KdV and BDO equations are restricted to modelling small amplitude waves, whereas observations often show waves of large amplitude. In an attempt to model this, the BDO equation is extended to a higher order in amplitude. Second order in amplitude corrections to the wave speed and wave

length of the solitary wave are computed. In one case of interest, it is found that these second order terms decrease the wave speed relative to the first order theory, and increase the wave length for a given wave amplitude.

Finally, some solitary wave solutions of the full nonlinear equations are presented which are long, but unrestricted in amplitude. The solutions describe the "snake-like" deformation of a thin layer of stratified fluid, separating two regions of constant density. When this thin shear layer has constant Brunt-Väisalä frequency the solitary wave solutions are governed by the steady BDO equation.

SOME NOT-ALTOGETHER-INCOHERENT LARGE STRUCTURE IN TURBULENT CONVECTION AND A NOT-ALTOGETHER-COHERENT MODEL

L. N. Howard

Recent experiments of R. Krishnamurti have found that, in a certain range of Rayleigh number near 10^7, turbulent convection in the Benard configuration is accompanied by a large scale circulation, frequently filling the entire convection box, which appears to persist for long periods (days, in the experiments). These experiments were described in this lecture, together with others designed to investigate various possible perturbing influences which might be conjectured to be responsible for the large scale flow. Lack of proper levelling of the convection tank was, for example, found to have very little effect, even when the tank was tipped (in either direction) to an angle many times any possible experimental uncertainty. Differential heating of the ends of the tank, if large enough, has an effect -- it can reverse the direction of the large scale flow, but the new direction is retained when the differential heating is removed, or even reversed to a limited extent. On the whole it appears that this phenomenon is an au.onomous property of convection whose precise orientation depends on initial circumstances or minor extraneous perturbations, but which, when once established, appears to be fairly stable.

A six-dimensional truncated model illustrating a possible mechanism for this phenomenon has been constructed and explored by Krishmamurti and the speaker. This model contains the Lorenz model on a 3-dimensional invariant subspace, but has the potential of modelling also a large-scale flow. At low Rayleigh number the Lorenz subspace is attracting. Above the critical Rayleigh number at which steady convection sets in, but below the (sub-critical) oscillatory bifurcation of the latter in the Lorenz model, a second bifurcation to stable steady motions not in the Lorenz subspace occurs. These may be described as tilted cells with asymmetry between the clockwise and counterclockwise ones; this gives a non-zero horizontally-averaged horizontal velocity oppositely directed in the upper and lower halves of the layer, but no large scale Lagrangian transport. (We have seen analogs of these steady tilted cells in preliminary qualitative experiments on convection in a Hele-Shaw cell.) At higher R the tilted cell solution (in the mathematical model) undergoes a supercritical Hopf bifurcation to stable periodically oscillating "cells" which do have a net large scale Lagrangian transport. These periodic solutions are suggestive of the large scale motion seen in the turbulent experiments. Further increase of R in the model gives complicated other phenomena including sequences of period-doubling bifurcations,

hysteresis effects, and irregular oscillations. Some of these resemble phenomena familiar in iterations of certain one-dimensional maps, as well as in the Lorenz model, but also exhibit certain significant differences, notably in the hysteresis effects.

I.   ARCTIC OCEAN EDDIES AND BAROCLINIC INSTABILITY

Kenneth Hunkins

Baroclinic eddies with diameters of from 10 to 40 km have been observed in the deep Arctic Ocean north of Alaska. These eddies have a velocity maximum with orbital speeds which may reach 50 cm/s at a depth between 100 and 200 m. From 10 to 20% of the ocean area north of Alaska is covered by these eddies, and they account for almost all of the kinetic energy in the region, completely dominating the mean flow. The water mass within the eddy differs from the surrounding water and points to a source on the Alaskan shelf.

The origin and some of the characteristics of these eddies can be accounted for by the instability of the mean geostrophic shear at the Alaskan shelf edge. A generalized Eady model with exponential mean shear and stratification is applied using ocean parameters appropriate to this region. Small perturbations tend to grow with an e-folding time of 154 days, which is sufficiently short for large amplitude eddies to develop. The half-wavelength of the fastest-growing wave is 37 km in reasonable agreement with the observed eddy diameter. Application of the same model to the West Spitsbergen current between Greenland and Spitsbergen gives a growth rate of 7 days and a half-wavelength of 22 km suggesting that eddies similar to those north of Alaska may be expected on the other side of the Arctic Ocean.

II.   SOLITONS IN SENECA LAKE

During summer and fall when the lake is well stratified, internal surges are often observed traveling from south to north at a speed of 35 to 40 cm/s. Isotherms are as much as 20 m deeper after the surge has passed. The surges are accompanied by a wave train with two distinct parts. First there are a number of vertically coherent waves with broad peaks and sharp troughs, wavelength of about 250 m. This is followed by a train of lower amplitude and less coherent waves. The initial coherent waves are interpreted as the solitons of nonlinear wave theory. Numerical solutions of the Korteweg-deVries equation for an initial pulse are invoked to explain these weakly nonlinear waves.

LONG THERMOHALINE WAVES

E. A. Spiegel

This is an account of a calculation of two-dimensional convection in a plane layer of Boussinesq liquid carried out with S. Childress. The static vertical density contrast is of the form

$$\Delta \ln \rho = (\Delta \ln \rho)_S + (\Delta \ln \rho)_T \leq 0.$$
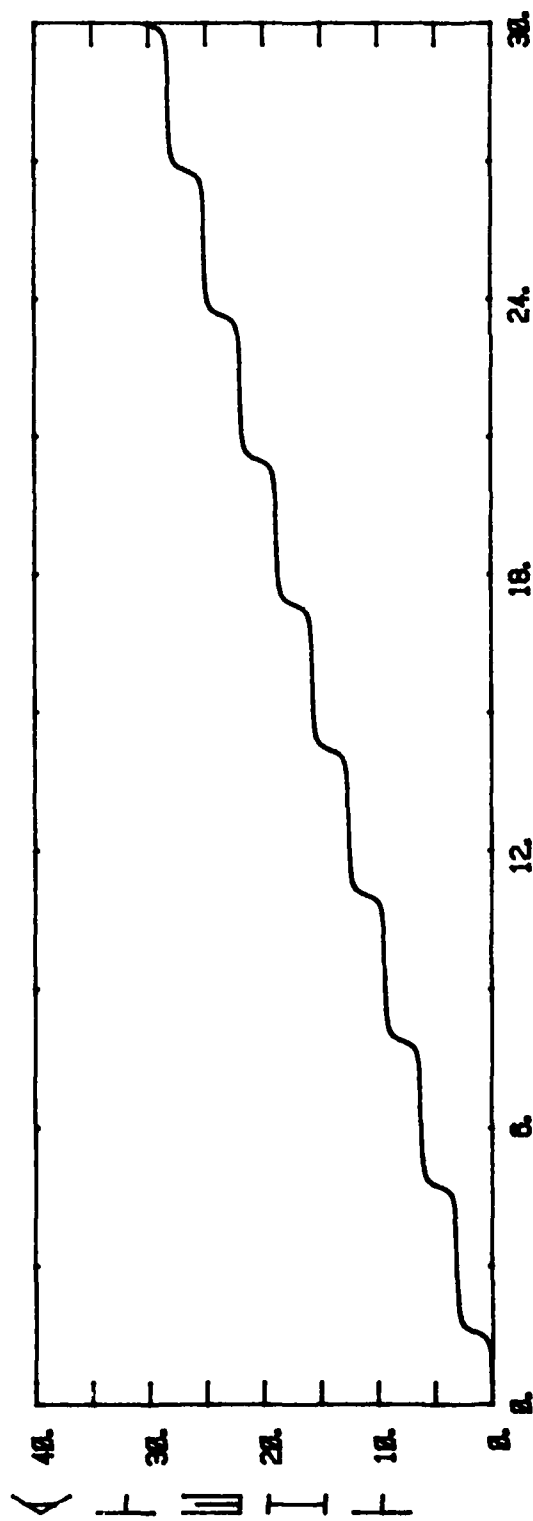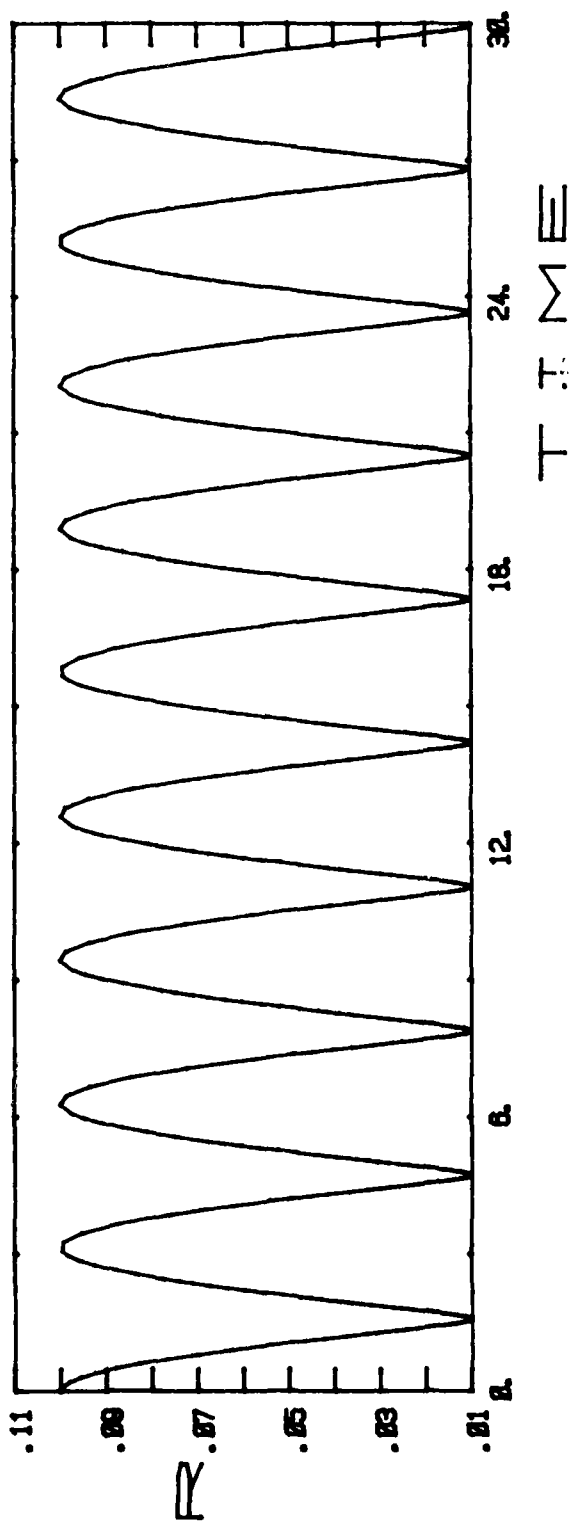
The Rayleigh number we use is

$$R = \frac{gd^3}{\nu}[(\Delta\ln\rho)_S/\kappa_S + (\Delta\ln\rho)_T/\kappa_T].$$

When the fluxes of salinity and heat are prescribed on the upper and lower boundaries, convection first appears t zero horizontal wave number. For small wave number, k, linear theory tells us that steady solutions occur when

$$R = R_o(k) = R_C(1+\alpha k^2),$$

Where R_C is the critical Rayleigh number for the onset of ordinary thermal convection and α is close to unity.

For the nonlinear case we may use a "shallow water" expansion for small amplitude and large horizontal scale. There results the evolution equation

$$f_{tt} - \tau(\frac{R}{R_C}-1)f_{xxxx} - \alpha\tau f_{xxxxxx} - \beta[(f_x)^3]_{xxx} = 0,$$

where

$$\tau = \kappa_T/\kappa_S,$$

$\mathbb{P}$ is nearly unity, and f(x,t) is proportional to the leading expressions for the temperature and salinity perturbations.

Let

$$\delta^2 = \tau(R-R_o)/R_C \ll 1$$

and

$$f = \delta R(\delta t)\sin[kx+\theta(\delta t)].$$

An ODE for R alone is obtained and the behavior shown in the accompanying figure emerges for small δ . The solution is in the form of a wave that hardly progresses for some time, then surges forward. The effort being apparently too great for it, it comes almost to rest, gathers its strength for a while, and then it hurtles forward once more - like progress in GFD.

Nigel Weiss and I have argued that in a suitable extension of the Boussinesq approximation, the equations governing magneto-convection, including the effects of magnetic buoyancy, are the same as those on which the foregoing results are based. Therefore, the figure showing R (δ t) is just an arm wave away from being a theory of the time dependence of the solar cycle. Or it would be if the results of Depassier elsewhere in these proceedings did not indicate that the Boussinesq approximation fails when the convection occurs on sufficiently large horizontal scales.

GULF STREAM AND KUROSHIO CYCLONIC RINGS

Thomas W. Spence

Gulf Stream cyclonic rings are strong mesoscale eddies formed from meanders of the Stream. During the past few years an interdisciplinary program, including biological, chemical, and physical oceanographers was engaged in observation of these features. One particular example (BOB) was observed on several cruises between its formation in February 1977 until its coalescence in September 1977. A summary of some results of the cruise and other measurements was presented, including the work of many investigators.

The CTD data were described insofar as they indicate the mean radially symmetric part of the density field. Quantities derivable from the density were shown; in particular, the velocity and potential vorticity (Olson, 1980). From the spatially distributed XBT data, non-axially symmetric perturbations can be identified and partitioned into modes ($\sim$ sin n θ) with the largest amplitudes in the lowest two modes (n = 1, 2). Mode two amplitude decreases with time and from satellite imaging rotates counterclockwise (Olson and Spence, 1978; Spence and Legeckis, 1980). Some preliminary computations from a numerical ring model with a non Gaussian height field show some similar effects (Smith, 1980). Observations of a cyclonic eddy in the Kuroshio system (Cheney, 1977) provided data for a comparison of features from the two systems. Velocity fields are somewhat stronger in the Gulf Stream ring, and the size is somewhat smaller. Non-dimensional parameters are rather comparable (Hua and Spence, 1980).

REFERENCES

Cheney, R. E., 1977. J. Geophys. Res., 82, 5459-5468.

Hua, G. C. and T. W. Spence, 1980. To be submitted.

Olson, D. B., 1980. J. Phys. Oceanogr., 10, 514-527.

Olson, D. B. and T. W. Spence, 1978. J. Geophys. Res., 83, 4691-4696.

Smith, D. C., 1980. PhD thesis. Texas A&M University.

Spence, T. W. and R. Legeckis, 1980. Submitted to J. Geophys. Res.

INTERNAL WAVE INTERACTIONS IN THE INDUCED DIFFUSION APPROXIMATION

J. D. Meiss

The Induced Diffusion (ID) approximation was introduced into the study of internal waves by McComas and Bretherton (1977). They present numerical computations of action transport rates for Garrett-Munk (1979) action spectra which show that for high frequency, small scale waves the transport is dominated by triads of the ID class; that is, diffusion of action in wave number space for small scale waves is induced by large amplitude, large scale waves with nearly inertial frequency.

The importance of the ID triads was demonstrated quantitatively by Pomphrey, Meiss and Watson (1980). In this paper two Langevin techniques are applied, yielding relaxation equations for wave amplitudes:

$$\frac{d}{d\tau} < a_{\underset{\sim}{k}} > + i \omega_k < a_{\underset{\sim}{k}} > = - \gamma(\underset{\sim}{k}) < a_{\underset{\sim}{k}} > \tag{1}$$

The first method utilizes the fluctuation-dissipation theorem and requires the assumption that the action spectrum, $< J_k >$, is nearly in "equilibrium". The relaxation rate derived by this method is denoted ν_F. A second

relaxation rate, derived by a multiple time scale perturbation theory, is denoted ν_p .

There is a formal relationship between these relaxation rates and the radiative transport equation used by McComas and Bretherton (1977). The transport equation (derived in a geophysical context by Hasselmann, 1967) can be formally written

$$\frac{d}{dt} < J_{\underset{\sim}{k}} > = 2\, \nu_\beta\, (\underset{\sim}{k}) < J_{\underset{\sim}{k}} > \tag{2}$$

The transport rate ν_β is, of course, a complicated functional of the spectrum -- and therefore evolves in time with the spectrum. Comparison of the expressions for the three rates introduced above yields the relationship

$$\nu_\beta = \nu_F - \nu_p \tag{3}$$

An "equilibrium" spectrum has $\nu_B = 0$ by definition. Equation (3) then implies $\nu_F\ \nu_p$. Recalling that the derivation of ν_F required that the spectrum be in equilibrium, we see that the two relaxation rates are equal when this assumption is satisfied.

Pomphrey, Meiss and Watson (1980) give analytic expressions for the rates ν_F , ν_p , and ν_β in the ID approximation. These expressions show that the ID triads dominate the interactions for frequencies $\omega_k > 3f$ and vertical mode numbers $\alpha > 5$. Furthermore, it is just in this region that $|\nu_\beta| << |\nu_p|$, implying that the Garret-Munk (1979) spectrum is nearly in equilibrium.

These calculations also imply, however, that in this region the derivation of Eqn. (1) is invalid. This derivation used a weak nonlinearity assumption which is only valid if

$$\nu(\underset{\sim}{k}) << \omega_k \tag{4}$$

where ω_k is the linear frequency. It is precisely in the ID region where the relaxation rate becomes comparable to the linear frequency.

To attempt to circumvent the weak nonlinearity approximation we consider the ID interactions from a dynamical viewpoint. Assuming that the large scale waves have large amplitudes we drive equations for the small scale waves:

$$\frac{d}{dt} b_{\underset{\sim}{k}} = \sum_{\underset{\sim}{m}} A_{\underset{\sim}{k}}^{\underset{\sim}{m}}(t)\, b_{\underset{\sim}{m}}\; ;\; b_{\underset{\sim}{k}} \equiv a_{\underset{\sim}{k}}\, e^{i\omega_k t} \tag{5}$$

Here the matrix $A_{\underset{\sim}{k}}^{\underset{\sim}{m}}$ depends linearly on the large scale wave amplitudes.

Since the large scale waves have large amplitudes, they are decoupled from the small scale waves. As a simplest model we assume that these waves form a stationary, homogeneous, Gaussian random field. Under these assumptions (Eqn. 5) becomes a stochastic differential equation.

If we make no further approximations, Eqn. (5) cannot be solved analytically, but it can be treated by perturbation theory (Van Kampen, 1974). At this point we note that for the internal wave case

$$A_{\underset{\sim}{k}}^{\underset{\sim}{m}} = f\,(\underset{\sim}{k} - \underset{\sim}{m}) + \mathcal{O}\left(\frac{|\underset{\sim}{k} - \underset{\sim}{m}|}{|\underset{\sim}{k} + \underset{\sim}{m}|}\right)^2 \qquad (6)$$

Since $\underline{k} - \underset{\sim}{m}$ is the large scale wave number, we can neglect the higher order corrections and assume that $A_{\underset{\sim}{k}}^{\underset{\sim}{m}}$ is a function of $\underline{k} - \underset{\sim}{m}$ only.

With this approximation, Eqn. (5) can be solved explicitly yielding

$$\frac{d}{dt} < b_{\underset{\sim}{k}} > = - K_L\,(t) < b_{\underset{\sim}{k}} > \qquad (7)$$

This equation is exact so long as the higher order terms in Eqn. (6) are neglected. Corrections to Eqn. (7) due to these terms can be obtained by Van Kampen's perturbation technique (1974).

In the weak interaction limit, K_L becomes time independent and equal to the relaxation rate ν_p . More generally, however, the relaxation implied by Eqn. (7) is slower than that of Eqn. (1). The effects of nonresonant triads are included in Eqn. (7).

A transport equation, similar to Eqn. (2) may also be derived using this technique. This equation is derived for the second moments $< b_{\underset{\sim}{k}}^* b_{\underset{\sim}{m}} >$. If we assume that the initial condition for the small scale waves is a wave packet, then this transport equation can be Fourier transformed to an equation for the Wigner function, $F(\underset{\sim}{k},\underset{\sim}{x})$.

For more details the reader is referred to Meiss and Watson (1980).

REFERENCES

Garret, C.J.R. and W. H. Munk, 1979. In: Ann. Rev. Fluid Mech. Van Dyke, Wehausen and Lumley (eds.).

Hasselmann, K., 1967. Proc. Roy. Soc. Lon. A299, 77.

McComas, C. H. and F. P. Bretherton, 1977. J. Geophys. Res. 82, 1397.

Meiss, J. D. and K. M. Watson, 1980. Internal wave interactions in the induced diffusion approximation. (Preprint)

Pomphrey, N., J. D. Meiss and K. M. Watson, 1980. J. Geophys. Res. 85, 1085.

Van Kampen, N. G., 1974. Physica 74, 239.

SURFACE VISCOSITY, THE PARTIALLY FILLED ROTATING CYLINDER AND OSCILLATING DROPS

Roger F. Gans

When a cylinder, partially filled with a liquid, is rotated rapidly about its principal symmetry axis, held horizontally, the liquid is held against the curved sidewalls by centrifugal force. The action of gravity on the density contrast between central core of air and the annulus of liquid induces a secondary circulation. The most easily measured feature of this secondary flow is the "retrograde rotation"" of the interface: the difference between the container rotation rate and the (slower) interface rotation rate.

A weak nonlinear and boundary layer double expansion, based on the smallness of $\mathcal{E} = g/\Omega^2 a$ and $E = \nu/\Omega a^2$, where g, Ω, a and ν denote gravity, rotation rate, container radius and liquid kinematic viscosity, allows one to calculate the retrograde rotation. Its magnitude is sensitive to the nature of the interface. For an ideal free surface, the magnitude is $\mathcal{E}^2$; for a rigid free surface (a buoyant straw), $\mathcal{E}^2 E^{-1/4}$. Measurements give an intermediate result, suggesting partial "rigidity" of the surface. This ability to support some shear stress can be parameterized by surface viscosity coefficients.

Because the relation between surface viscosity and retrograde rotation is indirect, and because surface viscosity is not well-understood, a simpler problem is useful: the effect of surface viscosity on the free oscillations of a drop. If the viscous diffusion lengths are small compared to the drop radius in both media, a boundary layer analysis works for any values of the surface viscosity coefficients to the decay rate of the normal modes by means of an expansion essentially in terms of the length scale ratio.

At lowest order the result is the inviscid Lamb result. At the next order the decay rate and a frequency correction appear. In the limit of zero surface viscosities it agrees with the leading term found by Marston (1980) from Miller and Scriven's (1968) integral formulation. A novel feature of the first order solution is that the surface viscosity effects drop out when

$$n \left(\rho_2\, \mu_2 \right)^{1/2} = (n+1) (\rho_1\, \mu_1)^{1/2}$$

where n_1, ρ and μ denote mode number, density and viscosity and the subscripts 1 and 2 refer to the drop and surrounding fluids.

REFERENCES

Marston, P. L., 1980. J. Acous. Soc. Am., 67, 15.

Miller, C. A. and L. E. Scriven, 1968. J. Fluid Mech., 32, 417.

FRONTOGENESIS IN THE ATMOSPHERE

William Blumen

The formalism for studying the frontogenesis problem within the framework of the geostrophic momentum approximation has been presented by Hoskins (1975). Under this approximation, geostrophic momentum is advected by the geostrophic and ageostrophic three-dimensional velocity field. In addition, the motions are constrained to be adiabatic and hydrostatic.

The Eady baroclinic instability problem, posed in this system, can be solved exactly if the motions are restricted to the (x,z) plane. Although this latter restriction limits application to real flows, the fundamental dynamical mechanism that concentrates gradients of cross-front geostrophic velocity and temperature may be exposed. The amplitude of the motion increases exponentially, as a consequence of baroclinic instability. Simultaneously, the cross-isobaric ageostrophic motions increase gradients until an infinity in the vertical component of relative vorticity occurs in a finite time at a horizontal boundary. The physical mechanism that produces the discontinuity is that which is inherent in the rudimentary one-dimensional advection equation.

Comparison of the solution, before the discontinuity forms, with detailed observations of an intense cold front indicates that the model captures fundamental aspects of frontal motions down to scales of a few hundred kilometers. Extension to smaller scales of motion is limited by the neglect of latent heat release, a boundary layer and small-scale mixing processes.

REFERENCES

Andrews, D. G. and B. J. Hoskins, 1978. J. Atmos. Sci., 35, 509-512.

Blumen, W., 1979. J. Atmos. Sci., 36, 3-11.

Blumen, W., 1980a. J. Atomos. Sci., 37, 64-77.

Blumen, W., 1980b. J. Atmos. Sci., in press.

Hoskins, B. J., 1975. J. Atmos. Sci., 32, 233-242.

Hoskins, B. J., 1976. Quart. J. Roy. Meteorol. Soc., 102, 103-122.

Hoskins, B. J. and N. V. West, 1979. J. Atmos. Sci., 36, 1663-1690.

Platzman, G. W., 1964. Tellus, 16, 422-431.

EFFECT OF SIDEWALL ON WAVE NUMBER SELECTION
IN RAYLEIGH-BENARD CONVECTION

P. C. Hohenberg

An analysis is presented of the steady states of two-dimensional convection in a laterally finite container near threshold. It is shown that the presence of sidewalls severely restricts the allowed wave vectors which can occur in the bulk of the container. This effect provides a possible mechanism to explain the observed wavelength increase of convective rolls with increasing Rayleigh number.

SMALL SCALE SYSTEMS IN THE MEDITERRANEAN

Ettore Salusti

I was interested in small scale systems detected in the Mediterranean Sea. A first example has been seen by French researchers of LOP, Museum d'Histoire Naturelle, Paris.

During the 1975 Medoc cruise in the northwestern Mediterranean basin, cyclonic and anticyclonic eddies where detected in the presence of a system of unstable baroclinic currents (Jeannin, 1976; Gascard, 1977). The observations were made by CTD casts Swallow floats and by moored current meters.

Gascard (1977) has interpreted these data as two eddies of a baroclinic unstable wave of wave-length λ = $2 \pi R_d$, where R_d is the internal Rossby radius of deformation; g the gravity; D the depth $\simeq$ 2300 m; N the Brunt-Väisälä frequency $\simeq 10^{-4} \mathrm{sec}^{-1}$

$$\lambda = 2\pi \frac{ND}{f} = 2\frac{\pi}{f} D\sqrt{\frac{g}{\rho_0}\frac{d}{d\zeta}\rho_0} \simeq 30 \div 40 \text{ Km.}$$

From eleven stations in the East-West section of the two eddies, temperature, salinity and σ_θ were calculated. Lagrangian floats gave the velocity of the cyclonic eddy. The velocity has a tangential component averaged over 12 h, and a weak radial component of less than 2 cm/sec. For the inner region ($r < 5$ kms, r being the distance from the middle of the eddy), the data came from Swallow float measurements and are in agreement with the hydrographic results. A strong Mistral wind started to blow on March 8 and the cyclonic eddy moved northwards at 4.5 cm/sec speed. At this time the anticyclonic eddy was not being tracked.

To summarize, the cyclonic eddy was a 5 km-large, rather rigidly rotating system. Its Brunt-Väisälä frequency N was about $2.5 \cdot 10^{-4} \mathrm{sec}^{-1}$; the velocity distribution V in the region $r < 7$ km, was shaped like a bell and at $r < 5$ km, $Z \simeq 600$ m, it resulted that $V/c \simeq 3.7 \cdot 10^{-5}$ sec^{-1}.

Another system has been seen in the North Tyrrhenian Sea, south of Genoa. Near a front $(\Delta \rho/\rho \sim 10^{-3})$, only $50 \div 100$ meters deep a small cyclonic eddy of 2-3 km of radius, $50 \div 100$ m of depth, has been found. One could also add that the system was seen (with one day of observations gap due to necessity of ship entailment) at its real beginning (Stocchino, 1980).

REFERENCES

Gascard, J. C., 1977. Quelques éléments de la dynamique de formation des Eaux Profondes Méditerranéennes. Thèse d'Etat, Paris VI.

Jeannin, P. F., 1976. Medoc 75 - Courantométrie à l'aide de flotteurs dérivants. Rapp. int. LOP-MUSEUM Paris.

Stocchino, C., et al., 1980. Studio dell'.evolozione termica del mar Ligure-IFAN, 1979. Preprint #192. Instituto di Fisica, Università di Roma.

SECONDARY FLOWS AND THE FORMATION OF SHEAR ZONE IN STRAINING NON-NEWTONIAN FLUIDS

Ron Smith

Starting with the Reiner-Rivlin equation reduced for two-dimensional, incompressible flow, and by allowing the viscosity function to depend on the pressure, a constitutive relation is developed which describes materials as they approach different types of plastic behavior. Von Mises (e.g., hot creep) and Coulomb (e.g., granular materials) plastics are included. The nature of these materials is examined by determining the secondary flow driven by a localized force, during straining. An analytic solution for the flow field is obtained which progressively takes on the form of narrow shear zones as the plastic limit is approached. In the pressure independent von Mises plastic the shear zones lie at $+45°$ to the principal axes of the background straining, but for a Coulomb material they are aligned more closely to the axis of compression. Intense far-reaching shear zones are possible even from weak point disturbances, as such a flow field can efficiently draw on energy stored in the basic flow.

NUMERICAL STUDIES OF MODONS

J. C. McWilliams

Numerical solutions of barotropic and equivalent barotropic (i.e., with finite deformation radius) modons are examined to assess the accuracy with which they can be calculated, their behavior under the influence of dissipation, their resistance to pertubations, and their ability to survive collisions. In brief summary, the results are the following:

(i) Modons can be successfully calculated by standard numerical techniques if the resolution scales in space and time are sufficiently small. In particular about 20 grid points per modon diameter are required to obtain greater than 95% accuracy in the bulk propagation rate using second-order finite difference techniques.

(ii) Under the influence of momentum dissipation, modons decrease in amplitude, reduce their zonal propagation rate, and expand their meridional scale. The first two processes occur in ways which are insensitive to gross aspects of the nature of the dissipation, and the third is rather simply related to the order of the dissipation law. After sufficient amplitude decay, the modon structures make a transition to a dispersive Rossby wave regime. While still within the modon regime, the decline in amplitude and speed crudely follows a modon dispersion curve.

(iii) Modons are resistant to perturbations of small amplitude and are destroyed by perturbations of moderate amplitude. The critical amplitude for destruction is dependent upon the scale content of the perturbation, in a manner consistent with larger-than-modon-scale advective shearing being the dominant destructive mechanism.

(iv) Collisions between initially non-interacting modons have much in common with classical soliton collisons, where, before and after collision, each of the structures are uniformly propagating and isolated, and the only residual consequences of the collision are phase jumps in the direction of propagation. For modons, however, there are some additional consequences of the collisions (e.g., the propagation speeds can be different before and after), and the modons collide by sliding around each other, with transient but large accompanying deformations of the structures, rather than passing through each other as solitons do.

A MODEL OF THE KUROSHIO MEANDER

Glenn R. Flierl

The Kuroshio off the coast of Japan appears to have two stable states: the "normal" path which stays fairly close to the coast and the "meander" pattern in which the Kuroshio turns near Shikoku in a loop of about 250 km and returns to near the coast at Honshu. The Kuroshio seems to switch rapidly from one path to the other and may remain in either state for long periods of time. This behavior is reminiscent of the response of a nonlinear oscillator to forcing.

Several models have been constructed to explore the possibility that the meander can be modelled as a nonlinear response to forcing near resonance by either topography or coastline shape. For a steady flow, the potential vorticity functional can be evaluated upstream if we assume that the topography vanishes or the coastline becomes zonal and the flow becomes zonal. If the upstream flow has shear, this functional will be nonlinear and the equation for the forced response become $L_2 (\psi) + N (\psi) = $ forcing, where $L_2(\psi)$ is a second order elliptic operator, $N (\psi)$ is a nonlinear function, and the forcing terms arise from interaction with the topography or coastline variations.

If we assume the downstream scale is long compared to the cross-stream scale, we end up with an equation similar to the KdV equation in the steady-state limit but with the inclusion of forcing. For a strongly-sheared

upstream flow in a semi-infinite region, stationary, long, neutral waves can exist given the correct current profile and speed. The nonlinearity will be quadratic in the downstream structure with the variations in coastline or topography entering as an inhomogeneous team. When this forcing is periodic, multiple equilibrium states may exist. For single-bump forcing, the existence of multiple states is more questionable. For weakly sheared flow, including a deformation radius term, a southern boundary and cubic nonlinearity, it is possible to find isolated responses to an isolated topographic bump where the amplitude of the response obeys a cubic equation and thus has multiple states: either an isolated inward or an isolated outward excursion of the jet. Transitions will occur for particular values of the mean flow speed and hysteresis would also be expected. Such models, while certainly over-simplified, do suggest that the meander may be modelled as a nonlinear response to forcing.

THE STRUCTURE AND STABILITY OF VORTICES IN A FREE SHEAR LAYER

R. T. Pierrehumbert

Many experiments have confirmed the presence of large scale organized vortex structures in the planar mixing region between two streams of fluid of different velocity (Wyganski, et al., 1979 and Browand and Weidman, 1976 present typical results). The character of steady configurations of vorticity, and the instabilities of such configurations, are therefore of considerable interest. We have exhibited a new family of steady solutions to the Euler equations corresponding to an infinite row of vortices of like sign arranged in the form of a shear layer. The family bifurcates from a parallel shear layer with constant vorticity and extends continuously to a state consisting of a row of point vortices. The intermediate states exhibit the flattened shape characteristic of observed shear layer vortices and have values of vorticity thickness/spacing comparable to those observed. Considera-tion of the energetic properties of the family has shown that the core size for a member of the family produced by rollup of a vortex sheet into vortices of a given spacing is bounded below, and that successive pairings may cause this lower bound to be attained if dissipation is sufficiently small.

We have also examined the two- and three-dimensional stability properties of periodic arrangements of vortices in the form of a shear layer. Two principal classes of instability were revealed. The first class is subharmonic, repeating in the streamwise direction with a wavelength twice the undistrubed vortex spacing. The subharmonic mode is most unstable for two-dimensional perturbations and has a cut-off for short spanwise wavelengths. The character and growth rate of this class of modes strongly suggest that it is associated with the observed pairing transition. The second class of instabilities has the same streamwise periodicity as the unperturbed state, and is most unstable at spanwise wavelengths 2/3 of the unperturbed vortex spacing. For sufficiently compact cores, the growth rate is comparable to that of the subharmonic instability. The spatial structure of the instability is similar to the pattern preceding transition to three-dimensionality observed by Breidenthal (1978).

REFERENCES

Breidenthal, R. E., 1978. Ph.D. Thesis, California Institute of Technology.

Browand, F. K. and P. D. Weidman, 1976. JFM 76, 127.

Wygnanski, I., D. Oster, H. Fiedler, and B. Dziomba, 1979. JRM 93, 325.

PROPERTIES OF ASYMMETRIC SOLITARY ROSSBY WAVES IN A ZONAL CHANNEL

Paola Malanotte Rizzoli

The barotropic, quasi-geostrophic potential vorticity conservation equation over variable topography is considered a zonal channel as the basic model capable of supporting nonlinear permanent form solutions, namely solitary Rossby waves. The considered solutions are asymmetric being characterized by a small aspect ratio $\delta^2 = L_1^2 / L_2^2$ if L_1 is the North-South length scale (channel width) and L_2 the East-West length scale. Then two kinds of solutions are possible. The first is the weak wave solution, for which $U \ll c$, U being the particle speed and c the wave phase speed. Weak solitary Rossby solutions can be shown to exist over the most general topographies in the zonal channel. The second kind of solution is the strong wave type, $(U \gg c)$ which can be obtained allowing for the relief to be quasi-linear in its argument.

For the weak wave type of solitary solutions, stability properties have been explored and collision experiments carried out, in analogy to the one-dimensional case.

The stability analysis of the solitary solution with respect to perturbations in the initial conditions has been investigated in the context of a linearized analytical theory. The results of the theory have been extended to finite amplitude perturbations through a series of numerical experiments, in which the perturbation intensity has been gradually increased. Thus, a threshold in the solitary solution stability can be shown to exist, separating a region of deterministic, wave-like behavior, from a region in which the permanent solution is being destroyed by the superimposed perturbation with with successive turbulent evolution of the flow field. For perturbations with energy concentrated at scales smaller than the basic field (for instance, random perturbations with an isotropic energy spectrum proportioned to k^3) this stability threshold can be qualitatively shown to be reached when

$$\left(\frac{u_{r.m.s.}}{\zeta_{r.m.s.}} \right) \text{PERTURBATION} \approx \left(\frac{u_{r.m.s.}}{\zeta_{r.m.s.}} \right) \text{SOLITARY SOLUTION}$$

if $u_{r.m.s.}$, $\zeta_{r.m.s.}$ are respectively the r.m.s. velocity and vorticity of the perturbation and basic field. The overpassing of the stability

threshold can be shown by the sudden loss of correlation in the locked Fourier phases of the solitary wave.

Collision experiments between two solitary solutions have also been carried out for the weak wave type. In them, the amplitude of one of the interacting waves is held fixed (A_1 = -0.02) while the amplitude of the other is gradually increased through the values

$$A_2 = -0.02; -0.05; -0.1; -0.5; -1; -2.$$

Until the two waves have comparable amplitude, one-dimensional soliton collision properties are respected insofar both waves maintain their permanence upon the interaction. Redekopp and Weidman's results are therefore maintained in the weak wave case, for two interacting wves of comparable intensity. However, when the stronger wave reaches an amplitude one order of magnitude bigger than the other (A_2 = -0.5), one is outside the range of values for the solutions to survive interaction, and the stability properties previously discussed are observed. Thus, the weaker solitary eddy A_1 is progressively distorted by the stronger-and larger scale-eddy A_2, showing the evolution of the flow towards final turbulent behavior. This is immediately evident in the extreme case A_2 = -2, where the weaker solitary wave can be regarded as a superimposed perturbation randomized by the strong (and stable) basic solitary field.

INTERMITTENCY IN FULLY DEVELOPED TURBULENCE

Mark Nelkin

The statistical properties of the small scale fluctuations of incompressible fluid turbulence are analyzed. The emphasis is on universal exponents defined by various correlation functions. After briefly reviewing the experimental support for the 1941 Kolmogorov theory, we consider the fluctuations in local dissipation rate. The simplest and least model dependent measure of intermittency is the dissipation autocorrelation $\langle \varepsilon (x) \varepsilon (x + r) \rangle$. This function is expected to have an inertial range form $(L/r)^\mu$. The exponent μ is expected to be universal. It has the geometrical interpretatin that $3-\mu$ is the fractal dimension of the non space filling objects in which the dissipation is concentrated. To determine μ experimentally required some model of the correlations in the dissipation range. Using a simple model of this behavior, the existing data are reanalyzed to give $\mu \approx 0.25$.

A variety cf other correlation functions can be measured, and several families of scaling exponents can be defined. Scaling theories give relations among these measurable exponents. A one exponent scaling theory expresses all of these exponents in terms of μ . One candidate for one exponent scaling is the 1962 theory of Kolmogorov and Obukhov. This theory is critically analyzed, and an alternative and simpler theory is proposed.

REFERENCES

Nelkin, M. and T. L. Bell, 1978. One exponent scaling for very high Reynolds number turbulence. Phys. Rev. A 17, 363.

Nelkin, M., 1980. Do the dissipation fluctuations in high Reynolds number turbulence define a universal exponent? (To be published in Phys. Fluids)

PERMANENT FORM SOLUTIONS AND THE INITIAL VALUE PROBLEM

Myrl C. Hendershott

The salient feature of the initial value problem for the barotropic potential vorticity equation (BPVE) $\Delta^2 \psi_t + J(\psi, \Delta^2 \psi + h) = 0$ without relief h is exponentially growing instability to infinitesmal perturbations of finite amplitude initial conditions (Lorenz, 1969, Tellus). But with zonal relief h(y), initial conditions having small aspect ratio δ = Y-scale/X-scale and small amplitude $\varepsilon = \delta^2 \ll 1$ evolve according to a set of coupled Kortweg deVries (KdV) equations. For initial conditions which are also the product of a function of A(x) and one of the cross-channel eigenfunctions ϕ_n (y) characterizing long linear topographic waves over the zonal relief, these coupled equations collapse to the well known KdV equation for A(x). This predicts the existence of permanent form (nonlinear Rossby) solutions of the BPVE with zonal relief (Rizzoli, 1980) and suggests very different properties for the initial value problem in the limit $\varepsilon = \delta^2 \ll 1$. These considerations motivate two numerical experiments. In the first experiment a uniformly progressing solution of the BPVE having $\varepsilon = \delta^2 \ll 1$ is perturbed in the x-direction with red noise and this solution is used as the initial condition for (a) the BPVE with zonal relief and (b) the corresponding set of coupled KdV equations. The coupled KdV equations do not anticipate the sharing of energy among different cross-channel modes which develops as the solution of the BPVE evolves. In the second experiment, initially random and isotropic but low amplitude initial conditions are imposed. The solution of the BPVE with zonal relief evolves towards small aspect ratio on account of the zonal relief, a special case of the general tendency for a strong correlation between relative vorticity and relief to develop in two dimensional turbulence over relief (Holloway, 1978). The solution is decomposed according to

$$\psi = \sum_{\substack{n = 1,3 \\ m = 1,3}} a_{nm} e^{inx} \phi_m(y).$$ Although a_{n1}, a_{n2} and a_{n3}

remain of comparable amplitude the a_{n2} evolve towards a state in which a_{n2} n x constant, i.e. in which $\sum a_{n2} e^{inx}$ $_2(y)$ progresses without change of form.

REFERENCES

Holloway, 1978. Jour. Phys. Oceanogr.

Lorenz, 1969. Tellus.Rizzoli, 1980. Dynamics of Atmpsheres and Oceans.

Rizzoli, 1980. Dynamics of Atmospheres and Oceans.

DIFFERENTIAL ROTATION IN THE SUN

Willem V. R. Malkus

It is proposed that the 40% difference in equatorial and polar rotation rates observed in the sun can be due to magnetic torque. Previous theories require significant meridional circulations in the convection zone and pole to equator temperature contrasts which are not observed. Here it is shown that solveabilities conditions imposed on the solar dynamo process require zonal circulation in the stably stratified region below the convection zone. This circulation must override the flow due to other causes or the growing magnetic field will produce large corrective forces. The non-linear eigenvalue problems which emerge from this formulation are derived. The order-one circulation required for solveability here is called the 'eigenflow'. Sample analytic solutions for eigenflows are found for the simplified problem of purely axisymmetric magnetic fields produced by   -dynamo effects confined to a spherical boundary layer. A more complete numerical study is in progress, oriented towards the determination of those macrodynamic flows which are most insensitive to details of the presumed   field.

WEAKLY NONLINEAR STABILITY OF FINITE AMPLITUDE FREE ROSSBY WAVE AND FORCED WAVE INSTABILITY

Richard Deininger

The weak nonlinear behavior of a slightly unstable perturbation to finite amplitude free Rossby and topographically forced waves has been investigated using a model consisting of a single layer of barotropic fluid on an infinite beta-plane. The nonlinear evolution equations

$$\frac{d^2 X}{dT^2} - \sigma_i^2 X - \sigma_i^2 X A + \gamma_1 F X = 0$$
$$\frac{dA}{dT} = - \gamma_2 \frac{d}{dT}(X^2) , \quad \gamma_2 > 0 \qquad \text{(1a,b,c)}$$
$$F = \gamma_3 X^2.$$

obtained by using the method of multiple scales describe the long time evolution of the free Rossby wave problem. In (1), X, A, and F are the perturbation amplitude and basic state wave amplitude and frequency cor-rections, respectively. σ_i is the growth rate obtained from the linear theory of Gill (1974) and γ_n (n = 1,2,3) are coefficients which depend upon the truncation of the perturbation field. These equations describe the stabilizing feedback that occurs between the perturbation amplitude and both

the amplitude and phase of the basic wave. Equation (1b) describes the change in amplitude of the basic wave via the tilted trough mechanism which does not necessarily involve a zonal flow. It is interesting to note that the system of equations reduces in form to that obtained by Pedlosky (1970) in the context of the inviscid baroclinic instability of a zonal flow when $\nu_3 = 0$. The additional result here is that of the additional feedback taking place between the phase of the basic state and the perturbation amplitude which occurs simultaneously with the amplitude feedback between the perturbation and Rossby wave which gives rise to an oscillatory exchange between the basic and perturbation fields.

The forced wave set up by a uniform zonal current U flowing over a sinusoidal topography of amplitude h, has an amplitude proportional to

$$\frac{Uh}{U-c}$$

which exhibits the topographic resonance where u = c. The linear stability analysis for this basic field was carried out by Charney and Flierl (1980). An analysis similar to that done for a free wave was carried out assuming U-c is order one. In this case, there was no frequency feedback so the basic wave remained stationary. Only an amplitude feedback exists. It is described by

$$\frac{d^2X}{dT^2} - \sigma^2 X + N X A = 0$$
$$A = X^2$$

where X and A are defined as before. The nonlinear coefficient N changes sign as U-c does. Thus the nonlinearity is stabilizing for subresonant flow (U > c) and destabilizing for super resonant flow (U > c). This seems to suggest the topographic instability of Charney and Devore (1979).

The analyses demonstrate fundamental differences between free and forced waves.

REFERENCES

Charney, J. G. and J. G. Devore, 1979. Multiple-flow equilbria in the atmosphere and blocking. J. Atmos. Sci., 36, 1205-1216.

Charney, J. G. and G. R. Flierl, 1980. Oceanic analogs of large-scale atmospheric motions.

Gill, A. E., 1974. The stability of planetary waves on an infinite beta-plane. Geophysical Fluid Dynamics, 6, 29-47.

Pedlosky, J., 1970. Finite-amplitude baroclinic waves. J. Atmos. Sci., 31, 15-30.

EXPERIMENTS ON THE STRUCTURE OF A TURBULENT JET

B. T. Chu

Recent experiments conducted at Yale University on the mixing mechanism and the structure of a turbulent jet are reviewed.* Fluid from a 4 mm round nozzle is seeded with uniformly dispersed submicron size aerosol particles. Assuming that each unit mass of the nozzle fluid is always "tagged" by approximately the same number of aerosol particles with approximately the same size distribution, the degree of mixing of the marked nozzle fluid with the unmarked surrounding air will be reflected in a change in the aerosol concentration. If a sheet of radiation is allowed to pass through the mixing layer, the instantaneous distribution of the aerosol (and, therefore, the nozzle fluid) concentration in the sheet can be monitored and inferred from the distribution of the elastically scattered radiation. The scattered light from the sheet is digitalized at 10,000 points in a 100x100 array and stored in the computer. Subsequently, the record allows one to examine both quantitatively and qualitatively the degree of mixing of the nozzle fluid with the surrounding air in a plane. By storing a large number of such records in the computer, statistical information relevant to turbulent mixing can be deduced. In particular, the distribution of the mean concentration and the rms fluctuation in a meridian plane are presented. The characteristic "shoulders" in the mean concentration profile and the "depressions" in the rms profile are shown to be consequences of the vortical mixing mechanism. A second mixing mechanism which dominates further downstream is responsible for the development of small scale concentration fluctuation and may be attributed to the instability and ultimate disintegration of vortex rings. The next effect of the instability is the production of bursts of nozzle fluid projected radially outward.

The spatial structure and coherence of the turbulent jet is characterized quantiatively by the longitudinal covariance. The instantaneous two-dimensional mapping of the constant concentrating contours also allows one to determine the various statistical properties of such contours. These contours are generally multi-valued functions of the axial distance. The average multiplicity of such contours and the increase of their length per unit axial distance in the direction of the flow have been computed.

LECTURES OF FELLOWS

WHAT DETERMINES THE VERTICAL STRUCTURE
THE GENERAL CIRCULATION?

William Young

I. Introduction

The wind driven homogeneous models of ocean circulation describe the qualitative horizontal features of the actual stratified flow remarkably well. The verisimilitude of these models can be attributed to the simplicity of the planetary-scale vorticity equation in a stratified fluid, viz.

$$\beta v = f \, \omega_z \tag{1.1}$$

(The notation here is standard; see Pedlosky (1979) section 6.19 for a careful explanation of the scaling arguments leading to (1.1)). If (1.1) is integrated over the depth of the ocean and the vertical velocity at the bottom is neglected we find

$$\beta \int_0^H v \, dz \;=\; f \omega_E \;=\; \nabla \times \left(\frac{\tau}{\rho_o f} \right) \cdot \hat{z} \tag{1.2}$$

where ω_E is the vertical velocity at the base of the Ekman layer produced by the curl of the wind stress, τ . Equation (1.2) is independent of the density profile and is identical to the Sverdrup relation used to determine the interior flow (away from boundary layers) in homogeneous circulation models.

The Sverdrup relation (1.2) tells us nothing about how the transport is distributed in the vertical. I shall use the simplest possible wind-driven stratified circulation model to investigate this question. The goal of this study is the vertical resolution of the interior flow, the boundary layer dynamics are of secondary interest here.

2. A Fundamental Difficulty of Completely Inviscid Circulation Models

The fundamental difficulty referred to in the heading is that in a sense we have too many solutions to the problem outlined at the end of section 1.

This is best illustrated by a specific example. For the sake of simplicity I shall solve the two layer quasigeostrophic equations,

$$J(\psi_1, q_1) \;=\; \omega_E \; + \text{dissipation} \tag{2.1}$$

$$J(\psi_2, q_2) \;=\; \text{dissipation} \tag{2.2}$$

$$\tag{2.3}$$

in a rectangular basin $0 < x < X_E$, $-1 < y < 1$. Eqns (2.1) - (2.3) are nondimensional using the scalings summarized in Table 1. The nonessential simplification of equal layer thickness is made.

Table 1. Scaling of the two layer equations. Dimensional quantities are starred.

W	=	magnitude of the Ekman pumping
L	=	horizontal dimension of the basin
H	=	depth of a layer
g'	=	reduced gravity between the two layers
f_o	=	Coriolis parameter
U	=	$(f_o W/\beta H)$ = magnitude of Sverdrup balanced horizontal velocities.
ψ_*	=	ψ UL
q_*	=	$\beta L\, q_i$
$w_e{}^*$	=	$W\, w_e$
ε^2	=	$(U/\beta L^2)$
F	=	$(f_o^2 U/g'\beta H)$

Now attempt to solve (2.1) - (2.3) in the interior of the basin where both dissipation and relative vorticity are negligible. In this case, the sum of (2.1) and (2.2) is just the Sverdrup relation

$$\psi_{\beta x} = \omega_E$$

where $\psi_\beta = \psi_1 + \psi_2$. If, say, $\omega_E = -\cos\left(\frac{\pi}{2}y\right)$ then the solution of (2.4) which satisfies a no flux Eastern boundary condition is

(2.4)

$$\psi_\beta = -(x - X_E)\cos\left(\frac{\pi}{2}y\right)$$

(2.5)

The Western boundary condition at x = 0 is satisfied by appending a boundary layer. The streamfunction in (2.5) is sketched in Fig. 1.
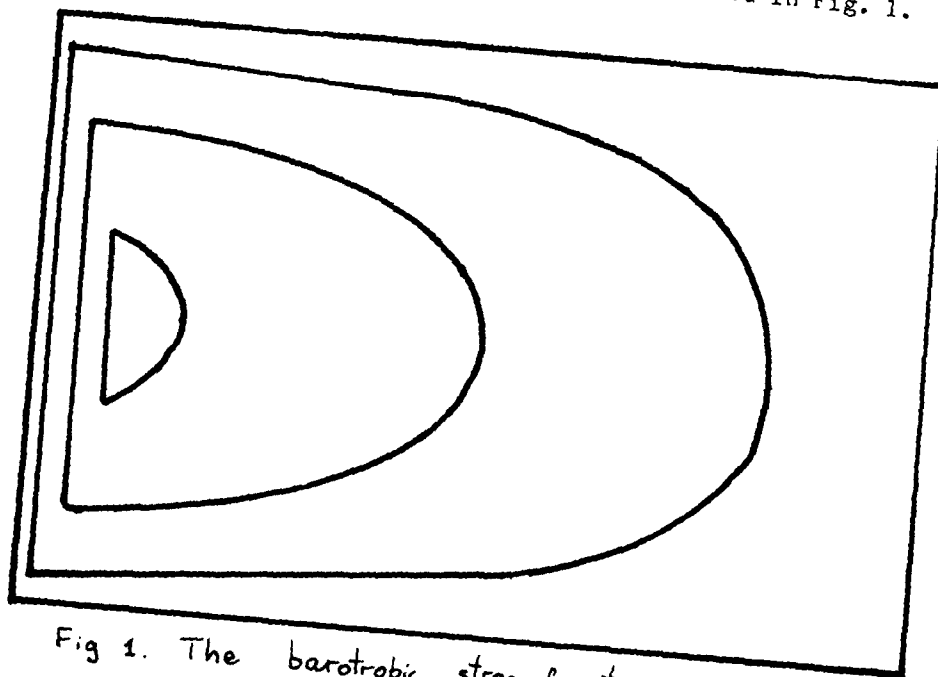
Fig 1. The barotropic streamfunction, ψ_β.

Now the lower layer equation in the interior is

$$J(\psi_2, q_2) = 0$$

or since

$$q_2 = y + F\psi_B - 2F\psi_2 + O(\varepsilon^2)$$

$$J(\psi_2, y + F\psi_B) = 0 \tag{2.6}$$

The solution of (2.6) is

$$\psi_2 = G(y + F\psi_B) \tag{2.7}$$

where G is an arbitrary function of $y + F\psi_B$. If a $y + F\psi_B$ contour hits an Eastern* boundary, where $\psi_2 = 0$, then G is determined,

$$G = 0 \tag{2.8}$$

The specification (2.8) implies that the lower layer is at rest at interior points threaded by $y + F\psi_B$ contours which reach the Eastern boundary. Rooth, Stommel and Veronis (1978) and Rhines and Holland (1979) gave a more general proof of this result. They proved that in a multi-layer model, where the density surfaces are allowed to strongly deform (i.e. the quasigeostrophic approximation is not made), the abyssal layers are quiescent wherever they are connected to Eastern boundaries by contours of $f/$(layer thickness).

Fortunately however, not all $y + F\psi_B$ contours reach Eastern boundaries; some close in the basin and the specification (2.8) is not forced on us by lateral boundary conditions. As the forcing w_E is increased (or equivalently F is increased) larger areas of the basins are threaded by closed $y + F\psi_B$ contours. This is shown in figures 2 - 5. The details of the Western boundary region are not shown in these figures. It is clear, however, that since $\psi_B = 0$ on the boundary, a contour which starts at $y = y_i$ on the Eastern boundary must also hit the Western boundary at $y = y_1$. Thus the details of the $y + F\psi_B$ contours in the Western boundary layer must look roughly like Figure 6, no matter what higher order dynamic process is used to form the barotropic Western boundary layer. In the closed regions G is undetermined and there may be nontrivial abyssal flows.

It is important to realize that within the context of the inviscid theory G is arbitrary. There is no physical reason for favouring one particular choice. It is in this sense that there are too many solutions; each choice of G provides an acceptable resolution of the vertical structure. I shall discuss three methods of removing this degeneracy (i.e.finding a preferred G):

---

*There is a bit of imprecision here; in a stratified fluid the deformation of the density surfaces can reverse the roles of Eastern and Western boundaries in much the same way as topography does in a homogeneous fluid (Pedlosky, 1979 Section 5.13). Specifically, if $\frac{d}{dy}(y + F\psi_B) < 0$ then it is the Western boundary at which a no flux condition must be satisfied by the interior solution.

$$F = \frac{1}{4}$$

-2-

$$F = \frac{1}{2}$$

-3-
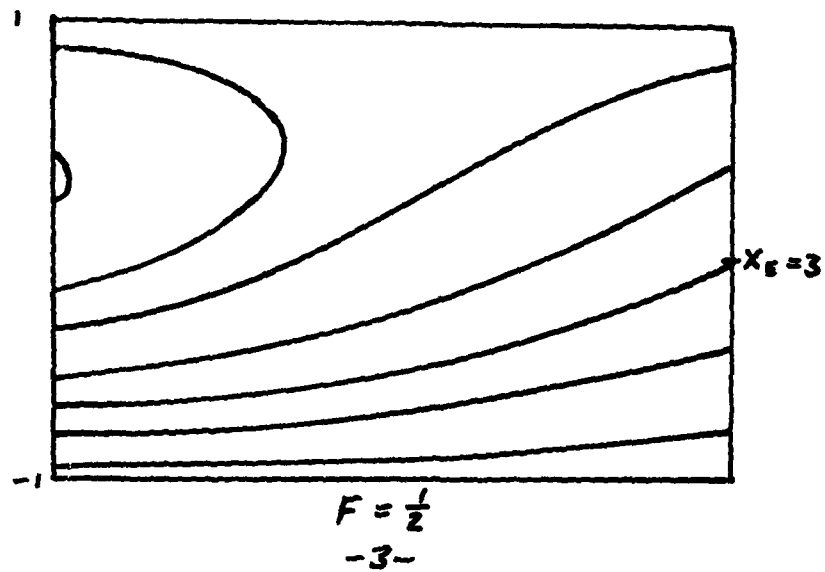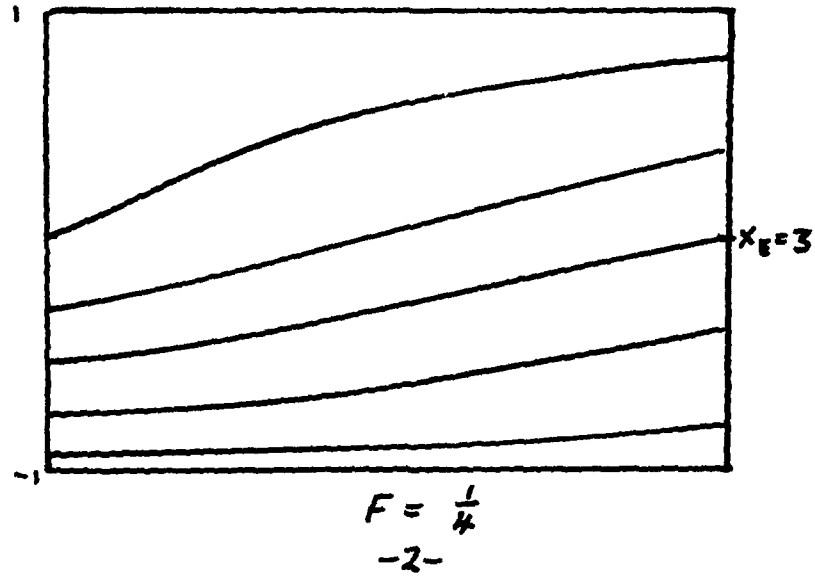
Figures 2-5. Contours of $y + F\psi_8$ for various values of F. As F increases larger areas of the basin are threaded by closed contours.

$-X_5=3$

$F = 1$

$-4-$

$-X_5=3$

$F = 2$

$-5-$

$y=y_1$

$y=y_1$

Closed $y + F\psi_B$ contours
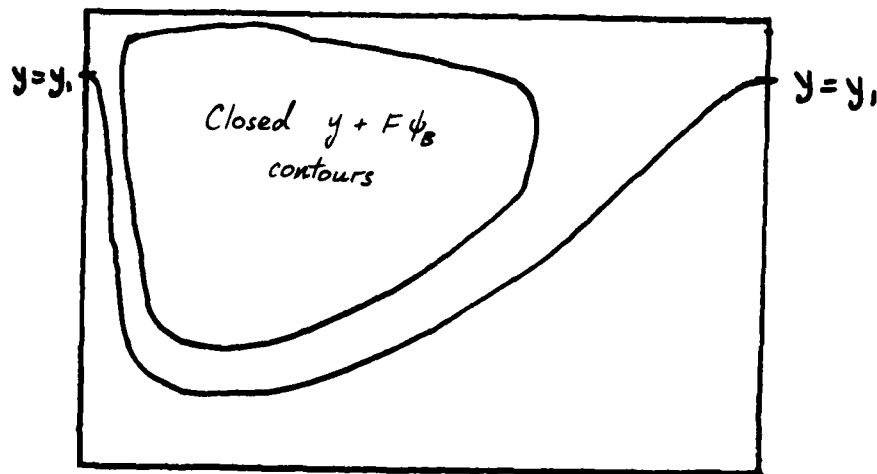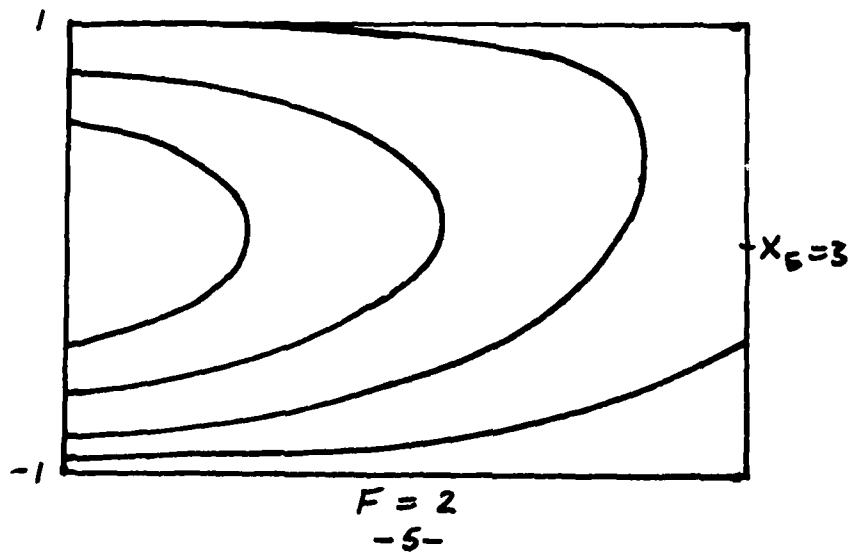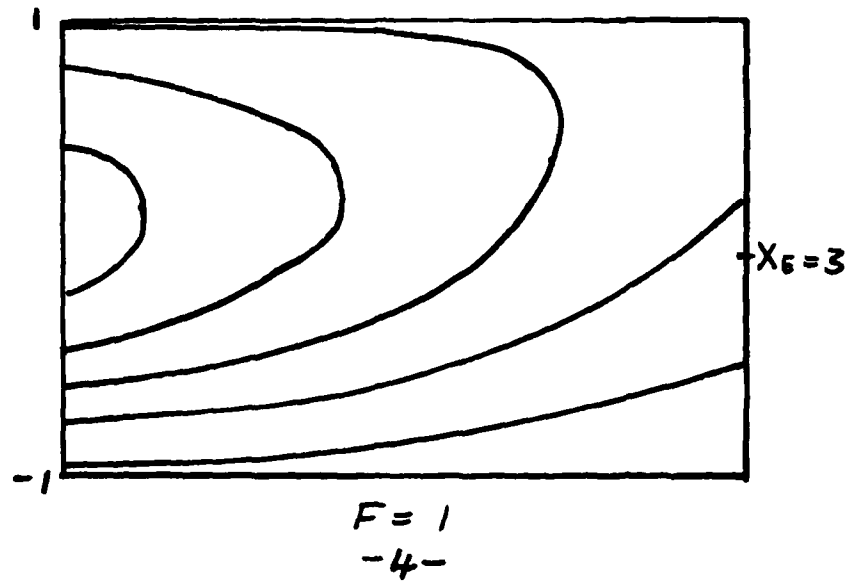
Fig 6 (Directly above) A schematic illustration of how $y + F\psi_B$ contours connect in the boundary layer.

(a)   Solve an inviscid nonlinear initial problem i.e. start with an ocean at rest, switch on the Ekman pumping and let the circulation evolve. Presumably the circulation will find its own q . (Actually this presumption is incorrect, in the closed $y + F\psi_B$ regions no steady state is ever reached, see section 3.)

(b)   Introduce some small dissipation and determine q using a Batchelor-Prandtl theorem, see section 4.

(c)   Introduce small dissipation and attempt to solve a complete general circulation model, see section 5.

3.An Initial Value Problem

The initial value problem discussed in this section is

$$q_{1t} + J(\psi_1, q_1) = \omega_E \tag{3.1}$$

$$q_{2t} + J(\psi_2, q_2) = 0 \tag{3.2}$$

where

$$\omega_E = \begin{cases} 0 & t < 0 \\ -\cos(\tfrac{\pi}{2}y) & t > 0 \end{cases} \tag{3.3}$$

and ψ_1 and ψ_2 are zero on the boundary of the rectangular basin   ,

Equations (3.1) and (3.2) have two linear wave solutions with different vertical structures. The first is the barotropic mode which crosses the basin East to West and establishes a barotropic flow like that in Fig. 1 in a few weeks. The second is the much more slowly propagating baroclinic mode which travels through a density and flow field produced by the barotropic mode. Its transit time across the basin is about a year. In solving (3.1) - (3.3) we will assume the barotropic mode has already gone through and produced as a new initial condition the barotropic flow given by:

$$\psi_B = \psi_1 + \psi_2 = (x_E - x)\cos\left(\tfrac{\pi}{2}y\right) \tag{3.4}$$

$$\psi_1 = \psi_2$$

The equation governing ψ_2 is then (the relative vorticity is neglected)

$$\psi_{2t} - (2F)^{-1} J(\psi_2, y + F\psi_B) = 0 \tag{3.5}$$

$$\psi_2 = \tfrac{1}{2}\psi_B \quad \text{at } t = 0$$

$$\psi_2 = 0 \quad \text{on the boundary of the basin.}$$

Note how (3.5) reduces to (2.6) if we seek steady solutions.

Equation (3.5) can be solved using the method of characteristics (Carrier and Pearson 1976). The characteristics are curves in (ψ_2, x , y , t) space parameterized by s.   From (3.5), the characteristic equations

$$\frac{dt}{ds} = 1 \tag{3.6}$$

$$\frac{d\psi_2}{ds} = 0 \tag{3.7}$$

$$\frac{dx}{ds} = -(2F)^{-1} \frac{\partial}{\partial y} (y + F \psi_B) \qquad (3.8)$$

$$\frac{dy}{ds} = (2F) \frac{\partial}{\partial x} (y + F \psi_B) \qquad (3.9)$$

Equations (3.6) and (3.7) imply that s can be replaced by t and that ψ_z is constant along characteristics, or equivalently the projections of the characteristics onto the (x, y) plane are just the familiar curves of constant $y + F \psi_B$.

It a characteristic intersects the boundary then the boundary condition $\psi_z = 0$ is propagated into the interior. If $\frac{\partial}{\partial y} (F \psi_B + \psi) > 0$ the characteristic leaves the Eastern boundary, while if $\frac{\partial}{\partial y} (F \psi_B + \psi) < 0$ the characteristic leaves the Western boundary. In either case, the result is the same; at points connected to boundaries by characteristics the abyssal flow is eventually "switched off" by the arrival of information from the boundary. Rhines (1977) gives an explicit example of this using the approximation $y + F \psi_B \simeq y$.

If a $y + F \psi_B$ contour closes then the corresponding characteristic is a helix in (x,y,t) space. This curve never intersects the boundary. No steady solution is ever produced. Thus in the closed regions although there are an infinite number of steady solutions, none are ever "found" by an inviscid initial value problem.

This last result makes it clear that in closed regions we must invoke some disspation to resolve the vertical structure of the circulation.

4. A Batchelor-Prandtl Theorem for Potential Vorticity

The degneracy associated with closed streamlines is familar in fluid mechanics. Thus usual method of overcoming this difficulty is to derive an integral constraint, based on the existence of the dissipation, which must be satisfied by the flow no mater how small the dissipation is (Batchelor, 1955).

The dissipative process discussed in this article is vertical diffusion of momentum, represented by the last term in

$$\frac{D \underline{v}}{Dt} + \hat{z} \times f \underline{v} = -\nabla p + (\gamma v_z)_z \qquad (4.1)$$

There are undoubtedly other important dissipative processes, such as vertical density diffusion

$$\frac{D \rho}{Dt} = (\kappa \rho_z)_z \qquad (4.2)$$

I shall, however, focus on vertical momentum diffusion since it is the most straightforward mathematically and the results can easily be interpreted physically. The small scale process (small compared to the general circulation that is) primarily responsible for vertical momentum transfer in the ocean is baroclinic instability. This is the underlying process crudely modelled by the last term in (4.1).

The planetary scale quasigeostrophic potential vorticity formulation follows from (4.1) and (4.2) in the usual way (Pedlosky 1979, section 6.19),

$$J(\psi, q) = (\nu \nabla^2 \psi_z)_z \tag{4.3}$$

$$q = y + F\psi_s \tag{4.4}$$

$$F(z) = \beta^{-1} \left(\frac{f_0 L}{NH}\right)^2 \tag{4.5}$$

$$F J(\psi, \psi_z) = \begin{cases} -w_E & \text{at } z=1 \\ 0 & \text{at } z=0 \end{cases} \tag{4.6}$$

w_E in (4.6) is the Ekman pumping at the top of the interior flow, the vertical velocity at the bottom Ekman layer has been neglected. ∇^2 is a horizontal Laplacian.

If $\nu = 0$ then (4.3) implies

$$q = Q(\psi, z) \tag{4.7}$$

As in section 2, if a streamline reaches the boundary of the basin the imposition of a no flux condition determines Q.

Now, to obtain the desired integral constraint, integrate (4.3) over the area enclosed by a closed streamline. The integral of the Jacobian vanishes since

$$\iint J(\psi, q) \, d^2 a = \iint \nabla \times (\psi \nabla q) \, da$$
$$= \oint \psi \nabla q \cdot d\underline{l}$$
$$= \psi \oint \nabla q \cdot d\underline{l} = 0$$

The second last step follows from the constancy of ψ on a streamline. The final result is

$$\iint (\nu \nabla^2 \psi_z)_z \, d^2 a = \oint (\nu \nabla \psi_z)_z \cdot \hat{n} \, dl$$
$$= 0 \tag{4.8}$$

The result (4.8) is valid for arbitrary ν. If ν is now very small it is plausible that (4.7) may also by valid (to $0 (\nu)$). In this case we (4.7) to cast (4.8) in the form

$$\hat{\nu} \frac{\partial Q}{\partial \psi} \oint \underline{v} \cdot d\underline{l} + \hat{\nu}_z F \oint \underline{v}_z \cdot d\underline{l} = 0 \tag{4.9}$$

where $\hat{\nu} = F^{-1}\nu$. In using (4.7) to rewrite (4.8) it is assumed that the viscous term is small everywhere on the closed streamline. This is certainly not the case for the streamline pattern shown in figure 1, every streamline passes through a viscous boundary layer. Similar objection to the use of (4.9) apply in many potentially important flow configurations. Thus, although interesting solutions can be constructed using (4.7) and (4.9) (Rhines, 1980), the general utility of (4.9) is open to question.

The consequences of (4.9) will be explored elsewhere, at the moment the difficulties associated with the application (4.9) motivate a third approach to the problem of resolving the vertical structure of the circulation.

5 A Stratified General Circulation Model

In this section I solve a very simple two layer general circulation model. The dissipation is provided by bottom drag and the layers are coupled by interfacial stress (a force proportional to the jump in velocity across the interface). This interfacial drag is the two layer analog of the last term in (4.1).

The two layer quasigeostrophic equations are

$$J(\psi_1, q_1) = \omega_E + \nu \nabla^2 (\psi_2 - \psi_1) \tag{5.1}$$

$$J(\psi_2, q_2) = \nu \nabla^2 (\psi_1 - \psi_2) - \delta \nabla^2 \psi_2 \tag{5.2}$$

where

$$q_1 = y + F(\psi_2 - \psi_1)$$

$$q_2 = y + F(\psi_1 - \psi_2)$$

The relative vorticity is neglected; in the interior it is unimportant because of the large length scale of the flow while in the boundary layers it is assumed that the viscous forces dominate. This last assumption is unrealistic, but once again I emphasize that the goal of this study is the vertical resolution of the <u>interior</u> flow.

The sum of (5.1) and (5.2) is

$$\psi_{Bx} = \omega_E - \delta \nabla^2 \psi_2 \tag{5.3}$$

In the interior the friction term is neglected and the Sverdrup balance is recovered. With $\omega_E = -\cos(\frac{\pi}{2} y)$ and using the same rectangular basin previously defined, the interior barotropic flow is

$$\psi_B = \psi_1 + \psi_2 = (x_E - x) \cos(\tfrac{\pi}{2} y) \tag{5.4}$$

As in section 2, the lower layer equation can be put in the form

$$J(\psi_2, y + F\psi_B) = \nu \nabla^2 \psi_B - (2\nu + \delta) \nabla^2 \psi_2 \tag{5.5}$$

Now, by inspection, an exact solution of (5.5) is

$$\psi_2 = \left(\frac{\nu}{2\nu + \delta}\right) \left(\frac{y + F\psi_B}{F}\right) \tag{5.6}$$

ψ_2 in (5.6) would be an exact solution of the problem if the no flux lateral boundary conditions are satisfied. This is the case if the $y + F\psi_B$ contour closes in the basin. In the regions threaded by $y + F\psi_B$ contours

which reach the boundary an alternative solution must be sought. In these regions ψ_2 is order ν and $\psi_1 \simeq \psi_B$. The streamfunctions are sketched in figures 7 and 8. For the moment, however, notice that if $\nu \sim \delta$, (5.6) gives an order one abyssal flow. Because (5.6) is the most important result in this article it's worthwhile attempting to interpret it physically. In the abyssal layer the "natural paths" for the circulation are $y + F\psi_B$ contours (essentially paths of f/(layer thickness)). A very weak force (such as interfacial stress) with a nozero circulation round a <u>closed</u> $y + F\psi_B$ contour accelerates a flow around the contour until a frictional force (in this case the bottom drag δ) becomes large enough to balance the driving force. This is a physical interpretation of (4.9). On the other hand if the contour does not close the forced flow is across rather than along the contour. The amplitude of this cross contour flow is determined by the driving rather than the friction.

As an example of this latter process consider the problem of solving (5.5) in regions where the $y + F\psi_B$ contours are open. For simplicity the weakly forced limit

$$y + F\psi_B \simeq y \tag{5.7}$$

will be investigated. The more general case can be discussed using similar method; see Welander (1968) for a similar calculation.

With (5.7) the equations of motion are reduced to

$$\psi_{Bx} = \omega - \delta \nabla^2 \psi_2 \tag{5.8}$$

$$\psi_{2x} = -(2\nu + \delta) \nabla^2 \psi_2 + \nu \nabla^2 \psi_B \tag{5.9}$$

Equations (5.8) and (5.9) are easily solved in the interior where the friction terms are negligible

$$\psi_B = -(x_E - x) \omega'(y) \tag{5.10}$$

$$\psi_2 = \tfrac{1}{2} \nu (x - x_E)^2 \omega'' \tag{5.11}$$

Note how the abyssal flow is order ν because its driven by the order ν forcing term $\nu \nabla^2 \psi_B$ in (5.9). The solutions (5.10) and (5.11) don't satisfy the boundary conditions at $x = o$ (the Western boundary). In this region we use a familiar boundary layer technique. Begin by introducing the boundary layer variables :

$$\zeta = \delta^{-1} x$$

$$\psi_B = (x_E - x) \omega + \varphi_B (\zeta, y)$$

$$\psi_2 = -\tfrac{1}{2} \nu (x_E - x)^2 \omega'' + \varphi_2 (\zeta, y)$$

which transform (5.8) and (5.9) to

$$\varphi_{B\zeta} = -\varphi_{2\zeta\zeta} + O(\delta) \tag{5.12}$$

$$\varphi_{2\zeta} = -(2\lambda + 1)\varphi_{2\zeta\zeta} + \lambda \varphi_{B\zeta\zeta} + O(\delta) \tag{5.13}$$

$$\lambda = \delta^{-1} \nu$$
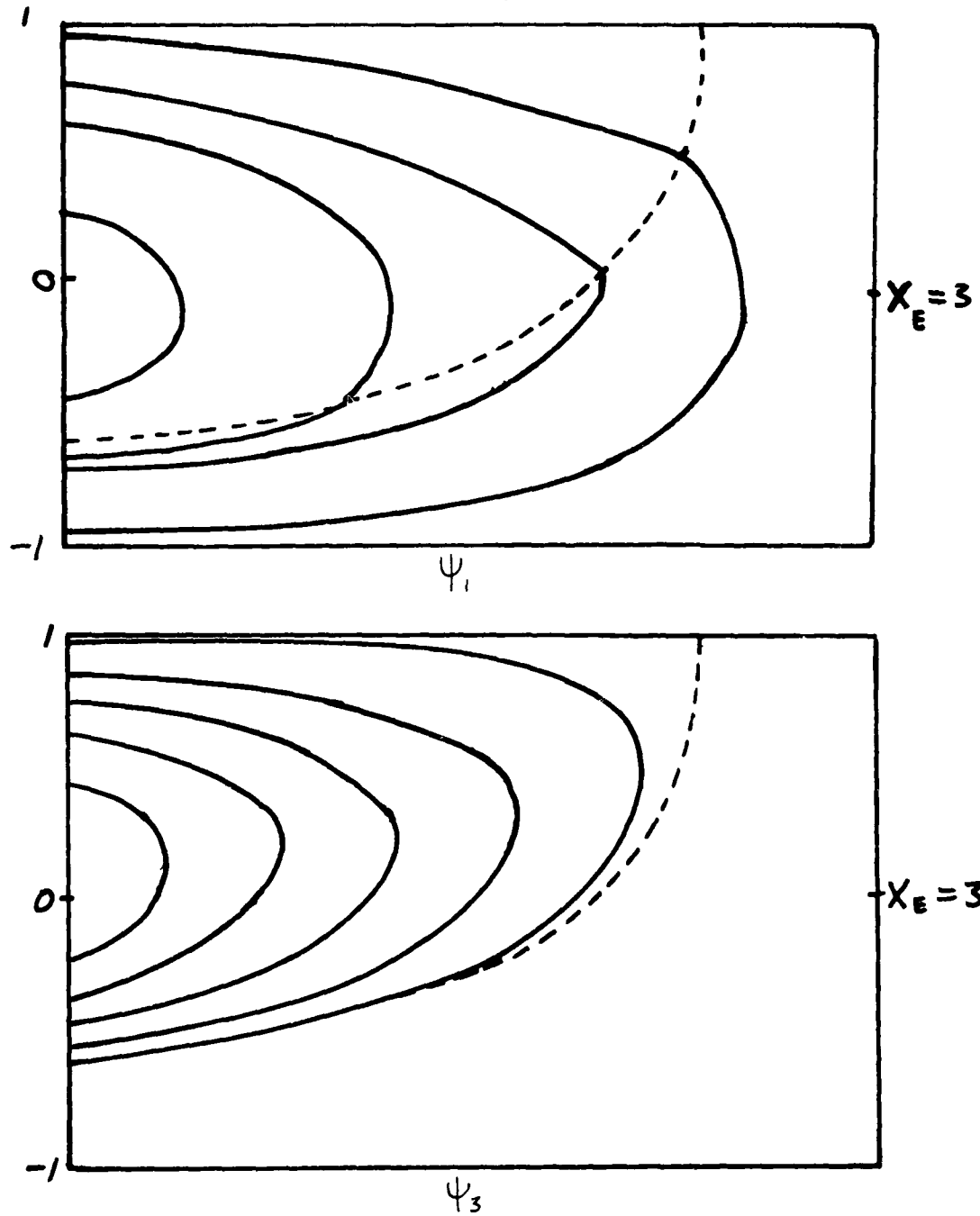
Figures 7 & 8   The upper and lower layer streamfunctions . $\nu = \delta$
and $F = 1$. In the regions where the contours of $y + F\psi_R$
close (see Fig. 4) ψ_2 is given by (5.6).

The final uniformly valid solution for the ψ_B and ψ_2 is constructed in the standard fashion,

$$\psi_B = (x - x_E)\omega\left[1 - (\kappa_2 - \kappa_1)^{-1}(\kappa_2 e^{-\kappa_1 \xi} - \kappa_1 e^{-\kappa_1 \xi})\right] + \tfrac{1}{2}\nu \kappa_1 \kappa_2 (\kappa_2 - \kappa_1)^{-1} x_E^2 \omega''\left[e^{-\kappa_1 \xi} - e^{-\kappa_1 \xi}\right] \quad (5.14)$$

$$\psi_2 = \tfrac{\gamma}{2}(x - x_E)^2 \omega''\left[1 - (\kappa_2 - \kappa_1)^{-1}(\kappa_2 e^{-\kappa_1 \xi} - \kappa_1 e^{-\kappa_1 \xi})\right] + x_E \omega(\kappa_2 - \kappa_1)^{-1}\left[e^{-\kappa_2 \xi} - e^{-\kappa_1 \xi}\right] \quad (5.15)$$

where

$$\kappa_1 = (2\lambda)^{-1}\left[2\lambda + 1 + (4\lambda^2 + 1)^{1/2}\right]$$

$$\kappa_2 = (2\lambda)^{-1}\left[2\lambda + 1 - (4\lambda^2 + 1)^{1/2}\right]$$

Note that ψ_2 in (5.15) is order 1, but only in a narrow region of thickness δ near the Western boundary. This is in contrast to (5.6) which gives an order one abyssal flow in the interior of the basin.

To summarize the conclusions of this section, in a region where the $y + F\psi_B$ close, very small vertical momentum transfer can create order one abyssal flows. By contrast in a region where the contours are open the interior abyssal flow is very weak (order ν).

6. A Three Layer Model

In this section the vertical resolution of the previous model is increased by considering a model with three identical layers. This model is interesting because the dynamics of the middle layer are qualitatively different from the upper layer (which is directly forced) and the lower layer (where the bottom drag provides the dissipation).

The three identical layer quasigeostrophic equations are

$$J(\psi_1, q_1) = \omega + \nu \nabla^2(\psi_2 - \psi_1) \quad (6.1)$$

$$J(\psi_2, q_2) = \nu \nabla^2(\psi_1 - 2\psi_2 + \psi_3) \quad (6.2)$$

$$J(\psi_3, q_3) = \nu \nabla^2(\psi_2 - \psi_3) - \delta \nabla^2 \psi_3 \quad (6.3)$$

where the potential vorticities are

$$q_1 = y + F(\psi_2 - \psi_1)$$

$$q_2 = y + F(\psi_1 - 2\psi_2 + \psi_3)$$

$$q_3 = y + F(\psi_2 - \psi_3)$$

In (6.1) - (6.3) the terms proportional to ν are the interfacial stress terms while the last term in (6.3) is the bottom drag.

The barotropic equation is obtained by adding (6.1) - (6.3),

$$\psi_{Bx} = \omega - \delta \nabla^2 \psi_3 \tag{6.4}$$

As before the last term in (6.4) is neglected in the interior, so that the barotropic flow field is know. This allows us to simplify (6.2) by observing that

$$q_2 = y + F\psi_B - 3F\psi_2$$

so that (6.2) can be rewritten as

$$J(\psi_2, y + F\psi_B) = \nu \nabla^2 \psi_B - 3\nu \nabla^2 \psi_2 \tag{6.5}$$

If the $y + F\psi_B$ contours close than an appropriate exact solution of (6.5) is

$$\psi_2 = (3F)^{-1}(y + F\psi_B) \tag{6.6}$$

If the contours are open an analysis similar to that in section   must be used. In this section we will focus on the more physically interesting case of closed contours. Now that ψ_2 is known, we can simplify (6.3) using (6.6). We have

$$q_3 = \tfrac{4}{3}y + \tfrac{1}{3}F\psi_B - F\psi_3$$

so that in the lower layer

$$J(\psi_2, \tfrac{4}{3}y + \tfrac{1}{3}F\psi_B) = \tfrac{1}{3}\nu \nabla^2 \psi_B - (\nu + \delta)\nabla^2 \psi_3 \tag{6.7}$$

Once again, in a region enclosed by a closed $\tfrac{4}{3}y + \tfrac{1}{3}F\psi_B$ contour, (6.7) can be solved exactly,

$$\psi_3 = \nu [F(\nu+\delta)]^{-1} [\tfrac{4}{3}y + \tfrac{1}{3}F\psi_B] \tag{6.8}$$

ψ_1 is now the residual when ψ_2 and ψ_3 given by (6.6) and (6.8) are subtracted from ψ_B . Note carefully the restriction on (6.8) (closed $\tfrac{4}{3}y$ + $\tfrac{1}{3}F\psi_B$) is stronger than the restriction on (6.6) (closed $y + F\psi_B$). This observation, together with Fig. 2-5, leads to the tentative prediction that the wind driven circulation in a stratified subtropical gyre should be deeper in the Northwest. Clearly it will be necessary to investigate a variety of models with increased vertical resolution to assess the importance of this prediction.

REFERENCES

Batchelor, G.K., 1956. On steady laminar flow with closed streamlines at large Reynolds number. J. Fluid Mech. $\underline{1}$, 177-190.

Carrier, G. and Pearson, C., 1976. Partial Differential Equations - Theory and Technique. Academic Press.

Pedlosky, J., 1979. Geophysical Fluid Dynamics. Springer Verlag.

Rooth, C., Stommel, H. and Veronis, G., 1978. On motions in steady layered geostrophic models. J. Oceanographical Soc. Japan. $\underline{34}$, 265-267.

Rhines, P., 1977. The Dynamics of unsteady currents. In: The Sea, Vol. VI, Wiley, New York, 189-318.

Rhines, P. and Holland, W., (1979) A theoretical discussion of eddy-driven mean flows. Dynamics of Atm. and Oceans. $\underline{3}$, 289-325.

Rhines, P., 1980. Personal Communication.

Welander, P., 1968. Wind-driven circulation in one- and two-layer oceans of variable depth. Tellus XX, 1-15.

BAROCLINICALLY GROWING SOLITARY WAVES

Richard Deininger

1. Introduction

Previous studies of solitary waves have for the most part, not dealt with their generation mechanisms except to say they evolve from general initial conditions. Possible generation mechanisms for solitary waves include localized forcing (e.g. mountains) and/or instability processes (e.g. baroclinic). This work represents an attempt to study the role of baroclinic instability in producing solitary waves.

It is well known the balance between dispersion and nonlinearity is responsible for the permanence of the solitary wave. Then, to allow for the possiblity for a growing solitary wave, we must simultaneously allow an instability (baroclinic in our case) to be present. It is also of interest to include a frictional process such as Ekman friction. The method to be used is the method of multiple scales. Each of the fundamental processes which are dispersion, instability, friction, and nonlinearity are assumed to be weak. As a result each fundamental process defines a slow time scale. The baroclinic instability time scale is a function of the small parameter which measures the degree of supercriticality of the zonal shear from its critical value (Pedlosky, 1970). The dispersive time scale is proportional to the ratio of the meridional scale to the zonal scale of the baroclinic wave. The frictional time scale is proportional to the Ekman number. To allow all of these processes to act simultaneously, we choose the respective measure of each process to give them the same long time scale. A weak cross channel topography produces the nonlinearity. Thus using the method of multiple scales we shall seek the evolution equation for a wave which is to lowest order neutrally stable and nondispersive. In doing so we hope to find growing solitary waves.

2. The Model

The model is the quasi-geostrophic two layer model with the equal layer depth, in a channel on a beta-plane, with bottom topography, and Ekman friction in the lower layer (Pedlosky, 1980). The nondimensional equations are

$$\left(\partial_t + \psi_{,x}\partial_y - \psi_{,y}\partial_x\right)\left[\nabla^2\psi_1 - F(\psi_1 - \psi_2) + \beta y\right] = 0$$

$$\left(\partial_t + \psi_{2x}\partial_y - \psi_{2y}\partial_x\right)\left[\nabla^2\psi_2 - F(\psi_2 - \psi_1) + \beta y + \eta_B\right] = -r\nabla^2\psi_2$$

$$(2.1a,b)$$

where

$$\nabla^2 = \delta^2\partial_{xx} + \partial_{yy}$$

and Ψ_1 and Ψ_2 are the stream functions in the upper and lower layers respectively. x and y are the zonal and meridional coordinates respectively and $\eta_B = \eta_B(y)$ represents the topography. The space and time coordinates and pressure have been nondimensionalized according to

$$(x', y', t', p_n) = (L x, \ell y, \tfrac{1}{U} t, \rho_n f_o U \ell \Psi_n)$$

where U is the velocity scale, f_0 is the Coriolis parameter, and ρ_n is the density in each layer. The parameters are:

$$S = \tfrac{\ell}{L} \qquad \text{(wave anisotropy)}$$

$$F = \frac{f_o^2 \ell^2}{g' D} \qquad \text{(Froude number)}$$

$$\beta = \frac{\beta' \ell^2}{U} \qquad \text{(planetary vorticity factor)}$$

$$\epsilon = \frac{U}{f_o \ell} \;,\; \epsilon = \frac{U}{f_o L} \qquad \text{(Rossby numbers)}$$

$$\eta_B = \frac{h_B}{\epsilon D} \qquad \text{(topographic variation)}$$

$$E = \frac{\nu}{2 f_o D^2} \qquad \text{(Ekman number)}$$

$$r = \frac{E_v^{\frac{1}{2}}}{\epsilon} \qquad \text{(friction parameter)}$$

where D is the depth of each layer, g' is the reduced gravity, β' is the meridional gradient of the vertical component of the earth's vorticity, h_B is the topographic variation, and ν is the viscosity coefficient. The boundary conditions are that there be no momentum source at the wall integrated over the length of the channel (or over a wavelength for periodic solutions) i.e.

$$\left. \begin{array}{l} \Psi_{n_x} = 0 \\[4pt] \lim\limits_{X \to \infty} \int_{-X}^{X} dx\, \Psi_{n_{y t}} = 0 \end{array} \right\} \quad at\ y = \pm \tfrac{1}{2} \qquad (2.2)$$

We now write the streamfunction in each layer as a zonal flow plus a small but finite deviation, i.e.

$$\Psi_n = -U_n y + \phi_n \qquad (2.3)$$

Using (2.3), (2.1) becomes

$$(\partial_t + u_1 \partial_x)[\nabla^2 \psi_1 - F(\psi_1 - \psi_2)] + [\beta + F(u_1 - u_2)] \psi_{1,x}$$
$$+ J[\psi_1, \nabla^2 \psi_1 - F(\psi_1 - \psi_2)] = 0$$

$$(\partial_t + u_2 \partial_x)[\nabla^2 \psi_2 - F(\psi_2 - \psi_1)] + [\beta - F(u_1 - u_2)] \psi_{2,x}$$

$$\hspace{3cm} (2.4a,b)$$

$$+ J[\psi_2, \nabla^2 \psi_2 - F(\psi_2 - \psi_1) + \eta_B] = -r \nabla^2 \psi_2$$

We now proceed to review the important points of the linear theory.

3. Linear analysis

Assume the ψ_n are infinitesimally small and for the time being neglect the topographic term. Eqns. (2.4a,b) now become

$$(\partial_t + u_1 \partial_x)[\nabla^2 \psi_1 - F(\psi_1 - \psi_2)] + [\beta + F(u_1 - u_2)] \psi_{1,x} = 0$$

$$(\partial_t + u_2 \partial_x)[\nabla^2 \psi_2 - F(\psi_2 - \psi_1)] + [\beta - F(u_1 - u_2)] \psi_{2,x} = -r \nabla^2 \psi_2 \quad (3.1a,b)$$

Taking a solution of the form

$$\psi_n = A_n e^{i(kx - \omega t)} \cos \pi y$$

results in the following dispersion relation

$$c = \frac{\omega}{k} = \frac{u_1 + u_2}{2} - \frac{\beta(K^2 + F)}{K^2(K^2 + 2F)} - \frac{ir}{k}\left(\frac{K^2 + F}{K^2 + 2F}\right) \pm \frac{1}{2 K^2(K^2 + 2F)}\left\{K^4(K^2 - 4F^2)(u_1 - u_2)^2\right.$$

$$\hspace{3cm} (3.2)$$

$$\left. + 4\beta^2 F^2 + 2i\frac{r}{k}K^2\left[K^2(K^2 + 2F)(K^2 - F)(u_1 - u_2) + 2\beta F^2\right] - (K^2 + F)^2 r^2 \frac{K^4}{k^2}\right\}^{\frac{1}{2}}$$

where

$$K^2 = S^2 k^2 + \pi^2 \hspace{3cm} (3.3)$$

In the nondispersive ($S = 0$) and frictionless (r=0) limits, baroclinic instability results when $\pi^2 < 2F$ and the vertical shear ($u_1 - u_2$) exceeds the critical value

$$U_c^2 = \frac{4\beta^2 F^2}{\pi^4(4F^2 - \pi^4)} \hspace{3cm} (3.4)$$

For a slightly supercritical shear

$$u_1 - u_2 = U_c + \Delta \quad , \quad \Delta \ll U_c \hspace{2cm} (3.5)$$

the growth rate due to the instability is given as

$$k c_i = \pm \frac{\sqrt{2} k \beta F}{\pi^2 (\pi^2 + 2F)} \left(\frac{\Delta}{u_c} \right)^{\frac{1}{2}} \tag{3.6}$$

and the real part of the frequency is

$$k c_r = \frac{k (u_1 + u_2)}{2} - \frac{\beta k (\pi^2 + F)}{\pi^2 (\pi^2 + 2F)} \tag{3.7}$$

Eqn. (3.6) suggests the long time scale corresponding to the instability, i.e.

$$T_i = |\Delta|^{\frac{1}{2}} t \tag{3.8}$$

The frequency corresponding to the dispersive correction to $k c_r$ of (3.7) is

$$k c_d = \pm \frac{u_c (\pi^2 - 2F^2)^{\frac{1}{2}}}{\pi (\pi^2 + 2F)} \delta k^2 \tag{3.9}$$

to leading order in δ. Note that when $\pi^2 < \sqrt{2} F$ this dispersive term contributes to the instability. We shall refer to this region of parameter space as the short wave side. We shall refer to the region in parameter space defined by $\sqrt{2} F < \pi^2 < 2F$ as the long wave side. In this latter region the long dispersive time scale from (3.9) is defined as

$$T_d = \delta t \tag{3.10}$$

It is important to realize that in this scaling k is O(1). The parameter δ measures the anisotropy of the wave. When $\delta \ll 1$ the wave is weakly dispersive. Similarly, if friction is small (r << 1) the frictional part of ω is

$$k c_f = \frac{\pm (1 + i) k}{2 \pi^2 (\pi^2 + 2F)} \left\{ r \frac{\pi^2}{k} \left[\pi^2 (\pi^2 + 2F)(k^2 - F) u_c + 2 \beta F^2 \right] \right\}^{\frac{1}{2}} \tag{3.11}$$

to leading order in r. From (3.11) we define the frictional long time scale

$$T_f = r^{\frac{1}{2}} t \tag{3.12}$$

We note that friction is destabilizing (Holopainen, 1961). In the finite amplitude analysis we shall make use of these long time scales.

4. Finite amplitude analysis

In order that the growth, dispersion, and friction act simultaneously, we choose the respective parameters so that the time scales defined in (3.8), (3.10), and (3.12) are the same. Therefore

$$|\Delta|^{\frac{1}{2}} = \delta = r^{\frac{1}{2}} \ll 1 \tag{4.1}$$

Now the time operator in (2.4) can be replaced by

$$\partial_t + |\Delta|^{\frac{1}{2}} \partial_T \tag{4.2}$$

where

$$T = |\Delta|^{\frac{1}{2}} t \tag{4.3}$$

To bring in nonlinearity we choose the topography to be

$$\eta_B = |\Delta|^{\frac{1}{2}} b \cos \pi y \tag{4.4}$$

and expand the streamfunction in each layer as

$$\psi_n = |\Delta|^{\frac{1}{2}} \psi_n^{(1)} + |\Delta| \psi_n^{(2)} + |\Delta|^{\frac{3}{2}} \psi_n^{(3)} + \cdots \tag{4.5}$$

Using (3.5), (4.2), (4.4) and (4.5) in (2.4) we obtain a sequence of problems for each power of $|\Delta|^{\frac{1}{2}}$.

The $O(|\Delta|^{\frac{1}{2}})$ problem is

$$[\partial_t + (u_2 + u_c)\partial_x][\psi_{1yy}^{(1)} + F(\psi_2^{(1)} - \psi_1^{(1)})] + (\beta + Fu_c)\psi_{1x}^{(1)} = 0$$

$$(\partial_t + u_2\partial_x)[\psi_{2yy}^{(1)} - F(\psi_2^{(1)} - \psi_1^{(1)})] + (\beta - Fu_c)\psi_{2x}^{(1)} = 0 \tag{4.6a,b}$$

Eqns. (4.6a,b) lead to the specification of the neutrally stable nondispersive disturbance whose evolution we seek, i.e.

$$\psi_1^{(1)} = A(kx - \omega t)\cos \pi y$$

$$\psi_2^{(1)} = \gamma A(kx - \omega t)\cos \pi y \tag{4.7a,b}$$

The $O(|\Delta|)$ problem after the inhomogeneous terms are evaluated using (4.7) is

$$[\partial_t + (u_2 + u_c)\partial_x][\psi_{1yy}^{(2)} + F(\psi_2^{(2)} - \psi_1^{(2)})] + (\beta + Fu_c)\psi_{1x}^{(2)}$$

$$= [\pi^2 - F(\gamma - 1)]A_T \cos \pi y$$

$$(\partial_t + u_2\partial_x)[\psi_{2yy}^{(2)} - F(\psi_2^{(2)} - \psi_1^{(2)})] + (\beta - Fu_c)\psi_{2x}^{(2)}$$

$$= [\pi^2 \gamma + F(\gamma - 1)]A_T \cos \pi y + \frac{\pi}{2}\gamma A_x b \sin 2\pi y \tag{4.8a,b}$$

The long time inhomogeneous terms are handled just as in Pedlosky (1970), his equations (4.15)-(4.19). They give rise to the particular solution

$$\psi_{1h}^{(2)} = 0$$

$$\psi_{2h}^{(2)} = \frac{1}{F}\frac{\beta + Fu_c}{(u_1 - c)^2}\cos \pi y \int dx\, A_T \tag{4.9}$$

The topographic inhomogeneous term produces a topographically forced wave which is due to the interaction of the neutrally stable, nondispersive wave with the topography. This forced solution is

$$\psi_{nf}^{(2)} = f_n A(kx - \omega t, T) \sin 2\pi y \qquad (4.10)$$

where

$$f_1 = -\frac{\pi}{2} \frac{\gamma}{F(\frac{\xi}{5}\bar{5} - 1)(U_2 - c)} \frac{b}{}$$

$$f_2 = -\frac{\pi}{2} \frac{\gamma \bar{5}}{F(\frac{\xi}{5}\bar{5} - 1)} \frac{b}{(U_2 - c)} \qquad (4.11a\text{-}d)$$

$$\zeta = \frac{4\pi^2 + F}{F} - \frac{\beta + F U_c}{F(U_1 - c)}$$

$$\bar{\zeta} = \frac{4\pi^2 + F}{F} - \frac{\beta - F U_c}{F(U_2 - c)}$$

We could add a solution consisting of a zonal flow which would depend on y and T only, since it is a trivial solution to the homogeneous problem. However, with the selection of the functional form (4.7), appropriate in the nondispersive limit, and looking for a solution which decays to zero as x approaches $\pm \infty$, there is no way to produce a zonal flow. Thus, this additional solution would be zero and need not be included.

The final order $O(|\Delta|^{3/2})$ can be written, after evaluating the inhomogeneous side using (4.7), (4.9), and (4.10);

$$[\partial_t + (U_2 + U_c)\partial_x][\psi_{1,yy}^{(6)} + F(\psi_2^{(4)} - \psi_1^{(3)})] + (\beta + F U_c)\psi_{1,x}^{(3)}$$

$$= -\frac{\beta + F U_c}{(U_1 - c)^2} \cos \pi y \int dx\, A_{TT} - (U_1 - c) \cos \pi y\, A_{xxx}$$

$$+ \frac{\Delta}{|\Delta|}\left(\frac{\beta + F U_c}{U_1 - c} - F\right) \cos \pi y\, A_x$$

$$(\partial_t + U_2 \partial_x)[\psi_{2,yy}^{(3)} - F(\psi_2^{(4)} - \psi_1^{(3)})] + (\beta - F U_c)\psi_{2,x}^{(3)} \qquad (4.12a,b)$$

$$= \frac{(\pi^2 + F)(\beta + F U_c)}{F(U_1 - c)^2} \cos \pi y \int dx\, A_{TT} - \gamma(U_2 - c)\cos \pi y\, A_{xxx}$$

$$+ \frac{\Delta}{|\Delta|}\gamma F \cos \pi y\, A_x + \pi b f_2 \sin \pi y \sin 2\pi y\, A_x + \pi^2 \gamma \cos \pi y\, A$$

$$- \frac{\pi^2}{4}\frac{\gamma^2 b}{(U_2 - c)}(2\cos \pi y \cos 2\pi y + \sin \pi y \sin 2\pi y)(A^2)_y$$

where we have written down only resonant terms. In (4.12) we see the presence

of all the desired processes, namely instability, dispersion, friction, and nonlinearity. Removal of these resonances results in the following evolution equation for A. It is

$$A_{,t} + \alpha_2 A_{xx} + \alpha_3 A_x + \alpha_4 A_{xxxx} + \alpha_5 (A^2)_{xx} = 0 \qquad (4.13)$$

where the α_n are given in Appendix I. The second through fifth terms are in order, the growth, frictional, dispersive, and nonlinear terms.

5. Inviscid exact solutions

From here on we shall concentrate our discussion on the inviscid form $\alpha_3 = 0$ of (4.13). The remaining coefficients of (4.13) change sign according to whether we are on the long wave or short wave side of parameter space (see Fig. 1), whether the term $\alpha_2 A_{xx}$ is actually a growth or decay term, and the sign of topography. Whether or not we are in the long or short wave side of parameter space depends upon the width of the channel relative to the internal deformation radius, i.e., the parameter F. On the long wave side

$$\frac{\pi^2}{2} < F < \frac{\pi^2}{\sqrt{2}},$$

while on the short wave side

$$F > \frac{\pi^2}{\sqrt{2}}$$

by definition.
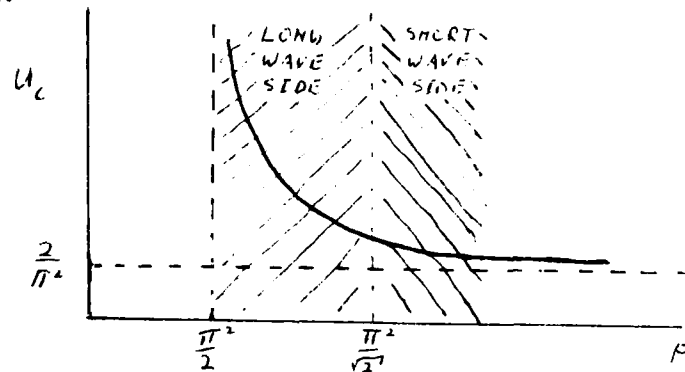
Figure 1: Schematically shows the region of parameter space covering the long wave and short wave sides of parameter space. U_c is the solid line.

We now rescale the variables in (4.13). On the long wave side we obtain for $b > 0$ (topography of elevation)

$$B_{\tau\tau} \pm B_{xx} + B_{xxxx} + (B^2)_{xx} = 0 \qquad (5.1)$$

where the (+) sign refers to the unstable case ($\alpha_c > C$) and the (-) sign refers to the stable case ($\alpha_c < C$). The following scaling was used

$$
\begin{aligned}
T &= d\,\tau \\
x &= a\,\chi \\
A &= N\,B
\end{aligned}
\tag{5.2}
$$

where

$$
a = \sqrt{\pm \frac{\alpha_4}{\alpha_c}}
$$

$$
d = \pm \frac{\sqrt{\alpha_4}}{\alpha_c}
\tag{5.3}
$$

$$
N = \sqrt{\pm \frac{\alpha_c}{\alpha_5}}
$$

and ($\pm$) sign has the same meaning as in (5.1). On the short wave side (4.13) becomes for b > 0.

$$
B_{\tau\tau} \pm B_{\chi\chi} - B_{\chi\chi\chi\chi} - (B^2)_{\chi\chi} = 0
\tag{5.4}
$$

where (4.15) was again used and

$$
a = \sqrt{-(\pm)\frac{\alpha_4}{\alpha_c}}
$$

$$
d = \pm \sqrt{-\frac{\alpha_4}{\alpha_c}}
\tag{5.5}
$$

$$
N = \sqrt{-(\pm)\frac{\alpha_c}{\alpha_5}}
$$

For topography of depression (b < 0) the sign of the nonlinear term in (5.1) and (5.4) is changed and (5.3c) and (5.5c) are interchanged.

We look for the solitary wave solution

$$
B = G\,\operatorname{sech}^2\left[k'(x - C\tau) \right]
\tag{5.6}
$$

to (5.1) and (5.4). In order for (5.6) to be a solution to (5.1), we must satisfy the following conditions

$$
6\,k'^2 = G
$$
$$
C^2 = -(\pm)1 + 4k'^2 > 0
\tag{5.7a,b}
$$

the first of which is the nonlinear-dispersive balance. Equation (5.7a) tells us that only solitary waves of elevation are possible ($G > 0$). If b < 0 (5.7a) would become $6k'^2 = -G$ and only solitary waves of depression ($G < 0$) would be possible. Equation (5.7b) says that there are no solutions of the type (5.6) when the unstable case ((+) sign of 5.7b) is considered since that would imply $C^2 < 0$. In the stable case ((-) sign of 5.7b), (5.6)

is a solution when $4k'^2 > 1$. On the short wave side similar arguments
apply. Equation (5.7a) still applies but the phase speed condition becomes

$$C^2 = 4k'^2 - (1)| > 0 \qquad (5.8)$$

which is satisfied for all wavenumbers in the stable case ((-) sign of 5.8)
and only for $4k'^2 > 1$ in the unstable case. See Table 1 for a summary of
these results. It is important to realize that in Table 1 $k' = 1/2 k$. It
is interesting to note that when the signs of F_{xx} and F_{xxxx} are opposite
only long wave ($0 < k < 1$) solitons are possible on the long wave side and
only short wave ($k^2 > 1$) solutions are possible on the short wave side. N
soliton solutions are also possible. The reader is referred to Hirota (1973)
for a discussion of this.

We have still not found solutions for some wavenumbers on the short and
long wave sides of parameter space. We shall look for some of these missing
solutions in the next section.

6. Envelope solitary wave solutions

In this section we look for envelope solitary waves to (5.1). To do this
we derive a nonlinear Schrodinger equation (NSE) from (5.1) for the amplitude
$a(X, \tau_1)$ of the wave packet solution

$$a(X, \tau_1) e^{i(kx - \Omega \tau)}$$

where τ_1 and X are the long time and space scales, respectively. These are
defined

$$\tau_1 = \epsilon^2 \tau \qquad (6.1a,b)$$

$$X = \epsilon(x - v_g \tau)$$

where v_g is the group velocity of the packet and ϵ measures the width of
the packet in wavenumber space (ϵ in this context is not the Rossby number as
in section 2). Using (6.1) the time operator ∂_τ and the space operator
can be replaced by

$$\partial_\tau - \epsilon v_g \partial_x + \epsilon^2 \partial_{\tau_1} \qquad (6.2)$$

$$\partial_x + \epsilon \partial_X$$

If we expand

$$\beta = \epsilon b_1 + \epsilon^2 b_2 + \epsilon^3 b_3 + \cdots \qquad (6.3)$$

and use (6.2) to replace the time and space operators of (5.1) we obtain a
sequence of problems in successive powers of ϵ . To 0 (ϵ) we have

$$b_{,\tau\tau} \pm b_{,xx} + b_{,xxxx} = 0 \qquad (6.4)$$

As a solution to (6.4) we take

$$b_1 = a(X, \tau_1) e^{i\theta} + * \qquad (6.5)$$

where * denotes the complex conjugate and

$$\theta = kx - \omega t \tag{6.6}$$

The dispersion relation is

$$\omega = k(k^2 - (t)1)^{\frac{1}{2}} \tag{6.7}$$

When the (+) is chosen (possible instability) we must have $k^2 > 1$ so actual instability is not allowed. The group velocity corresponding to (6.7) is

$$v_g = \frac{2k^2 - (1)1}{(k^2 - (1)1)^{\frac{1}{2}}} \tag{6.8}$$

From (6.8) we note that in order to avoid an infinite group velocity we must have $k^2 \neq 1$. The $0(\epsilon^2)$ problem is

$$b_{2tt} + b_{2xx} + b_{2xxxx} = -i(2\omega v_g \pm 2k - 4k^3)a_x e^{i\theta} + \omega k^2 a^2 e^{2i\theta} + *$$

where (6.5) was used to evaluate the righthand side. Using (6.7) and (6.8) the inhomogeneous term proportional to $e^{i\theta}$ vanishes. The inhomogeneous term proportional to $e^{2i\theta}$ yields the forced solution

$$b_2 = \frac{1}{3k} a^2 e^{2i\theta} + * \tag{6.9}$$

At $\epsilon(\epsilon^3)$ we have

$$b_{3tt} + b_{3xx} + b_{3xxxx} = -(2\partial_{ty} \partial_{xy} + \partial_{xx} + 4\partial_{xxxx})b_1$$
$$- 2\partial_{xx}(b_1)^2 - (2\partial_{tt_1} + v_g^2 \partial_{xx} + \partial_{xx} + 6\partial_{xxxx})b_1$$
$$- 2\partial_{tx}(b_1 b_2) \tag{6.10}$$

The only resonant terms of (6.10) are proportional to b_1 and $b_1 b_2$. Using (6.5) and (6.9) in their removal yields

$$i a_{t_1} + \lambda a_{xx} = \mu |a|^2 a \tag{6.11}$$

where

$$\lambda = \frac{k(2k^2 - (1)3)}{2(k^2 - (1)1)^{1/2}}$$

$$\mu = -\frac{1}{3k(k^2 - (1)1)^{\frac{1}{2}}} \tag{6.12,a,b}$$

It is well known that envelope soliton solutions of the form

$$a \sim \left(2\nu'\mu^{-1}\right)^{\frac{1}{2}} \operatorname{sech}\left[(-\nu'\lambda^{-1})^{\frac{1}{2}} x\right] e^{-i\nu' T} \tag{6.13}$$

exist if

$$\lambda \nu' < 0 \tag{6.14}$$

On the long wave side for which this analysis was just carried out, (6.14) is true for $k^2 > 3/2$ in the unstable case and always true for the stable case. On the short wave side λ is replaced by λ' where

$$\lambda' = -\lambda$$

In this case the condition $\lambda'\nu' < 0$ is satisfied and the analysis is valid for $0 < k^2 < 1$ in the stable case and the analysis cannot be done on the unstable side because ω is not real for any wavenumber. This is summarized in Table 1.

Table 1.

LONG WAVE SIDE	EXACT SOLITARY WAVE	ENVELOPE SOLITARY WAVE
UNSTABLE	NONE	$k^2 > 3/2$
STABLE	$0 < k^2 < 1$	ALL k
SHORT WAVE SIDE		
UNSTABLE	$k^2 > 1$	NONE
STABLE	ALL k	$0 < k^2 < 1$

A comparison of the wavenumber space which allows exact solitary and envelop solitary waves on both the short wave and long wave sides of parameter space. Note k' of (5.6) is 1/2 k.

8. Discussion

We have discussed some special solutions to the inviscid form of (4.13). The search for viscous solutions has not as yet proved fruitful. The exact solitary and envelop solitary solutions have complimented each other. It is interesting that on the long wave side there are no solitary waves with a wavenumber that would give rise to instability through the linear dispersion relation (6.7). However, on the short wave side the exact solitary wave exists for wavenumbers for which there is instability according to the dispersion relation

$$\nu^2 = k^2 \left(-(1)_1 - k^2 \right)$$

which is the counter part to (6.7) on the shortwave side. As a result we might conjecture that there may be a difference in the way these solitary waves evolve from initial conditions on the long and short wave sides if they do at all. To test this the initial value problem must be attempted which may be possible in some parameter regimes through inverse scattering techniques and/or a combination of numerical and asymptotic expansion techniques.

Pedlosky (1972) has sought wave packet solutions directly from (2.4). The essential difference between that analysis and this is that in the nondispersive limit we have considered, the zonal flow cannot be altered when we seek solutions which decay towards $\pm \mathcal{Y}$ in the zonal coordinate. This modification of the zonal flow is essential for the eventual quelling of the initially exponential instability. Therefore, the inital value problem corresponding to (4.13) may not always have bounded solutions in time since the feedback with the zonal flow is not present.

We have not reached the ultimate goal of this work which was to find growing solitary wave solutions. It seems if they exist in this model, that they are tangled up in the initial value problem for (4.13). Furthermore, it seems likely that one must abandon the idea of the growing classical soliton and to give way to finding a growing isolated feature (i.e., at the very least we should allow a different spatial structure). However, the classical solitary wave is certainly a useful concept in reaching that goal in that the necessary physics may be contained within it. Namely, as we have suggested in this paper that combining an instability with the classical nonlinear dispersive balance of a solitary wave may produce a growing isolated feature. Although growing isolated solutions have not yet been obtained we have succeeded in deriving a relatively simple equation which contains the physical mechanisms which may lead to such solutions.

ACKNOWLEDGEMENT

REFERENCES

Hirota, R., 1973: Exact N-soliton solutions of the wave equation of long waves in shallow-water and in nonlinear lattices. J. Math. Phys., 14, 810-814.

Holopainen, E. O., 1961: On the effect of friction in baroclinic waves. Tellus, 13, 363-367.

Pedlosky, J., 1970: Finite-amplitude baroclinic waves, J. Atmos. Sci., 29, 680-686.

_____,1972: Finite amplitude baroclinic wave packets, J. Atmos. Sci., 29, 680-686.

_____,1980: Geophysical Fluid Dynamics, Springer-Verlag, 624 pp.

APPENDIX I

The coefficients are

$$\alpha_1 = \frac{2 b^2 F^2}{\pi^4 (\pi^2 + 2F)^2} \frac{1}{U_c}$$

$$\alpha_2 = -\frac{\pi^2 b^2 \gamma^2 \xi}{4F(U_2 - c)D(\xi \xi - 1)}$$

$$\alpha_3 = \frac{1}{2\pi^2(\pi^2 + 2F)^2} \left[\pi^2 (\pi^2 + 2F)(\pi^2 - F) U_c + 2\beta F^2 \right]$$

$$\alpha_4 = \frac{U_c^2 (\pi^4 - 2F^2)}{\pi^2 (\pi^2 + 2F)^2}$$

$$\alpha_5 = -\frac{3\pi^2 \gamma^3 b(U_1 - c)}{\gamma D(U_2 - c)}$$

$$\alpha_6 = \alpha_1 + \alpha_2$$

where

$$D = \left(\frac{3FFU_c}{U_1 - c} \right) \left[\gamma \left(\frac{\pi^2 + F}{F} \right) - \left(\frac{U_2 - c}{U_1 - c} \right) \right]$$

α_1, α_3, and α_4 agree with the results of the linear analysis, i.e. with (3.6), (3.11), and (3.9) respectively. We note that the total growth term α_c consists of the baroclinic part α_1 and a topographic part α_2 due to the interaction of the topographically forced wave with the topography.

A FORCED BURGERS EQUATION

James Meiss and William Young

1. Introduction

It is now well known that rather mild looking systems of third order, ordinary differential equations such as the Lorenz model have chaotic, or more precisely aperiodic, solutions. Although the Lorenz model was derived by modally truncating the partial differential equations describing two dimensional convection, its chaotic solutions are found only for parameter values at which the modal truncation is unjustified. Thus one could argue that the Lorenz model, and other similarly constructed ordinary differential systems, tell us litle about the chaotic solutions of partial differential equations.

This report began as an attempt to find a simple model partial differential equation which exhibited chaotic behaviour. Our hope was that the equation would be simple enough to allow an exhaustive numerical study, thus we restricted ourselves to two independent variables. Although we were not successful we felt it would be pedagogicaly useful to summarize our attempts. The one conclusion we can unequivocally draw is that forcing, dissipation and nonlinearity are not sufficient to ensure the existence of a chaotic regime in a partial differential system.

2. The First Model

The first model we consider is the nonlinear eigenvalue problem

$$u_t = u u_x + R u + u_{xx} \tag{1a}$$

$$u(o) = u(1) = o \tag{1b}$$

Burgers considered this model in 1939. We will reexamine it from a more modern prospective.

First $u = o$ is a steady solution of (1). When $R < \pi^2$ it's also linearly stable. To see this, represent u as a sin series:

$$u(x,t) = \sum_{n=1}^{\infty} a_n(t) \sin(n\pi x) \tag{2}$$

The linear evolution equations for the a_n's are

$$\dot{a}_n = (R - n^2 \pi^2) a_n$$

If $R - \pi^2 < o$ then all the a_n's decay exponentially to zero.

We can prove a much stronger result than this using a variational argument viz when $R < \pi^2$ all initial conditions decay to $u = o$.

Begin by multiplying (1a) by u and integrating over the interval. One has

$$\frac{1}{2}\frac{d}{dt}\langle u^2\rangle = R\langle u^2\rangle - \langle u_x^2\rangle \tag{3}$$

where

$$\langle\cdot\rangle = \int_0^1 (\cdot)\, dx$$

Equation (3) is an energy equation, the left hand side is forced by $R\langle u^2\rangle$ and $\langle u_x^2\rangle$ provides dissipation. A simple variational argument shows that the smallest value of the functional

$$\mathcal{F}[\omega] = \frac{\langle \omega_x^2\rangle}{\langle \omega^2\rangle}$$

$$\omega(0) = \omega(1) = 0$$

is π^2. Thus (3) becomes

$$\frac{d}{dt}\langle u^2\rangle \leq 2(R-\pi^2)\langle u^2\rangle$$

so that if $R-\pi^2 < 0$ then $\langle u^2\rangle \to 0$.

Eqn. (1) is so simple that all the steady solutions can be reduced to quadratures by introducing

$$v = R^{-1}u_x$$

and writing (1a) in the form

$$u_x = Rv \tag{5a}$$

$$v_x = -u(1+v) \tag{5b}$$

The trajectories of this system are sketched in Figure 1. Eqns. (5) are now simplified by eliminating x and using v as an independent variable,

$$\frac{du}{dv} = -\frac{Rv}{u(1+v)}$$

or

$$u = \pm(2R)^{1/2}\sqrt{A + \log(1+v) - v} \tag{6}$$

where A is the constant of integration. A is determined by requiring that (6) satisfy (1b). Using (5a) and (5b)

$$x = \int_0^x dx' = \int_0^u \frac{du}{Rv}$$

$$= -\frac{1}{R}\int_0^u du' - \int_{v_1}^v \frac{dv}{u} \tag{7}$$

where v_1 is the value of v at $x = 0$. At $x = 1$, where $u = 0$ and $v = v_2$, (6) and (7) imply

$$m^{-1}(2R)^{1/2} = \int_{v_1}^{v_2} \frac{dv}{\sqrt{A+\log(1+v)-v}} \tag{8}$$

m is an integer which determines the number of zeroes in the interval. Equation (8) determines A as a function of R and m. This is equivalent to choosing a particular trajectory in Fig. 1 and traversing it $(\frac{1}{2}m + \frac{1}{2})$ times starting at $u = 0$.
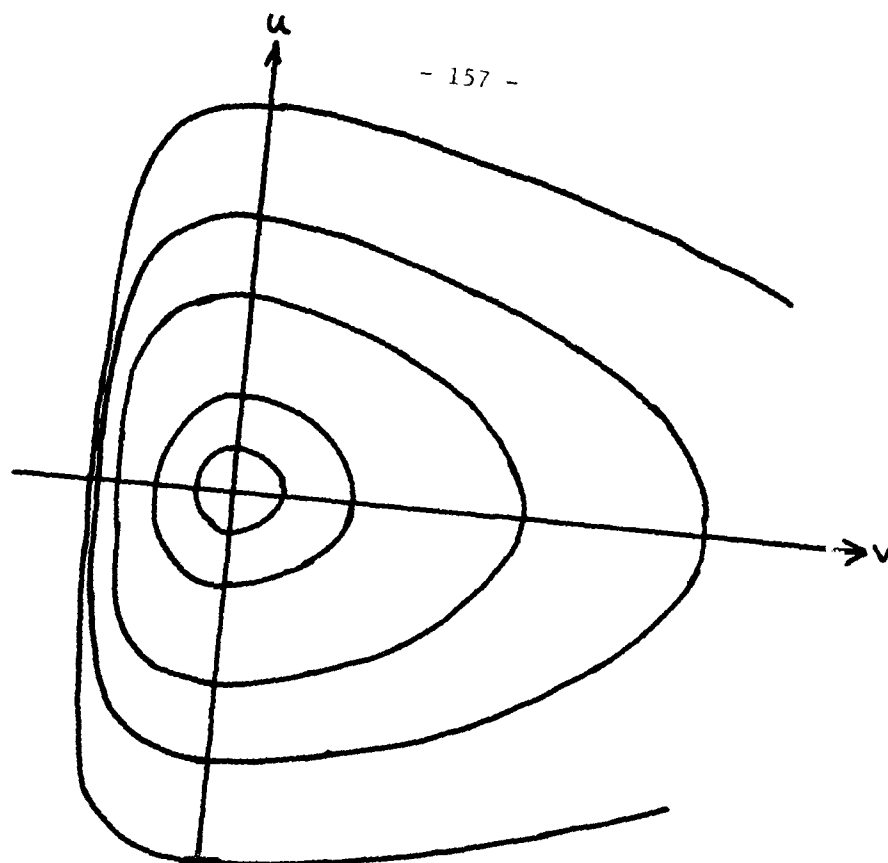
Fig. 1: The trajectories of the system (5a,b) in the (u,v) plane.
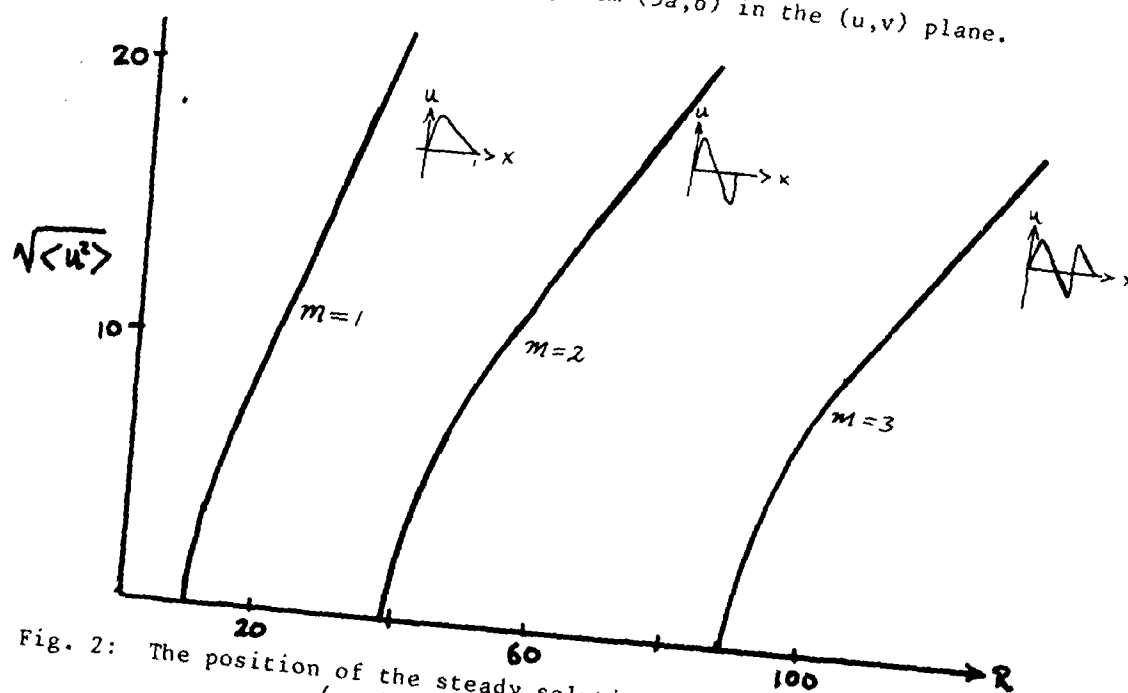
Fig. 2: The position of the steady solutions of (1a,b) in the (amplitude, R) plane.

The results of a numerical evaluation of (8) are summarized in Figure 2 (Burgers discusses some analytic approximations). Instead of plotting A against R we use a more conventional measure of the amplitude of the solution. The linear solutions are at R = ($n\pi$)2 on the $\sqrt{<u^2>}$ = 0 line. The steady solutions we have found using (5) all bifurcate from these points.

We shall discuss the first bifurcation at R = π^2 in detail. Let

$$\varepsilon = R - \pi^2 > 0$$

and substitute (2) into (1a) retaining the nonlinear term uu_x. When $\varepsilon \ll 1$ it is only necessary to retain two modes to capture the leading order behaviour;

$$\dot{a} = \varepsilon a - \frac{\pi}{2} ab \tag{9a}$$

$$\dot{b} = (-3\pi^2 + \varepsilon^2) b + \frac{\pi}{2} a^2 \tag{9b}$$

where u = a $\sin(\pi x)$ + b $\sin(2\pi x)$ + $\cdots$. Now use the usual scaling which applies in a slightly supercritical situation:

$$a = \sqrt{\varepsilon} A \qquad b = \varepsilon B \qquad T = \varepsilon t$$

and to leading order (9a,b) reduces to the Landau equation

$$A_T = A - \frac{1}{12} A^3 \tag{10}$$

Equation (10) shows that when R > π^2 the solution u = o is unstable and the system bifurcates to a new steady (and also stable) solution.

Before discussing the stabiity of these steady solutions we will investigate them in the limit R $\gg$ 1, $u \sim$ R using boundary layer techniques. This investigation supplements the exact solutions in (6) - (8) and provides useful insight into the stability problem.

If

$$\tilde{u} = R^{-1} u$$

then (1a) is

$$o = \tilde{u} + \tilde{u}\tilde{u}_x + R^{-1} \tilde{u}_{xx} \tag{11}$$

If the term $R^{-1} \tilde{u}_{xx}$ is neglected we get

$$\tilde{u} = -x + c \tag{12}$$

This solution cannot satisfy all the boundary conditions and must be supplemented by thin boundary layer regions in which the neglected term is important. To resolve the boundary layers introduce

$$\xi = R (x - x_0)$$

where $x_\bullet$ is the position of the boundary layer. With this new variable (11) is

$$0 = R^{-1} \tilde{u} + \tilde{u}\tilde{u}_\xi + \tilde{u}_{\xi\xi} \tag{13}$$

The relevant solution of (13) is

$$\tilde{u} = 2\alpha \tanh\left[\alpha R(x - x_0)\right] \tag{14}$$

The constant α is chosen to satisfy the various boundary and matching conditions. For example to construct the solution sketched in Fig. (3a) we have $c = 1$ in (12) and $\alpha = 1/2$, $x_\bullet = 0$ in (14).
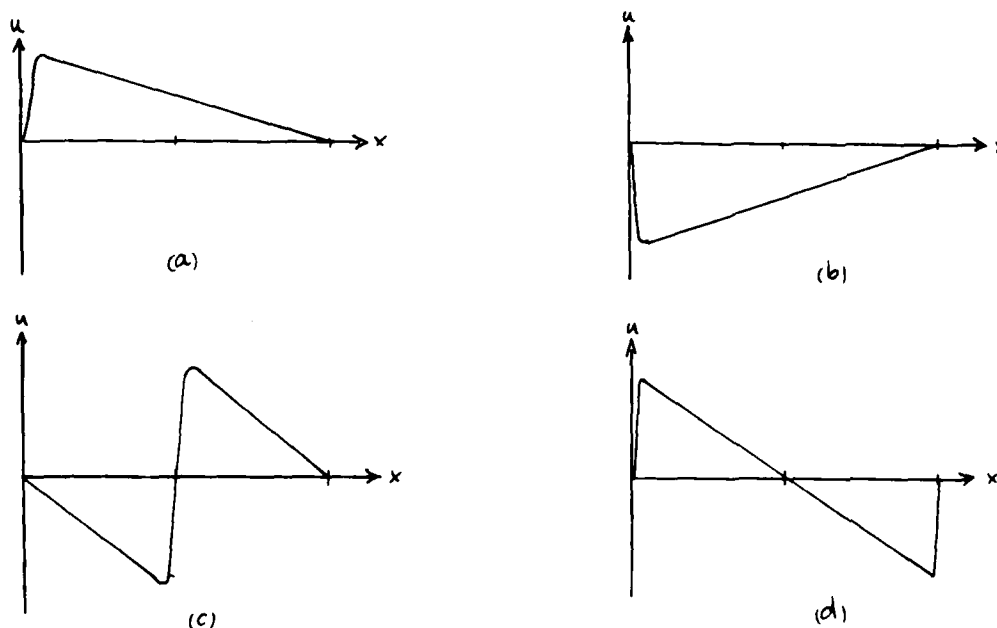
Fig. 3: A schematic illustration of the boundary layer solutions constructed in using the limit $R \gg 1$, $u \sim R$.

The other solutions sketched in Fig. 3 can be constructed in a similar fashion.

We turn now to a discussion of the stability of the steady solutions. This is an issue which Burgers completely ignored and it is of course vitally important in deciding whether (1a,b) has chaotic (or even periodic) solutions.

Linearize about the steady solution

$$u = \bar{u}(x) + u'(x,t)$$

where $\bar{u}(x)$ is now the steady solution. The linearized equation for u' can be reduced to

$$-\psi_{xx} + \left\{ \sigma - R - \tfrac{1}{2}\bar{u}_x^2 + \tfrac{1}{4}\bar{u}^2 \right\} \psi = 0 \qquad (15)$$

using the substitution

$$u' = e^{\sigma t}\, e^{-\int_0^x \bar{u}\, dx'}\, \psi(x)$$

Equation (15) is the time independent Schrodinger equation. It tells us immediately that σ is real, so there are no oscillatory instabilities. This is disappointing since the appearance of chaos in ordinary differential systems is frequently preceeded by the overstable oscillations characteristic of the Hopf bifurcation.

It is possible to use (15) combined with the large R solution to discuss the stability of the solutions sketched in Fig. 3. Using just the interior solution (12), the potential in (15) is very simple and the eigenmodes and eigenvalues can be discussed using the well known solution of the simple harmonic oscillator. This analysis suggests that the solutions in the (3a,b) are stable while those in (3c,d) are unstable. This analysis is not conclusive since it is hard to assess the importance of perturbations to the potential resulting from the boundary layers and higher order terms in the R^{-1} expansion. However, a numerical solution of (1a,b) using spectral methods confirmed this tentative conclusion and strengthened it to fully nonlinear perturbations. No matter what the initial condition was the system always evolved to a final state resembling (3a) or (3b). The nature of this instabilty is sketched in Fig. 4 for the solution in Fig. (3c). Basically a small first mode perturbation to a solution with a boundary layer at x = 1/2 breaks the symmetry about x = 1/2 and causes the shock to propagate (initially with a speed $\tfrac{1}{2}\epsilon$). As the shock moves towards x = o it evolves into an m = 1 solution.
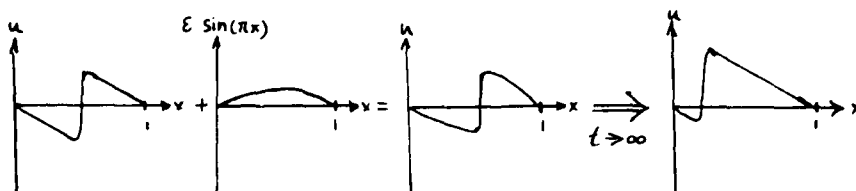
Fig. 4: A hueristic illustration of the m = 2 solution. A small first mode perturbation breaks the symmetry about x = 1/2 and causes the shock to propagate.

To summarize, (1a,b) is not a successful model. If $R < \pi^2$, u = o is an absolutely stable solution. If $R > \pi^2$ the solutions sketched in Fig. (3a,b) and located on the uppermost, m = 1, curve in Fig. 2 are absolutely stable. In no case did we find any interesting (even periodic) time dependent behaviour. These conclusions were supported by a numerical solution of (1a,b).

3.   The Second Model

In an attempt to find more interesting behaviour we considered a more complicated model, also proposed by Burgers in 1939. The idea is to make R time dependent in a way which depends on the integral properties of u

$$R_t = P - R - \sigma <u^2> \tag{16a}$$

$$u_t = R u + u u_x + u_{xx} \tag{16b}$$

$$u(0) = u(1) = 0 \tag{16c}$$

P and σ are constants, Burgers only considered the case $\sigma = 1$.

The energy equation for (16a,b,c) depends on the sign of σ . Let

$$\zeta = \frac{1}{|\sigma|} (R-P)^2 + <u^2>$$

then

$$\zeta_t = P<u^2> - <u_x^2> - \frac{1}{|\sigma|} (R-P)^2 + (1 - \text{sgn}\, \sigma)(R-P)<u^2>$$

If $\sigma > o$ then using a variational argument we can prove as before that when $P < \pi^2$, $\zeta \to 0$ as $t \to \infty$.

The nature of the solutions when P is just supercritical:

$$P = \pi^2 + \varepsilon \qquad \text{and} \qquad \varepsilon \ll 1$$

can be determined as before. Once again a = $\sqrt{\varepsilon}$ A satisfies a Landau equation

$$A_T = A - \frac{1}{12}(6\sigma+1)A^3 \tag{17}$$

Note that the bifurcation is subcritical if $\sigma < -\frac{1}{6}$.

The steady solutions can again be reduced to quadratures. The amplitude is plotted against P for the m = 1 solution in Figure 5. If $\sigma > o$ the curve bends down closer to the P axis for a given amplitude. When $\sigma = -\frac{1}{6}$ the curve is perpendicular to the P axis at P = π^2 . This is in agreement with (17) which shows that at this value of σ there is a transition from super to subcritical instability.
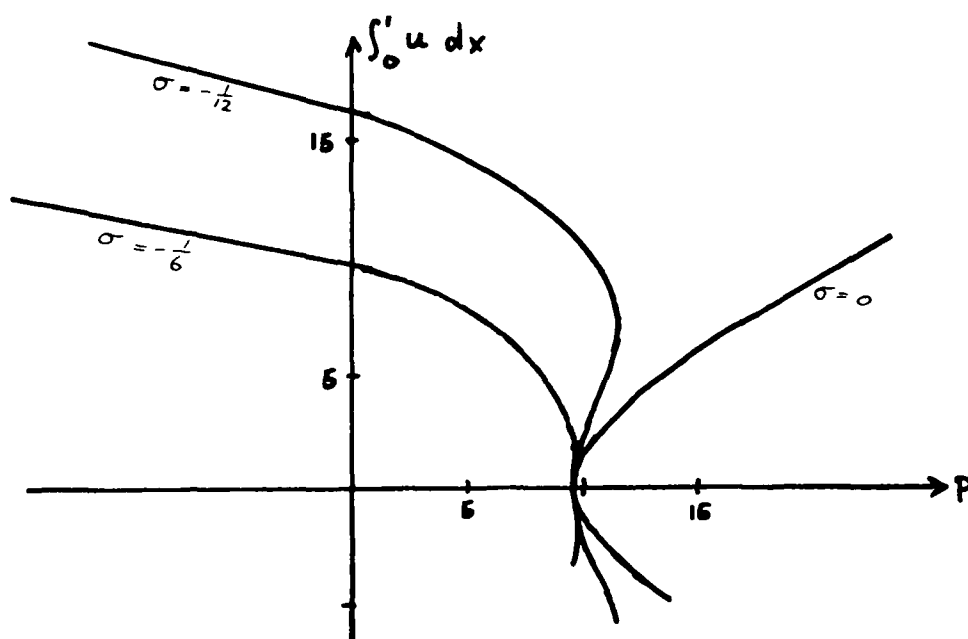
Fig. 5: The position of the m = 1 steady solutions of (16) in the (amplitude, R) plane for various

Now consider the range $0 > \sigma > -\frac{1}{6}$, say $\sigma = -1/12$ to be specific. We originally thought there would be interesting time dependent solutions for sufficiently large P. We reasoned as follows. Suppose P = 10 say. Then from Fig. 5 there is an m = 1 steady solution which a given initial condition can evolve into. The model 1 results suggest this steady solution is stable. This was confirmed numerically. When P is increased past the "turn over point" A of the $\sigma = -1/12$ the curve in Fig. 5 there is no longer an m = 1 steady stable solution available to trap the system. There is an m = 2 steady solution with a very large amplitude, but it is probably unstable. Thus we expected some interesting time dependent behaviour for P in this range. Instead what was observed numerically, and later proven analytically, was that the system goes to infinity in this parameter range. In fact it does so in a finite time. The analytic proof is based on the observation that when R is large then

$$u = -Rx$$

so that

$$\langle u^2 \rangle = \frac{1}{2} R^2 + O(R)$$

Thus, when $\sigma < 0$, (16a) is forced by an R^2 term which can produce explosive instability. Presumably this is what's responsible for the rapid growth observed numerically when P is taken past the turnover point on Figure 5.

4. Modal Truncations

We also investigated the three mode truncation of (16a,b,c). By this stage we had abandoned all hope of finding chaotic behaviour in (16). The aim of this investigation was simply to see how the behaviour of the modally truncated system differed from that of the partial differential equation.

The three mode truncation is

$$\dot{\mathcal{R}} = P - \mathcal{R} - \tfrac{1}{2}\sigma\,(a^2 + b^2) \tag{18a}$$

$$\dot{a} = (\mathcal{R} - \pi^2)a - \tfrac{1}{2}\pi\,ab \tag{18b}$$

$$\dot{b} = (\mathcal{R} - 4\pi^2)b + \tfrac{1}{2}\pi\,a^2 \tag{18c}$$

We will discuss the case $\sigma = 0$ in detail. Apart from a few unresolved questions, the $\sigma \neq 0$ case appears to be qualitatively similar in the regions we explored using primarily linear stability theory.

With $\sigma = 0$ and $R = P > 0$, (18a,b,c) reduce to

$$\dot{a} = (P - \pi^2)a - \tfrac{1}{2}\pi\,ab \tag{19a}$$

$$\dot{b} = (P - 4\pi^2)b + \tfrac{1}{2}\pi\,a^2 \tag{19b}$$

An "energy" equation follows immediately

$$\frac{d}{dt}\,\tfrac{1}{2}(a^2 + b^2) = (P - \pi^2)a^2 + (P - 4\pi^2)\,b^2 \tag{20}$$

Eqn. (20) implies that

(i) If $(P - \pi^2) < 0$ then all solutions fall into the attractor $(a,b) = (0,0)$.

(ii) If $P - 4\pi^2 > 0$ then all solutions go to infinity as $t \to \infty$.

One of the unresolved questions alluded to at the start of this section is the behaviour of the system with $\sigma \neq 0$ and $P - 4\pi^2 > 0$. It does not appear to be possible to determine the asymptotic state of the system using a clear cut energy argument as above.

The case not covered by the energy argument is

$$\pi^2 \leqslant P \leqslant 4\pi^2$$

In this case its convenient to use

$$\mu = \ln a^2$$

as an independent variable. The equation for μ is

$$\ddot{\mu} + \gamma_2 \dot{\mu} + \tfrac{1}{2}\pi^2 e^\mu - \gamma_1\gamma_2 = 0 \qquad (21)$$

$$\gamma_1 = 4\pi^2 - P \geqslant 0 \qquad \text{+} \qquad \gamma_2 = 2(P-\pi^2) > 0$$

If $\gamma_2 \neq 0$ the system has a steady solution at

$$e^\mu = \tfrac{2}{\pi^2}\gamma_1\gamma_2$$

$$\alpha = \pm \tfrac{2}{\pi}\sqrt{(4\pi^2-P)(P-\pi^2)}$$

Moreover its clear from (21) that this equilibrium position is stable even under finite amplitude perturbations. However, linear stability theory shows that the return to the equilibrium position takes the form of damped oscillations if

$$P \geqslant \tfrac{4}{3}\pi^2$$

This is in contrast to partial differential equation where the corresponding solution is also stable under finite amplitude perturbations but linear stability theory shows that all the eigenvalues are real so that the return to equilibrium is an exponential decay. This qualitative difference in behaviour occurs at a not too large value of the supercriticality.

REFERENCES

J. M. Burgers (1939), Mathematical examples illustrating relations occurring in the theory of turbulent fluid motion. Verhandel. Kon. Nederl. Akad. Wetenschappen Amsterdam, Afdeel. Natuurkunde (1st sect.), 17, No. 2, 1-53.

CONVECTION WITH TEMPERATURE DEPENDENT MATERIAL PROPERTIES

M. Cristina Depassier

I. Introduction

We want to consider what are the non-linear effects introduced by assuming that the material properties of the fluid are included in the Boussinesq equations. This was first done by Palm (1960) and Busse (1962) for the case of fixed temperature on the boundaries and for a single wave number k. Here we will consider a continuous finite band of linearly unstable modes. There are two extreme cases of interest, one is the case of fixed temperatures on the boundaries for which the critical wavelength is of the same order as the depth of the layer of fluid. When the flux across the boundaries is fixed instead, the most unstable wave number is zero (Hurle, Jakeman and Pike (1967)). In the first situation there are two relevant horizontal scales and it can be approached using the method of Newell & Whitehead (1969). In the second case, since the wavenumber and the amplitude are small, one can use shallow water methods (Childress & Spiegel). We consider only this last case here. We find that for large wavenumbers (large in the small scale) there is no qualitative effect. The bifurcation from the static state is supercritical; however, for small enough wavenumbers, small in a sense which will become clear later, the bifurcation is subcritical.

II. Equations of the Problem

We will consider a two dimensional fluid contained between two insulating plates at $z = \pm D/2$ under the influence of a constant gravitational field $\vec{g} = g\hat{z}$ and heated from below with the flux held constant at both boundaries. The equations that describe the problem are

$$\vec{\nabla} \cdot \vec{v} = 0 \tag{1}$$

$$\rho_o \left(\frac{d\vec{v}}{dt} \right)_j + (\vec{\nabla} p)_j = \sum_i \frac{\partial}{\partial x_i} \left[\mu \left(\frac{\partial v_i}{\partial x_j} + \frac{\partial v_j}{\partial x_i} \right) \right] + (g \rho \hat{z})_j \tag{2}$$

$$\frac{dT}{dt} = \vec{\nabla} \cdot (\kappa \vec{\nabla} T) \tag{3}$$

$$\rho = \rho_o \left[1 - \alpha (T - T_o) + \varepsilon \alpha f (T - T_o) \right] \tag{4}$$

$$\mu = \mu_o \left[1 + \varepsilon \frac{dg}{dT} (T - T_o) \right] \tag{5}$$

$$\kappa = \kappa_o \left[1 + \varepsilon \frac{dh}{dT} (T - T_o) \right] \tag{6}$$

with

$$f(0) = \frac{dg}{dT}(0) = \frac{dh}{dT}(0) = h(0) = g(0) = 0 \tag{7}$$

The functions f, g and h which contain the temperature dependence of the material, except for the properties stated above are arbitrary. The parameter ε will be considered a small quantity.

The boundary conditions are

$$K \frac{\partial T}{\partial z} = F$$
$$\qquad\qquad\qquad \text{on} \qquad z = \pm D/2 \tag{8}$$
$$w = \frac{\partial v}{\partial z} = 0$$

We have chosen free-free boundary conditions for simplicity but everything can be repeated for rigid boundaries.

Static solution and dimensionless form of the equations

Equation (3) can be integrated at once. Choosing $T_S(0) = T_0$ we obtain

$$K_0 (T_s - T_0) + \varepsilon K_0 h(T_s - T_0) = F z \tag{9}$$

Letting $T_s - T_0 = \sum \varepsilon^n T_{sn}$ we find

$$T_{s0} = F z / K$$

$$T_{s1} = - h(T_{s0})$$

$$T_{s2} = h(T_{s0}) h'(T_{s0})$$

Prime denotes differentiation with respect to the argument. Since both μ and K depend on the temperature, the Rayleigh and Prandtl numbers depend on z:

$$R = \frac{\rho_0 g D^3 \alpha}{K \mu} \left(T_s(D/2) - T_s(-D/2) \right) \qquad , \qquad \sigma = \frac{\mu}{K \rho_0} \tag{10}$$

It is convenient to evaluate them at the middle of the layer, where $T_s = T_0$. Choosing units in which $D = 1$, $\rho_0 = 1$, $K_0 = 1$ and $F = 1$ we find

$$\sigma (z = 0) = \mu_0 \qquad , \qquad R(z = 0) = \frac{g^3 \alpha}{\mu_0} \left(1 + \varepsilon \Delta h + \cdots \right) \tag{11}$$

where

$$\Delta h = h(1/2) - h(-1/2)$$

Since $\nabla \cdot \vec{v} = 0$, we introduce the stream function ψ defined by $\vec{v} = (\psi_z, 0, -\psi_x)$. We also let the temperature be $T = T_s + \theta$. The equations then reduce to

$$\mu \nabla^4 \psi - \frac{1}{\sigma} \nabla^2 \psi_t + \frac{1}{\sigma}[\psi_x \nabla^2 \psi_z - \psi_z \nabla^2 \psi_x] + 2\mu_z \nabla^2 \psi_z$$

$$+ 2\mu_x \nabla^2 \psi_x + 4\mu_{xz} \psi_{zx} + (\mu_{zz} - \mu_{xx})(\psi_{zz} - \psi_{xx}) =$$

$$- R(1 + \epsilon \Delta R + \cdots)(1 - \epsilon \beta'(T_s - T_c + \Theta))\Theta_x \tag{12}$$

$$\Theta_t + (\psi_z \Theta_x - \psi_x \Theta_z) - \psi_x T_{sz} = \frac{d}{dz}\left\{(1 + \epsilon k'(T_s - T_c + \Theta))(\Theta_z + T_{sz})\right\} \tag{13}$$

$$+ \frac{d}{dx}\left\{(1 + \epsilon k'(T_s - T_c + \Theta))\Theta_x\right\}$$

with boundary conditions

$$\psi = \psi_{zz} = 0 \qquad\qquad\qquad\qquad \text{on } z = \pm\, 1/2$$

$$[1 + \epsilon k'(T_s - T_c + \Theta)](T_{sz} + \Theta_z) = 1 \tag{14}$$

Scaling and Expansions

If the Rayleigh number is above its critical value Ro by an amount of order ϵ, then a bandwidth of wavenumbers of order ϵ 1/2 is linearly unstable. Therefore, we introduce the new horizontal variable $\xi = \epsilon 1/2 x$. The scaling for the time comes from the fact that if in linear theory we let the time dependence be e^{pt} we find that $p(R_0 + \epsilon) = \epsilon 2$. This leads to the slow time scale $\tau = \epsilon^2 t$. We also introduce a scaled stream function $\hat{\psi} = \epsilon^{1/2}\psi$. At this stage we also identify ϵ with the small parameter introduced in eqns. (4) – (6).

Expanding in ϵ

$$\hat{\psi} = \psi_0 + \epsilon \psi_1 + \cdots$$

$$\Theta = \Theta_0 + \epsilon \Theta_1 + \cdots$$

$$R = R_0 + \epsilon R_1 + \cdots$$

we obtain in leading order:

$$\Theta_{0zz} = 0$$

$$\psi_{0zzzz} = - R_0 \Theta_{0\xi} \tag{15}$$

with B. C. $\quad \psi_0 = \psi_{0zz} = \Theta_{0z} = 0 \quad$ on $z = \pm\, 1/2$

$$\tag{16}$$

$$\Rightarrow \qquad\qquad \Theta_0 = f(\xi, \tau)$$

$$\psi_0 = R_0 f_\xi \Phi_0(z) \tag{17}$$

where $\qquad$ (18)

$$\Phi_c(z) = \frac{1}{48} \left(-2z^4 + 3z^2 - \frac{5}{8} \right)$$

and $j(\xi, \zeta)$ is an arbitrary function, and Ro, the critical Rayleigh number.

In order ε we obtain the equations

$$\frac{d}{dz} \left(T_{3,z} + \Theta_{1z} + k'(T_{3c} + \Theta_c) \right) = \Psi_{,z}\Theta_{c\xi} - \Psi_{c\xi}\Theta_{,z} - \Psi_{,\xi} - \Theta_{c\xi\xi} \tag{19}$$

$$\Psi_{1zzzz} = -R_1\Theta_{c\xi} - R_o\Theta_{1\xi} - 2\Psi_{c\xi\xi zz} - \frac{1}{\tau}(\Psi_{c\xi}\Psi_{czzz} - \Psi_{cz}\Psi_{czz\xi})$$

$$- R_o\Theta_{c\xi}\Delta k + R_o\Theta_{c\xi}f'(T_{3c}+\Theta_c) - g'''(T_{3c}+\Theta_c)\Psi_{czz} \tag{20}$$

$$- 2g''(T_{3c}+\Theta_c)\Psi_{czz} - g'(T_{3c}+\Theta_c)\Psi_{czzz}$$

with boundary conditions

$$T_{3,z} + \Theta_{1,z} + k'(T_{3c}+\Theta_c) = 0$$

$$\Psi_1 = \Psi_{1zz} = 0 \qquad\qquad \text{on} \quad z = \pm\frac{1}{2} \tag{21}$$

Integrating the energy equation between $z = -1/2$ and $z = +1/2$ we see that the right hand side must vanish in order to satisfy the boundary condition. This implies

$$R_o = -\left[\int_{-1/2}^{1/2} \Phi_o(z)\,dz \right]^{-1} = 120 \tag{22}$$

We can then solve for Θ_1 and Ψ_1. The solution is

$$\Theta_1 = j_{\xi\xi}T_1(z) + \frac{1}{2}j_\xi^2 T_2(z) + k(z) + k(j) - k(z+j) \tag{23}$$

We have not included an arbitrary function of ξ and ζ since we only go to order $\varepsilon 2$. The function h(j) has been introduced for convenience only. T_1 and T_2 are defined by

$$T_1(z) = -\int_o^z dz' \int_{-1/2}^{z'} dz'' \left(1 + R_o\Phi_o(z'') \right)$$

$$T_2(z) = \int_o^z dz' \int_{-1/2}^{z'} dz'' R_o\Phi_o'(z'')$$

The solution for Ψ_1 is

$$\Psi_1(z) = R_1\Phi_o(z)j_\xi + P_2(z)j_{\xi\xi\xi} + (j_\xi^2)_\xi P_3(z) - R_o(j_\xi\Delta k + k(j))_\xi \Phi_o(z)$$

$$+ R_o j_\xi \left(p(j+z) + Az^3/6 + Bz^2/2 + Cz + D \right) \tag{24}$$

$$- R_o j_\xi \left[\int_{-1/2}^z dz' \int_{-1/2}^{z'} dz'' \Phi_o''(z'')g'(z''+j) - (z+1/2)\int_{-1/2}^{1/2} dz' \int_{-1/2}^{z'} dz'' g'(z''+j)\Phi_o''(z'') \right]$$

where we have introduced the following notation:

P_2 is the solution to

$$P_{2zzzz} = -R_0 T_1 - 2R_0 \Phi_{0zz} \qquad \text{with} \qquad P_2 = P_{2zz} = 0 \quad \text{on } z = \pm 1/2.$$

and P_3 is the solution to

$$P_{3zzzz} = -R_0 T_2 + R_0^2 (\Phi_{0z}\Phi_{0zz} - \Phi_0 \Phi_{0zzz})/2\sigma \qquad \text{with} \quad P_{3zz} = P_3 = 0 \quad \text{on } z = \pm 1/2.$$

$$A = -p''(j + 1/2) + p''(j - 1/2)$$

$$B = [\, p''(j + 1/2) + p''(j - 1/2) \,]/2$$

$$C = -A/24 + p(j - 1/2) - p(j + 1/2)$$

$$D = -B/8 - [\, p(j + 1/2) + p(j - 1/2) \,]/2$$

where

$$p'''(j) \equiv h(j) + f(j)$$

In order $\varepsilon 2$ we only need the energy equation

$$\frac{d}{dt}(\hat{z}\,\vec{F}lux) = \theta_{0\tau} + (\Psi_{0z}\theta_{1\xi} + \Psi_{1z}\theta_{0\xi} - \Psi_{0\xi}\theta_{1z} - \Psi_{1\xi}\theta_{0z}) \tag{25}$$

$$- \Psi_{0\xi}T_{s1z} - \Psi_{1\xi} - \frac{d}{d\xi}[\,h'(T_{s0} + j)\,j_\xi\,]_\xi - \theta_{1\xi\xi}$$

Again,

$$\int_{-1/2}^{1/2} dz \, \frac{d}{dz}(\hat{z}\,\vec{F}lux) = 0 \implies$$

$$\int_{-1/2}^{1/2}\theta_{0\tau}dz + \int_{-1/2}^{1/2}(\Psi_{0z}\theta_1)_\xi dz + \int_{-1/2}^{1/2}\Psi_{0\xi}h'(z)dz - \int_{1/2}^{1/2}\Psi_{1\xi}dz = \int_{-1/2}^{1/2}\theta_{0\xi\xi}dz + \left[\int_{-1/2}^{1/2}h'(z+j)\,j_\xi dz\right]_\xi$$

where we have used the expression for T_{s1}, and the fact that $\theta_{0\tau} = 0$

and that $\Psi_1(0) = \Psi_1(1) = 0$

Introducing the expressions for θ_1, Ψ_1 and Ψ_0 we obtain an evolution equation for $j(\xi,\tau)$ with which the solution of order one is completely

determined:

$$j_\tau + 0.196 \, j_{\xi\xi\xi\xi} + j_{\xi\xi} \left(\Delta k + \frac{R_i}{R_j} \right) - 1.23 \left(j_\xi^3 \right)_\xi + R_0 \left[g(j + \tfrac{1}{2}) + g(j - \tfrac{1}{2}) \right]_{\xi\xi}$$

$$+ \left\{ R_0 \left[\Phi_c * (2k + f + 6g + \tfrac{1}{2} g'') \right] (j) \right\}_{\xi\xi} = 0 \qquad (26)$$

where * denotes the convolution $\qquad (\Phi_c * F)(j) = \int_{-1/2}^{1/2} dz \; \Phi_c(z) \, F(z + j)$

Finally we consider two examples which show some of the main features of this equation.

Example 1

Consider the simple laws $\quad f = \frac{\lambda}{2} z^2 \;, \quad g = \frac{\beta}{2} z^2 \;, \quad k = \frac{\mu}{2} z^2$

which correspond to

$$\rho = \rho_0 \left[1 - \alpha (T - T_0) + \varepsilon \alpha \lambda (T - T_0)^2 / 2 \right]$$
$$\mu = \mu_0 \left[1 + \varepsilon \beta (T - T_0) \right]$$
$$\kappa = \kappa_0 \left[1 + \varepsilon \mu (T - T_0) \right] .$$

we obtain

$$j_\tau + 0.196 \, j_{\xi\xi\xi\xi} + \frac{R_i}{R_j} \, j_{\xi\xi} - 1.23 \left(j_\xi^3 \right)_\xi - \tfrac{1}{2} (j^2)_{\xi\xi} (2\mu + \lambda - \beta) = 0$$

At this stage we recall that there are two contributions to R_1, one is a purely linear contribution R_{1L} which is obtained from the linear theory for marginal stability. The other is the nonlinear correction which we call R_2.

Let us look for solutions which satisfy the boundary conditions
by expanding in a new small parameter δ :

$$j_\xi = j_{\xi\xi\xi} = 0 \quad \text{on } \xi = 0, \; 2\pi/a \, ,$$

$$j = \delta (j_1 + \delta \, j_2 + \cdots)$$
$$\frac{R_1}{R_0} = \frac{R_{1L}}{R_0} + \delta^2 \, \frac{R_2}{R_0} + \cdots$$

We find then that

$$j_1 = A(s) \cos a \xi \qquad\qquad \text{where } s = \delta^2 t$$
$$R_{1L} = 0.196 \, a^2 \, R_0$$

and that $A(s)$ obeys the Landau equation

$$\dot{A}(s) = a^2 \frac{R_2}{R_0} A + \frac{3}{8} \left[\frac{(2\mu + \lambda - \beta)^2}{9 \times 0.196} - 2 \times 1.23 a^4 \right] A^3$$

We see that we can have finite amplitude instability for

$$\Delta = \frac{3}{8}\left[\frac{1}{9\times0.196}(2\beta+\lambda-\beta)^2 - 2\times1.23\,a^4\right] > 0$$

that is, for $\quad a < a_c = 0.6\,(2\beta+\lambda-\beta)^{1/2}\quad$. Then for a given set of parameters δ,λ,β there is a critical aspect ratio $2\tilde{a}/a_c$ which separates stable from unstable solutions.

Example 2

To see further what happens for small a, we can take for example

$$\beta = \eta_1(1+\tau_0)^2 + \eta_2(1-\tau_0)^3 + \eta_3(\tau-\tau_0)^5$$

The equation for j becomes

$$j_\tau + 0.196\,j_{\xi\xi\xi\xi} + \left(\frac{R_1}{R_0} - \frac{\eta_2}{7} - \frac{25\,\eta_3}{16\times63}\right)j_{\xi\xi} - 1.23\left(j_\xi^3\right)_\xi$$

$$- \eta_1(j^2)_{\xi\xi} - \left(\eta_2 + \frac{10\,\eta_3}{21}\right)(j^3)_{\xi\xi} - \eta_3(j^5)_{\xi\xi} = 0$$

The corrections to R_1 are linear, so we call the coefficient of $j_{\xi\xi}$, r. We can include the effect of j^5 by assuming

$$-\left(\eta_2 + 10\,\eta_3/21\right) = \delta^2\,\bar{n}_2 \quad, \quad -\eta_3 = \bar{n}_3 \,, \quad -\eta_1 = \delta^2\,\bar{n}_1$$

$$r = \delta^2\,\bar{r}$$

and scaling $x' = \epsilon\xi$, $\Delta = \epsilon^6 t$, we expand as in the previous example. This time we find

$$j_1 = A(s)\cos a\,x'$$

where

$$\dot{A}(s) = a^2\,\frac{R_2}{R_0}\,A + A^3\left[\frac{\bar{n}_1^2}{6\times.196} + \frac{3}{4}\,a^2\,\bar{n}_2 - \frac{3}{4}\times1.23\,a^4\right] + \frac{5}{8}\,a^2\,\bar{n}_3\,A^5$$

so that for $\bar{n}_3 < 0$ the solutions can be stabilized, however if we plot A^2 vs R_2/R_0 for the steady solution $\dot A = 0$, the turning point $\hat{R}_2/R_0$ is proportional to a^{-4} and the amplitude $\hat{A}^2$ to a^{-2} so that for very small wavenumbers the assumption of small amplitude is not valid anymore
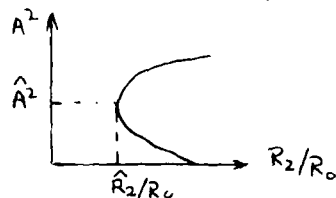
We do not know if this can be avoided by considering small but finite conductivity of the boundaries.

The main point we wanted to show is that small departures from the Boussinesq approximation can alter the nature of the solutions in a way which depends on the horizontal scale involved, at least for the boundary conditions we have used here. Only for large enough values of the wave number, the bifurcation is supercritical as in the Boussinesq problem (Chapman, 1979).

Acknowledgements

I would like to thank Dr. E. A. Spiegel for suggesting this problem and Drs. L. N. Howard, J. Keller, and G. Veronis for helpful discussions.

REFERENCES

Busse, F. H., 1962. Dissertation, University of Munich.

Chapman, C. J., 1979. Woods Hole Summer School Fellowship Lectures, 2, 1-17.

Childress, S. and Spiegel, E. A., (1978). Submitted to JFM.

Hurle, D. T. J., Jakeman, E. and Pike, E. R. (1967). Proc. Roy. Soc., A296, 469-475

Palm, E., 1960. J.F.M., 8, 183.

Newell, A. C. and Whitehead, J. A. (1969). JFM 38, 279-303

EFFECTS OF VISCOSITY AND VERTICAL THERMAL GRADIENT ON SHALLOW WATER SOLITONS

Richard W. Gregory-Allen

Introduction

The equations of inviscid shallow water theory have soliton solutions with an infinite set of conservation laws. The inclusion of viscous dissipation effects will of course damp the wave- the conservation laws (at least some of them) are lost. In an effort to model a physical system capable of sustaining a soliton in the presence of viscosity, the fluid is heated from below and cooled from above—the hope being that the wave could somehow extract energy from this thermal gradient. The equations are formulated in a Boussinesq approximation and surface tension effects are ignored. Perturbation expansions in the dimensionless wavenumber k and λ (related to viscosity) are used to break the problem into solvable pieces. Made necessary by the boundary conditions are a viscous boundary layer at the bottom and a thermal boundary layer at the free surface (the effects of a viscous boundary layer at the free surface are beyond the order of this calculation). These two boundary layers and the region of the main flow will be referred to as TOP, MIDDLE, and BOTTOM. The leading order approximation, in the limit of no thermal gradient, gives the KdV equation. Higher order corrections yield the time evolution of the amplitude.

The equations governing the flow to be studied are

$$u_t + uu_x + wu_z + p_x/\rho = \nu(u_{xx} + u_{zz})$$
$$w_t + uw_x + ww_z + p_z/\rho + g[1 - \alpha(T - T_{bot})] = \nu(w_{xx} + w_{zz})$$
$$T_t + uT_x + wT_z = \kappa(T_{xx} + T_{zz})$$
$$u_x + w_z = 0$$

$$(1)$$

subject to the boundary conditions

on $z = 0$:

$$u = w = T = 0$$

on $z = h + \eta$:

$$\eta_t + u\eta_x = w$$
$$T = -\Delta T$$
$$[-p\delta_{ij} + \mu(u_{i,j} + u_{j,i})] \cdot n_j = 0$$

or expressing the surface stress in normal and tangential components

$$p = \frac{2\mu}{\sqrt{1 + (\eta_x)^2}} [u_x(\eta_x)^2 + w_z - \eta_x(u_z + w_x)]$$
$$\frac{1 - (\eta_x)^2}{2}(u_z + w_x) + \eta_x(w_z - u_x) = 0.$$

The boundary conditions to be used in the horizontal direction are that everything dies at infinity with the exception of the horizontal velocity and pressure gradient which only vanish to leading order. This
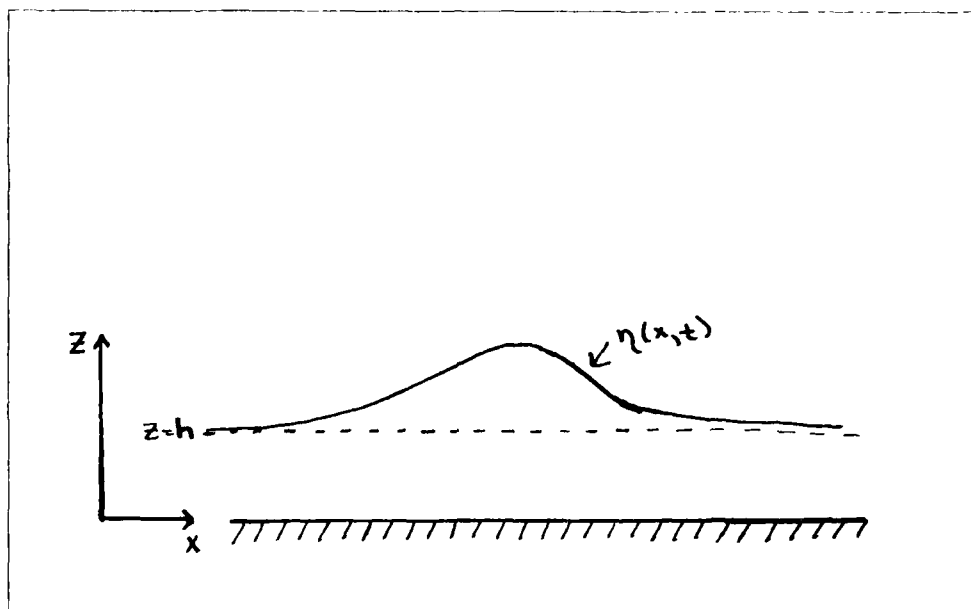
Figure 1.

is a result of the fact that as a wave damps, the fluid, once displaced, must leave the system at the ends. This will be made more precise when some notation is in place.

The governing equations are scaled using the dimensionless wavenumber k by the substitutions

$$x = hx'/k$$
$$z = hz'$$
$$t = \frac{1}{k}\sqrt{\frac{h}{g}}t'$$
$$u = k^2\sqrt{gh}u'$$
$$w = k^3\sqrt{gh}w' \tag{2}$$
$$T = \Delta T(k^2 T' - z')$$
$$p = \rho gh\left[1 - z' + \frac{a\Delta T}{2}(1 - z'^2) + k^2 p'\right]$$
$$\eta = k^2 h\eta'.$$

Defining the parameters

$$\epsilon^2 = \frac{\nu}{kh\sqrt{gh}}$$
$$\sigma = \frac{\nu}{\kappa}$$
$$\gamma^2 = a\Delta T$$

the scaled equations become (dropping the primes)

$$u_t + k^2(uu_x + wu_z) + p_x = \epsilon^2(k^2 u_{xx} + u_{zz})$$

$$k^2 u_t + k^4(uw_x + ww_z) + p_z - \gamma^2 T = \epsilon^2 k^2(k^2 w_{xx} + w_{zz})$$

$$T_t + k^2(uT_x + wT_z) - w = \frac{\epsilon^2}{\sigma}(k^2 T_{xx} + T_{zz}) \tag{3}$$

$$u_x + w_z = 0$$

with boundary conditions

on $z = 0$:

$$u = w = T = 0$$

on $z = 1 + k^2 \eta$:

$$\eta_t + k^2 u \eta_x = w$$

$$T = \eta$$

$$p - \eta - \frac{\gamma^2}{2}(2\eta + k^2 \eta) - 2k^2 \epsilon^2 w_z = O(k^4)$$

$$u_z + k^2 w_x = O(k^4).$$

Balancing the time derivative and the viscous diffusion terms in the momentum equations defines a slow diffusion time scale to be $\tau = \epsilon t$. Let the x position of the wave be given by $x = \phi(\tau)/\epsilon$ so that the peak of the wave stays fixed in the variable $\xi = x - \phi(\tau)/\epsilon$. The viscous boundary condition at $z = 0$ requires a boundary layer at the bottom and the thermal boundary condition at the free surface makes necessary a boundary layer at the top of the fluid. Then at the bottom, let $\varsigma = z/\epsilon$ so that $\partial_z \mapsto \partial_\varsigma/\epsilon$ and $\partial_\xi \mapsto \partial_\xi$. At the top we define $s = (1 + k^2 \eta - z)\sqrt{\sigma}/\epsilon$ so that $\partial_z \mapsto -(\sqrt{\sigma}/\epsilon)\partial_s$ and $\partial_\xi \mapsto \partial_\xi + k^2(\sqrt{\sigma}/\epsilon)\eta_\xi \partial_s$. The lines of constant s are "parallel" to the free surface ($s = 0$ is the surface) so that this is not an orthogonal coordinate system and the Jacobian mixes the derivatives. Introducing the parameter λ by $\epsilon = \lambda^2 k^2$ establishes a relation between the viscous and long-wave parameters to bring the corresponding terms in at the proper order. Thus the working equations are:

TOP

$$-(\phi_\tau \eta_\xi + \hat{w})\sqrt{\sigma}\hat{u}_s + \lambda^2(\hat{p}_\xi - \phi_\tau \hat{u}_\xi - \sigma \hat{u}_{ss}) + k^2[\sqrt{\sigma}\eta_\xi \hat{u}\hat{u}_s + \lambda^2 \hat{u}\hat{u}_\xi + \lambda^4 \hat{u}_\tau] = O(k^6)$$

$$\hat{p}_s + k^2 \lambda^2 \frac{\gamma^2}{\sqrt{\sigma}}\hat{T} = O(k^4)$$

$$-(\phi_\tau \eta_\xi + \hat{w})\sqrt{\sigma}\hat{T}_s - \lambda^2(\phi_\tau \hat{T}_\xi + \hat{w} + \hat{T}_{ss}) + k^2[\sqrt{\sigma}\eta_\xi \hat{u}\hat{T}_s + \lambda^2 \hat{u}\hat{T}_\xi + \lambda^4 \hat{T}_\tau] = O(k^6) \tag{4}$$

$$\hat{w}_s - k^2\left[\eta_\xi \hat{u}_s + \frac{\lambda^2}{\sqrt{\sigma}}\hat{u}_\xi\right] = 0$$

subject to the free surface boundary conditions at $s = 0$:

$$\phi_\tau \eta_\xi + \hat{w} - k^2[\hat{u}\eta_\xi + \lambda^2 \eta_\tau] = 0$$

$$\hat{p} - \eta(1 + \gamma^2) - k^2 \frac{\gamma^2}{2}\eta^2 = O(k^4)$$

$$\hat{u}_s = O(k^4)$$

$$\hat{T} = \eta$$

MIDDLE

$$-\phi_\tau u_\xi + p_\zeta + k^2[uu_\xi + wu_\zeta + \lambda^2 u_\tau] = O(k^1)$$
$$p_\zeta - \gamma^2 T - k^2\phi_\tau w_\zeta = O(k^1)$$
$$-\phi_\tau T_\xi - w + k^2[uT_\xi + wT_\zeta + \lambda^2 T_\tau] = O(k^1) \tag{5}$$
$$u_\xi + w_\zeta = 0$$

BOTTOM

$$\tilde{w}\tilde{u}_\zeta + \lambda^2(\tilde{p}_\xi - \phi_\tau\tilde{u}_\xi - \tilde{u}_{\zeta\zeta}) + k^2[\lambda^2\tilde{u}\tilde{u}_\xi + \lambda^4\tilde{u}_\tau] = O(k^1)$$
$$\tilde{p}_\zeta - k^2\lambda^2\gamma^2 T = O(k^1)$$
$$\sqrt{\sigma}\tilde{w}\tilde{T}_\zeta - \lambda^2\left(\phi_\tau\tilde{T}_\zeta + \tilde{w} + \frac{1}{\sigma}\tilde{T}_{\zeta\zeta}\right) + k^2[\lambda^2\tilde{u}\tilde{T}_\xi + \lambda^4\tilde{T}_\tau] = O(k^1) \tag{6}$$
$$\tilde{w}_\zeta + k^2\lambda^2\tilde{u}_\xi = 0$$

subject to the condition at $\zeta = 0$:

$$\tilde{u} = \tilde{w} = \tilde{T} = 0.$$

Notice that the horizontal stress condition at the free surface is zero to the order considered in this paper so that there is essentially no viscous boundary layer at the free surface in the calculations to follow. The horizontal boundary conditions can now be considered in detail. As η decreases on the slow viscous time scale, the fluid from the crest must exit the system at $\xi = \pm\infty$ and thus since the model is incompressible, the sound speed is infinte and

$$u(\pm\infty, z) = \pm\frac{1}{2}\int_{-\infty}^{\infty} \eta_t\, d\xi = \pm\frac{\epsilon}{2}\int_{-\infty}^{\infty} \eta_\tau\, d\xi = O(\epsilon).$$

This expression replaces the first conservation law for a soliton in an inviscid fluid and must be used if derivatives of u or p are integrated over ξ at $O(k^2)$. In the following calculation these integrations are avoided.

Now assume a perturbation expansion in powers of k^2 for each of the dependent variables, ie..

$$u = u_0 + k^2 u_2 + \cdots$$
$$\eta = \eta_0 + k^2\eta_2 + \cdots$$

etc. then substitute these expansions into the above equations and separate into problems for each order in k^2.

$O(k^0)$

The equations in the top boundary layer are;

$$-(\phi_{0\tau}\eta_{0\xi} + \hat{w})\sqrt{\sigma}\hat{u}_{0s} + \lambda^2(\hat{p}_{0\xi} - \phi_{0\tau}\hat{u}_{0\xi} - \sigma\hat{u}_{0ss}) = 0 \tag{7a}$$
$$\hat{p}_{0s} = 0 \tag{7b}$$
$$-(\phi_{0\tau}\eta_{0\xi} + \hat{w})\sqrt{\sigma}\hat{T}_{0s} - \lambda^2(\phi_{0\tau}\hat{T}_{0\xi} + \hat{u}_0 + \hat{T}_{0ss}) = 0 \tag{7c}$$
$$\hat{w}_{0s} = 0 \tag{7d}$$

with boundary conditions at $s = 0$

$$\phi_{0\tau}\eta_{0\xi} + \hat{u}_0 = 0 \tag{7e}$$

$$\hat{p}_0 - \eta_0(1 + \gamma^2) = 0 \tag{7f}$$

$$\hat{u}_{0s} = 0 \tag{7g}$$

$$\hat{T}_0 - \eta_0 = 0. \tag{7h}$$

Eqns. (7d) and (7e) yield immediately

$$\hat{u}_0 = -\phi_{0\tau}\eta_{0\xi}$$

and likewise Eqns. (7b) and (7f) give

$$\hat{p}_0 = \eta_0(1 + \gamma^2).$$

Then the terms with coefficient λ^0 in Eqns. (7a) and (7c) vanish, so that

$$\phi_{0\tau}(\hat{T}_{0\xi} - \eta_{0\xi}) + \hat{T}_{0ss} = 0$$

together with the boundary condition Eqn. (7h) gives

$$\hat{T}_0 = \eta_0,$$

and

$$\phi_{0\tau}\hat{u}_{0\xi} - \eta_{0\xi}(1 + \gamma^2) + \sigma\hat{u}_{0ss} = 0$$

with Eqn. (7g) gives

$$\hat{u}_0 = \frac{\eta_0}{\phi_{0\tau}}(1 + \gamma^2).$$

Thus the $O(k^0)$ results in the top layer are

$$\hat{u}_0 = \frac{\eta_0}{\phi_{0\tau}}(1 + \gamma^2) \qquad \hat{p}_0 = \eta_0(1 + \gamma^2)$$

$$\hat{w}_0 = -\phi_{0\tau}\eta_{0\xi} \qquad \hat{T}_0 = \eta_0 \tag{8}$$

In the middle the equations are

$$-\phi_{0\tau}u_{0\xi} + p_{0\xi} = 0 \tag{9a}$$

$$p_{0z} - \gamma^2 T_0 = 0 \tag{9b}$$

$$-\phi_{0\tau}T_{0\xi} - w_0 = 0 \tag{9c}$$

$$u_{0\xi} + w_{0z} = 0. \tag{9d}$$

Eqn. (9a) is integrated to give

$$p_0 = \phi_{0\tau}u_0$$

while Eqn. (9c) is differentiated with respect to z to give

$$u_{0z} = -\phi_{0\tau} T_{0\xi z}$$

which can be combined with Eqn. (9d) and integrated over ξ to get

$$u_0 = \phi_{0\tau} T_{0z}$$

so that

$$p_0 = (\phi_{0\tau})^2 T_{0z}$$

and

$$(\phi_{0\tau})^2 T_{0zz} - \gamma^2 T_0 = 0.$$

Letting $\omega = \gamma/\phi_{0\tau}$,

$$T_{0zz} - \omega^2 T_0 = 0.$$

The solution matching with $\hat{T}_0$ at $z = 1 + O(k^2)$ is

$$T_0 = (\eta_0 - a)\frac{\sinh \omega z}{\sinh \omega} + a\frac{\cosh \omega z}{\cosh \omega}$$

where $a = a(\xi)$ is a function to be determined. This gives

$$u_0 = -\phi_{0\tau}\left[(\eta_{0\xi} - a_\xi)\frac{\sinh \omega z}{\sinh \omega} + a_\xi\frac{\cosh \omega z}{\cosh \omega}\right]$$

and since the equations in the bottom boundary layer give $\tilde{u}_0 = 0$, $a_\xi = 0 \Rightarrow a = $const. But $p_0 = (\phi_{0\tau})^2 T_{0z}$ or

$$p_0 = (\phi_{0\tau})^2\frac{\gamma}{\phi_{0\tau}}\left[(\eta_0 - a)\frac{\cosh \omega z}{\sinh \omega} + a\frac{\sinh \omega z}{\cosh \omega}\right]$$

so that matching at $z = 1$ to $\hat{p}_0 = \eta_0(1 + \gamma^2)$ gives

$$\eta_0(1 + \gamma^2) = \gamma\phi_{0\tau}[(\eta_0 - a)\coth \omega + a\tanh \omega]$$

or

$$\frac{1 + \gamma^2}{\gamma\phi_{0\tau}} = \frac{\eta_0 - a}{\eta_0}\coth \omega + \frac{a}{\eta_0}\tanh \omega.$$

The quantity on the left is a pure number; so then must the right so that $a = 0 \bmod \eta_0$, but then $a = $constant$\Rightarrow a = 0$. This gives the results

$$\begin{aligned}
u_0 &= \gamma\eta_0\frac{\cosh \omega z}{\sinh \omega} \\
u_0 &= -\phi_{0\tau}\eta_{0\xi}\frac{\sinh \omega z}{\sinh \omega} \\
p_0 &= \gamma\phi_{0\tau}\eta_0\frac{\cosh \omega z}{\sinh \omega} \\
T_0 &= \eta_0\frac{\sinh \omega z}{\sinh \omega}
\end{aligned} \qquad (10)$$

where ϕ_{0_τ} is given by

$$\tanh \frac{\gamma}{\phi_{0_\tau}} = \frac{\gamma \phi_{0_\tau}}{1 + \gamma^2}.$$

Now we can solve for the flow in the bottom boundary layer. The equations (using $\hat{u}_0 = 0$) are:

$$\tilde{p}_{0\xi} - \phi_{0_\tau} \tilde{u}_{0\xi} - \tilde{u}_{0_{ss}} = 0 \qquad (11a)$$

$$\tilde{p}_{0\varsigma} = 0 \qquad (11b)$$

$$\phi_{0_\tau} \tilde{T}_{0\xi} + \frac{1}{\sigma} \tilde{T}_{0\varsigma\varsigma} = 0. \qquad (11c)$$

Since the pressure is independent of ς, matching with the middle gives

$$\tilde{p}_0 = \frac{\gamma \phi_{0_\tau}}{\sinh \omega} \eta_0.$$

The solution to the heat-like equation for $\tilde{T}_0$ is $\tilde{T}_0 = 0$ since the boundary condition at both the top and bottom of the layer is $\tilde{T}_0 = 0$. Then Eqn. (11a) becomes

$$\gamma \phi_{0_\tau} \eta_{0\xi} \operatorname{csch} \omega - \phi_{0_\tau} \tilde{u}_{0\xi} - \tilde{u}_{0\varsigma\varsigma} = 0$$

with the boundary conditions

$$\tilde{u}_0(\xi, \infty) = \gamma \eta_0 \phi_{0_\tau} \operatorname{csch} \omega$$

$$\tilde{u}_0(\xi, 0) = 0.$$

Let $v = \tilde{u}_0 - \gamma \eta_0 \operatorname{csch} \omega$ so that

$$\phi_{0_\tau} v_\xi + v_{\varsigma\varsigma} = 0$$

with

$$v(\xi, \infty) = 0$$

$$v(\xi, 0) = -\gamma \eta_0 \operatorname{csch} \omega.$$

This heat equation with $-\xi$ as the time-like variable determines the diffusion of the viscous boundary layer into the main flow behind the wave. The equation is solved by taking its Fourier sine transform

$$\phi_{0_\tau} \int_0^\infty \sin \alpha \varsigma \, v_\xi \, d\varsigma + \int_0^\infty \sin \alpha \varsigma \, v_{\varsigma\varsigma} \, d\varsigma = 0.$$

Two integrations by parts gives an ordinary differential equation for $\hat{v}$ (where $\hat{v}$ is the sine transform of v). The first step is

$$(\phi_{0_\tau} \hat{v})_\xi + \sin \alpha \varsigma \, v_\varsigma |_0^\infty - \alpha \int_0^\infty \cos \alpha \varsigma \, v_\varsigma \, d\varsigma = 0$$

but the evaluation vanishes at both ends so

$$(\phi_{0_\tau} \hat{v})_\xi - \alpha \cos \alpha \varsigma \, v |_0^\infty - \alpha^2 \int_0^\infty \sin \alpha \varsigma \, v_\varsigma \, d\varsigma = 0 \qquad (12)$$

and the BC give

$$(\phi_{0_\tau} \hat{v})_\xi - \alpha \gamma \eta_0 \operatorname{csch} \omega - \alpha^2 \hat{v} = 0$$

which is multiplied by $\exp\left(-\frac{a^2}{\phi_{0_\tau}}\xi\right)$ to yield the exact differential

$$\frac{d}{d\xi}\left[\exp\left(-\frac{a^2}{\phi_{0_\tau}}\xi\right)\bar{v}\right] = \exp\left(-\frac{a^2}{\phi_{0_\tau}}\xi\right)\frac{a\gamma}{\phi_{0_\tau}}\eta_0\,\text{csch}\,\omega.$$

Taking $-\int_\xi^\infty(\quad)d\xi' \Rightarrow$

$$\bar{v} = -\frac{a\gamma}{\phi_{0_\tau}\sinh\omega}\int_\xi^\infty \exp\left[-\frac{a^2}{\phi_{0_\tau}}(\xi'-\xi)\right]\eta_0(\xi')\,d\xi'$$

so that

$$v = -\frac{2\gamma}{\pi\phi_{0_\tau}\sinh\omega}\int_0^\infty a\sin a\varsigma \int_\xi^\infty \exp\left[-\frac{a^2}{\phi_{0_\tau}}(\xi'-\xi)\right]\eta_0(\xi')\,d\xi'\,da$$

and

$$\tilde{u}_0 = \gamma\eta_0\,\text{csch}\,\omega + v.$$

The value of $\tilde{u}_{0_\varsigma}$ at the bottom will be needed later so notice that Eqn. (12) gives

$$\int_0^\infty \cos a\varsigma\,\tilde{u}_{0_\varsigma}\,d\varsigma = \gamma\eta_0\,\text{csch}\,\omega - \frac{a^2\gamma}{\phi_{0_\tau}\sinh\omega}\int_\xi^\infty \exp\left[-\frac{a^2}{\phi_{0_\tau}}(\xi'-\xi)\right]\eta_0(\xi')\,d\xi'.$$

So

$$\tilde{u}_{0_\varsigma} = \frac{2}{\pi}\int_0^\infty \cos a\varsigma\left\{\gamma\eta_0\,\text{csch}\,\omega - \frac{a^2\gamma}{\phi_{0_\tau}\sinh\omega}\int_\xi^\infty \exp\left[-\frac{a^2}{\phi_{0_\tau}}(\xi'-\xi)\right]\eta_0(\xi')\,d\xi'\right\}da$$

or

$$\tilde{u}_{0_\varsigma} = -\frac{2\gamma}{\pi\sinh\omega}\int_0^\infty \eta_{0\xi}(\xi+\beta)\int_0^\infty \cos a\varsigma\,\exp\left(-\frac{a^2}{\phi_{0_\tau}}\beta\right)da\,d\beta$$

where $\beta = \xi'-\xi$. At $\varsigma = 0$,

$$\tilde{u}_{0_\varsigma}(\xi,0) = -\sqrt{\frac{\phi_{0_\tau}}{\pi}}\gamma\,\text{csch}\,\omega\int_0^\infty \beta^{-1/2}\eta_{0\xi}(\xi+\beta)\,d\beta. \tag{13}$$

This completes the $O(k^0)$ problem.

$O(k^2)$

TOP

The equations are:

$$(\hat{p}_{2\xi} - \phi_{0\tau}\hat{u}_{2\xi} - \sigma\hat{u}_{2ss}) + \left(\frac{1+\gamma^2}{\phi_{0\tau}}\right)^2\eta_0\eta_{0\xi} + \lambda^2\left(\frac{1+\gamma^2}{\phi_{0\tau}}\right)\eta_{0\tau} = 0 \qquad (14a)$$

$$\hat{p}_{2s} + \lambda^2\frac{\gamma^2}{\sqrt{\sigma}}\eta_0 = 0 \qquad (14b)$$

$$\phi_{0\tau}\hat{T}_{2\xi} + \phi_{2\tau}\eta_{0\xi} + \hat{w}_2 + \hat{T}_{2ss} - \left(\frac{1+\gamma^2}{\phi_{0\tau}}\right)^2\eta_0\eta_{0\xi} - \lambda^2\left(\frac{1+\gamma^2}{\phi_{0\tau}}\right)\eta_{0\tau} = 0 \qquad (14c)$$

$$\hat{w}_{2s} - \lambda^2\frac{1+\gamma^2}{\sqrt{\tilde{\sigma}}\phi_{2\tau}}\dot{\eta}_{0\xi} = 0. \qquad (14d)$$

Integrating Eqns. (14b) and (14d) from $s = 0$ gives

$$\hat{p}_2 = -\frac{\gamma^2}{\sqrt{\sigma}}\eta_0\lambda^2 s + \eta_2(1+\gamma^2) + \frac{\gamma^2}{2}(\eta_0)^2 \qquad (15)$$

and

$$\hat{w}_2 = \frac{1+\gamma^2}{\sqrt{\sigma}\phi_{0\tau}}\eta_{0\xi}\lambda^2 s - \phi_{0\tau}\eta_{2\xi} - \phi_{2\tau}\eta_0\xi + \frac{1+\gamma^2}{\phi_{0\tau}}\eta_0\eta_{0\xi} + \lambda^2\eta_{0\tau}. \qquad (16)$$

Using this expression for $\hat{w}_2$ in Eqn. (14c) gives

$$\phi_{0\tau}\hat{T}_{2\xi} + \hat{T}_{2ss} + \frac{1+\gamma^2}{\sqrt{\sigma}\phi_{0\tau}}\eta_0\xi\lambda^2 s - \phi_{0\tau}\eta_{2\xi} = 0$$

so that

$$\hat{T}_2 = \eta_2 - \frac{1+\gamma^2}{\sqrt{\sigma}(\phi_{0\tau})^2}\eta_0\lambda^2 s + \theta \qquad (17)$$

where θ is a linear function of s, i.e., $\theta = as$, where a is some constant. An expression for $\hat{u}_2$ will not be needed.

BOTTOM

The only feature of the flow in the bottom layer that will be needed from this order is $\tilde{w}_2$. The equation is

$$\tilde{w}_{2\varsigma} + \lambda^2\tilde{u}_{0\xi} = 0$$

but from the $O(k^0)$ equations $\tilde{u}_{0\xi} = \gamma\eta_{0\xi}\,\mathrm{csch}\,\omega - \tilde{u}_{0\varsigma\varsigma}/\phi_{0\tau}$ so that

$$\tilde{w}_{2\varsigma} = \lambda^2\left(\frac{\tilde{u}_{0\varsigma\varsigma}}{\phi_{0\tau}} - \gamma\eta_{0\xi}\,\mathrm{csch}\,\omega\right)$$

and $\int_0^\varsigma (\quad) d\varsigma'$ gives

$$\tilde{w}_2 = \lambda^2 \left(\frac{\tilde{u}_{0\varsigma}}{\phi_{0\tau}} - \gamma \eta_{0\xi} \, \text{csch} \, \omega \varsigma - \frac{\tilde{u}_{0\varsigma}(\xi, 0)}{\phi_{0\tau}} \right). \tag{18}$$

MIDDLE

The equations are:

$$-\phi_{0\tau} u_{2\xi} - \phi_{2\tau} \frac{\gamma \cosh \omega z}{\sinh \omega} \eta_{0\xi} + p_{2\xi} + \left(\frac{\gamma}{\sinh \omega} \right)^2 \eta_0 \eta_{0\xi} + \lambda^2 \gamma \frac{\cosh \omega z}{\sinh \omega} \eta_{0\tau} = 0 \tag{19a}$$

$$p_{2z} - \gamma^2 T_2 + (\phi_{0\tau})^2 \frac{\sinh \omega z}{\sinh \omega} \eta_{0\xi\xi} = 0 \tag{19b}$$

$$-\phi_{0\tau} T_{2\xi} - \phi_{2\tau} \frac{\sinh \omega z}{\sinh \omega} \eta_{0\xi} - w_2 + \lambda^2 \frac{\sinh \omega z}{\sinh \omega} \eta_{0\tau} = 0 \tag{19c}$$

$$u_{2\xi} + w_{2z} = 0. \tag{19d}$$

Take the z-derivative of Eqn. (19c) ,

$$-\phi_{0\tau} T_{2\xi z} + \frac{\gamma}{\phi_{0\tau}} \frac{\cosh \omega z}{\sinh \omega} (\lambda^2 \eta_{0\tau} - \phi_{2\tau} \eta_{0\xi}) = w_{2z},$$

and combine it with Eqn. (19d) to substitute into Eqn. (19a) giving

$$-(\phi_{0\tau})^2 T_{2\xi z} + 2\gamma \frac{\cosh \omega z}{\sinh \omega} (\lambda^2 \eta_{0\tau} - \phi_{2\tau} \eta_{0\xi}) + p_{2\xi} + \left(\frac{\gamma}{\sinh \omega} \right)^2 \eta_0 \eta_{0\xi} = 0.$$

Eliminating the pressure between this and Eqn. (19b) by cross differentiating gives

$$-(\phi_{0\tau})^2 T_{2\xi zz} + \frac{2\gamma^2}{\phi_{0\tau}} \frac{\sinh \omega z}{\sinh \omega} (\lambda^2 \eta_{0\tau} - \phi_{2\tau} \eta_{0\xi}) + \gamma^2 T_{2\xi} - (\phi_{0\tau})^2 \frac{\sinh \omega z}{\sinh \omega} \eta_{0\xi\xi\xi} = 0$$

so that

$$T_{2zz} - \omega^2 T_2 = - \frac{\sinh \omega z}{\sinh \omega} \left[\eta_{0\xi\xi} + \frac{2\gamma^2}{(\phi_{0\tau})^3} \left(\phi_{2\tau} \eta_{0\xi} - \lambda^2 \int_{-\infty}^\xi \eta_{0\tau} \, d\xi' \right) \right]$$

which has as the solution for T_2

$$T_2 = A(\xi) \frac{\sinh \omega z}{\sinh \omega} + B(\xi) \frac{\cosh \omega z}{\cosh \omega} - \frac{z}{\gamma} \frac{\cosh \omega z}{\sinh \omega} F(\xi, \gamma, \lambda) \tag{20}$$

where

$$F(\xi, \gamma, \lambda) = \frac{\phi_{0\tau}}{2} \eta_{0\xi\xi} + \left(\frac{\gamma}{\phi_{0\tau}} \right)^2 \left(\phi_{2\tau} \eta_{0\xi} - \lambda^2 \int_{-\infty}^\xi \eta_{0\tau} \, d\xi' \right) \tag{21}$$

Now match T with Eqn. (17) in the top layer to $O(k^4)$ at $z = 1$

$$T = \eta_0 + k^2 \left[\frac{\gamma}{\phi_{0\tau}} \coth \omega (\eta_0)^2 + A + B - \frac{\coth \omega}{\gamma} F \right] - k^2 \lambda^2 s \frac{\gamma \coth \omega}{\sqrt{\sigma} \phi_{0\tau}} \eta_0 + O(k^4)$$

and

$$\hat{T} = \eta_0 + k^2\left[\eta_2 - \lambda^2\frac{1+\gamma^2}{\sqrt{\sigma}(\phi_{0_\tau})^2}\eta_0 s + \theta\right] + O(k^4)$$

so

$$A = \eta_2 + \frac{1+\gamma^2}{\gamma^2\phi_{0_\tau}}F - \frac{1+\gamma^2}{(\phi_{0_\tau})^2}(\eta_0)^2 - B. \tag{22}$$

Matching w with Eqn. (18) at the bottom will determine A_ξ and B_ξ. Using Eqn. (20), Eqn. (19c) becomes

$$w_2 = -\phi_{0_\tau}\left[A_\xi\frac{\sinh\omega z}{\sinh\omega} + B_\xi\frac{\cosh\omega z}{\cosh\omega} - \frac{z}{\gamma}\frac{\cosh\omega z}{\cosh\omega}F_\xi\right] - \frac{\sinh\omega z}{\sinh\omega}(\phi_{2_\tau}\eta_{0\xi} - \lambda^2\eta_{0_\tau}).$$

Combining this with u_0 from Eqn. (10) and expressing w in the boundary layer coordinates,

$$w = -\lambda^2 k^2\frac{\gamma\eta_{0\xi}}{\sinh\omega}\varsigma - k^2\frac{\phi_{0_\tau}}{\cosh\omega}B_\xi + O(k^4).$$

Since $\tilde{u}_1 = 0$ and in the expression for $\tilde{w}_2$ the term $\tilde{u}_{0\xi}/\phi_{0_\tau}$ dies for large ς then

$$\tilde{w} = \lambda^2 k^2\left[\frac{\gamma\,\mathrm{csch}\,\omega}{\sqrt{\pi\phi_{0_\tau}}}\int_0^\infty \beta^{-1/2}\eta_{0\xi}(\beta + \xi)\,d\beta - \frac{\gamma\eta_{0\xi}}{\sinh\omega}\varsigma\right] + O(k^4).$$

Thus

$$B_\xi = -\lambda^2\frac{1+\gamma^2}{(\phi_{0_\tau})^2\sqrt{\pi\phi_{0_\tau}}}\int_0^\infty \beta^{-1/2}\eta_{0\xi}(\beta + \xi)\,d\beta \tag{23}$$

and then

$$A_\xi = \eta_{2\xi} - 2\frac{1+\gamma^2}{(\phi_{0_\tau})^2}\eta_0\eta_{0\xi} + \frac{1+\gamma^2}{\gamma^2\phi_{0_\tau}}F_\xi - B_\xi. \tag{24}$$

A substitution of Eqn. (20) for T_2 in

$$-(\phi_{0_\tau})^2 T_{2\xi z} + p_{2\xi} + 2\gamma\frac{\cosh\omega z}{\sinh\omega}(\lambda^2\eta_{0_\tau} - \phi_{2_\tau}\eta_{0\xi}) + \left(\frac{\gamma}{\sinh\omega}\right)^2\eta_0\eta_{0\xi} = 0$$

gives

$$p_{2\xi} - (\phi_{0_\tau})^2\left(\frac{\gamma}{\phi_{0_\tau}}\frac{\cosh\omega z}{\sinh\omega}\left[\eta_{2\xi} - 2\frac{1+\gamma^2}{(\phi_{0_\tau})^2}\eta_0\eta_{0\xi} + \frac{1+\gamma^2}{\gamma^2\phi_{0_\tau}}F_\xi - B_\xi\right] + \frac{\gamma}{\phi_{0_\tau}}\frac{\sinh\omega z}{\cosh\omega}B_\xi\right.$$

$$\left. - F_\xi\left[\frac{z}{\phi_{0_\tau}}\frac{\sinh\omega z}{\sinh\omega} + \frac{\cosh\omega z}{\gamma\sinh\omega}\right]\right) + 2\gamma\frac{\cosh\omega z}{\sinh\omega}(\lambda^2\eta_{0_\tau} - \phi_{2_\tau}\eta_{0\xi}) + \left(\frac{\gamma}{\sinh\omega}\right)^2\eta_0\eta_{0\xi} = 0.$$

Near $z = 1$

$$p_{2\xi} = (\phi_{0_\tau})^2\left(\frac{\gamma}{\phi_{0_\tau}}\left[\eta_{2\xi} - 2\frac{1+\gamma^2}{(\phi_{0_\tau})^2}\eta_0\eta_{0\xi} + \frac{1+\gamma^2}{\gamma^2\phi_{0_\tau}}F_\xi - B_\xi\right]\coth\omega + \frac{\gamma}{\phi_{0_\tau}}B_\xi\tanh\omega\right.$$

$$\left. - F_\xi\left[\frac{1}{\phi_{0_\tau}} + \frac{\coth\omega}{\gamma}\right]\right) + 2\gamma\coth\omega(\phi_{2_\tau}\eta_{0\xi} - \lambda^2\eta_{0_\tau}) - \left(\frac{\gamma}{\sinh\omega}\right)^2\eta_0\eta_{0\xi} + O(k^2)$$

and

$$p_0 = \gamma\phi_{0\tau}\eta_0 \coth\omega + \gamma^2\eta_0 k^2\left(\eta_0 - \lambda^2\sqrt{\sigma}s\right) + O(k^4)$$

so

$$p_\xi = \eta_0(1 + \gamma^2) - \lambda^2 k^2 \frac{\gamma^2}{\sqrt{\sigma}}s\eta_{0\xi} + k^2\left\{2\gamma^2\eta_0\eta_{0\xi} + (1 + \gamma^2)\eta_{2\xi} - 2\left(\frac{1 + \gamma^2}{\phi_{0\tau}}\right)^2\eta_0\eta_{0\xi}\right.$$

$$+ F_\xi\left[\frac{(1 + \gamma^2)^2 - (\phi_{0\tau})^2(1 + 2\gamma^2)}{\gamma^2(\phi_{0\tau})^2}\right]v + \frac{\gamma}{\phi_{0\tau}}B_\xi(\tanh\omega - \coth\omega)$$

$$\left. + 2\frac{1 + \gamma^2}{\phi_{0\tau}}(\phi_{2\tau}\eta_{0\xi} - \lambda^2\eta_{0\tau}) - \gamma^2\left[\left(\frac{1 + \gamma^2}{\gamma\phi_{0\tau}}\right)^2 - 1\right]\eta_0\eta_{0\xi}\right\} + O(k^4).$$

But

$$\tilde{p}_\xi = \eta_{0\xi}(1 + \gamma^2) - \lambda^2 k^2 \frac{\gamma^2}{\sqrt{\sigma}}s\eta_{0\xi} + k^2[\eta_{2\xi}(1 + \gamma^2) + \gamma^2\eta_0\eta_{0\xi}] + O(k^4)$$

so these can be matched (being careful about the mixing of derivatives) to give

$$3\left[\gamma^2 - \left(\frac{1 + \gamma^2}{\phi_{0\tau}}\right)\right]\eta_0\eta_{0\xi} + \left[\left\{1 + \left(\frac{1 + \gamma^2}{\phi_{0\tau}}\right)\right\}\frac{\phi_{2\tau}}{\phi_{0\tau}}\right]\eta_{0\xi} + \left[\frac{(1 + \gamma^2)^2 - (\phi_{0\tau})^2(1 + 2\gamma^2)}{2\gamma^2\phi_{0\tau}}\right]\eta_{0\xi\xi\xi}$$

$$= \lambda^2\left\{\left[\frac{(\gamma\phi_{0\tau})^2 - (1 + \gamma^2)^2}{\sqrt{\pi}\phi_{0\tau}(\phi_{0\tau})^4}\right]\int_0^\infty \beta^{-1/2}\eta_{0\xi}(\beta + \xi)\,d\beta\right.$$

$$\left. + \left[\frac{(1 + \gamma^2)^2 - (\phi_{0\tau})^2(1 + 2\gamma^2)}{(\phi_{0\tau})^4} + \frac{2(1 + \gamma^2)}{\phi_{0\tau}}\right]\eta_{0\tau}\right\}$$
(25)

where the expression for B and F have been substituted back in. Naming the functions of γ in square brackets and allowing $\phi_{2\tau}$ to vary with τ makes this equation a bit more manageable,

$$3P\eta_0\eta_{0\xi} + QA(\tau)\eta_{0\xi} + R\eta_{0\xi\xi\xi} = \lambda^2\left[L\int_0^\infty \beta^{-1/2}\eta_{0\xi}(\beta + \xi)\,d\beta + M\eta_{0\tau}\right].$$
(26)

Before solving this equation, an expression for the τ evolution of η_0 can be obtained by multiplying through by η_0 and integrating over all ξ. This is written

$$3\int_{-\infty}^\infty \eta_0(\eta_0\eta_{0\xi})\,d\xi + A\frac{Q}{P}\int_{-\infty}^\infty \eta_{0\xi}\,d\xi + \frac{R}{P}\int_{-\infty}^\infty \eta_0\eta_{0\xi\xi\xi}\,d\xi$$

$$= \frac{\lambda^2}{P}\left[L\int_{-\infty}^\infty \eta_0\int_0^\infty \beta^{-1/2}\eta_{0\xi}(\beta + \xi)\,d\beta\,d\xi + \frac{M}{2}\frac{d}{d\tau}\int_{-\infty}^\infty (\eta_0)^2\,d\xi\right].$$

Several integrations by parts finds the terms on the left hand side to be 0 so that

$$\frac{d}{d\tau}\int_{-\infty}^\infty (\eta_0)^2\,d\xi = -\frac{2L}{M}\int_{-\infty}^\infty \eta_0\int_0^\infty \beta^{-1/2}\eta_{0\xi}(\beta + \xi)\,d\beta\,d\xi$$
(27)

Now the equation for η_0 will be solved by expanding η_0 in powers of λ^2, i.e. let

$$\eta_0 = \eta_0^0 + \lambda^2 \eta_0^2 + \cdots$$

and assuming $\lambda \ll 1$ the $O(\lambda^0)$ problem is written

$$3P\eta_0^0\eta_{0\xi}^0 + QA\eta_{0\xi}^0 + R\eta_{0\xi\xi\xi}^0 = 0.$$

So $\int_{-\infty}^{\xi} (\quad) d\xi'$ to get

$$\frac{3P}{2}(\eta_0^0)^2 + QA\eta_0^0 + R\eta_{0\xi\xi}^0 = 0$$

and then $\int_{-\infty}^{\xi} \eta_{0\xi}^0 (\quad) d\xi'$ gives

$$\frac{P}{2}(\eta_0^0)^3 + \frac{QA}{2}(\eta_0^0)^2 + \frac{R}{2}(\eta_{0\xi}^0)^2 = 0.$$

At $\xi = 0$, the wave is at its maximum so $\eta_0^0 = A(\tau)$ and $\eta_{0\xi}^0 = 0$ so evaluating at this point gives

$$Q = -P$$

so that

$$\phi_{2\tau}^0 = -\phi_{0\tau} \frac{\left[\gamma^2 - \frac{1+\gamma^2}{(\phi_{0\tau})^2}\right]}{\left[1 + \left(\frac{1+\gamma^2}{\phi_{0\tau}}\right)^2\right]} A(\tau). \tag{28}$$

The evolution of η_0^0 is governed by

$$3\eta_0^0\eta_{0\xi}^0 - A\eta_{0\xi}^0 + \frac{R}{P}\eta_{0\xi\xi\xi}^0 = 0$$

which has the solution

$$\eta_0^0 = A \operatorname{sech}^2 \sqrt{\frac{AP}{4R}}\xi. \tag{29}$$

Substituting this into Eqn. (27) gives for the long time evolution of η_0 (let $a = \sqrt{\frac{AP}{4R}}$)

$$\frac{d}{d\tau} \int_{-\infty}^{\infty} A^2 \operatorname{sech}^4 a\xi \, d\xi = \frac{2L}{M} \int_{-\infty}^{\infty} A \operatorname{sech}^2 a\xi \int_0^{\infty} \beta^{-1/2} Aa \operatorname{sech}^2 a(\beta + \xi) \tanh a(\beta + \xi) \, d\beta \, d\xi.$$

Making the substitutions

$$\chi = \sqrt{\frac{AP}{4R}}\xi \qquad \psi = \sqrt{\frac{AP}{4R}}\beta$$

leads to the expression

$$A^{-5/4}A_\tau \int_{-\infty}^{\infty} \operatorname{sech}^4 \chi \, d\chi = \frac{L}{M}\left(\frac{P}{4R}\right)^{1/4} I$$

where

$$I = \int_{-\infty}^{\infty} \operatorname{sech}^2 \chi \int_0^{\infty} \psi^{-1/2} \operatorname{sech}^2(\psi + \chi) \tanh(\psi + \chi) \, d\psi \, d\chi$$

or

$$A^{-5/4} A_\tau = -4N$$

where

$$N = -\frac{L}{2^{3/2}M} \left(\frac{P}{R}\right)^{1/4} I.$$

So

$$\frac{d}{d\tau} A^{-1/4} = N$$

$$A^{-1/4} = N\tau + A(0)^{-1/4}$$

$$A(\tau) = \frac{A(0)}{(1 + NA(0)^{1/4}\tau)^4} \tag{30}$$

Replacing τ with dimensional time gives the more illuminating expression

$$A(t) = A(0) \left(1 + NA(0)^{1/4} \sqrt{\frac{\nu}{kh\sqrt{gh}}} t\right)^{-4}$$

$$= ghk^2 \frac{A(0)}{\left((k^2 gh^3)^{1/4} + NA(0)^{1/4}\nu^{1/2}t\right)^4} \tag{31}$$

which should be considered in the limits $\nu \to 0$ (the inviscid limit) and $\Delta T \to 0$ (no thermal gradient). When $\nu = 0$, $A = A(0)$ and the wave is unchanged in time—a genuine soliton. In the limit $\gamma \to 0$; $P \to -1$, $R \to -\frac{1}{3}$, $L \to -\frac{1}{\sqrt{\pi}}$, and $M \to 2$ so that

$$\eta = A(t) \operatorname{sech}^2 \frac{\sqrt{3A}}{2} \xi$$

$$A(t) = ghk^2 \frac{A(0)}{\left((k^2 gh^3)^{1/4} + N'A(0)^{1/4}\nu^{1/2}t\right)^4} \qquad N' = \frac{3^{1/4}}{\sqrt{\pi} 2^{5/2}} I.$$

Notice that there is no situation where the wave doesn't damp since $L = 0$ would imply that $\tanh \omega = 1$, certainly not within the range of the Boussinesq approximation. Higher order calculations and changing the thermal boundary conditions to constant flux (rather than constant temperature) still hold some promise for achieving a true soliton in the presence of viscous dissipation.

Acknowledgements

A SIMPLE MODEL OF THE KUROSHIO MEANDER

Spahr Webb

I. Introduction

The Kuroshio takes one of two distinct paths as it flows along the south coast of Japan. The Kuroshio will flow along the upper part of the shelf for several years and then suddenly shift to a path which loops far offshore near the northern end of the island of Shikoku and then back onshore before it passes over the Izu ridge. This second path is known as the Kuroshio meander and may remain in existence for several years (Robinson and Taft, 1972) (see Figure 1). This phenomena has been observed for several decades, Stommel and Yoshida, (1972), provides a summary of the older references. The path of Kuroshio flucuates widely around either the meander or the coastal path.

A model is needed which explains the bimodel character of the path of Kuroshio. Robinson and Taft (1972) base a theory on the theory of steady free inertial jets. They suggest bottom topography strongly constrains the path of Kuroshio when it lies on the shelf. They then hypothesize a weakening of the bottom current velocity which reduces the topographic steering and allows the current to flow offshore. Once offshore the current no longer feels the bottom. The possibility of weak or strong topographic constraint forces a bimodality in the possible paths.

White and McCreary (1976) noted that since the bottom slope near the shelf is large the change in depth across the width of the Kuroshio is also large and the gentle topographic steering of Robinson and Taft (1972) is not an appropriate model. An experiment by Taft, Robinson and Schmitz (1973) measured the bottom current velocity under the Kuroshio over a 64 day period and found the mean bottom current was not generally in the same direction as the surface current and is small. A later paper, Taft (1978), based on the same experiment suggests a deep countercurrent may exist.

McCreary and White (1976) model the Kuroshio meander as a Rossby lee wave excited by a bump in the coastline, the Island of Kyushu. Their model was based on a two layer ocean and the equivalent barotropic quasigeostrophic potential vorticity equation. The lower layer is stationary so bottom topography is not in the problem except as a bounding coastline. The wavelength of the Rossby lee wave is larger for larger current velocities. They invoked a secondary effect due to the Izu ridge "water gate" to explain the bimodality of the current paths.

The model to be discussed will include the Izu ridge specifically as an "outlet". Nonlinearity in the equations will allow several steady states to occur given one set of boundary conditions. Charney and Devore (1979) presented another geophysical phenomena where multiple stable states arising from nonlinearity may be important in their examination of atmospheric blocking. Charney and Flierl (1980) included nonlinearity in a model of Kuroshio also, but their solutions require several "bumps" in the coastline to get more than one steady state.
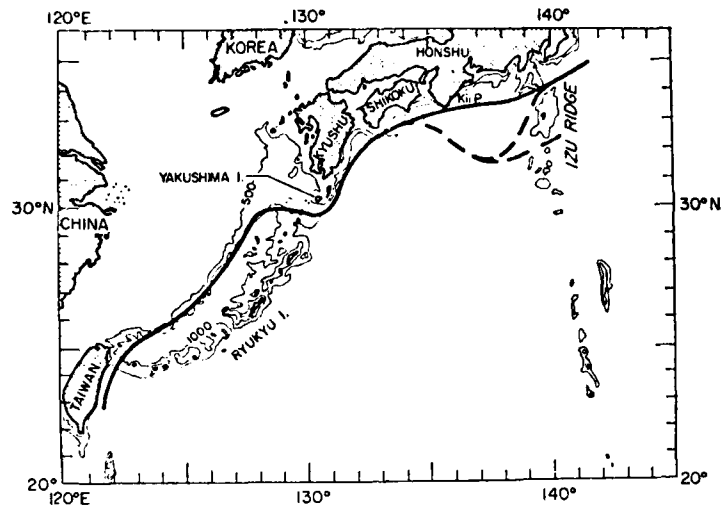
Fig. 1. The geometry of the Kuroshio meander.
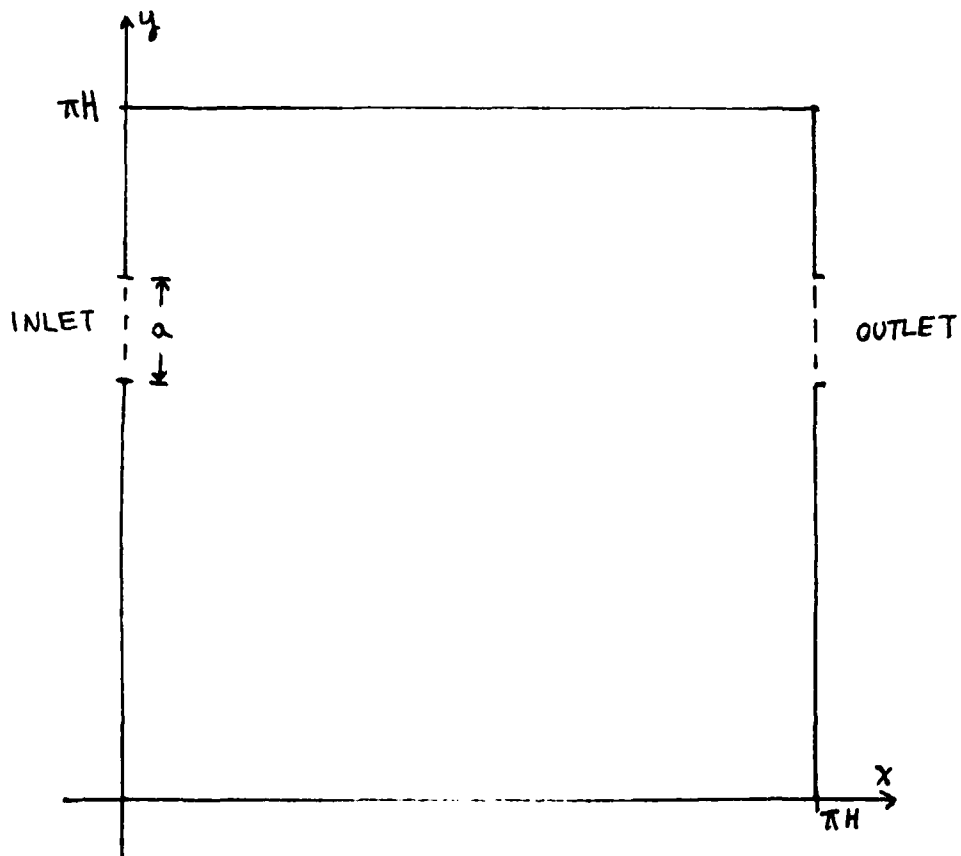
Fig. 2. The model with inlet and outlet.

Three solutions will be found for the same boundary conditions for a small range of the parameters in the problem. The last section of this report will examine the stability of these solutions to show that two of the solutions may be stable. One stable solution includes a la ge cyclonic eddy and is similar to observations of the Kuroshio meander. In the other stable solution the current is held tightly to the coast.

II. The Model

The coastlines of Kyushu, Shikoku and Honshu and the Izu ridge will be modeled as three sides of a square box with an inlet on the west and outlet on the east side (Fig. 2). The Izu ridge is mostly quite shallow, less than 500m deep but is cut by a steep walled channel approximately 100km south of Honshu. The Kuroshio usually follows the coastlines of Kyushu and Shikoku with separation (when the meander is present) occuring near the northern tip of Shikoku. It is then reasonable to use a model which assumes a fixed location for the inlet. It seems to be necessary to require the fourth side of the box to be closed also. No resonant modes are possible in an open geometry unless there is a reversal in the direction of the mean flow. The box was made square, but the character of the solutions is independent of the aspect ratio.

The ocean will be taken to have two layers, with a rigid lid condition at the surface and the lower layer stationary. Computations of the geostrophic current by Worthington and Kawai (1972) and Taft (1978) found that current speeds above 100 cm/s were confined to the upper 500m and nearly all the northward transport was in the upper kilometer of the ocean.

The appropriate equation is the equivalent barotropic quasigepstrophic potential vorticity equation.

$$\partial_t \left(\nabla^2 \psi - \frac{f_o^2}{gD} \psi \right) + J \left(\psi, \nabla^2 \psi + \beta y \right) = 0 \tag{1}$$

Here ψ is the streamfunction, the coriolis parameter is $f = f_o + \beta y$ and D is the depth of the fluid. The north-south coordinate is y, and the east-west, x. If the solutions are required to be steady:

$$\nabla^2 \psi + \beta y = F(\psi) \tag{2}$$

$F(\psi)$ is now an arbitrary function and needs to be determined. This equation requires the potential vorticity to be constant along a streamline. The streamfunction at the inlet is assumed to be of the form:

$$\psi_I = -ua \left(\frac{y - y_o}{a} + \frac{\epsilon^3 (y - y_o)^3}{a^3} \right) \tag{3}$$

The width of the stream is a, u is a characteristic velocity and y_o is the coordinate of the southern end of the inlet. The streamline at the outlet may be chosen arbitrarily and will be chosen to match the

inlet streamfunction. In the model presented here the outlet is at the same latitudes as the inlet. The Kuroshio usually crosses the Izu ridge 200km north of the path near Shikoku. It is not difficult to do the same problem as presented here, but with the outlet moved northward. It does not alter the character of the solutions.

The stream velocity at the inlet is

$$U = u\left(1 + 3\,\frac{\epsilon^3(y-y_0)^2}{a^2}\right)$$ (eastward velocity)   (4)

The current is approximately constant across the stream, but the maximum velocity at the inlet occurs at the northern edge of the current. This is in rough agreement with observations which show the current is asymmetrical and the largest velocities are more to the North.

The function $F(\psi)$ in equation 2 can be determined by a upstream condition at the inlet. Some justification of this procedure can be found by considering a slightly altered model with a long channel connecting smoothly to the box.
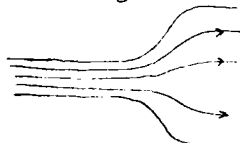
Then from equation 2)

$$\nabla^2 \psi_I + \beta y = 6\,\frac{\epsilon^3(y-y_0)}{a^2}u + \beta y = F(\psi)$$ (5)

Equation 3 can be inverted for y as a function of ψ if ϵ is small

$$y_I(\psi) = -\frac{\psi}{u} + \frac{\epsilon^3 \psi^3}{a^2 u^3} + y_0 + O(\epsilon^6)$$ (6)

Therefore

$$F(\psi) = \beta\left(-\frac{\psi}{u} + \frac{\epsilon^3 \psi^3}{a^2 u^3}\right) - \frac{6\epsilon^3 \psi}{a^2} + \beta y_0 + O(\epsilon^6)$$ (7)

Here it is seen that a cubic form of the streamfunction (eqn. 3) leads to a cubic nonlinearity in the governing equation:

$$\nabla^2\psi + \beta(y-y_0) + \frac{\beta\psi}{u} = \frac{\epsilon^3 \psi^3 \beta}{a^2 u^3} - \frac{6\epsilon^3 \psi}{a^2} + O(\epsilon^6)$$ (8)

A quadratic form for the streamfunction at inlet might have been tried. It will be shown that with cubic nonlinearity three solutions are possible but at most two are stable. It was expected that for a quadratic nonlinearity in the inlet streamfunction there would be two solutions, of which one was stable. Charney and Flierl (1980) found this was true for their model of the Kuroshio meander.

Nondimensionalizing x and y by H, the length of the box over pi and the streamfunction by βH^3 leads to

$$\nabla^4 \psi + (y-R) + K\psi = \frac{\epsilon^3 K^3 \psi^3}{q^2} + 6\frac{\epsilon^3 \psi}{q} + O(\epsilon^6)$$

$$K = \frac{\beta H^2}{u} \qquad R = y_0/H \qquad q = a/H \tag{9}$$

If ϵ is small the streamfunction may be expanded in powers of ϵ. The zeroth order equation is

$$\nabla^2 \psi_0 + (y-R) + K\psi_0 = 0 \tag{10}$$

A resonant mode of the form

$$\psi = \sin jx \sin \ell y \qquad\qquad j, \ell \text{ integer} \tag{11}$$

is possible if $K = j^2 + 1^2$. This mode is zero on the boundary of the box. Off resonance ($K \neq j^2 + 1^2$) a solution for ψ_0 can be found which satisfies the boundary conditions:

$$\psi = -(1 + \epsilon^3)q/K \qquad y \geq R + q$$

$$\psi = -\left(\frac{y-R}{q} + \frac{\epsilon^3(y-R)^3}{q^3}\right)q/K \qquad R + q \geq y \geq R \tag{12}$$

$$\psi = 0 \qquad\qquad y \leq R$$

The solution is

$$\psi_0 = \frac{-(y-R)}{K} + \sum_{n=1}^{\infty} B_n \sin ny \cosh\left(\sqrt{n^2 K}\left(x - \pi/2\right)\right) + A_1 \sin\sqrt{K} y + A_2 \cos\sqrt{K} y$$

$$A_1 = (\pi - R + R\cos\sqrt{K}\,\pi - q)/(K\sin\sqrt{K}\,\pi) \tag{13}$$

$$A_2 = -R/K$$

$$B_n = \frac{2}{\pi K}\left[\left(\cos n\pi(\pi - R - q) + R/q\right)\left(n/(n^2 - K) - 1/4\pi\right) + \cdots\right. \tag{14}$$

$$\left.\left(\sin nR - \sin(n(R+q))\right)\right]\frac{1}{\cosh\left(\sqrt{n^2 K}\,\pi/2\right)}$$

The higher order in ϵ equations are all linear and show small forced corrections due to the nonlinear terms

$$\nabla^2 \psi_1 + K\psi_1 = 0$$

$$\nabla^2 \psi_3 + K\psi_3 = -\frac{6\psi_0}{q^2} + \frac{K^3 \psi_0^3}{q^2} \tag{15}$$

If the parameter $K = \beta H^2/u$ is near a value for resonance, there will exist an integer N such that $(N^2 - K)^{1/2}$ is complex and almost an integer times $\sqrt{-1}$. Then $\cosh(\sqrt{N^2 K}\,\pi/2)$ is small and B_N will be large. The expansion outlined above breaks down since $\epsilon^3 \psi^3$ may be of order unity.

It will be assumed that K is approximately two, a value appropriate for resonance of the lowest mode in the box:

$$\psi_R = \sin x \sin y \tag{16}$$

If K is two, and u_0 is 100 cm/s, and β is evaluated at 30°N, then H times pi, (the width of the box) must be about 700 km. This is not an unreasonable scale for the meander.

Rewrite u as $u_0 + \epsilon u_1$ with u_0 such that $\beta H^2/u_0 = K_0 = 2$ and

$$K = K_0\left(1 - \frac{\epsilon u_1}{u_0} + \frac{\epsilon^2 u_1^2}{u_0^2} - \frac{\epsilon^3 u_1^3}{u_0^3}\right) + O(\epsilon^4) \tag{17}$$

Then equation 8 becomes:

$$\nabla^2\psi + (y-R) + k_0\psi = K_0\left(\frac{\epsilon u_1}{u_0} - \frac{\epsilon^2 u_1^2}{u_0^2} + \frac{\epsilon^3 u_1^3}{u_0^3}\right)\psi + \frac{\epsilon^3 K_0^3 \psi^3}{q^2} - \frac{6\epsilon^3\psi}{q^2} + O(\epsilon^4) \tag{18}$$

The coefficient B_1 will of order $1/\epsilon$ if u_1/U_0 is of order one. It is then reasonable to look for an expansion of the form:

$$\psi = \frac{A\psi_R}{\epsilon} + \phi_1 + \epsilon\phi_2 \tag{19}$$

The order $1/\epsilon$ equation is
$$A\nabla^2\psi_R + A K_0 \psi_R = 0$$
which is just the equation for the resonant mode. The amplitude A must be determined by the order one equation:

$$\nabla^2\phi_1 + K_0\phi_1 = \frac{K_0 u_1}{u_0}A\psi_R + \frac{K_0^3 \psi_R^3 A^3}{q^2} \tag{20}$$

and ϕ_1 must satisfy the boundary conditions (eqn. 12)

Expanding the ψ_R^3 term:
$$\nabla^2\phi_1 + K_0\phi_1 = \left(\frac{K_0 u_1 A}{u_0} + \frac{9K_0^3 A^3}{16 q^2}\right)\sin x \sin y + \frac{K_0^3 A^3}{q^2 16}\left(-3\sin 3x \sin y - 3\sin x \sin 3y + \sin 3x \sin 3y\right) \tag{21}$$

The first term on the righthand side introduces a term which can eliminate the singularity in the series (eqn. 13) provided
$$A^3 - \frac{16}{9}\frac{u_1}{u_0}\frac{q^2}{K_0^3} A + \frac{16}{9}\frac{q^2}{K_0^3} B_1' = 0 \tag{22}$$
$$B_1' = \frac{-4}{\pi^2 K_0}\left((\pi - 2R + q)2 + \sin R - \sin(R+q)\right)$$
B_1' is the projection of the boundary conditions on $\pi/2 \sin y$.

The solution for ϕ_1 is
$$\phi_1 = -\frac{(y-R)}{K_0} + B_1'(x-\pi/2)\cos x \sin y + \sum_{n=2}^{\infty} B_n \sin ny \cosh(\sqrt{n^2 K_0}(x - \pi/2))$$
$$+ A_1 \sin\sqrt{K_0}\, y + A_2 \cos\sqrt{K_0}\, y + \phi_F \tag{23}$$

There are several other forced terms besides the B_1 term but all are zero on the boundary

$$\varphi_F = \frac{A^3}{16}\left(-\frac{1}{8}\sin 3x \sin 3y + \frac{3}{4}\left(\sin 3x \sin y + \sin x \sin 3y\right)\right) \qquad (24)$$

The three roots to the cubic equation for the amplitude of the resonant mode (eqn. 22) are plotted in Figure 3 for $R = .6\pi$ and $q = .15\pi$. For inlet velocities slightly greater than the value appropriate for resonance, $(u_1/u_o > 0)$ only one solution is found. Contours of the streamfunction for this solution with $u_1/u_o = 1.0, \epsilon = .2$ and $A = -.25$ are plotted in Fig. 4.

The flow is directed far south of the inlet and then returns north to the outlet. A large cyclonic eddy is present.

This solution looks similar to the meander of the Kuroshio. There is strong observational evidence for a recirculating region inside of the meander of the Kuroshio. Taft (1972) and Shoji (1972) found the transport downstream of Kyushu was generally 30% larger than the transport at the island. The maximum velocity in the meander region may be more than twice the velocity near Kyushu.
This solution looks most like the physical situation for large values of the small parameter ϵ. Increasing ϵ reduces the amplitude of the cyclonic eddy. Equation 7 is not necessarily valid inside a closed streamline, but since $F(\Psi)$ can be chosen arbitrarily inside a closed steamline it can be taken as in equation 6. This assumption is probably not the most physically reasonable one.

Two additional solutions are possible if the velocity is reduced below the resonant value ($u_1/u_o < -2.3$). The amplitude of the resonant solution (A) in both these solutions is positive, and these solutions contain large anticyclonic eddies: (Figures 5, 6). The Kuroshio is forced tightly against the northern boundary.

White and McCreary (1976) cite Taft (1972) and Shoji (1972) for evidence that meandering usually disappears when the transport of the Kuroshio e ceeds a critical value. The model presented here would suggest the coastal path of the Kuroshio would revert to the meander path as the velocity of the Kuroshio was increased. (This is true for $R = .6\pi$ and $q = .15\pi$). A reexamination of equation 21 reveals that for $2R + q < \pi$, B_1 is negative. In this case the diagram in Figure 3 should be flipped around the x axis. A positive amplitude solution will exist for all u_1/u_0, and two negative amplitude solutions for $u_1/u_0 < 0$.

Stability

The stability of the solutions is of fundamental importance to this problem. The nonlinearity was introduced into the problem to allow three solutions. It will be shown that two of these solutions may be stable, while the third is not stable to small perturbations.
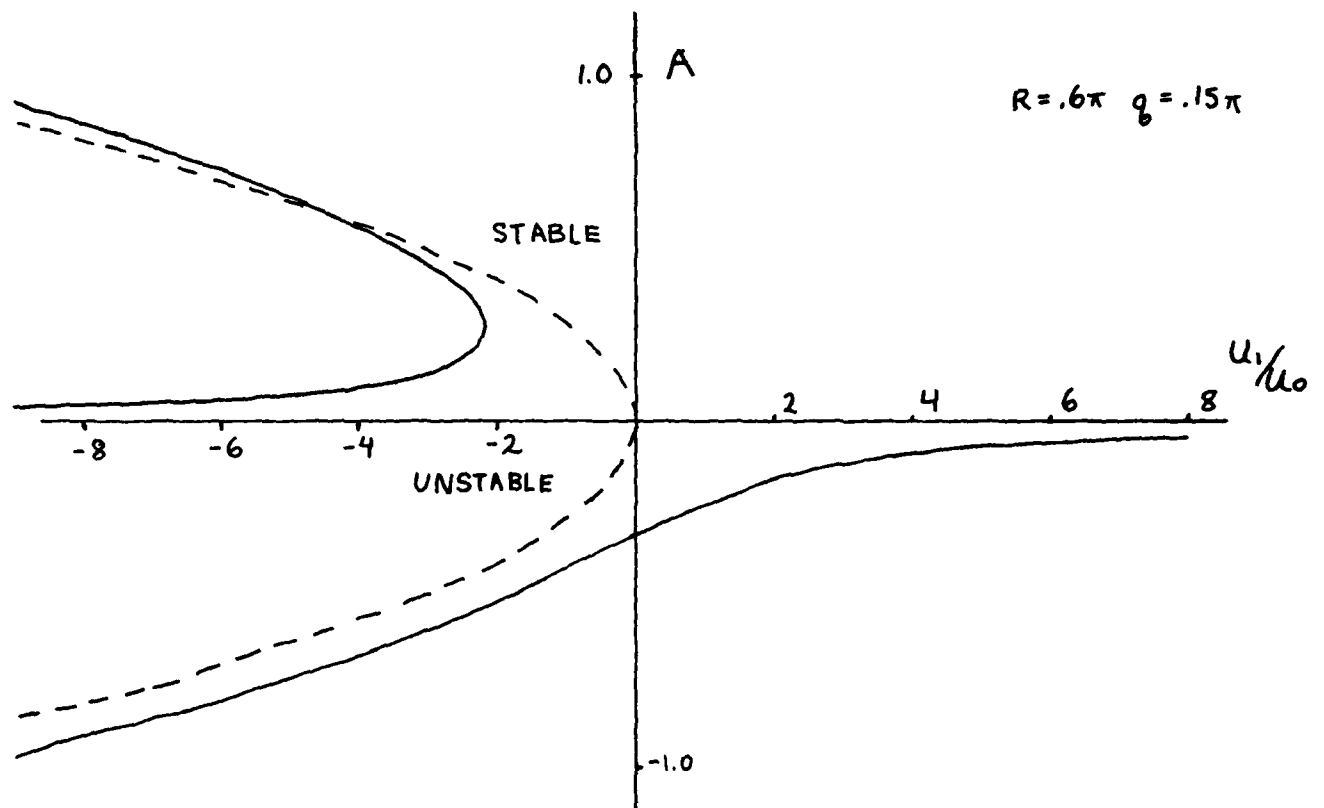
Fig. 3. Roots of equation 22.
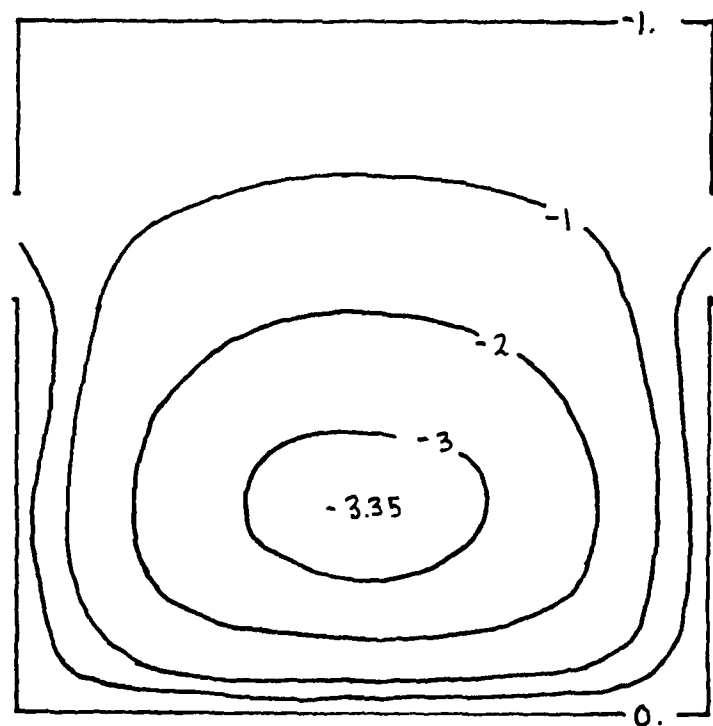
Fig. 4. Stream function of a solution.
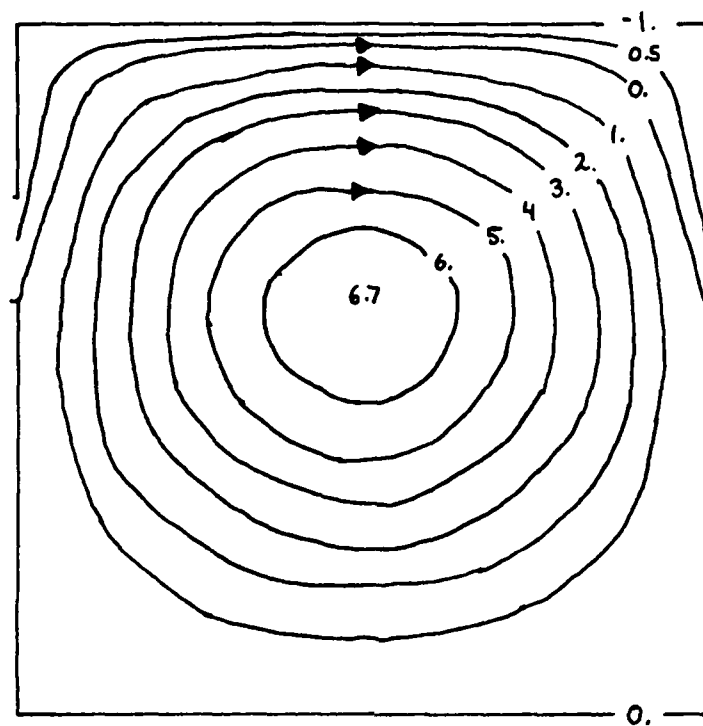
$\epsilon = .2 \quad u_1/u_0 = -2.5$

$A = .184$

Fig. 5.   Stream function of a solution.
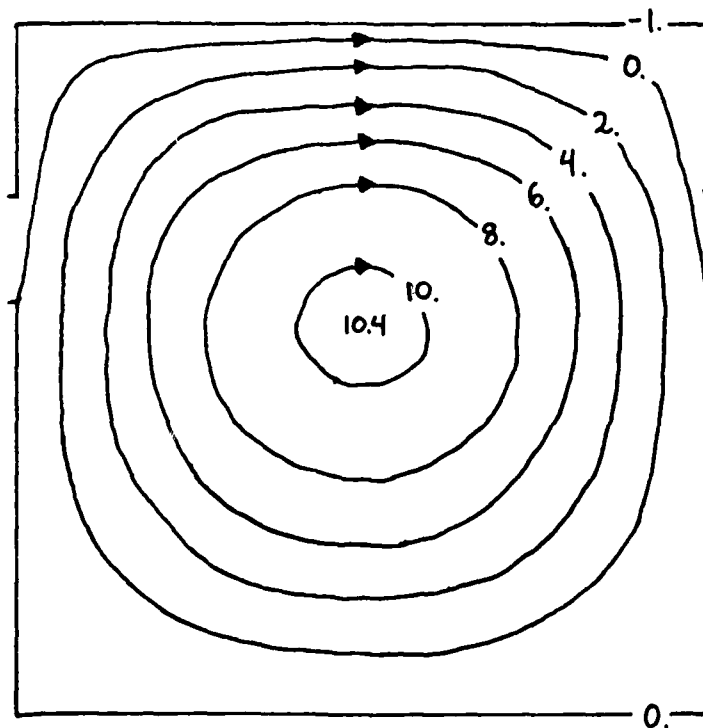
$\epsilon = .2 \quad u_1/u_0 = -2.5$

$A = .379$

Fig. 6.   Stream function of a solution.

Begin with the equation

$$\partial_t \nabla^2 \psi + J(\psi, \nabla^2 \psi + y) = 0 \qquad (25)$$

A small perturbation to the streamfunction ψ', with time dependence $e^{\sigma t}$ can be added to the solutions found in the preceeding section (eqn. 23).

$$\psi = \psi_R A/\epsilon + \phi + \psi' \qquad\qquad \phi = \phi_1 + \epsilon \phi_2 + \qquad (26)$$

$$\partial_t \nabla^2 \psi' + J\left(\psi', \underbrace{\nabla^2 \psi_R A}_{\epsilon} + \nabla^2 \phi + y\right) + J\left(\frac{\psi_R A}{\epsilon} + \phi, \nabla^2 \psi'\right) + J(\psi', \nabla^2 \psi') = 0 \quad (27)$$

The last term will be dropped. The perturbation is assumed to be small. The perturbation streamfunction can be described as a sum of orthogonal modes which are zero on the boundary.

$$\psi' = \sum_n \delta_n \psi_n e^{\sigma t} \qquad \nabla^2 \psi_n = -k_n^2 \psi_n \qquad \psi_n = \sin jx \, \sin \ell y$$

$$k_n^2 = j^2 + \ell^2 \qquad\qquad j, \ell \text{ integer} \qquad (28)$$

Equation 9 allows equation 25 to be rewritten as:

$$\sigma \sum_n -k_n^2 \psi_n \delta_n + \sum_m \delta_m J\left[\psi_m, (k_m^2 - k_0(1 - \epsilon \tfrac{u_1}{u_0}))\left(\frac{\psi_R A}{\epsilon} + \phi\right) + \right.$$
$$\left. \frac{\epsilon^3}{q^2}\left(\frac{\psi_R A}{\epsilon} + \phi^3\right)\right] = 0 \qquad (29)$$

This equation leads to an eigenvalue problem for σ.

$$\sigma \delta_n = B_{nm} \delta_m \qquad (30)$$

The modes ψ_n can be made orthonormal. Multiply equation 29 by ψ_n and integrate over x and y then:

$$B_{nm} = \frac{1}{k_n^2} \iint dx\, dy\, \psi_n J\left[\psi_m, (k_m^2 - k_0(1 - \epsilon \tfrac{u_1}{u_0}))\left(\frac{\psi_R A}{\epsilon} + \phi\right) + \frac{k^3 \epsilon^3}{q^2}\left(\frac{\psi_R A}{\epsilon} + \phi\right)^3\right] \quad (31)$$

If σ is real and positive for any eigenmode then the solution must be unstable. It is helpful to rewrite Bnm as

$$B_{nm} = \lambda_1 A/\epsilon + \lambda_2 A^3 + \epsilon \lambda_3 + \epsilon \lambda_4 A^2 + O(\epsilon^2)$$
$$\lambda_1 = \langle \psi_n J(\psi_m, \psi_R)\rangle (k_m^2 - k_0(1 - \epsilon \tfrac{u_1}{u_0}))\, 1/k_n^2$$
$$\lambda_2 = \langle \psi_n J(\psi_m, \psi_R^3)\rangle k_0^3/(q^2 k_n^2) \qquad (32)$$
$$\lambda_3 = \langle \psi_n J(\psi_m, \phi_1)\rangle (k_m^2 - k_0(1 - \epsilon \tfrac{u_1}{u_0}))$$
$$\lambda_4 = \langle \psi_n J(\psi_m, 3\psi_R^2 \phi_1)\rangle k^3/q^2$$

The brackets mean integration over x and y. This form is a little misleading since φ_1 is a function of A through the forced terms φ_F (equation 24). These integrals were calculated numerically for a small set of modes. The notation $\psi_{j\ell}$ will refer to a term

$$\psi_{j\ell} = \sin jx \sin \ell y \qquad\qquad j, \ell \text{ integer}$$

Modes with any of the first three integral wave numbers in the x or y directions are included in a table of Bnm (Fig. 7). Only a few elements of the matrix have order $1/\epsilon$ terms since

$$J(\psi_{mn}, \psi_R) = \frac{m+n}{4}\left(\psi_{m+1\,n-1} - \psi_{m-1\,n+1}\right) + \frac{m-n}{4}\left(\psi_{m+1\,n-1} - \psi_{m-1\,n+1}\right) \tag{33}$$

For example consider a truncated form for the perturbation:

$$\psi' = \delta_1 \psi_{13} + \delta_2 \psi_{22} \tag{34}$$

The eigenvalue equation is

$$\sigma^2 + \frac{6}{16} A/\epsilon = 0 \tag{35}$$

Then σ is strictly imaginary. The solutions are stable to this perturbation which represents two modes interacting with the resonant mode. All such pairs are stable since $J(\psi_A, \psi_B) = -J(\psi_B, \psi_A)$.

The elements of B_{nm} which seem to be important in determining the stability occur in the first column. All terms are at most order ϵ because $k_m^2 = K_0$.

A perturbation of the form

$$\psi' = \delta_1 \psi_{11} + \delta_2 \psi_{2j} \qquad j = 1, 2 \cdots 3 \tag{36}$$

leads to an eigenvalue equation

$$\sigma^2 + C_1\left(A^2 + \frac{u_1}{u_0} C_2\right) = 0 \qquad C_1 \geq 0, \ C_2 \geq 0 \tag{37}$$

Any solution is stable (σ complex) for $u_1/u_0 > 0$. But only one solution exists in this region (Figure III).

For $u_1/u_0 < 0$ any solution with

$$|A| \leq \sqrt{C_2 \left|\frac{u_1}{u_0}\right|} \tag{38}$$

is unstable. This curve is plotted on Figure 3 for the largest value or C_2 found. The mode ψ_{2L} gives the largest value of C_2. The smaller of the two solutions with a positive amplitude for the resonant mode is certainly unstable.

The other two solutions appear stable for at least part of the range of u_1/u_0.

B_{nm}

n \ $m \rightarrow$	11	12	13	21	22	23	31	32	33
11	0	0	0	$-.0039$	$-.3506$	$.2024$	0	0	0
12	0	0	0	$-.45\frac{A}{\epsilon}$	$.1644$	$.550\frac{A}{\epsilon}$	0	0	0
13	0	0	0	$.0729$	$-.6\frac{A}{\epsilon}$	$.1727$	0	0	0
21	$\epsilon(.00264\frac{u_1}{u_0}+.0536A^2)$	$.45\frac{A}{\epsilon}$	$-.3880$	0	0	0	$.0272$	$-.55\frac{A}{\epsilon}$	$.3552$
22	$\epsilon(.0283\frac{u_1}{u_0}+.04605A^2)$	$-.050$	$1.00\frac{A}{\epsilon}$	0	0	0	$-1.00\frac{A}{\epsilon}$	$.3454$	$-.3552$
23	$\epsilon(.00564\frac{u_1}{u_0}+.067A^2)$	$-.0576\frac{A}{\epsilon}$	$-.0944$	0	0	0	$.220$	$1.0582\frac{A}{\epsilon}$	$.3504$
31	0	0	0	$-.0015$	$.60\frac{A}{\epsilon}$	$-.3938$	0	0	0
32	0	0	0	$.05\%\frac{A}{\epsilon}$	$-.1104$	$1.058\frac{A}{\epsilon}$	0	0	0
33	0	0	0	$-.0186$	$.0576$	$-.1672$	0	0	0

Fig. 7. The stability matrix B_{nm}.

Calculations based on a truncated form of the matrix B_{nm} are not sufficient to show stability. It is also likely that other physics, not included in these solutions will influence stability.

Conclusions

A simple model for the bimodality of the path of the Kuroshio has been presented. This model depends on nonlinearity introduced by imposing a form of the stream function upstream and the existence of a resonant mode in the box modeling the basin between Japan and the Izu ridge.

Three solutions are found if the nonlinearity is cubic. One of these solutions is unstable to small perturbations.

REFERENCES

Charney, J. G. and J. G. DeVore, 1979. Multiple flow equilibrium in the atmosphere and blocking, J. Atmos. Sci., 36, 1205-1216.

Charney and Flierl, 1980. Oceanic analogues of large-scale atmosphere motions. MIT Press.

Robinson, A. R. and B. A. Taft, 1972. A numerical experiment for the path of the Kuroshio, J. Mar. Res., 20, 65-101.

Shoji, D., 1972. Time variation of the Kuroshio south of Japan, in Kuroshio: Physical aspects of the Japan Current. Stommel, H. and K. Yoshida, eds. Univ. of Wash. Press.

Stommel, H. and K. Yoshida, eds., 1972. Kuroshio: Physical Aspects of the Japan Current. Univ. of Wash. Press, 517 pp.

Taft, B. A., 1972. Characteristics of the flow of the Kuroshio south of Japan, in Kuroshio: Physical aspects of the Japan Current, Stommel, H. and K. Yoshida, eds., Univ. of Wash. Press.

Taft, B. A., 1978. Structure of Kuroshio south of Japan, J. Mar. Res., 36, 77-117.

Taft, B. A., A. R. Robinson and W. J. Schmitz, Jr., 1973. Current path and bottom transport of Kuroshio, J. Phys. Oceanogr. 3,347-3,350.

White, W. B., and J. P. McCreary, 1976. On the formation of the Kuroshio meander and its relationship to the large-scale ocean circulation, Deep-Sea Res., 33-47.

Worthington, L. V. and H. Kawai, 1972. Comparison between deep sections across the Kuroshio and the Florida Current and Gulf Stream, in Kuroshio: Physical Aspcts, Univ. of Washington Press.

THE STABILITY OF CURRENTS BOUNDED BY TWO FREE
STREAMLINES IN A ROTATING SYSTEM

Ross Griffiths

Introduction

Density fronts in the atmosphere and oceans are often highly unstable features and are the site of active mixing between fluids of unequal densities. Their instability also leads to the production of smaller scale but long lived flow features. Three possible instability mechanisms have been studied. For a two layer fluid, there is the barotropic shear instability which requires that the sign of the potential vorticity gradient changes somewhere within the flow, the two-layer baroclinic instability, which requires the presence of both upper and lower boundaries and that the potential vorticity gradient take opposite signs within the fluid (Pedlosky, 1964) and the Kelvin-Helmholtz shear instability, which requires an inflection in the velocity profile. None of these mechanisms are able to cause instability if only one layer is active and has a uniform vorticity.

While most density fronts have one line of intersection with an upper boundary (such as the ocean surface) or a lower boundary (such as the ocean bottom), there are some situations in which the same density surface has two intersections with the same boundary. This occurs whenever buoyant water forms a narrow current at the ocean surface (away from coastal boundaries) or when dense water flows in a narrow stream over the ocean bottom under the influence of buoyancy forces. One such case is the flow of cold, dense Norwegian Sea Water through the Denmark Strait and along the sloping bottom south of the strait (Worthington, 1969; Mann, 1969). The Coriolis force is able to inhibit spreading in the direction perpendicular to the direction of flow but not in the downstream direction (due to the presence of the bottom slope).

The presence of two free streamlines (at the intersections of the density interface with the horizontal boundary) gives rise to another mechanism for instability that has not previously been considered. Here we concentrate upon single-layer flows (in which a deep second layer is stationary) with a uniform potential vorticity distribution, and show that a rectilinear current adjacent to a horizontal boundary is always unstable. It is first shown that variations of the current width, in the limit of a very large downstream length scale, will give rise to a meandering instability with linear growth rate. Then normal modes with finite wavelengths are shown to have exponential growth. Both meandering and varicose modes grow with time, and they lead to release of both potential and kinetic energy from the original flow. For a current with zero potential vorticity, the wavelength with maximum growth rate is estimated to be eight times the Rossby radius based on the maximum depth of the current. Qualitatively, our conclusions do not appear to depend upon the simplifying assumption of uniform potential vorticity and the 'single-layer' instability is likely to continue to contribute to the behavior of a two-layer system in which baroclinic instability is important. Our analysis is readily modified to describe a current that flows along a sloping bottom, and a similar instability will occur in that case.

The very unstable nature of a current with two free streamlines is
demonstrated by laboratory experiments. A narrow current of buoyant
fluid was produced at the free surface of a deep lower layer by floating
a layer of fresh water on top of a salt solution between two axisymmetric
cylindrical walls in a rotating system. When the walls were withdrawn,
gravitational collapse produced a narrow annular flow with uniform
potential vorticity. Wave-like disturbances appeared on each front and
regions of closed circulation rapidly developed within the current. The
preferred downstream length scale was equal to seven times the Rossby
radius of deformation, independent of current width. The structure of
the disturbances also appears to be very similar to that predicted.

2. Governing equations

We begin with the hydrostatic momentum and continuity equations

$$\frac{\partial \underline{V}}{\partial t} + (f + \zeta)\underline{k} \times \underline{V} = -\nabla\left(g'\eta + \frac{V^2}{2}\right), \tag{2.1}$$

$$\frac{\partial \eta}{\partial t} + \nabla \cdot (\eta \underline{V}) = 0, \tag{2.2}$$

where y is the height of the interface from the rigid horizontal
(geopotential) boundary, $g' = g\Delta\rho/\rho$ is the reduced gravity, $\underline{V}$ is the
horizontal velocity, f is the Coriolis parameter about the vertical axis
of rotation, $\underline{k}$ is a vertical unit vector, and $\zeta = \underline{k} \cdot (\nabla \times \underline{V})$ is the
relative vorticity. Equations (2.1) and (2.2) together imply that the
potential vorticity $(f + \zeta)/\eta$ is conserved by fluid columns. Hence

$$\frac{f + \zeta}{\eta} = \frac{f}{Ho}, \tag{2.3}$$

where Ho would be the fluid depth when the relative vorticity is zero.

Let the undisturbed flow be parallel to the x-axis, and $H = \eta$ (y = o)
be the maximum depth of the current. The flow is then characterized by
the Rossby radius of deformation $(g'H)^{1/2}f^{-1}$ and the time scale
f^{-1}. Because we will be interested in downstream (x) variations with
some large length scale λ, say, we define a dimensionless wavenumber
$\varepsilon = 2\pi(g'H)^{1/2}f^{-1}\lambda^{-1}$. The dimensionless variables are then
defined by

$$x^* = x\,\varepsilon^{-1}(g'H)^{1/2}f^{-1}, \quad y^* = y(g'H)^{1/2}f^{-1}, \quad t^* = t\varepsilon^{-1}f^{-1},$$

$$u^* = u(g'H)^{1/2}, \quad v^* = v\varepsilon(g'H)^{1/2}, \quad \eta = hH, \quad H_o = \mathcal{H}H, \tag{2.4}$$

where x is the downstream coordinate, t is the time, y is the
cross-stream coordinate, u is the downstream velocity, v is the cross
stream velocity, h is the layer depth and $\mathcal{H}^{-1}$ is the dimensionless
potential vorticity. The stars denote dimensional variables. Equations

(2.1) and (2.2) become in dimensionless form

$$\frac{\partial u}{\partial t} + v\left(\frac{\partial u}{\partial y} - 1\right) = -\frac{\partial}{\partial x}\left(h + \frac{1}{2}u^2\right) , \tag{2.5}$$

$$\varepsilon^2 \frac{\partial v}{\partial t} + u\left(\varepsilon^2 \frac{\partial v}{\partial x} + 1\right) = -\frac{\partial}{\partial y}\left(h + \frac{1}{2}\varepsilon^2 v^2\right) \tag{2.6}$$

and

$$\frac{\partial h}{\partial t} + \frac{\partial}{\partial x}(uh) + \frac{\partial}{\partial y}(vh) = 0 . \tag{2.7}$$

The potential vorticity equation (2.3) becomes

$$\frac{\partial u}{\partial y} - \varepsilon^2 \frac{\partial v}{\partial x} = 1 - \frac{h}{\mathcal{H}} . \tag{2.8}$$

The undisturbed flow is assumed to be the steady solution of (2.5-2.7) with $v \equiv 0$. Then (2.6) reduces to the geostrophic relation

$$\bar{u} = -\frac{d\bar{h}}{dy} \tag{2.9}$$

while (2.8) gives the relative vorticity as

$$\frac{d\bar{u}}{dy} = 1 - \frac{\bar{h}}{\mathcal{H}} , \tag{2.10}$$

where the bars denote the basic flow whose stability is to be investigated. Together (2.9) and (2.10) can be solved for $\bar{h}$ and $\bar{u}$, the boundary conditions being $\bar{h} = 1$ at $y = o$ and $\bar{h} = o$ at $y = \pm L$. If the potential vorticity is assumed to take a constant value across the stream the solution takes the form

$$\bar{h} = \mathcal{H}\left[1 - \frac{\cosh y/\mathcal{H}^{1/2}}{\cosh L/\mathcal{H}^{1/2}}\right] , \quad \bar{u} = \mathcal{H}^{1/2}\frac{\sinh y/\mathcal{H}^{1/2}}{\cosh L/\mathcal{H}^{1/2}} . \tag{2.11}$$

Thus the flow involves the two length scales L and $\mathcal{H}$. In the limit of zero potential vorticity ($\mathcal{H} \to \infty$), the relative vorticity (2.10) becomes the constant value $d\bar{u}/dy = 1$, the current is described by the single dimensional length scale H, and the solution (11) reduces to

$$\bar{h} = 1 - \frac{1}{2}y^2 , \quad \bar{u} = y . \tag{2.12}$$

The current width is fixed at $L = \sqrt{2}$.

3. The long wave limit

An interesting observation is possible when a disturbance with a very large length scale is imposed on the basic flow. In the limit $\varepsilon \to 0$, the momentum and vorticity equations (2.6) and (2.8) become, respectively,

$$u = -\frac{\partial h}{\partial y} \tag{3.1}$$

and

$$\frac{\partial u}{\partial y} - 1 = -\frac{h}{h_t} ,$$

(3.2)

while the longitudinal momentum and continuity equations are unchanged.

We consider a spatial variation of the width L of an otherwise parallel current, maintaining symmetry about the midpoint of the stream. If the midpoint is defined to be at $y = y_0$ (x,t) at subsequent times, as shown in Figure 1, then $h = 0$ at $y-y_0 = L(x,t)$.

The current depth is of the form $h(x,y,t)$. However, we know it to be symmetric at $t = 0$. By assuming that the depth remains symmetric at subsequent times, it may be written in the form

$$h = h(Y = y - y_0 , L).$$

(3.3)
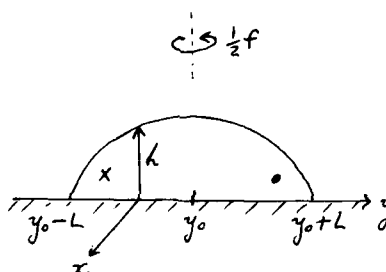
Figure 1. Coordinates for a symmetric current.

When the continuity equation (2.7) is integrated across the current, the geostophic velocity (3.1) (or, alternatively, the symmetry of the flow) can be used to show that the net flow of fluid through any cross-section is zero. Hence, the continuity equation implies

$$\int_{-L}^{L} \frac{\partial h}{\partial t} dY = 0 .$$

(3.4)

If the functional form (3.3) is to satisfy (3.4) we require

$$\frac{\partial L}{\partial t} = 0 .$$

(3.5)

Thus the variations of width are stationary in time and L is a function of x alone.

Returning to the vorticity equation (3.2) and evaluating it on the two free streamlines $y = \pm L(x)$, where $h = 0$, yields

$$\frac{\partial u}{\partial y}\bigg|_{\pm L} = 1 .$$

(3.6)

When this result is used in the (non-linear) momentum equation (5), the time-dependence of the velocity on the free-streamline is given by

$$\frac{\partial u}{\partial t} = -\frac{\partial}{\partial x}\left(h + \tfrac{1}{2}u^2\right) \quad on \quad y = \pm L. \tag{3.7}$$

Along with the geostrophic velocity (3.1), (3.7) leads to an equation in h alone. Then, the form (3.3) for h and the result that $\partial L/\partial t = 0$ give

$$\frac{\partial^2 h}{\partial Y^2}\cdot\frac{\partial y_0}{\partial t} - \frac{\partial h}{\partial Y}\left[\frac{\partial^2 h}{\partial Y^2}+1\right]\frac{\partial y_0}{\partial x} + \left[\frac{\partial h}{\partial L} + \frac{\partial h}{\partial Y}\cdot\frac{\partial^2 h}{\partial L\partial Y}\right]\frac{dL}{dx} = 0$$

on the free streamlines. However, (3.1) and (3.6) imply that $\partial^2 h/\partial Y^2 = -1$ on y = ±L, so that

$$\frac{\partial y_0}{\partial t} = \left[\frac{\partial h}{\partial L} + \frac{\partial^2 h}{\partial L\partial Y}\cdot\frac{\partial h}{\partial Y}\right]_{\pm L}\frac{dL}{dx}. \tag{3.8}$$

The term inside the brackets in (3.8) is independent of time. This result suggests that variations of current width with very large length scales will cause the current to meander, the amplitude of the meanders growing linearly with time. The stream is expected to wander most rapidly at those positions where dL/dx is greatest. However, (3.8) also suggests that short waves will grow more rapidly then long waves. This contradicts the approximations used ($\varepsilon \to$ o) and indicates that we need to consider the stability of the uniform current to perturbations of finite wavelength. The stability of normal modes is discussed in the following sections, first for the special but simpler case of a current with zero potential vorticity and then for the more general case with finite but uniform potential vorticity.

4. Flow with zero potential vorticity

4.1 The eigenvalue problem

If a small perturbation is imposed on the basic flow (2.12) and each variable is written in the form $\phi = \bar{\phi} + \phi'$, where $\bar{\phi}$ is the steady flow, then ϕ must satisfy equations (2.5-2.8). From the momentum equations the perturbation quantities must satisfy

$$\frac{\partial u'}{\partial t} + \left(\bar{u} + u'\right)\frac{\partial u'}{\partial x} + v'\left(\frac{d\bar{u}}{dy}-1\right) = -\frac{\partial h'}{\partial x} \tag{4.1}$$

and

$$\varepsilon^2\frac{\partial v'}{\partial t} + \varepsilon^2 v'\frac{\partial v'}{\partial y} + \varepsilon^2\bar{u}\frac{\partial v'}{\partial x} + u' = -\frac{\partial h'}{\partial y}. \tag{4.2}$$

When the potential vorticity is zero, (2.12) gives $d\bar{u}/dy - 1 = 0$, and this simplifies (4.1).

The continuity and vorticity equations (2.7) and (2.8) give

$$\frac{\partial h'}{\partial t} + \bar{u}\frac{\partial h'}{\partial x} + \bar{h}\frac{\partial u'}{\partial x} + \frac{\partial}{\partial y}(v'\bar{h}) = 0 \tag{4.3}$$

and

$$\frac{\partial u'}{\partial y} - \varepsilon^2\frac{\partial v'}{\partial x} = 0 \ . \tag{4.4}$$

If the perturbation takes the form $(u',v',h')=(\hat{u},\hat{v},\hat{h})e^{i(x-ct)}$ then (4.1), (4.3) and (4.4) give the following three linearized equations for the amplitudes:

$$(\bar{u}-c)\hat{u} + \hat{h} = 0 \ , \tag{4.5}$$

$$\bar{h}\hat{u} - i\frac{d}{dy}(\hat{v}\bar{h}) + (\bar{u}-c)\hat{h} = 0 \tag{4.6}$$

and

$$\frac{d\hat{u}}{dy} - i\varepsilon^2\hat{v} = 0 \ . \tag{4.7}$$

Elimination of $\hat{h}$ and $\hat{v}$ from the continuity equation (4.6) yields an eigenvalue problem for the growth rate c:

$$\frac{d}{dy}\left(\bar{h}\frac{d\hat{u}}{dy}\right) - \varepsilon^2\left[\bar{h} - (\bar{u}-c)^2\right]\hat{u} = 0 \ . \tag{4.8}$$

This equation is singular at the edges of the current, where $\bar{h}(\pm L) = 0$, and we wish to find the solution for which the eigenfunction $\hat{u}$ is regular at $y = \pm L$. That is, $d\hat{u}/dy$ (L) must be finite in order that $\hat{v}$ be finite on the free streamline. Therefore, when (4.8) is integrated across the current we require

$$\int_{-L}^{L}\left[\bar{h} - (\bar{u}-c)^2\right]\hat{u}\ dy = 0 \ . \tag{4.9}$$

In order to solve (4.8-9) with a non-zero wavenumber ε, c and $\hat{u}$ are expanded in the power series

$$c = c_o + \varepsilon c_1 + \varepsilon^2 c_2 + \dots$$

$$\hat{u}(y) = u_o(y) + \varepsilon u_1(y) + \varepsilon^2 u_2(y) + \dots$$

and the amplitude is normalized by requiring (at a fixed value of x)

$$\hat{u}(0) = 1 \ . \tag{4.10}$$

4.2 Terms of the lowest order

When these expansions for c and $\hat{u}$ are placed in (4.8), the leading order terms imply that

$$\frac{d}{dy}\left(\bar{h}\frac{du_o}{dy}\right) = 0 \ .$$

For du_0/dy to be finite at $\bar{h} = o$, this requires

$$\frac{du_o}{dy} = 0 . \tag{4.11}$$

Hence the leading order downstream velocity perturbation is independent of y. From (4.10) we set $u_0 = 1$ and require that $u_1(o) = u_2(o) = \ldots = 0$. The eigenvalue c_0 is given by (4.9), in which the leading order terms imply

$$u_o \int_{-L}^{L} \left[\bar{h} - (\bar{u} - c_o)^2 \right] dy = 0$$

This is a quadratic equation for c_0 but, with $\bar{h}$ and $\bar{u}$ given by (12) and $L = \sqrt{2}$, can only be satisfied by

$$c_0 = 0 . \tag{4.12}$$

Thus normal modes are stable in the limit $\varepsilon \to 0$, as was predicted by the long wave analysis in section 3.

The terms of order ε obtained from (4.8) imply that $du_1/dy = 0$. In order to satisfy (4.10), this requires $u_1 = 0$. Using this result along with (4.12) leads to the expansion

$$\hat{u}\left[\bar{h} - (\bar{u} - c)^2 \right] = \bar{h} - \bar{u}^2 + 2\varepsilon \bar{u} c_1 +$$
$$+ \varepsilon^2 \left[2\bar{u} c_2 - c_1^2 + u_2(\bar{h} - \bar{u}^2) \right]$$
$$+ \varepsilon^3 \left[2\bar{u}(c_3 + u_2 c_1) - 2c_1 c_2 + u_3(\bar{h} - \bar{u}^2) \right]$$
$$+ \varepsilon^4 \left[2\bar{u}(c_4 + u_2 c_2 + u_3 c_1) - 2c_1 c_3 - c_2^2 - u_2 c_1^2 + u_4(\bar{h} - \bar{u}^2) \right]$$
$$+ O(\varepsilon^5),$$

where the arbitrary amplitude u_0 has been set to $u_0 = 1$.

4.3 Terms of order ε^2 and higher

Equating the terms of order ε^2 obtained from (4.8) yields an equation for the second eigenfunction u_2:

$$\frac{d}{dy}\left(\bar{h} \frac{du_2}{dy} \right) = \bar{h} - \bar{u}^2 . \tag{4.13}$$

By applying the conditions that du_2/dy be finite at $\bar{h} = o$ and $u_2(o) = 0$, we find

$$u_2 = \tfrac{1}{2} y^2 . \tag{4.14}$$

The condition (4.9) becomes

$$2L c_1^2 - \int_{-L}^{L} u_2 (\bar{h} - \bar{a}^2) dy = 0 ,$$

giving $c_1^2 = -4/15$. Hence the growth rate c_1 is pure imaginary and the positive root $c_1 = 2i/\sqrt{15}$ describes exponentially growing modes that are stationary in space. Disturbances with large but finite wavelengths are therefore always unstable.

The calculation can be continued to higher orders in ε in order to investigate the dependence of the growth rate upon the wavenumber and determine the higher order structure of the growing disturbances. At order ε^3, (4.8) gives

$$\frac{d}{dy}\left(\bar{h}\,\frac{du_3}{dy}\right) = 2c_1\bar{u}$$

which reduces to the regular solution with $u_3(o) = 0$:

$$u_3 = -2c_1 y \tag{4.15}$$

From (4.9)

$$4L c_1 c_2 - 2 c_3 \int_{-L}^{L} \bar{u}\,dy - 2c_1 \int_{-L}^{L} u_2 \bar{u}\,dy - \int_{-L}^{L} u_3 (\bar{h} - \bar{a}^2) dy = 0$$

and this implies that $c_2 = 0$.

Repeating this procedure at order ε^4 yields the eigenfunction

$$u_4 = \tfrac{1}{5} y^2 \left(\tfrac{2}{3} + \tfrac{3}{8} y^2\right)$$

and the imaginary eigenvalue $c_3 = 104/(315 c_1)$. The positive (unstable) root for c_1 corresponds to

$$c_3 = -(52/315)\sqrt{15}\, i . \tag{4.16}$$

At order ε^5, the downstream velocity perturbation is

$$u_5 = -2y\left(c_1 + c_3 + \tfrac{1}{3} c_1 y^2\right)$$

while $c_4 = 0$. From the order ε^6 terms we find that $c_1 c_5 = -(32672/165375)$, and from order ε^7 terms that $c_6 = 0$. Similarly we find $c_8 = c_{10} = c_{12} = 0$, $c_1 c_7 = 0.1851$, $c_1 c_9 = -0.06139$ and $c_1 c_{11} = 0.2976$. Taking the positive root for c_1, we have

$$c_5 = 0.3826 i ,\quad c_7 = -0.3585 i ,\quad c_9 = 0.1189 i ,\quad c_{11} = -0.5762 i . \tag{4.17}$$

Since the eigenvalues up to $O(\varepsilon^{12})$ are all imaginary, the growing disturbances are stationary in space. Their growth factor e^{-ict} can be written as $e^{\varepsilon|c|ft*}$, where $t*$ is the dimensional time and

$$\varepsilon|c| = \varepsilon^2|c_1| - \varepsilon^4 c_3 + \varepsilon^6 c_5 + O(\varepsilon^8) \;.$$

The dimensionless growth rate $\varepsilon|c|$ is plotted in figure 2 as a function of wavenumber, with each curve including extra terms. The growth rate increases as the wavenumber increases at least until $\varepsilon \approx 0.7$. The growth rates have converged sufficiently for us to conclude that the maximum growth rate is close to 10^{-1}, and that this occurs at a wavenumber between $\varepsilon = 0.7$ and $\varepsilon = 0.8$.

4.4 The eigenfunctions

The form of the downstream velocity perturbation is given by the sum of $\hat{u} = u_0 + \varepsilon^2 u_2 + \varepsilon^3 u_3 + \ldots$ Use of these individual functions in the longitudinal momentum equation (4.5) and the vorticity equation (4.7) yields the depth and cross-stream velocity perturbations respectively, for successive orders in ε . Some of these functions are real, others are imaginary. Since the normalized amplitudes of all perturbation quantities have the downstream dependence e^{ix}, the real parts of the lower order eigenfunctions are

$$u_0 = \cos x \;, \qquad v_0 = y\sin x \;, \qquad\qquad h_0 = -y\cos x \;,$$

$$v_1 = \frac{-4}{\sqrt{15}}\cos x \;, \qquad\qquad h_1 = -\frac{2}{\sqrt{15}}\sin x \;,$$

$$u_2 = \tfrac{1}{2}y^2\cos x \;, \quad v_2 = \tfrac{i}{5}y\left(\tfrac{4}{3} + \tfrac{3}{2}y^2\right)\sin x \;, \quad h_2 = -\tfrac{i}{2}y^3\cos x, \qquad\qquad (4.18)$$

$$u_3 = \frac{4}{\sqrt{15}}\sin x \;, \quad v_3 = \frac{4}{\sqrt{15}}\left(\tfrac{5}{21} - y^2\right)\cos x \;, \quad h_3 = \frac{1}{\sqrt{15}}\left(\tfrac{52}{21} - 5y^2\right)\sin x \;.$$

The structure of the zeroth order eigenfunctions is sketched in figure 3(a). Because the cross-stream velocity v_0 is directed away from the midpoint of the stream at $x = \pi/2$, and toward the midpoint at $x = 3\pi/2$, while the undisturbed longitudinal flow is positive for positive y but negative for negative y, the zeroth order perturbation corresponds to a meandering of the stream. The corresponding depth perturbation is linear with y, so that the total depth profile, $\bar{h} + h_0$, remains symmetric (parabolic) about the local midpoint of the current. This behaviour is consistent with that found for the limit $\varepsilon \to 0$, described in section 3.

The first order perturbation h_1, also maintains the symmetry about the midpoint of the current. The cross-stream velocity v_1, on the other hand, is independent of position across the stream and corresponds to variations in the current width, as sketched in figure 3b. Its amplitude also has a phase that is $\pi/2$ radians ahead of v_0 and h_0. The depth increases uniformly at the widest section of the current and decreases at the narrowest section. Higher order eigenfunctions have the same structure as those already described, but tend to concentrate perturbations near the two free streamlines.
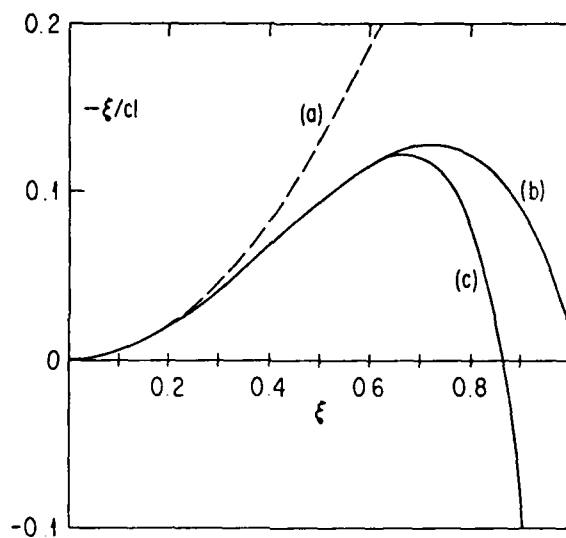
Figure 2. The growth rates (a) to $O(\varepsilon^2)$, (b) to $O(\varepsilon^{10})$, (c) to $O(\varepsilon^{12})$ for disturbances on a current with zero potential vorticity.
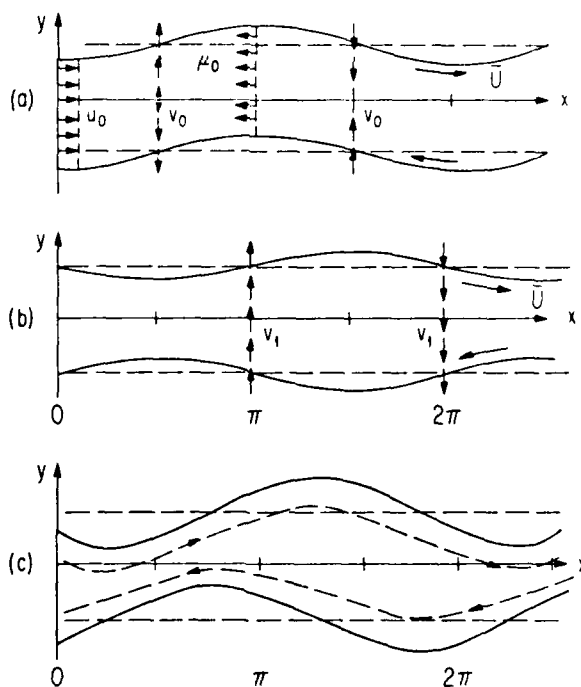

Figure 3. The structure of the eigenfunction at (a) zeroth order in ε (b) first order in ε , and (c) the superposition of these two lowest order modes.

When the perturbations sketched in figures 3a and 3b are superimposed, assuming comparable amplitudes, the structure of the flow becomes that sketched in figure 3c. There is still a uniform reduction of the current depth at $x = \pi/2$ and a uniform increase at $x = 3\pi/2$. At sufficiently large amplitudes, it is likely that regions of closed circulation will develop within the broader, deeper parts of the stream.

4.5 Energy transports

The source of energy for the growing disturbances may be determined from the structure of the depth and velocity perturbations. In order to calculate the potential energy changes, we begin with the longitudinally averaged continuity equation

$$\left\langle \frac{\partial h}{\partial t} \right\rangle + \left\langle \frac{\partial}{\partial y} (h v') \right\rangle = 0. \qquad (4.19)$$

The braces denote an average over the x coordinate and $h = \bar{h} + h'$ is the total depth. Since $h' \ll \bar{h}$, (4.19) gives

$$\left\langle \frac{\partial}{\partial t} (h^2/2) \right\rangle + \bar{h} \frac{\partial}{\partial y} \langle h' v' \rangle \approx 0$$

and by integrating across the stream the rate of change of potential energy becomes

$$\frac{\partial}{\partial t} \int_{-L}^{L} \left\langle \frac{h^2}{2} \right\rangle dy \approx - \int_{-L}^{L} \bar{h} \frac{\partial}{\partial y} \langle h' v' \rangle dy. \qquad (4.20)$$

The lefthand side of (4.20) involves the cross-stream divergence of the mass flux. Using the power series expansions for $\hat{h}$ and $\hat{v}$ in the normal modes form of h' and v', the mass flux can be written as

$$h' v' = h_o v_o + \varepsilon (h_o v_1 + h_1 v_o) + O(\varepsilon^2).$$

Then the individual functions in (4.18) give, to an arbitrary amplitude,

$$\frac{\partial}{\partial y} \langle h' v' \rangle = \varepsilon / \sqrt{15} + O(\varepsilon^2).$$

Hence, the lefthand side of (4.20) is negative. The potential energy decreases with time. This is a result of the coupling between the meandering and varicose modes. The individual isolated modes would be unable to decrease the total potential energy of the current.

The superposition of the meandering and varicose modes, with a phase difference of $\pi/2$, also removes kinetic energy from the mean flow. The velocity correlation is $\langle u' v' \rangle = \langle u_o v_o \rangle + \varepsilon \langle u_o v_1 \rangle + O(\varepsilon^2)$, where (4.18) implies that $\langle u_o v_o \rangle = 0$. Then

$$\langle u' v' \rangle = -2\varepsilon / \sqrt{15} + O(\varepsilon^2).$$

Thus the perturbations induce a positive Reynolds stress which transports momentum across the stream.

5. Flow with finite potential vorticity

5.1 The eigenvalue problem

When the potential vorticity $\mathcal{H}^{-1}$ is finite and uniform across the stream, the undisturbed flow is given by (2.9-2.11) and is characterized by an extra length scale L. This case is of greater oceanographic relevance and involves more interesting behavior. The dimensionless perturbation equations (4.1-4.3) are unchanged but the vorticity equation (4.4) is replaced by

$$\frac{\partial u'}{\partial y} - \varepsilon^2 \frac{\partial v'}{\partial x} = -\frac{h'}{\mathcal{H}} \ . \tag{5.1}$$

In (4.1), the undisturbed flow now has $d\bar{u}/dy - 1 = -\bar{h}/\mathcal{H}$.

The normal mode amplitudes $\hat{u}$, $\hat{v}$ and $\hat{h}$ are then related by the linearized equations

$$(\bar{u}-c)\hat{u} + i\frac{\bar{h}}{\mathcal{H}}\hat{v} + \hat{h} = 0 \ , \tag{5.2}$$

$$\bar{h}\hat{u} - i\frac{d}{dy}(\hat{v}\bar{h}) + (\bar{u}-c)\hat{h} = 0 \ , \tag{5.3}$$

$$\frac{d\hat{u}}{dy} - \varepsilon^2 i\hat{v} + \frac{\hat{h}}{\mathcal{H}} = 0 \ . \tag{5.4}$$

Eliminating $\hat{v}$ from (5.2) and (5.4) and eliminating $\hat{h}$ from the same two equations gives $\hat{h}$ and $\hat{v}$, respectively, in terms of $\hat{u}$. These can be used in the continuity equation (5.3) to find the differential equation that corresponds to (4.8):

$$\left(\frac{1}{\mathcal{H}^2}+\varepsilon^2\right)\frac{d}{dy}\left(\bar{h}\frac{d\hat{u}}{dy}\right) - \frac{1}{\mathcal{H}}\left(\frac{1}{\mathcal{H}^2}+\varepsilon^2\right)\frac{d}{dy}\left[\bar{h}(\bar{u}-c)\hat{u}\right] +$$

$$+ \left\{\left(\bar{h}/\mathcal{H}^4+\varepsilon^2\right)\frac{(\bar{u}-c)\bar{h}}{\mathcal{H}} + \frac{\bar{h}\bar{u}}{\mathcal{H}^4}\right\}\frac{d\hat{u}}{dy} \tag{5.5}$$

$$- \left\{\bar{h}^3/\mathcal{H}^6 + \frac{\bar{h}\bar{u}(\bar{u}-c)}{\mathcal{H}^5} + \frac{\varepsilon^2\bar{h}}{\mathcal{H}^2}\left[2\bar{h}+(\bar{u}-c)^2\right]+\varepsilon^4\left[\bar{h}-(\bar{u}-c)^2\right]\right\}\hat{u} = 0.$$

The above equation is presented in order to point out the nature of the problem. For non-zero values of ε and the limit $\mathcal{H}^{-1} \to 0$, (5.5) reduces to (4.8). Since an expansion of the variables in powers of the wavenumber ε, about the limit $\varepsilon \to 0$, will again be used to find the eigenvalues $c_0, c_1 \ldots$ at finite values of $\mathcal{H}$, we must require that $\varepsilon \ll \mathcal{H}^{-1}$. Hence our solution is not expected to be valid in the limit $\mathcal{H}^{-1} \to 0$.

Rather than using (5.5) we note that the cross-stream momentum equation (4.2) is unchanged for finite potential vorticity and reduces to the linearized form

$$\hat{u} + \varepsilon^2 (\bar{u} - c) i \hat{v} + \frac{d\hat{h}}{dy} = 0 \qquad (5.6)$$

for the normal modes. Using (5.6) in (5.4) yields

$$\frac{d^2 \hat{h}}{dy^2} - \frac{\hat{h}}{\mathcal{H}} = -i \varepsilon^2 \left[\hat{v} + \frac{d}{dy} (\bar{u} - c) \hat{v} \right] , \qquad (5.7)$$

while (5.6) and (5.3) give

$$\hat{v} = \frac{-i}{\bar{h}} \int^y \left[(\bar{u} - c)(\hat{h} - i \varepsilon^2 \hat{v} h) - \bar{h} \frac{d\hat{h}}{dy} \right] dy . \qquad (5.8)$$

The last two equations may be solved for $\hat{h}$ and $\hat{v}$, and then $\hat{u}$ is given by (5.6). Since $\bar{h} = 0$ on the two free streamlines, the downstream momentum equation (5.2) indicates that the solution is subject to the condition $(\bar{u} - c) \hat{v} + \hat{h} = 0$ on $y = \pm$ L. Replacing $\hat{v}$ from (5.6), these boundary conditions become

$$(\bar{u} - c) \frac{d\hat{h}}{dy} - \hat{h} + i \varepsilon^2 \hat{v} (\bar{u} - c)^2 = 0 \quad on \quad y = \pm L . \qquad (5.9)$$

It is interesting to note that (5.9) is no longer a boundary condition on the free streamlines in the limit of zero potential vorticity, but is then satisfied at all values of y.

The variables are again expanded in the form

$$c = c_o + \varepsilon c_1 + \varepsilon^2 c_2 + \ldots .$$

and

$$\hat{h} = h_o(y) + \varepsilon h_1(y) + \varepsilon^2 h_2(y) + \cdots$$

Similarly for $\hat{u}$ (y) and $\hat{v}(y)$. Then a suitable normalization of the amplitudes is again

$$\hat{u}(o) = 1 . \qquad (5.10)$$

and this requires that $u_1(o) = u_2(o) = \ldots = 0$. Because solution of this problem is more protracted than that of the zero potential vorticity problem we will proceed to calculate only the lower order eigenfunctions and the first non-zero eigenvalue.

5.2 The zeroth order solution

When the power series expansions are substituted into (5.7) the terms of leading order in ε give

$$h_{o\,yy} - \frac{h_o}{\mathcal{H}} = 0 \qquad (5.11)$$

and the boundary conditions become

$$(\bar{u} - c_o) \frac{dh_o}{dy} - h_o = 0 \qquad at \quad y = \pm L . \qquad (5.12)$$

The general solution to (5.11), is $h_o = A \sinh y/\mathcal{H}^{1/2} + B \cosh y/\mathcal{H}^{1/2}$, and by substituting this into (5.12) we obtain, at y = L,

$$\left[B \frac{(U - c_o)}{\mathcal{H}^{1/2}} - A \right] \sinh \frac{L}{\mathcal{H}^{1/2}} + \left[A \frac{(U - c_o)}{\mathcal{H}^{1/2}} - B \right] \cosh \frac{L}{\mathcal{H}^{1/2}} = 0$$

and at y = -L

$$\left[B\frac{(U-c_0)}{\mathcal{H}^{1/2}}+A\right]\sinh\frac{L}{\mathcal{H}^{1/2}}+\left[-A\frac{(U+c_0)}{\mathcal{H}^{1/2}}-B\right]\cosh\frac{L}{\mathcal{H}^{1/2}}=0,$$

where $U = \bar{u}(L) = \mathcal{H}^{1/2}\tanh(L/\mathcal{H}^{1/2})$ and $\bar{u}(-L) = -U$. Addition and subtraction of these two identities shows that $B = 0$ and $c_0 = 0$. Hence normal modes are again stable in the limit $\varepsilon \to 0$. The leading order terms from (5.6) imply that $u_0 = -dh_0/dy$. Hence $u_0 = -(A/\mathcal{H}^{1/2})\cosh(y/\mathcal{H}^{1/2})$, where the normalization (5.10) requires that $A = -\mathcal{H}^{1/2}$. The zeroth order eigenfunctions are now

$$h_0 = -\mathcal{H}^{1/2}\sinh y/\mathcal{H}^{1/2},$$
$$u_0 = \cosh y/\mathcal{H}^{1/2},$$

$$(5.13)$$

with v_0 given by (5.8):

$$v_0 = \frac{-i}{\bar{h}}\int^y\left(\bar{u}h_0 - \bar{h}\frac{dh_0}{dy}\right)dy.$$

$$(5.14)$$

Substituting (5.13) into (5.14), with $\bar{h}$ given by (2.11), and requiring v_0 to be finite on the free streamline, where $y = \pm L$ and $\bar{h} = 0$, the cross-stream velocity perturbation is found to be

$$v_0 = -i\mathcal{H}^{1/2}\sinh y/\mathcal{H}^{1/2}$$

$$(5.15)$$

5.3 Terms of order ε.

By equating terms of order ε obtained from (5.7), (5.8) and (5.9) we find

$$h_{1,yy} - \frac{h_1}{\mathcal{H}} = 0,$$

$$(5.16)$$

$$v_1 = \frac{-i}{\bar{h}}\int^y\left(\bar{u}h_1 - c_1 h_0 - \bar{h}\frac{dh_1}{dy}\right)dy$$

$$(5.17)$$

and

$$\bar{u}\frac{dh_1}{dy} - h_1 - c_1\frac{dh_0}{dy} = 0 \quad \text{on} \quad y = \pm L.$$

$$(5.18)$$

The general solution for h_1 is $h_1 = C\sinh(y/\mathcal{H}^{1/2}) + D\cosh(y/\mathcal{H}^{1/2})$. This time, the terms involving the constant C cancel from (5.18), leaving one equation relating D and the eigenvalue c_1:
$D = c_1\cosh^2(L/\mathcal{H}^{1/2})$.

The first order longitudinal velocity is geostrophic, $u_1 = -dh_1/dy$, as was the case for u_0. Then $u_1(0) = 0$ requires that $C = 0$ and the solution becomes

$$h_1 = c_1 \cosh^2(L/\mathcal{H}^{\frac{1}{2}}) \cosh(y/\mathcal{H}^{\frac{1}{2}})$$

$$u_1 = -c_1 \mathcal{H}^{-\frac{1}{2}} \cosh^2(L/\mathcal{H}^{\frac{1}{2}}) \sinh(y/\mathcal{H}^{\frac{1}{2}}).$$

(5.19)

The solution for v_1 that is finite at $y = \pm L$ is

$$v_1 = i c_1 \left(1 + \cosh\frac{L}{\mathcal{H}^{1/2}} \cosh\frac{y}{\mathcal{H}^{1/2}}\right) \cosh\frac{L}{\mathcal{H}^{1/2}}.$$

(5.20)

5.4 Terms of order ε^2

In order to find the first non-zero eigenvalue it is necessary to evaluate h_2. From (5.7), (5.8), and (5.9) the second order terms give

$$h_{2yy} - \frac{h_2}{\mathcal{H}} = -i v_0 - i\frac{d}{dy}(\bar{u} v_0) ,$$

(5.21)

$$v_2 = \frac{-i}{\bar{h}} \int^y \left(\bar{u} h_2 - c_1 h_1 - c_2 h_0 - i\bar{u} v_0 \bar{h} - \bar{h}\frac{dh_2}{dy}\right) dy$$

(5.22)

and

$$\bar{u}\frac{dh_2}{dy} - c_1\frac{dh_1}{dy} - c_2\frac{dh_0}{dy} - h_2 + i\bar{u}^2 v_0 = 0 \quad \text{on } y = \pm L,$$

(5.23)

while (5.6) implies that

$$u_2 = -\frac{dh_2}{dy} - i v_0 \bar{u} .$$

(5.24)

Substituting for v_0 from (5.15) into (5.21) gives an equation for h_2,

$$h_{2yy} - h_2/\mathcal{H} = -\mathcal{H}^{1/2}\left[\sinh y/\mathcal{H}^{\frac{1}{2}} + \sinh(2y/\mathcal{H}^{\frac{1}{2}})/\cosh(L/\mathcal{H}^{\frac{1}{2}})\right].$$

For this equation the general solution is

$$h_2 = \alpha \sinh\frac{y}{\mathcal{H}^{1/2}} + \beta\cosh\frac{y}{\mathcal{H}^{1/2}} - \frac{\mathcal{H}}{2}y\cosh\frac{y}{\mathcal{H}^{1/2}} - \frac{\mathcal{H}^{3/2}}{3}\sinh\left(\frac{2y}{\mathcal{H}^{1/2}}\right)\cosh^{-1}\left(\frac{L}{\mathcal{H}^{1/2}}\right).$$

Two algebraic equations in c_1, c_2 and β are now obtained from (5.23) and the known forms of h_2, h_1, h_0 and v_0. By adding these equations it is found that $\beta = c_2 \cosh^2(L/\mathcal{H}^{1/2})$. The constant α is then evaluated by finding u_2 from (5.24) and requiring $u_2(0) = 0$. This procedure gives $\alpha = \frac{1}{2}\mathcal{H}^{3/2}\left[1 + \frac{2}{3}\cosh^{-1}(L/\mathcal{H}^{1/2})\right]$.

On the other hand, by subtracting the two equations obtained from the boundary conditions (5.23) we are left with an equation for c_1 alone:

$$\frac{2c_1^2}{\mathcal{H}^2}\cosh^2\left(\frac{L}{\mathcal{H}^{1/2}}\right) = -1 + \frac{2}{3}\tanh^2\left(\frac{L}{\mathcal{H}^{1/2}}\right) + \frac{2L/\mathcal{H}^{1/2}}{\sinh(2L/\mathcal{H}^{1/2})}$$

It is preferable to rewrite this expression in terms of the parameter $L/\mathcal{H}^{1/2}$ alone. From the shape of the undisturbed current (2.11), where $\bar{h}(0) = 1$, the dimensionless potential vorticity can be expressed as

$$\mathcal{H}^{-1} = \frac{\cosh L/\mathcal{H}^{1/2} - 1}{\cosh L/\mathcal{H}^{1/2}} ,$$

(5.25)

whence the growth rate c_1 is given by

$$c_1^2 = -\frac{1}{2}\left[\cosh\frac{L}{\mathcal{H}^{1/2}} - 1\right]^{-2}\left[1 - \frac{2}{3}\tanh^2\left(\frac{L}{\mathcal{H}^{1/2}}\right) - \frac{2L/\mathcal{H}^{1/2}}{\sinh(2L/\mathcal{H}^{1/2})}\right] \cdot (5.26)$$

5.5 The growth rate and structure

Before discussing the first order growth rate further it is useful to introduce a new parameter that will enable a more direct comparison between our predictions and experiments. In terms of the dimensional parameters of the problem we have $L/\mathcal{H}^{1/2} = fL^*/\sqrt{g'H_o}$, where L^* is the dimensional half-width of the current. A similar dimensionless group can be defined in terms of the cross-sectional area, A, of the current:

$$\mathcal{F} = \frac{fA}{2H_o(g'H_o)^{1/2}} \cdot \qquad (5.27)$$

Then, by integrating the depth profile (2.11) across the stream,
$\mathcal{F} = L/\mathcal{H}^{1/2} - \tanh(L/\mathcal{H}^{1/2})$.

The square of the first order growth rate (5.26) is plotted in figure 4 as a function of $\mathcal{F}$. The value of c_1^2 is negative for all values of $\mathcal{F}$ (or $L/\mathcal{H}^{1/2}$) and so normal modes are always unstable. As $\mathcal{F} \to \infty$, $c_1^2 \to -4/3 \, exp(-L/\mathcal{H}^{1/2})$, indicating that disturbances grow much more slowly when the current width is large compared to the length scale $(g'H_o)^{1/2}f^{-1}$ than they do when these length scales are comparable. Note that Ho is the (uniform) depth that the current would have to assume if the fluid was to be stationary in the rotating reference frame. In the opposite limit of $\mathcal{F} \to 0$, c_1^2 approaches its minimum value -0.5. In order to reach this limit it is necessary that Ho $\to \infty$ at a finite value of the area A (or of the width L*), or that $A \to 0$ (L* $\to$ 0) at a finite value of Ho. However, both of these cases imply that $\mathcal{H}^{-1} \to 0$ and the analysis is not expected to be valid in that limit, since then $\mathcal{E} > \mathcal{H}^{-1}$ for all non-zero wavenumbers. Indeed, the eigenvalue c_1 does not correspond to that found earlier ($c_1^2 = -4/15$) from the equations with zero potential vorticity. Thus the growth rates obtained at $\mathcal{F} \ll 1$ have no significance. At $\mathcal{F} \gtrsim 0(1)$, on the other hand, c_1 is a close approximation to the eigenvalue c for all wavenumbers $\mathcal{E} \ll 1$. The structure of the problem with zero potential vorticity also suggests that the value of c_1 will be an upper bound for c at larger values $\mathcal{E} < 1$.

Having shown that the first order growth rate is imaginary, the structure of the growing disturbances can be described. Both the zeroth and first order eigenfunctions (5.13, 5.15, 5.19, 5.20) have forms similar to those found for the flow with zero potential vorticity (sketched in figure 3) and are modified only by the hyperbolic functions of v, which tend to concentrate the perturbation energy into regions close to the two free streamlines. This tendency is stronger for wider currents, flows for which we know that the disturbances grow much more slowly. There is again a superposition of a meandering mode in which the width and depth are constant along the current and a varicose mode with a longitudinal width and depth variation. The two modes have a phase difference of $\pi/2$, producing a decrease in the potential energy of the

flow and a transport of momentum across the stream. The eigenfunctions of higher order in ε simply reinforce the structure of the lower modes and, for larger wavenumbers ε , further restrict the release of energy to regions adjacent to the edges of the current.

6. Laboratory experiments

6.1 Apparatus

In order to establish an initially "parallel" current of uniform potential vorticity in a rotating container it was necessary to adopt an axisymmetric geometry. A cylindrical tank 92 cm in diameter was filled with a layer of sodium chloride solution which in most experiments was 40 cm deep. Two rigidly connected cylindrical walls that formed an annulus were then partially immersed into this deep layer, as sketched in figure 5. The annulus was suspended, and held concentric with the vertical axis of rotation, by three guides attached to the rim of the tank. The annulus width ($2L*_o$) was 7cm, its inner diameter 36cm, and its outer diameter 50cm.

After the salt solution had come to the desired rotation rate $f/2$, dyed fresh water was carefully floated onto the free surface inside the annulus to form the shallow upper layer shown in figure 5. After filling to the required depth H_o the system was left for at least 30 minutes to reach solid body rotation. The depth H_o was most accurately determined by measuring the volume of fluid placed in the annulus. At a time $t=0$, the annulus was carefully drawn vertically upward and removed. The subsequent flow was visualised by the dye in the upper layer and small pellets of paper floating on the free surface. Photographs were taken with a camera mounted in the rotating reference frame and time exposures of about one half of a rotation period were used to obtain streaks. Such streaks revealed no motion before the annulus was withdrawn.

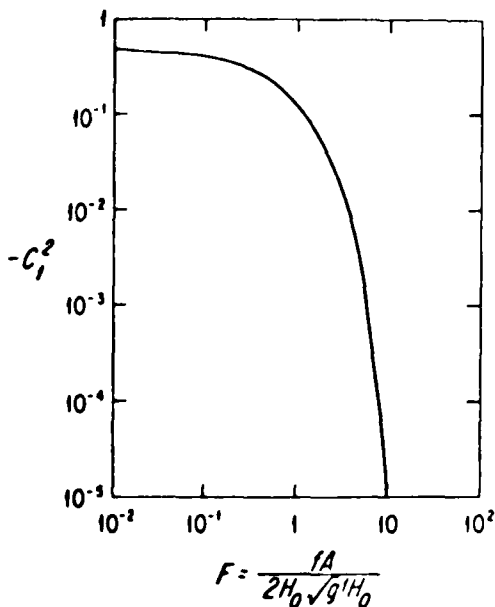$$F = \frac{fA}{2H_o\sqrt{g'H_o}}$$

Figure 4.   The first order eigenvalue $-c_1^2$ for normal modes on a current with uniform finite potential vorticity.
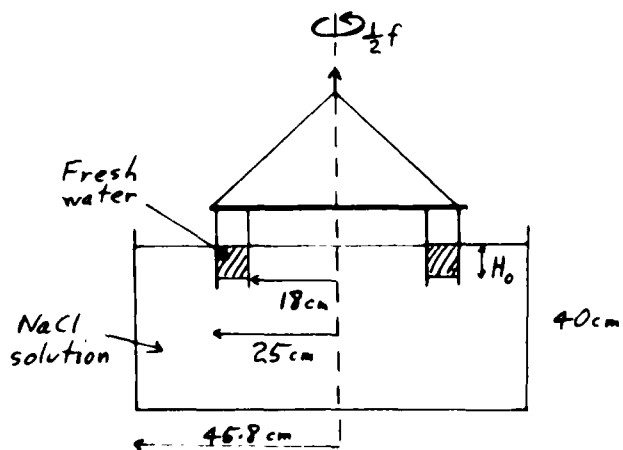
Figure 5.   The laboratory apparatus.

Values of the Coriolis parameter used ranged from $0.38s^{-1}$ to $2.5s^{-1}$, while the reduced gravity g' lay in the range $0.8 \leqslant g' \leqslant 12cms^{-2}$. The initial depth of the upper layer was always between 4 and 6 cm. This gave a ratio of layer depths less than 0.16 when the lower layer was 40 cm deep. However, two experiments were carried out with shallow lower layers in order to observe the influence of the lower boundary upon the flow. In these cases the initial depth ratios were 0.6 and 0.84.

6.2 Observations and results

The flow was observed to be very unstable at all values of the parameters. When the annulus was removed the buoyant upper layer first spread radially toward and away from the axis of rotation by a distance that was measured to be close to the initial Rossby radius $(g'Ho)^{1/2}f^{-1}$. As a result there formed an anticyclonic (clockwise) flow in the outer region of the upper layer and a cyclonic flow in the inner half of the dyed fluid. This collapsing phase occupied a time scale of order f^{-1}. Large disturbances to this flow became obvious within two or three revolutions and the current broke up into a chain of eddies within about six revolutions.

In figure 6 are shown four stages during the evolution of a current that was formed when the initial Rossby radius was 10% greater than the half width $L*_o$ of the annulus. In (i) the flow is largely axisymmetric and some of the curvature in the streaks is probably due to the later stages of the collapsing phase. However, some meandering is already present and in (ii) there have appeared five regions of closed anticyclonic circulation within the current. The fronts (edges of the dyed fluid) also reveal a wavelike structure. Although the circular geometry confuses the nature of the flow at this stage, there appears to be some meandering away from a circular line as well as variations in current width. The meandering becomes more obvious in (iii), where the flow is qualitatively very similar to that sketched in figure 3(c). In (iv), individual eddies have broken off from their neighboring eddies. The flow subsequently evolves very slowly, with the anticyclonic eddies becoming more circular and motions slowly decaying due to friction.

In figure 7 is shown a similar sequence in the evolution of a current for which the initial Rossby radius was only 45% of the annulus half-width $L*_o$. Frame (i) again shows an almost axisymmetric flow with some turbulence produced in the wake of the annulus. Large disturbances are obvious in (ii). In this case, though, the waves have a much smaller wavelength and there are more waves around the outer front than around the inner front. However, the meandering mode can be clearly seen. In (iii) the varicose and meandering modes are both clear. The wider and deeper parts of the current form closed eddy circulations which, after a relatively slow evolution, make up the broad and turbulent current shown in (iv).
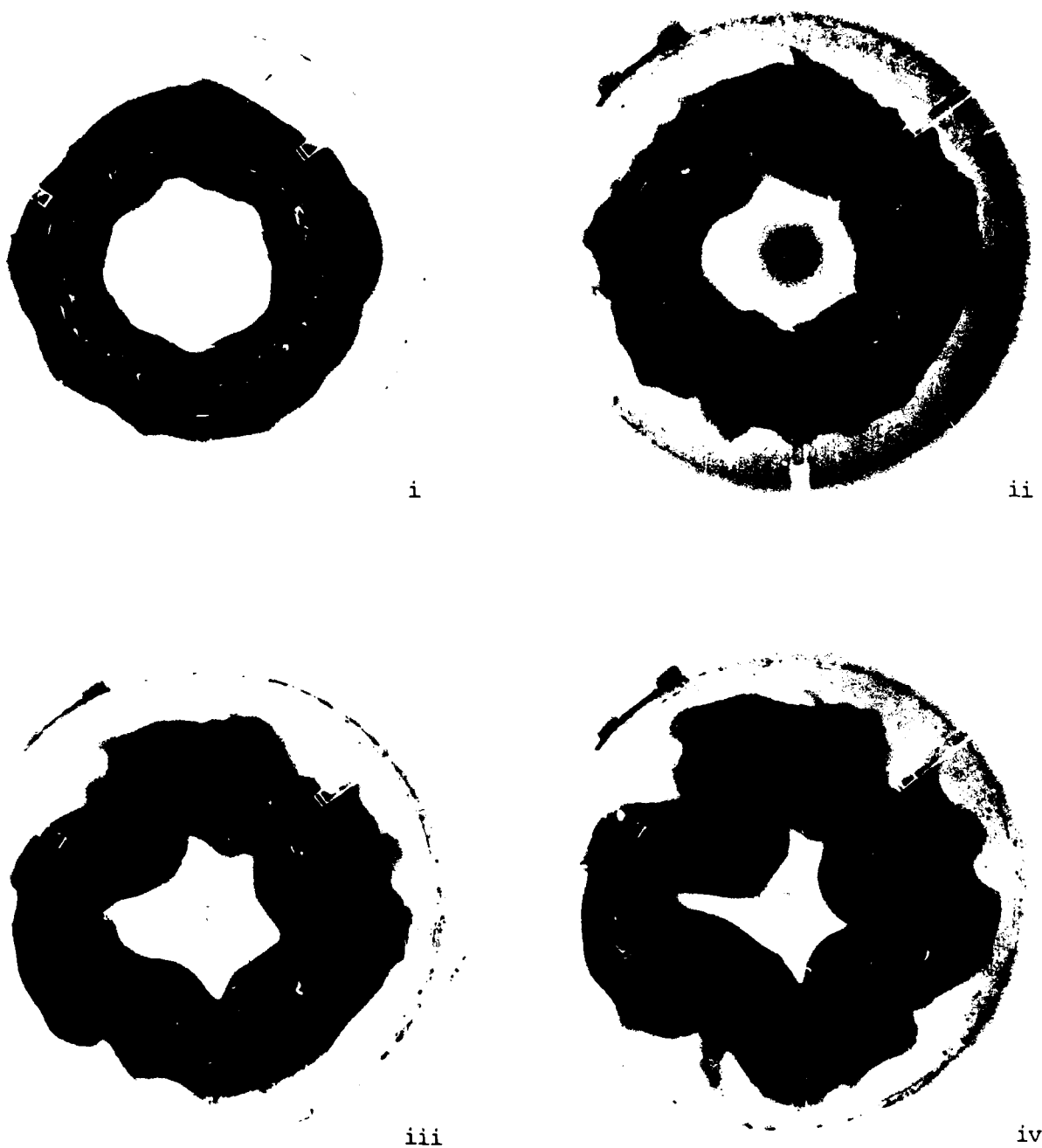
i

ii

iii

iv

Figure 6.   The evolution of a current with $f = 2.07s^{-1}$ and $F = 0.90$.
             (i)   t = 2 days
             (ii)   t = 4 days
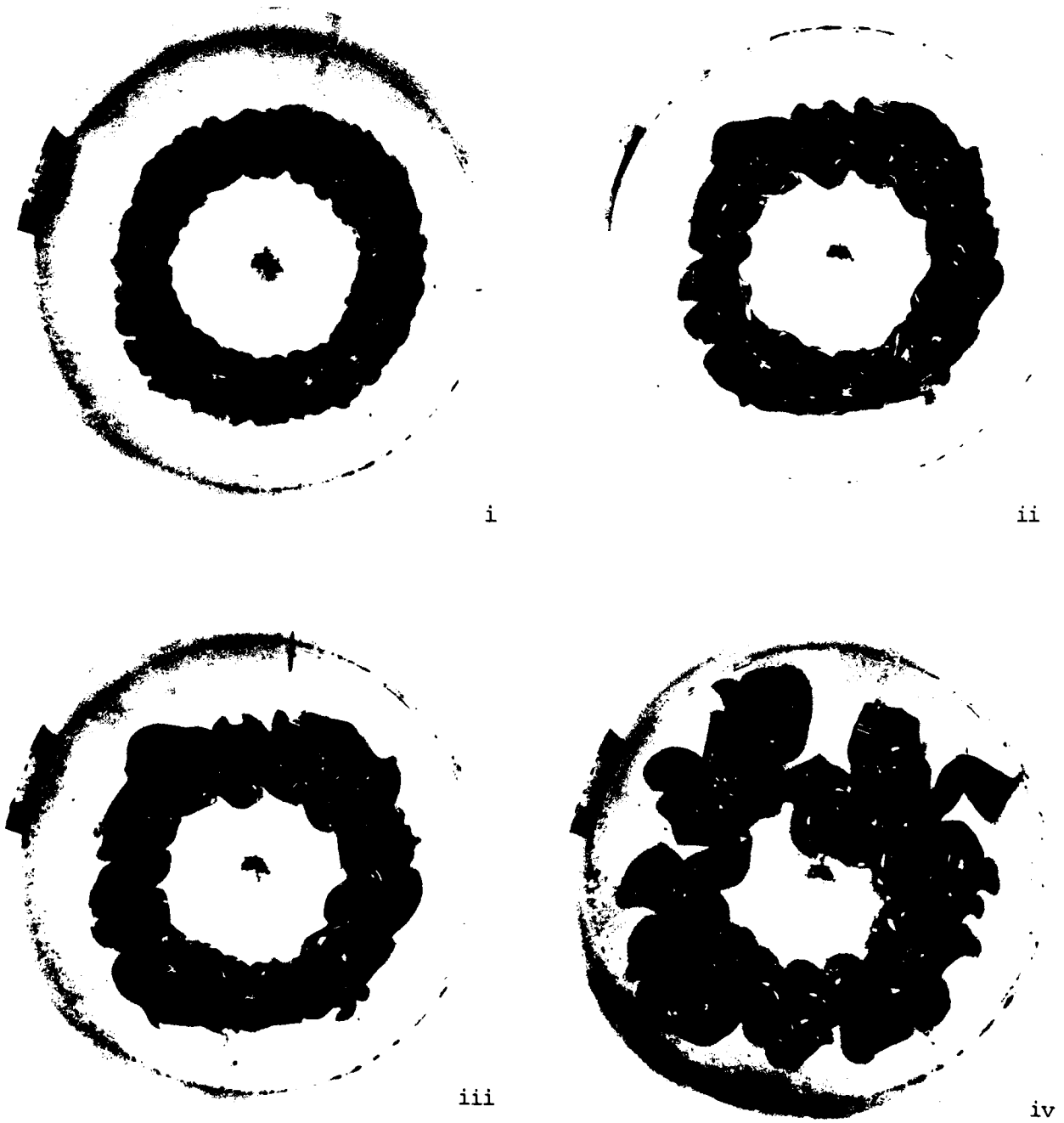   (iii) t = 6 days
             (iv)   t = 8 days.

Figure 7   The evolution of a current with f = 1.45s⁻¹ and $\tilde{F}$ = 2.2
(i)   t = 1 day
(ii)   t = 4 days
(iii) t = 5 days
(iv)   t = 17 days

If we assume for the moment that the deep bottom layer is stationary and that there is no mixing between the layers, then the laboratory current is described by the single dimensionless parameter $fL*_o/(g'H_o)^{1/2}$, and this is exactly the quantity $\mathcal{F}$ defined in (5.27). In figure 8 is plotted n, the number of waves that appeared around the annular current. The straight line is a fit by eye to the data and indicates that the wavenumber increases roughly linearly with $\mathcal{F}$. In figure 9, the same data is presented as the dimensionless wavelength $f\lambda/(g'H)^{1/2}$, where the wavelength λ is calculated from $\lambda = 2\pi r/n$ and r is the radius of the inner or outer front. The depth H at the midpoint of the current is given by Ho, the measured width L* after collapse and equation (2.11), but was always within 10% of Ho. We see that this dimensionless wavelength is independent of $\mathcal{F}$ and is therefore independent of the width of the current. The constant value $f\lambda/(g'H)^{1/2} = 6.9 \pm 0.7$ corresponds to the wavenumber $\mathcal{E} = 0.9 \pm 0.1$. Thus energy is most efficiently released on a length scale that is determined solely by the Rossby radius and that is not influenced by the distance between the two fronts. Note that a most rapidly growing mode with $\mathcal{E} = 0.8$ is consistent with our analysis for zero potential vorticity while this wavenumber has not been predicted for currents with finite potential vorticity.

Two remarks can be made about the growth rates of the observed disturbances. First, their appearance within about two revolutions after the annulus was withdrawn implies a growth rate $c > 4\times10^{-2}$. This lower limit is significantly less than calculated first order growth rate c_1 at values of $\mathcal{F} < 5$. Since c_1 is expected to greatly over-estimate the real growth rate at $\mathcal{E} \sim 1$, the two values are vaguely consistent. On the other hand, the growth rate is predicted to decrease rapidly with increasing $\mathcal{F}$. This is difficult to verify within the experimental range of parameters because the appearance and growth of small amplitude disturbances is poorly defined. A more clearly defined time scale, and one that will be of importance in oceanographic observations, is that time required for the initial current to form isolated eddies whose circulations have pinched off from their neighbors. For the two experiments shown in figures 6 and 7 this time scale was, respectively, 5 and 6 rotation periods.

6.3 Other instabilities

Immediately after the buoyant upper layer collapsed, some small scale structure was visible at the fronts. This was probably the result of turbulence produced in the wake of the withdrawn annulus walls. No evidence of Kelvin-Helmholtz instability was observed.

Of greater importance is the influence of a two-layer baroclinic instability. Griffiths and Linden (1980) have found that the wavelength of unstable waves that appear on an isolated two-layer vortex in a rotating laboratory tank is dependent upon the ratio of layer depths. They conclude that the instability is primarily baroclinic when the ratio of the upper to lower layer depths is greater than 10^{-1}. At such depth ratios the unstable waves led to the formation of cyclone-anticyclone pairs which propagated away from any remaining central vortex. In figure 10 are shown two stages in the evolution of an annular current when the
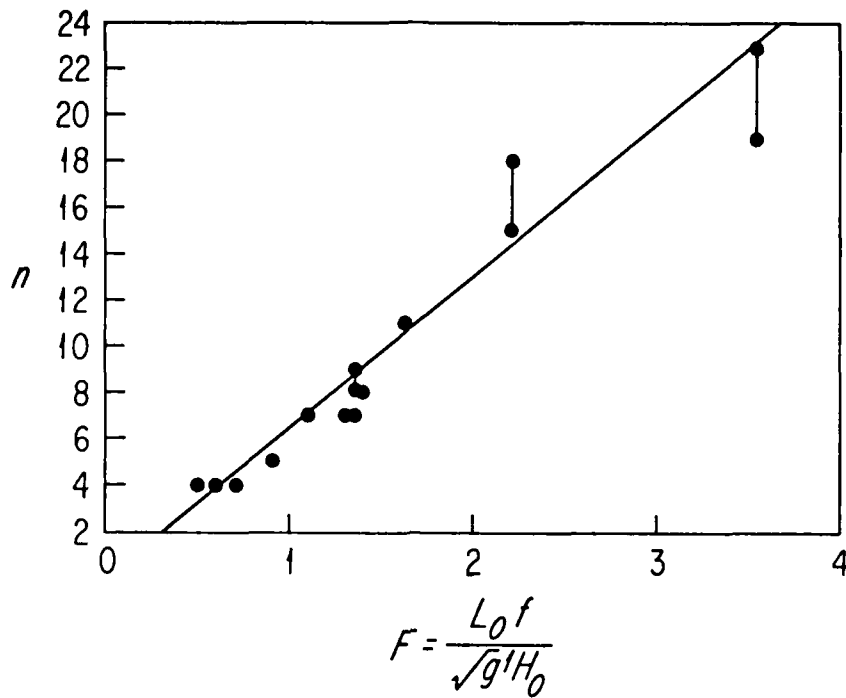
Figure 8. The number of waves observed around the annulus, and a straight line fitted by eye to the data.

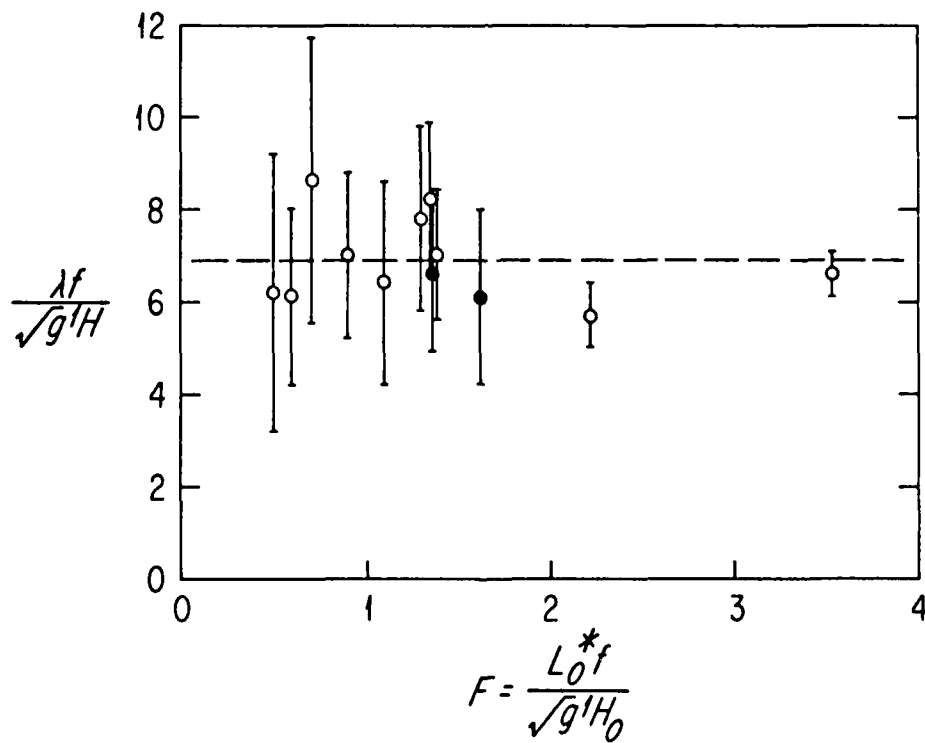

Figure 9. The dimensionless wavelength $\lambda f/(g'H)^{1/2}$ as a function of $\mathcal{F} = fL^*_o/(g'Ho)^{1/2}$. The horizontal line is the mean value 6.9 ± 0.7. The filled circles are those cases in which the lower layer was shallow.

initial depth ratio is 0.6. While of smaller amplitude, each wave was observed to "break" on the up-stream side, where vortices of opposite sign appeared in the lower layer. At the later stage shown in (ii) there are a number of cyclone-anticyclone pairs present and one dipole has escaped from the vicinity of the current. On the other hand, the dominant wavelength observed on the annular currents does not depend upon the ratio of layer depths (the wavelengths from experiments with large depth ratios are shown as filled cir les in figure 9). There was also no marked difference in the time that elapsed before large disturbances appeared. We conclude that the lower layer is no longer stationary at the larger depth ratios and that the two-layer baroclinic mechanism is able to help release potential energy. However, it seems likely that the single-layer instability caused by the presence of two free streamlines selects the most unstable wavenumber and assists the energy transfer, even in the distinctly two-layer flow.

7. Conclusions

A single-layer model of a narrow buoyant current that is bounded by two free streamlines predicts that such a flow is very unstable. In the limit of infinitely long waves, disturbances grow linearly with time and normal modes are stable. For flows with uniform potential vorticity an analysis of normal modes with finite wavelengths indicates that disturbances will grow exponentially with time and be stationary in space. A superposition of meandering and 'varicose' modes is predicted to release both potential and kinetic energy from the undisturbed current. When the flow has zero potential vorticity, the wavelength of the mode with the maximum growth rate is estimated to be $8 \ (g'H)^{1/2} f^{-1}$, where H is the maximum depth of the current.

Our analysis for flows with finite potential vorticity leads to a first order growth rate that depends upon the ratio of width and depth scales of the current. Two limits are of interest. First, the analysis is not valid in the limit where the potential vorticity approaches zero. The correct limit is that given by the equations with the potential vorticity set identically to zero. Second, when the current width becomes large compared to the Rossby radius based on H_o (the depth at which the relative vorticity is zero) the growth rate of disturbances becomes very small. This suggests that a single front (at the edge of an infinitely wide current) is stable to normal modes in a one-layer model.

Laboratory experiments with a shallow current at the free surface of a deep lower layer confirm that such a current is very unstable and show that the dominant downstream length scale is approximately $7 \ (g'H)^{1/2} f^{-1}$. The observed structure of growing disturbances corresponds closely to that predicted. The experiments also indicate that the single-layer frontal instability is likely to continue to be important when the second layer is of finite depth and the two-layer baroclinic instability mechanism assists the release of potential energy.

The analysis could be extended to investigate the stability of a circular eddy that is bounded by a sharp density front. In this case, there is a single free streamline. However, there may be a coupling

i

ii

Figure 10.   Two stages in the evolution of an annular current when the
lower layer is shallow.   f = 0.89s^{-1}, F = 1.36 and
initial ratio of layer depths 0.6
(i)   t = 2.5 days
(ii) t = 6 days

between the antipodes of the front. A current flowing along a sloping
bottom can also be described by a minor modification to the cross-stream
momentum equation (2.9). For a planar bottom with a slope $d\mathcal{S}/dy$,
perpendicular to the direction of the undisturbed flow, (2.9) becomes
$\bar{u} = -d\bar{h}/dy - d\mathcal{S}/dy$ and the perturbation equations are otherwise
unchanged. There is now a net flux of fluid along the stream and it can
be shown that the velocity is even unidirectional when $|d\mathcal{S}/dy| >$
$\mathcal{H}^{1/2}$ tanh $(L/\mathcal{H}^{1/2})$. As the symmetry of the original problem has now
been removed, the structure of the growing disturbances will be altered
and they will no longer be stationary in the spatial reference frame
moving with the velocity of the midpoint of the current.

Acknowledgements

References

Griffiths, R. W. and Linden, P. F. (1980) The stability of vortices in a
   rotating, stratified fluid, J. Fluid Mech., in press.

Mann, C. R. (1969) Temperature and salinity characteristics of the
   Denmark Strait overflow. Deep-Sea Res., 16, 125-137.

Pedlosky, J. (1964) The stability of currents in the atmosphere and
   ocean. Part I. J. Atmos. Sci. 21, 201-219.

Worthington, L. V. (1969) An attempt to measure the volume transport of
   Norwegian Sea overflow water through the Denmark Strait. Deep-Sea
   Res., 16, 421-432.

RATIONAL SOLUTIONS TO PARTIAL DIFFERENTIAL EQUATIONS

James Meiss

A soliton is usually defined as a localized solution to a partial differential equation (pde) which "asymptotically preserves its shape and velocity upon collison with other solitons." (Scott, Chu, and McLaughlin, 1973). One explanation for this remarkable stability derives from the inverse spectral transform: in "spectral space" a soliton is represented by an eigenvalue (of the associated linear problem) which is time independent.

Another possible explanation for the particle-like nature of solitons was first suggested by Kruskal in 1974. In his view a soliton is represented by a point, or an array of points, moving in the complex plane. In this report we review the development of this idea over the past six years for a number of pde's.

For historical reasons, consider first the Korteweg-de Vries (KdV) equation

$$u_t + uu_x + u_{xxx} = 0 \; , \tag{1}$$

which has the soliton solution

$$u(x,t) = 3v \, \text{sech}^2\left(\frac{\sqrt{v}}{2}(x-vt)\right) \; . \tag{2}$$

Noticing that the function sech2(y) has double poles evenly spaced along the imaginary axis we could rewrite (2) in terms of a summation over poles:

$$\text{sech}^2(y) = -\sum_{n=0}^{\infty} \frac{1}{\left(y+i\left(n+\frac{1}{2}\right)\pi\right)^2} + c.c. \; . \tag{3}$$

The KdV soliton therefore can be thought of as an infinite line of points in the complex plane with spacing $2\pi/\sqrt{v}$. In the single soliton, each pole moves with constant velocity v in the "real" direction. To obtain a two soliton solution we begin with two well separated lines at poles, each with spacing depending on its velocity. The subsequent evolution of the poles depends in detail on the ratio $\sqrt{v_1/v_2}$, for if this is rational then the entire structure is periodic in the imaginary direction (Thickstun, 1976). This suggests interpreting the poles as point particles which interact due to the nonlinearity of the KdV equation. We will see that this is indeed the case and suggest that this particle interpretation is connected to the stability of the solitons.

To generalize the soliton solution (2-3), assume that the function u(x,t) can be decomposed into a set of mth order poles with positions $a_j(t)$ and residues $R_j(t)$:

$$u(x,t) = \sum_{j=1}^{N} \frac{R_j(t)}{(x-a_j(t))^m} \; . \tag{4}$$

Substitution of this ansatz into (1) shows that (4) is a solution only if m = 2 and R_j = -12 (Airault, McKean, and Moses, 1977; Choodnovsky[2], 1977). In addition, the pole positions must satisfy the ordinary differential equations (ode's)

$$\dot{a}_j(t) = -12 \sum_{k=1}^{N}{}' \frac{1}{(a_j - a_k)^2} \qquad , \quad j = 1, 2, \cdots N \tag{5}$$

Finally, the initial conditions are constrained by the requirement

$$\sum_{k=1}^{N}{}' \frac{1}{(a_j - a_k)^3} = 0 \qquad j = 1, 2, \ldots N \tag{6}$$

In these sums the prime indicates the omission of the singular terms k = j.

We thus have a correspondence between the pde (1) and the N ode's (5). The set of solutions (4) includes as a special case the multi-soliton solutions. For finite N it has been shown (Airault, McKean, and Moses, 1977) that the constraint (6) can be satisfied only when

$$N = \frac{d(d+1)}{2} \qquad d = 1, 2, \cdots \tag{7}$$

The simplest case of (7), d = 1, yields a time independent solution

$$u(x) = \frac{-12}{(x-a)^2} \tag{8}$$

where a is a complex constant

The next case, d = 2, has pole positions, proportional to $\sqrt[3]{-1}$ and

$$u(x,t) = \frac{-36x(x^3 - 4t)}{(x^3 + 2t)^2} \tag{9}$$
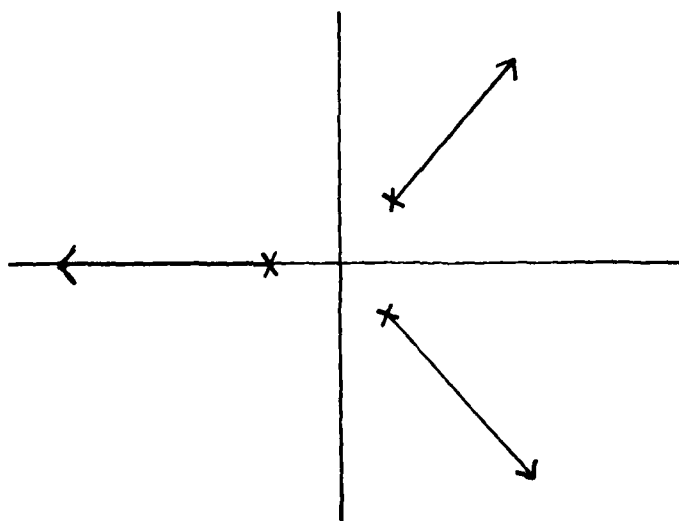
Figure 1 displays the trajectories of the poles for this case.

Airault (1978) has presented solutions for higher values of d; however, not much is known about the $N \rightarrow \infty$ case other than the existence of the multi-soluton solutions.

The pole equations (5) can be derived directly by substituting the ansatz (4) into the pole or alternatively by Fourier transformation. We will describe this latter method for another pde - the Benjamin-Ono equation ((Len, Lee, and Pereira, 1979). This equation results in the simpliest possible pole equations and is for that reason pedagogically preferable.

The Benjamin-Ono equation (see Redekopp, this volume) is

$$u_t + uu_x + H u_{xx} = 0 \tag{10}$$

where H is the Hilbert transform

$$H u \equiv \frac{1}{\pi} \oint_{-\infty}^{\infty} \frac{u(z)}{z-x} \, dz \tag{11}$$

Defining the Fourier transform by $\quad \tilde{u}(k) = \int_{-\infty}^{\infty} e^{-ikx} u(x) dx$ and applying this to (10) yields

$$\tilde{u}_t + \frac{ik}{2} (\widetilde{u^2}) - ik|k| \, \tilde{u} = 0 \tag{12}$$

where we have used $\widetilde{Hu} = i \, \text{sgn}(k) \tilde{u}$. If the ansatz (4) is again used, we will see that (12) can be satisfied only when m = 1. For this case the Fourier transform of u is

$$\tilde{u}(k,t) = -\text{sgn}(k) \, 2\pi i \sum_{j\pm} R_j \, e^{-ika_j(t)} \tag{13}$$

where the summation is only over those poles in the upper (lower) half plane for $k < 0$ $(k > 0)$. We will assume below that $k < 0$ for simplicity; however, it is easy to see that the case $k > 0$ yields equivalent results. Using the form (13) in the three terms of (12) yields

$$\tilde{u}_t = 2\pi i \sum_{j+} R_j e^{-ika_j} \left(-ika_j + \frac{\dot{R}_j}{R_j}\right) \tag{14a}$$

$$\frac{ik}{2}(\widetilde{u^2}) = 2\pi i \left\{ \frac{k^2}{2} \sum_{j+} R_j^2 \, e^{-ika_j} + \sum_{j+} R_j \, e^{-ika_j} \sum_{\ell}' \frac{R_\ell}{(a_j - a_\ell)} \right\} \tag{14b}$$

$$-ik|k| \tilde{u} = 2\pi i \, (ik^2) \sum_{j+} R_j \, e^{-ika_j} \tag{14c}$$

In (14b) the first term on the right arises from the double poles in the Fourier integral. The three terms (14) must sum to zero for all k; in particular, the $\mathcal{O}(k^2)$ terms must vanish

$$2\pi i \, k^2 \left[\sum_{j+} e^{-ika_j} \left(\frac{R_j^2}{2} + i R_j \right) \right] \implies R_j = -2i \tag{15}$$

Vanishing all of the $\mathcal{O}(k)$ term implies

$$\dot{a}_j = \sum_\ell{}' \frac{R_\ell}{(a_j - a_\ell)} \tag{16}$$

and finally the $\mathcal{O}(k^0)$ term gives $\dot{R}_j = 0$ which is consistent with (15).

The known solutions of the many-body problem (16) include the case $N = 1$ where u is trivally time independent, $N = 2$ with complex conjugate poles where u is the single soliton solution

$$u(x,t) = \frac{4v}{v^2(x-vt)^2 + 1} \tag{17}$$

and similarly $N = 2n$ when the poles are complex conjugate pairs where   is the n-solution (Joseph, 1977; Case, 1979; Matsumo, 1979, 1980). We will see below that (16) can be embedded into an integrable Hamiltonian system and hence all solutions are known in principle.

The above analysis applies almost without change to the Burgers-Benjamin-Ono (BBO) equation as defined by

$$u_t + u u_x + \alpha H u_{xx} - \beta u_{xx} = 0 \tag{18}$$

This equation has solutions of the form (4) with $m = 1$, $R_j = -2(\beta + i\alpha)$ and

$$\dot{a}_j = -2(\beta + i\alpha) \sum_k{}' \frac{1}{(a_j - a_k)} \tag{19}$$

Consider for example the N=2 case for which the equations (19) are easily solved

$$a_1 = C + \sqrt{D^2 - 2(\beta + i\alpha)t} \tag{20}$$

$$a_2 = C - \sqrt{D^2 - 2(\beta + i\alpha)t}$$
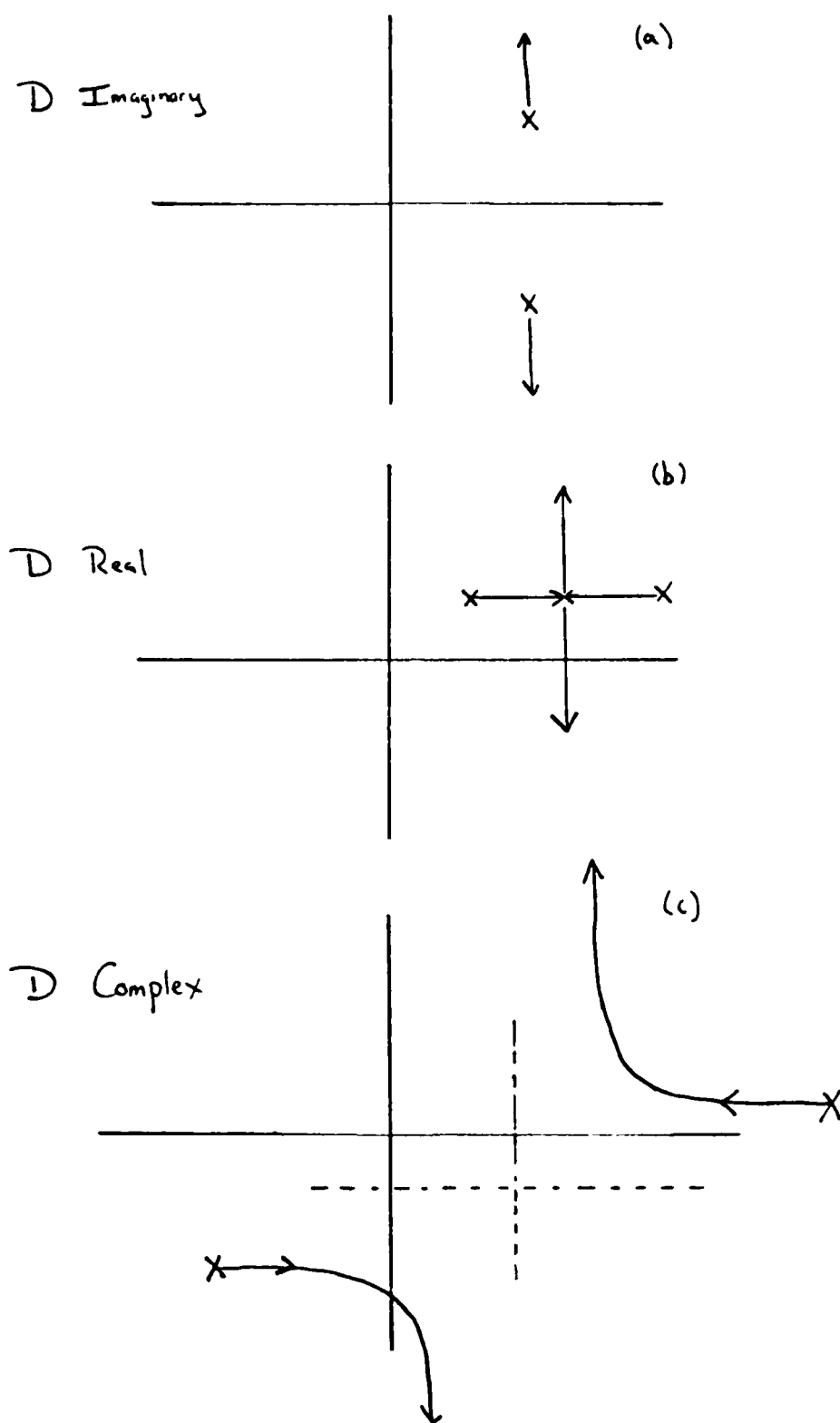
Fig. 2 Pole Trajectories for the Burgers Equation from (20).

Figure 2 displays the three types of trajectories for this equation when $\alpha =$ 0. Note that if D is real, the poles collide and the velocity, according to (19), becomes infinite.

The pole equations for the BBO equation can be embedded into a Hamiltonian system. Begin by differentiating (19) with respect to time and substituting for a_k on the right hand side to obtain

$$\ddot{a}_j = 8(\beta + i\alpha)^2 \sum_k{}' \frac{1}{(a_j - a_k)^3} \tag{21}$$

This set of equations is derivable from the Hamiltonian

$$H = \frac{1}{2} \sum_j (\dot{a}_j)^2 + 4(\beta + i\alpha)^2 \sum_{k<j} \frac{1}{(a_j - a_k)^2} \tag{22}$$

which is the complex version of the Calogero-Moser lattice (Calogero, 1971). This system can be shown to be integrable by Lax's method (Moser, 1975). It must be noted that there are trajectories of the Hamiltonian (22) which are not solutions to (19); however, the particular solutions of (21) that have initial conditions satisfying (19) are also solutions of (19). This is the meaning of the term "embedded" as used above.

The embedding of the pole equations into a Hamiltonian system is also possible for the KdV system (5) (Airault, Moser, and McKean, 1977). In this case one obtains a particle system with an inverse fourth power potential. This Hamiltonian is also integrable - only however when the constraint (6) is satisfied (Choodnovsky, 1977).

It is interesting, in view of the above connections between integrable pde's and integrable ode's, to speculate that there is some deeper connection between those pde's which can be pole decomposed and integrability. Consider, for example, the more general equation

$$u_t + u^p u_x + \mathcal{L} u = 0 \tag{23}$$

where p is an integer and $\mathcal{L}$ a linear pseudo-differential operator of order n (that is, the Fourier transform of $\mathcal{L}$ is a power series in k, and perhaps $|k|$, with the highest power n). We can easily find a necessary requirement for the validity of the ansatz (4) by considering the highest order poles generated by substitution into (23). The diagonal part of the nonlinear term is a pole of order $mp + m + 1$; while the highest order of the poles in the dispersive term is $m + n$. These two terms must balance since if $n \geq 1$ the time derivative has no poles of order larg enough. Thus we must have

$$mp + m + 1 = m + n,$$
$$mp = n - 1 \tag{24}$$

in order for the nonlinearity to balance the dispersion. This necessary requirement for the solution (4) already eliminates most equations (Table 1).

For example, when n = 3 only

P \ n	1	2	3	4	5
0	Wave Eq.				
1	BBO	KdV	✓	✓
2		mKdV		✓
3			✓	
4				✓

no pole solutions

Table 1: Equations with pole solutions

the p = 1 (KdV) and p = 2 (modified KdV) equations have pole solutions. We note that these are also the only two n = 3 equations with an infinite set of polynomial conservation laws. It is possible, although apparently not yet proved, that such a set of conservation laws is required for integrability.

It the connection between pole solutions and conservation laws is true for other n then (24) implies that the only n = 2 equations which are integrable are the BBO equations. Similarly there are only two integrable equations for n = 4 and only three with n = 5, etc.

As a final remark we note that it is also possible to look for solutions consisting of periodic arrays of poles. For the KdV equation there is a solution

$$u(x,t) = \sum_j \wp(x - a_j(t)) \tag{25}$$

where $\wp$ is the Weierstrass elliptic function (Airault, McKean, and Moser, 1977, Chudnovsky, 1977). We recall that the $\wp$ function consists of a doubly periodic array of second order poles. In a similar fashion we can expect to find solution for the BBO equation which is a sum of Jacobi elliptic functions, although this has apparently not been done.

REFERENCES

Airault, H., McKean, H. P., Moser, J., 1977; Rational and Elliptic Solutions of the Korteweg-De Vries Equation and a Related Many Body Problem, Comm. on Pure and Appl. Math, $\underline{30}$, 95-148.

Airault, H., 1978; Poles of Nonlinear Evolution Equations and Integrable Dynamical Systems; in Nonlinear Evolution Equations Solvable by the Spectral Transform, F. Caloger (ed.), Pitman; London

Calogero, F.; Solution of the One-Dimensional N-Body Problems with Quadratic and/or Inversely Quadratic Pair Potentials, J. Math. Phys. $\underline{12}$, 419-436.

Case, K. M., 1979; Properties of the Benjamin-Ono Equation; J. Math. Phys. $\underline{20}$, 972-977.

Choodnovsky, D. V., and Choodnovsky, G. V.; Pole Expansions of Nonlinear Partial Differential Equations; Nuovo Cimento $\underline{40}$, 339-352.

Joseph, R. I.; 1977; Multi-Soliton-Like Solutions to the Benjamin-Ono Equation; J. Math. Phys. $\underline{18}$, 2251-2258.

Kruskal, M., 1974; in Lect. in Appl. Math, A. Newell (ed.) $\underline{15}$, 61-83.

Matsuno, Y., 1979, Exact Multi-Soliton Solution of the Benjamin-Ono Equation, J. Phys. A. $\underline{12}$, 619-621.

Matsuno, Y., 1980; Interaction of the Benjamin-Ono Solitons, J. Phys. A. $\underline{13}$, 1519-1536.

Moser, J.; 1975; Three Integrable Hamiltonian Systems Connected with Isospectral Deformations; Adv. Math $\underline{16}$, 197-220.

Scott, A. C., Chu, F.Y.F., McLaughlin, D. W., 1973; The Soliton; Proc. IEEE $\underline{61}$, 1443-1490.

Thickstun, W. R.; 1976; A System of Particles Equivalent to Solitons; J. Math. Anal. and Appl. $\underline{55}$, 335-346.

COHERENT FEATURES BY THE METHOD OF POINT VORTICES

Hassan Aref

1. Introduction

This investigation arose from a desire to apply to the barotropic potential vorticity equation the method of point vortex decomposition that has proved so useful in nonrotating two-dimensional flow. In particular, it seemed that point vortices (and the vortex-in-cell method, see § 3) might considerably reduce the computing time necessary to calculate numerically a coherent feature such as a modon. The recent work by McWilliams, Flierl, Larichev and Reznik (1980; henceforth referred to as MFLR) provided a useful benchmark with which to compare.

In this work I assess the accuracy and reliability with which one can calculate certain dipole vortex structures in nonrotating two-dimensional flow. As shown in § 2 these dipoles turn out to be the $\beta \to 0$ limit of the two-dimensional Rossby solitons found by Larichev & Reznik (1978) and studied in MFLR. The dipoles, called 2D Euler solitons here by analogy, can be calculated by the vortex-in-cell method. At comparable accuracy and resolution this method is shown to be at least a factor 25 faster than a straightforward finite difference calculation (§ 3). This considerable saving of necessary resources allows collision experiments between coherent features to be studied with ease (§ 4). The results obtained here suggest that application of the vortex method to flow features with finite β should be pursued.

2. The two-dimensional Rossby soliton (2DRS)

These special solutions, originally presented by Larichev & Reznik (1978), consist of a dipole-like vortex on the infinite β-plane. The streamfunction ψ in the restframe of such a "coherent feature" has the form:

$$\psi = -\beta a \sin\theta \times \begin{cases} -\left[\dfrac{J_1(\kappa r)}{\kappa^2 J_1(\kappa a)} - \dfrac{r}{a}\left(\dfrac{1}{\kappa^2} + \dfrac{1}{\rho^2}\right)\right] ; & r < a \\[3ex] \dfrac{K_1(\rho r)}{\rho^2 K_1(\rho a)} ; & r > a \end{cases} \tag{2.1}$$

where $J_1(K_1)$ is the (modified) Besselfunction of order 1. As written the solution contains three parameters: a, κ and ρ. a is the radius of the feature. κ and ρ are inner and outer wavenumbers characterizing the feature. They are related by the condition:

$$\frac{J_2(\kappa a)}{\kappa a\, J_1(\kappa a)} = -\frac{K_2(\rho a)}{\rho a\, K_1(\rho a)} \tag{2.2}$$

which results from demanding that the tangential velocity be continuous at r = a. The dipole (2.1) translates with uniform speed:

$$U = \beta/\rho^2 \tag{2.3}$$

to the East (x increasing). The relative vorticity of the feature, $\zeta = -\Delta\psi$, is given by the simple expression:

$$\zeta = -\beta a \sin\theta \times \begin{cases} J_1(\kappa r)/J_1(\kappa a) \; ; \; r < a , \\ K_1(\rho r)/K_1(\rho a) \; ; \; r > a . \end{cases} \tag{2.4}$$

Two limits of the above result are worth noting. First, keep β and a fixed but let $\rho \to \infty$ so that $U \to 0$ and $\psi \to 0$ for $r > a$. Then

$$\psi \to -\frac{\beta a}{\kappa^2}\left(\frac{J_1(\kappa r)}{J_1(\kappa a)} - \frac{r}{a}\right) \sin\theta \qquad ; \qquad r < a \tag{2.5}$$

and the matching condition (2.2) becomes:

$$J_2(\kappa a) = 0. \tag{2.6}$$

Hence we recover the modon solution originally found by Stern (1975).

The second limit to consider arises for a and U fixed but $\rho \to 0$ so that $\beta \to 0$. For $r > a$ we then get:

$$\psi = \frac{U a^2}{r} \sin\theta \tag{2.7a}$$

while for $r < a$

$$\psi = -U\left(\frac{J_1(\kappa r)}{\kappa J_0(\kappa a)} - r\right) \sin\theta . \tag{2.7b}$$

The matching condition becomes:

$$J_1(\kappa a) = 0 \tag{2.8}$$

These solutions are discussed by Lamb (1916) and Batchelor (1967). Note that U is now a free parameter (independent of a and κ). I shall call these solutions two-dimensional Euler solitons (2DES).

A couple of pertinent results about 2DES follow. First, note that κ is an average wavenumber of the flow in the sense that $\zeta = \kappa^2\psi$ for $r < a$ or equivalently that

$$\kappa^2 \mathcal{E}_{kin} = \Omega \tag{2.9}$$

where $\mathcal{E}_{kin}$ is the kinetic energy of the flow (in the frame of reference where the fluid is at rest at infinity) and Ω is the enstrophy.

Secondly, note that the nonvanishing component of the fluid impulse

$$P \equiv \iint dx\, dy\ y\varsigma = 2\pi a^2 U \tag{2.10}$$

For $\iint dx\, dy\ \varsigma = 0$ (as is the case here) P equals the total momentum of the fluid (in the same reference frame as above). Finally,

$$\varepsilon_{kin} = \tfrac{1}{2}\left(2\pi a^2\right) U^2 \tag{2.11}$$

The formulae (2.10), (2.11) are analogous to the expressions for momentum and kinetic energy of a classical free particle with mass $2\pi a^2$ and velocity U. I shall return to these formulae in §3 and §4.

3. Numerical simulation of a 2DES

A sequence of numerical calculations were performed to assess how well a 2DES, Eqn. (2.7), can be simulated using the vortex-in-cell algorithm. A description of this algorithm is given in Christiansen (1973). The actual code used here is the same as in previous work (Aref & Siggia 1980). The basic independent variables of this algorithm are the coordinates (x_n, y_n) and the strengths κ_n, $n = 1,\ldots,N$ of an assembly of N point vortices. However, in calculating the motion of the vortices a grid (of dimension M x M say) is used, and at each timestep Poisson's equation for the streamfunction is solved and velocities calculated (by finite differences) on the grid. At first sight one might therefore assume that a vortex-in-cell calculation employing an M x M grid would have a spatial resolution comparable to a finite difference calculation on a grid of the same dimensions. However, it is possible to have many vortices per grid square and so the spatial resolution of the vortex-in-cell approach depends on both the grid size M and the available number of point vortices N. Note that an FFT on an M x M grid requires $O(M^2 \log_2 M)$ operations. Hence, in a finite difference code that employs FFT technique to solve for the streamfunction the operation count goes up by at least a factor of 4 if M is increased by a factor of 2. In the vortex-in-cell algorithm on the other hand the operation count increases only linearly with N as the number of vortices is increased on a grid of fixed size.

When calculating a structure like (2.7) the vortex-in-cell method turns out to be much more efficient than a finite difference algorithm. The reason is that M can be kept relatively small (M = 64 or 128 in the calculations reported here) and all the vortices can be piled into the vorticity containing regions of the flow field. The resulting resolution is considerably beyond that of a finite difference code on an M x M grid. By comparing with recent results in MFLR the spatial resolution of my vortex-in-cell calculations with $N = O(M^2)$ seems comparable to the spatial resolution of a finite difference code on a grid approximately 5M x 5M! The necessary computing resources are thus reduced by at least a factor 25.

Now let me describe the numerical calculations performed. The setup is shown schematically in the top half of Fig. 1. The numerical box has rigid boundaries top and bottom, periodic boundaries left and right. The 2DES which is a solution for the unbounded plane is initialized in this channel and its evolution followed in time. This procedure is repeated for several values of the ratio a/L of structure radius to channel width.
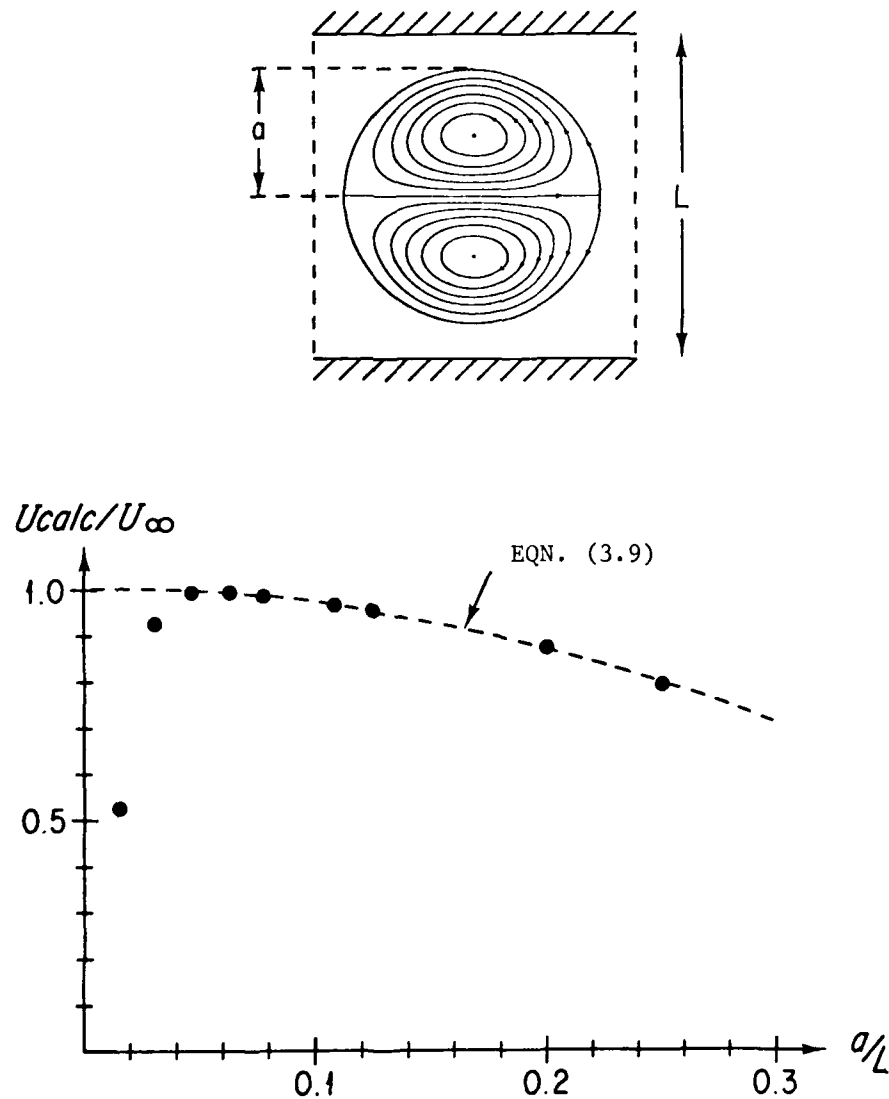

Fig. 1   Defining sketch for numerical experiments (top).   Calculated propagation speeds for different sizes of 2DES (bottom).

In order to exploit the potential additional resolution of the vortex method the 2DES were initialized as follows: First, using a 64 × 64 grid, a 2DES of radius $a = L/2$ was initialized by placing at each grid site a point vortex of the appropriate strength. In all 3142 point vortices were needed. Then the 2DES was contracted to the desired size. To see how this works let $\mathfrak{Z}(r)$ be the vorticity of the solution (2.7) with radius a

$$\mathfrak{Z}(r) = \begin{cases} 2U\kappa\sin\theta \, \dfrac{J_1(\kappa r)}{J_0(\kappa a)} & ; \quad r < a \\[2ex] 0 & ; \quad r > a \end{cases} \tag{3.1}$$

and consider

$$\hat{\mathfrak{Z}}(r) \equiv \left(\frac{a}{b}\right)^2 \mathfrak{Z}\left(r\frac{a}{b}\right) = 2\hat{U}\hat{\kappa}\sin\theta \, \frac{J_1(\hat{\kappa}r)}{J_0(\hat{\kappa}b)} \quad ; \quad r < b \tag{3.2}$$

where

$$\hat{\kappa} = \kappa\frac{a}{b} \quad , \quad \hat{U} = U\frac{a}{b} \quad . \tag{3.3}$$

This vorticity distribution produced by contracting and rescaling is again of the form (2.7). Thus, in the calculations reported on here 3142 point vortices are used to represent the vorticity distribution regardless of the size of the radius. Note that the product of propagation speed and radius is the same for all 2DES obtained in this way.

The following values of a/L were considered: 1/64, 1/32, 3/64, 1/16, 5/64, 7/64, 1/8, 1/5, 1/4 and κa equal to the first zero of J_1. In each case the propagation velocity, U_{calc}, was calculated from the simulation by following the motion of the centroids of positive and negative vorticity. In Fig. 1 (lower half) the ratio U_{calc}/U_∞ , where U_∞ is the propagation velocity expected for the 2DES on the infinite plane, is plotted versus a/L. Two effects are apparent in this figure. For $a/L \gtrsim 0.1$ the simulated propagation speed is smaller than U_∞. This is due to the effects of the boundaries on the structure (see the discussion surrounding Eqns. (3.8) - (3.9)). For $a/L \lesssim 0.025$, U_{calc}/U_∞ again drops below unity. This is due to loss of resolution (cf. Fig. 3). To calculate the velocities plotted in Fig. 1 the 2DES was allowed to move 1-3 radii, i.e. the calculation lasted for a time interval, $0 < t < t_{fin}$, where $U t_{fin}/a \cong 2$. Such a calculation consumed approximately 10 sec of CRAY-1 CPU time. In the finite difference calculations of MFLR similar calculations consumed several minutes of CRAY-1 time (McWilliams, private communication).

Fluctuations in the value of U_{calc}/U_∞ over the duration of the run were smaller than the width of the dots in Fig. 1. The flag on the point $a/L = 0.125$ signifies that this value of U_{calc}/U_∞ was reproduced with a longer run, $U t_{fin}/a \gtrsim 5$, and for a run with κa equal to the second zero of J_1. For the longer run the vorticity profile

$$\bar{\zeta}(y, t_j) \equiv \frac{1}{L} \sum_{\ell=1}^{M} \zeta\left(\frac{\ell-1}{M} L, y, t_j\right) \tag{3.4}$$

for y on the grid, i.e. $y \times M/L = 0, \pm 1,$, was also calculated at several instants of time $t_1, \ldots, t_S$. The histogram in Fig. 2 gives the average

$$\langle \bar{\zeta}(y) \rangle \equiv \frac{1}{S} \sum_{j=1}^{S} \bar{\zeta}(y, t_j) \tag{3.5}$$

and the error bars give the size of the standard deviation $[\langle\bar{\zeta}^2\rangle - \langle\bar{\zeta}\rangle^2]^{\frac{1}{2}}$, where

$$\langle \bar{\zeta}^2(y) \rangle \equiv \frac{1}{S} \sum_{j=1}^{S} \bar{\zeta}^2(y, t_j). \tag{3.6}$$

It is obvious that the vorticity profile is well preserved. This check on the accuracy of the simulation is more sensitive than just evaluating the propagation speed. For, as is seen from Eqns. (2.10) - (2.11), the propagation speed is simply

$\langle\bar{\zeta}\rangle$	$[\langle\bar{\zeta}^2\rangle - \langle\bar{\zeta}\rangle^2]^{1/2}$
1.915	± .014
3.412	± .048
4.229	± .055
4.266	± .048
3.550	± .045
2.308	± .031
0.950	± .012
0.102	± .007
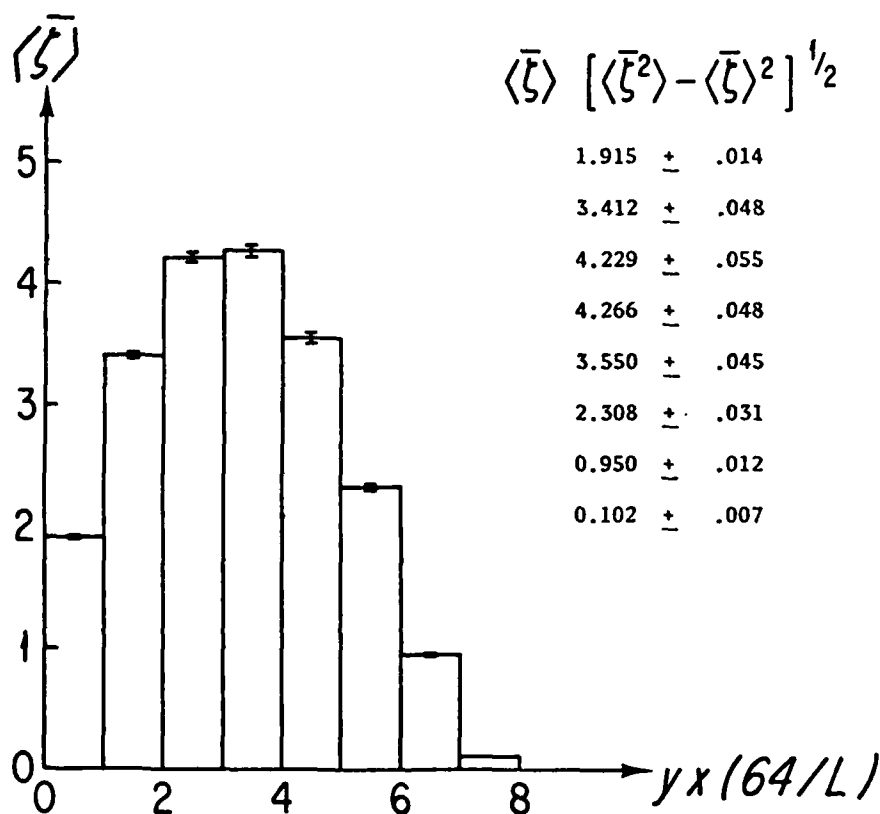
Fig. 2   Numerical check on persistence of 2DES vorticity profile.

$$U = 2\mathcal{E}_{kin}/P \tag{3.7}$$

and is constant for a code that preserves P and $\mathcal{E}_{kin}$.

To substantiate the claim that U_{calc}/U_{∞} for the large a/L values is less than unity because of boundary interactions I have calculated the analogous ratio of speeds for a pair of point vortices of opposite strengths. Let U_L denote the propagation speed of the pair with the boundary conditions of Fig. 1 (top) and let U_{∞} denote the propagation speed on the infinite plane. Then using results given by Oberhettinger & Magnus (1949) I find

$$U_L/U_{\infty} = \frac{\pi s}{L}\cot\frac{\pi s}{L} + \frac{\pi s}{L}\sin\left(\frac{2\pi s}{L}\right)\sum_{m=1}^{\infty}\left(\cosh^2 m\pi - \cos^2\frac{\pi s}{L}\right)^{-1} \tag{3.8}$$

where s is the distance between the point vortices. Expanding in powers of $\pi s/L$

$$U_L/U_{\infty} \cong 1 - 0.318\left(\frac{\pi s}{L}\right)^2 \tag{3.9}$$

The dashed line in Fig. 1 (bottom) is this parabola with the identification s = a.

To discuss the small a/L results I have replotted in Fig. 3 the data points for a/L = 1/64, 1/32, 3/64, 1/16, 5/64 and 7/64. The ordinate is again U_{calc}/U_{∞} but the abcissa now gives the number of grid intervals within the diameter of the 2DES. Since my
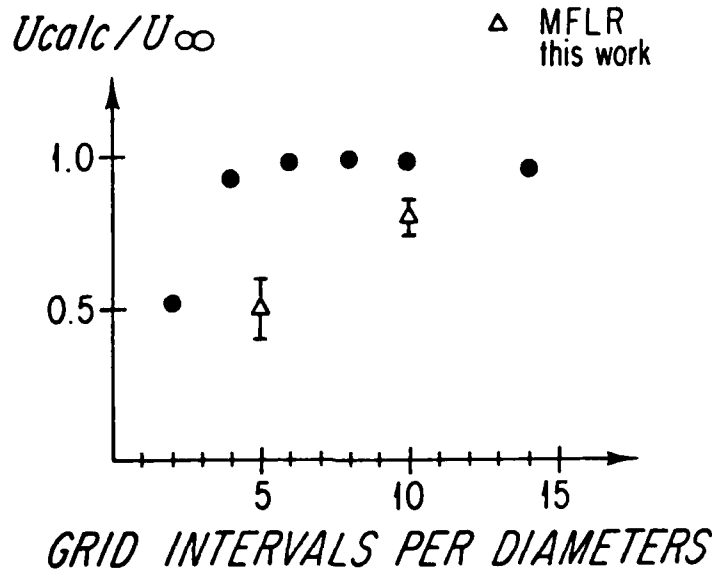
Fig. 3 Comparison of vortex-in-cell and finite difference code
        resolutions

grid is 64 x 64, a/L = 1/64 corresponds to 2 grid intervals per diameter and so on. As already surmised, piling up vortices within the bounding streamline increases the numerical resolution. To emphasize this point I have also plotted in Fig. 3 the results obtained by MFLR for a 2DRS using a finite difference code. (Results for the 2DES should be identical). It is clearly seen that the point vortices enhance the numerical resolution of the vortex-in-cell scheme well beyond that of the finite difference code. As discussed before the overall savings of computational resources are substantial.

Finally, consider contour plots of the streamfunction for the case a/L = 0.25 (Fig. 4a and b). The streamlines in the evolved structure match the initial streamlines identically when shifted back. On the other hand we know from Fig. 1 that the propagation speed is only about 0.8 of U_∞ and so the vortex must be adjusting to the imposed boundary conditions. Figs. 5a, b give an indication of how this is happening. Apparently waves propagate around the vortex lobes. Propagating waves on vortices have been studied by Zabusky and coworkers (cf. Deem & Zabusky (1979)) for the case of uniform vortices of finite area. I would like to believe that the waves seen in Fig. 5b represent dynamically possible modes and are not numerical artifacts. For a/L = 0.125 the boundary effects should be much reduced. The vorticity contour plots in Fig. 6a,b show that such is indeed the case.

4. Vortex collisions

In § 3 it was shown that the vortex-in-cell method can accurately calculate a 2DES, Eqn. (2.7). In this section we venture beyond the simulation of known analytical solutions and consider one of the simplest dynamical processes involving the 2DES: the collison of two of them. We shall see that calling these features solitons is not completely appropriate.

The three numerical experiments performed all involve coaxial pairs in which a 2DES of radius a_1 and speed U_1 collides with another of radius a_2 and speed U_2. Table 1 summarizes the runs

Table 1: Collision experiments with 2 DES

Experiment	Figure	a_1	a_2	Qualitative description
A	7	3/64	1/4	"Elastic collision"
B	8	1/16	1/8	"Inelastic collision"
C	9	1/8	1/8*	"Inverse cascade"

In experiments A and B all 2DES correspond to the gravest mode, κa_1 and κa_2 are both equal to the first zero of J_1. Furthermore, in these two experiments $U_1 a_1 = U_2 a_2$. In experiment C the second
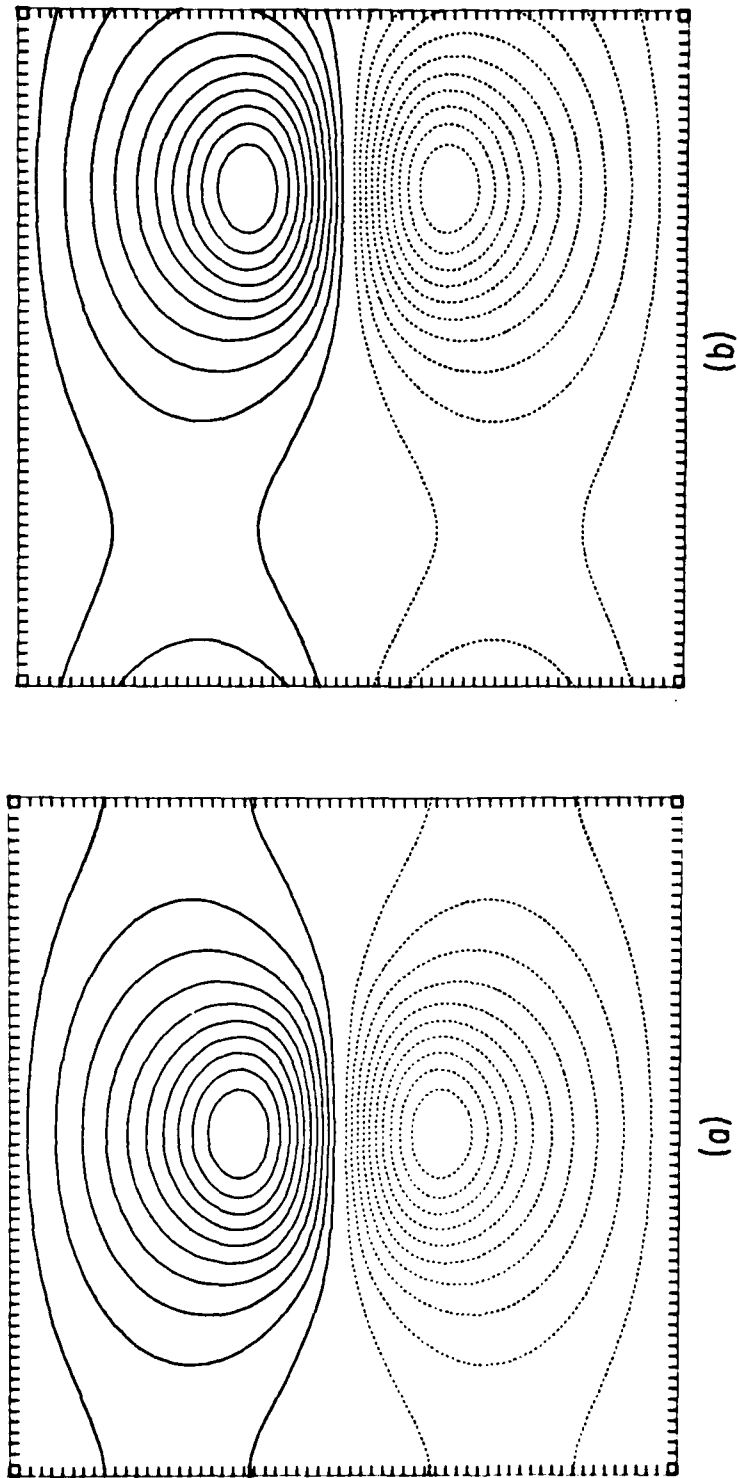
Fig. 4. Initial (a) and time evolved (b) streamline pattern for 2DES with a/L = 0.25.
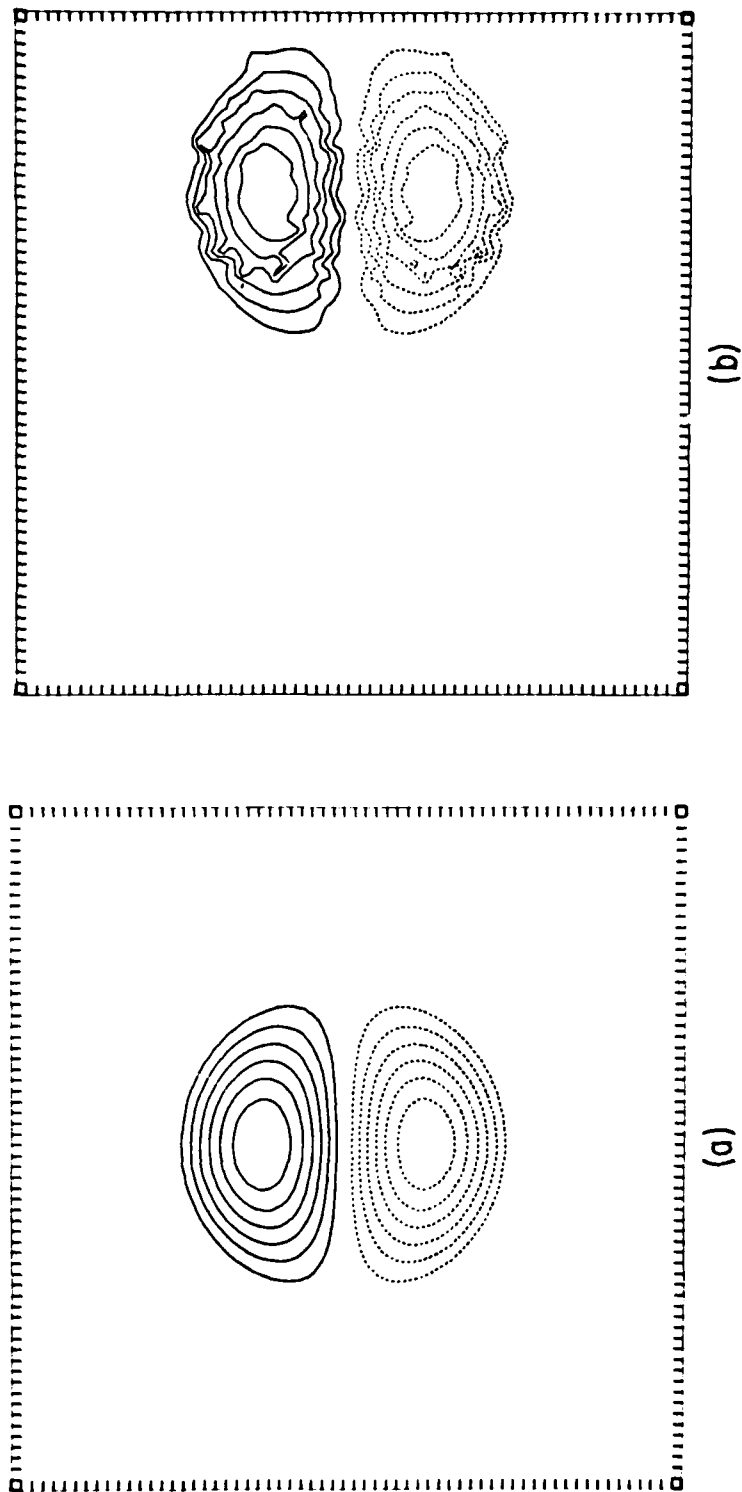
Fig. 5. Initial (a) and time evolved (b) vorticity pattern for the same run as in Fig. 4.
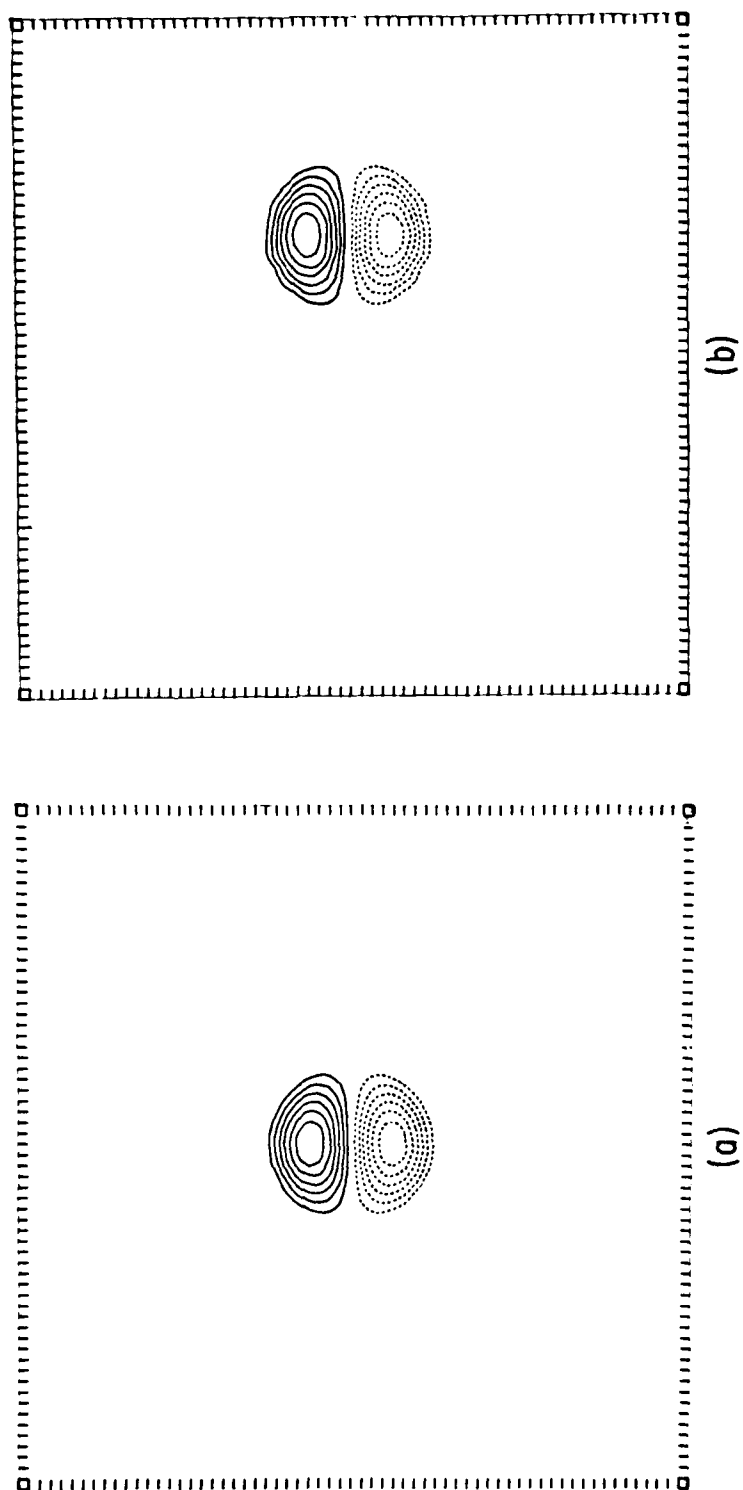
Fig. 6. Initial (a) and time-evolved (b) vorticity contours for 2DES with a/L = 0.125.

vortex is in the "first excited state", κa_2 equals the second zero of J_1. (This is the significance of the * in Table 1). This "quadrupole vortex" moves slowly to the left (x decreasing). Pictures of streamlines for the three sequences appear in Figs. 7-9.

Qualitatively the three sequences may be described as follows: In sequence A the smaller pair passes straight through the larger one, and in Table 1 this was characterized as an "elastic collision." In sequence B the small pair first passes through the large pair, then the large pair starts to contract and passes through the "small" pair. However, in the process the like-signed blobs merge and a single dipole results. Notice that in the lowest panels of Figs. 7 and 8 a vortex pair has passed through the periodic boundary at the right and reappeared at the left.

Finally in the sequence C (Fig. 9) the low κ pair absorbs the small vorticity nucleus of the high κ pair. Hence high wavenumber excitation is obliterated and two relatively low wavenumber structures remain. This process has been labelled "inverse cascade" in Table 1.

Expectations for experiments A and B are conditioned by knowledge of the sequence of events for two point vortex pairs. An early analysis by Love (1894) gives the following results for the initial value problem sketched in Fig. 10. The vortices all have the same absolute strength. Love showed that in every case all four vortices are collinear at some instant. There are then two possible regimes according as

$$\left(3+2\sqrt{2}\right)^{-1} = 3 - 2\sqrt{2} < \lambda/\Lambda < 3 + 2\sqrt{2} \tag{4.1}$$

at the instant the vortices are collinear or λ/Λ is outside this interval. If λ/Λ is within the interval (4.1) the two pairs perform a periodic leapfrogging motion in which one overtakes the other by passing through it. If λ/Λ is outside the range (4.1) the relative motion is aperiodic and the pairs separate. Two pairs started infinitely far apart as $t \rightarrow -\infty$ always belong to this regime and the only net effect of the collision is a forward shift of the smaller pair and a retardation of the larger
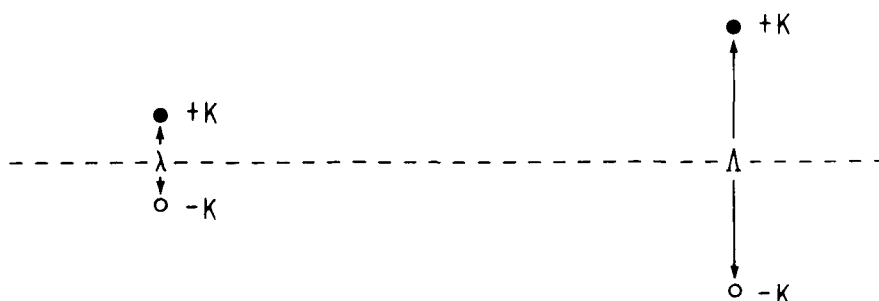
Fig. 10 Case of coaxial vortex pairs analyzed by Love (1894).

Fig. 7. Six consecutive streamline patterns for the "elastic collision" of two 2DES (experiment A, Table 1).
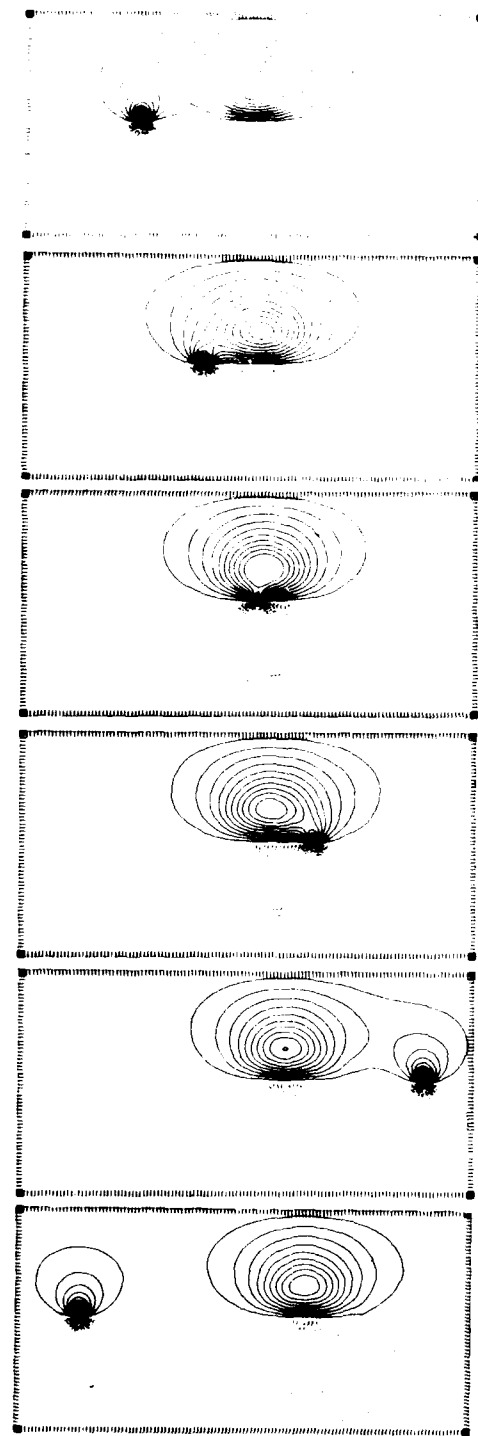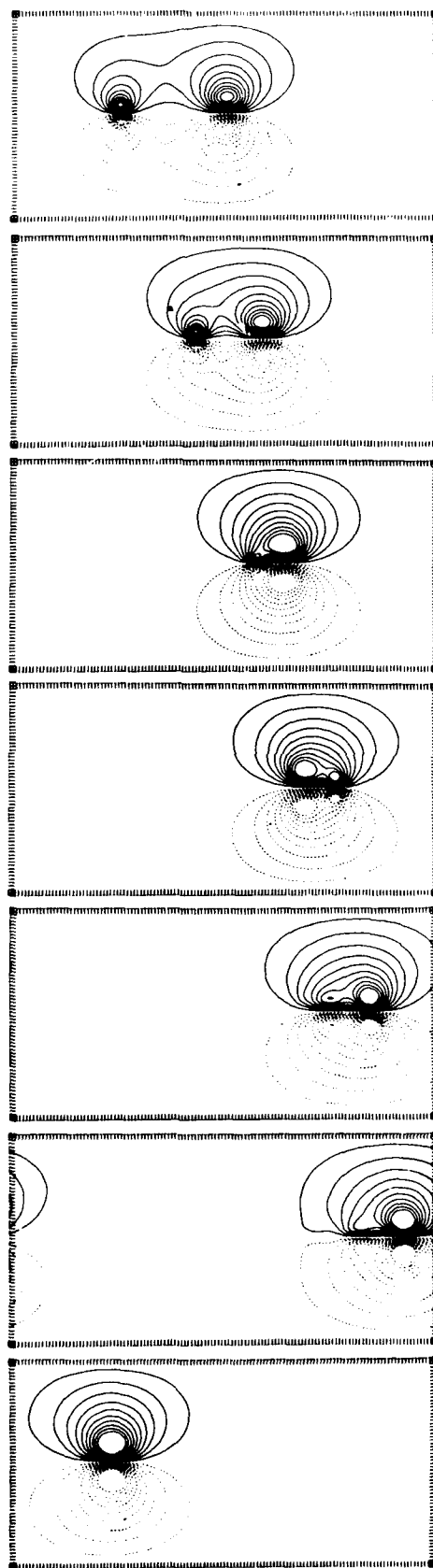
Fig. 8. Seven consecutive streamline patterns for the "inelastic collision" of two 2DES (experiment B, Table 1).
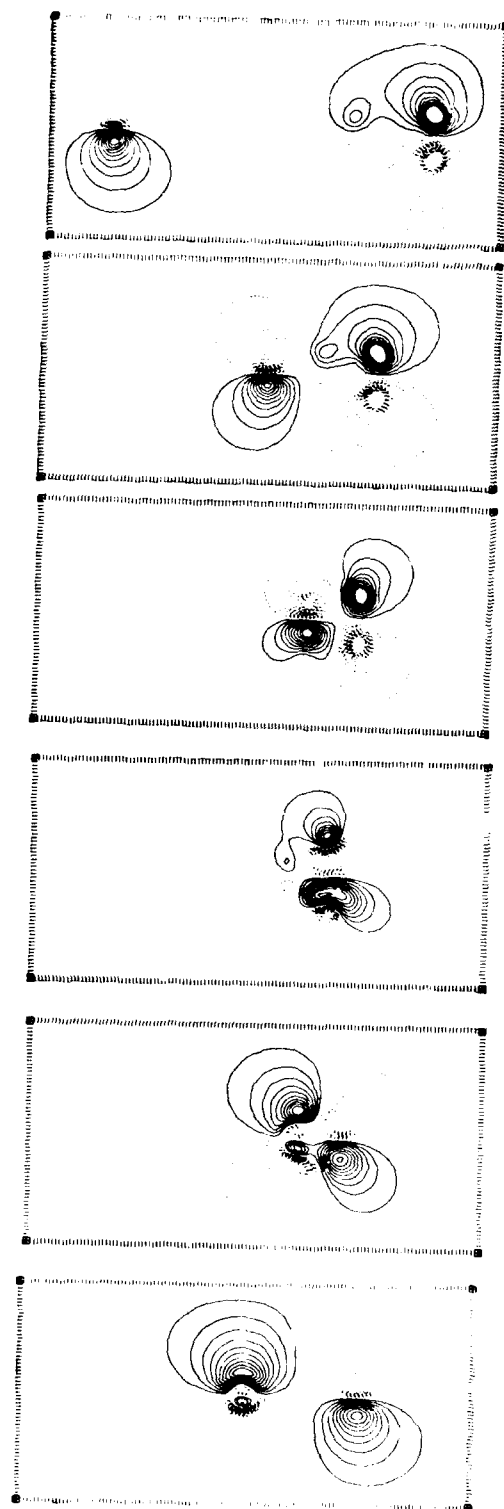
Fig. 9. Six consecutive streamline patterns for the collision of a "ground state" and a "first excited state" 2DES with the same radius (experiment C, Table 1).

relative to where they would have been if they had propagated without encountering one another. This case then is very reminiscent of the collision of solitons in one space dimension.

When initializing the colliding 2DES for experiments A and B care was taken to assure that the total circulation of each lobe had the same absolute magnitude. Using (3.1) one can show that the dimensionless ratio

$$\iint_{y>0} dxdy\, \zeta \Big/ Ua \;=\; 2\pi\, H_1(\kappa a) \tag{4.2}$$

where H_1 is a Struve function. Since the vorticity distributions rescaled according to (3.2) all have the same value of Ua it is seen that this rescaling in fact produces 2DES of the desired type. Hence the ratio of impulses for the colliding 2DES, which is the analogue of λ/Λ for point vortex pairs, is equal to the ratio of radii a_1/a_2 according to (2.10). It is then clear that experiment B with point vortex pairs would lead to periodic leapfrogging. Due to the distributed cores the vortex merging intervenes for 2DES after about 1.5 periods. Experiment A on the other hand has a much larger value of a_2/a_1 and produces the slip-through quasi-elastic collision in Fig. 7. Hence analogues of both the modes known for point vortex pairs appear to be present for the 2DES. It is apparent from Fig. 7 that even for the elastic collision small modifications result in the shape of resulting vortex dipoles. These may be thought of as the analogue of "dispersive tails" in solitary wave collisions.

The formulae (2.10), (2.11) may be applied to experiment B if one assumes that the resulting single vortex dipole is again of the form (2.7). The streamline picture indicates that this is approximately true. To proceed we also assume that the initial 2DES are so far apart that the total kinetic energy of the flow field is

$$\mathcal{E} \;=\; \pi a_1^2 U_1^2 + \pi a_2^2 U_2^2 \;. \tag{4.3}$$

The total impulse is initially

$$P \;=\; 2\pi a_1^2 U_1 + 2\pi a_2^2 U_2 \tag{4.4}$$

Using (2.10) and (2.11) we can obtain expressions for a, U of the final single vortex dipole. Since $a_1 U_1 = a_2 U_2$ one obtains

$$U \;=\; \frac{2\mathcal{E}}{P} \;=\; 2\,U_1 U_2 / (U_1 + U_2) \tag{4.5}$$

and

$$a \;=\; P/\sqrt{4\pi\mathcal{E}} \;=\; (a_1 + a_2)/\sqrt{2} \tag{4.6}$$

The expression (4.5) for U is about 10% larger than the actually measured value (from pictures). The value of a, (4.6), is difficult to measure from a streamline picture but is not unreasonable. The initial structures may have been too close for (4.3) to be valid.

Acknowledgments

References

Aref, H. and Siggia, E. D., 1980. "Vortex Dynamics of the Two-dimensional Turbulent Shear Layer", J. Fluid Mech., 100, 705-737.

Batchelor, G. K., 1967. "An introduction to Fluid Dynamics", Cambridge University Press, Chapter 7.

Christiansen, J. P., 1973. "Numerical Simulation of Hydrodynamics by the method of point vortices", J. Comp. Phys., 13, 363-379.

Deem, G. S. and Zabusky, N. J., 1978. "Vortex waves: Stationary 'V-states', interactions, recurrence and breaking", Phys. Rev. Lett., 40, 859-862.

Lamb, H., 1916. "Hydrodynamics" 4th ed., Cambridge University Press, Sec. 165.

Larichev, V. D. and Reznik, G. M., 1978. "Two-dimensional Rossby soliton: An exact solution" POLYMODE News 19 p. 3.

McWilliams, J. C., 1980. "Numerical Studies of Modons" This report, Vol. I.

McWilliams, J. C., Flierl, G., Larichev, V. D., and Reznik, G. M., 1980. "Numerical Study of barotropic modons", preprint.

Obernettinger, F. and Magnus, W., 1949. "Anwendung der Elliptischen Funktionen in Physik und Technik", Springer-Verlag, Chapter IV.

Stern, M. E., 1975. "Minimal properties of planetary eddies", J. Mar. Res., 33, 1-13.

MANDATORY DISTRIBUTION LIST

FOR UNCLASSIFIED TECHNICAL REPORTS, REPRINTS, AND FINAL REPORTS
PUBLISHED BY OCEANOGRAPHIC CONTRACTORS
OF THE OCEAN SCIENCE AND TECHNOLOGY DIVISION
OF THE OFFICE OF NAVAL RESEARCH

(REVISED NOVEMBER 1978)

1 Deputy Under Secretary of Defense
(Research and Advanced Technology)
Military Assistant for Environmental Science
Room 3D129
Washington, D.C. 20301

Office of Naval Research
800 North Quincy Street
Arlington, VA 22217
3 ATTN: Code 483
1 ATTN: Code 460
2 ATTN: 102B

1 CDR J. C. Harlett, (USN)
ONR Representative
Woods Hole Oceanographic Inst.
Woods Hole, MA 02543

Commanding Officer
Naval Research Laboratory
Washington, D.C. 20375
6 ATTN: Library, Code 2627

12 Defense Documentation Center
Cameron Station
Alexandria, VA 22314
ATTN: DCA

Commander
Naval Oceanographic Office
NSTL Station
Bay St. Louis, MS 39522
1 ATTN: Code 8100
1 ATTN: Code 6000
1 ATTN: Code 3300

1 NODC/NOAA
Code D781
Wisconsin Avenue, N.W.
Washington, D.C. 20235

Woods Hole Oceanographic Institution
WHOI-80-53

1980 SUMMER STUDIES PROGRAM IN GEOPHYSICAL FLUID DYNAMICS.
COHERENT FEATURES IN GEOPHYSICAL FLOWS by George Veronis, Director
and Florence K. Mellor, Editor. 249 pages. November 1980. Prepared
for the Office of Naval Research under Contract N00014-79-C-0671.

Four principal lecturers shared the task of presenting the subject
"Coherent Features in Geophysical Flows" to the participants of the
twenty-second geophysical fluid dynamics summer program. Glenn Flierl
introduced the topic and the Kortweg-de Vries equation via a model of
finite amplitude motions on the beta plane. He extended the analysis
to more complex flows in the ocean and the atmosphere and in the process
treated motions of very large amplitude. Larry Redekopp's three lectures
summarized an extensive body of the mathematical literature on coherent
features. Andrew Ingersoll focussed on the many fascinating features
in Jupiter's atmosphere. Joseph Keller supplemented an interesting
summary of laboratory observations with suggestive models for treating
the flows.

The seminars by participants and invited speakers, abstracts of
which are included, cover a broad range of topics in geophysical fluid
dynamics. Among the abstracts are the seminars presented by McWilliams,
Flierl, Redekopp, Rizzoli, Pierrehumbert and Hendershott during the one-
week workshop on coherent features.

The nine student lectures summarize the most creative product of
the summer program. This year was most unusual in that most of the
students worked on some aspect of the central theme. Some of these
projects will be reworked and extended for publication.

Woods Hole Oceanographic Institution
WHOI-80-53

1980 SUMMER STUDIES PROGRAM IN GEOPHYSICAL FLUID DYNAMICS.
COHERENT FEATURES IN GEOPHYSICAL FLOWS by George Veronis, Director
and Florence K. Mellor, Editor. 249 pages. November 1980. Prepared
for the Office of Naval Research under Contract N00014-79-C-0671.

Four principal lecturers shared the task of presenting the subject
"Coherent Features in Geophysical Flows" to the participants of the
twenty-second geophysical fluid dynamics summer program. Glenn Flierl
introduced the topic and the Kortweg-de Vries equation via a model of
finite amplitude motions on the beta plane. He extended the analysis
to more complex flows in the ocean and the atmosphere and in the process
treated motions of very large amplitude. Larry Redekopp's three lectures
summarized an extensive body of the mathematical literature on coherent
features. Andrew Ingersoll focussed on the many fascinating features
in Jupiter's atmosphere. Joseph Keller supplemented an interesting
summary of laboratory observations with suggestive models for treating
the flows.

The seminars by participants and invited speakers, abstracts of
which are included, cover a broad range of topics in geophysical fluid
dynamics. Among the abstracts are the seminars presented by McWilliams,
Flierl, Redekopp, Rizzoli, Pierrehumbert and Hendershott during the one-
week workshop on coherent features.

The nine student lectures summarize the most creative product of
the summer program. This year was most unusual in that most of the
students worked on some aspect of the central theme. Some of these
projects will be reworked and extended for publication.

DATE
ILMED

8